Dick Carrillo Melgarejo

IMPROVING THE DESIGN OF CELLULAR NETWORKS BEYOND 5G FOR SMART GRIDS

ACTA UNIVERSITATIS LAPPEENRANTAENSIS 1086

Dick Carrillo Melgarejo

IMPROVING THE DESIGN OF CELLULAR NETWORKS BEYOND 5G FOR SMART GRIDS

Dissertation for the degree of Doctor of Science (Technology) to be presented with due permis-sion for public examination and criticism at Lappeenranta–Lahti University of Technology LUT, Lappeenranta, Finland on the 22nd of September, 2023, at noon.

The dissertation was written under an agreement for dual-doctoral degree programme between Lappeenranta–Lahti University of Technology LUT, Finland and the University of Campinas (UNI-CAMP), Brazil and jointly supervised by supervisors from both universities.

Acta Universitatis
Lappeenrantaensis 1086

Supervisors Associate Professor (Tenure Track) Pedro Juliano Nardelli
LUT School of Energy Systems
Lappeenranta–Lahti University of Technology LUT
Finland

Associate Professor Gustavo Fraidenraich
Department of Communications
School of Electrical and Computer Engineering
University of Campinas
Brazil

Reviewers Associate Professor Jimmy Jessen Nielsen
Department of Electronic Systems
Aalborg University
Denmark

Associate Professor Jasmine Priscyla Leite de Araujo
Federal University of Pará
Brazil

Opponent Associate Professor Jimmy Jessen Nielsen
Department of Electronic Systems
Aalborg University
Denmark

ISBN 978-952-335-963-5
ISBN 978-952-335-964-2 (PDF)
ISSN 1456-4491 (Print)
ISSN 2814-5518 (Online)

Lappeenranta–Lahti University of Technology LUT
LUT University Press 2023

Abstract

Dick Carrillo Melgarejo
Improving the design of cellular networks beyond 5G for smart grids
Lappeenranta 2023
95 pages
Acta Universitatis Lappeenrantaensis 1086
Diss. Lappeenranta–Lahti University of Technology LUT
ISBN 978-952-335-963-5, ISBN 978-952-335-964-2 (PDF), ISSN 1456-4491 (Print), ISSN 2814-5518 (Online)

In the last decade, wireless technologies have emerged to support vertical applications. For instance, many wireless communication technologies are becoming key enablers of specialized smart grid applications. However, critical applications are still in the evaluation phase, and they are not deployed commercially yet. At present, 5th generation of mobile network (5G) is not yet capable of enabling critical applications that require a low latency and a high reliability. Bridging this gap is the main target of the present doctoral dissertation.

The doctoral dissertation considers the standard International Electrotechnical Commission (IEC) 61850 as a reference benchmark. This standard defines the foundation of a widely used protocol in smart grid applications, which is currently deployed mostly in wired networks.

To enable the application of the standard IEC 61850, the wireless communication interface should meet certain requirements. These requirements define specialized key performance indicators (KPIs) on latency, throughput, and reliability. As the complexity of functionalities to support the IEC 61850 KPIs goes beyond the current 5G design, a generic framework is proposed to enable and facilitate the identification, design, and integration of wireless cellular networks with the protocol IEC 61850.

The umbrella defined by the proposed framework aims to enable the radio access network (RAN) slicing, which is a cellular network functionality adopted recently by the wireless industry to add isolation between services sharing the same radio resource. Under this umbrella, this doctoral dissertation focuses on specialized cellular communication functions at the physical layer (PHY) and media access control (MAC) layer to enable each RAN slice.

In the PHY layer, a mathematical framework is provided to evaluate the generalized frequency division multiplexing (GFDM) waveform without the necessity of longer simulations. Based on this framework, key metrics like bit error rate (BER), sum rate, and outage probability can be derived analytically.

In the MAC layer, a dynamic allocation of RAN slices is proposed using deep-reinforcement

learning (DRL) to enable IEC 61850 messages. Here, the performance of the solution is measured based on each service-level agreement (SLA) defined for each RAN slice.

In the final chapter, a summary of the dissertation and other complementary information is provided. The chapter discusses the key outcomes of the study and its potential impact on the 3rd Generation Partnership Project (3GPP) standard toward 5G-advanced and 6th generation of mobile network (6G). The chapter also highlights the impact of the proposed framework on other industrial verticals, such as mining, oil, and gas industry.

Keywords: Connectivity in smart grids, RAN slicing, GFDM, deep reinforcement learning, sub-1GHz bands

Resumo

Dick Carrillo Melgarejo
Aprimorando o design de redes celulares além do 5G para smart grids
Lappeenranta 2023
95 páginas
Acta Universitatis Lappeenrantaensis 1086
Diss. Lappeenranta–Lahti University of Technology LUT
ISBN 978-952-335-963-5, ISBN 978-952-335-964-2 (PDF), ISSN 1456-4491 (Print), ISSN 2814-5518 (Online)

Na última década, surgiram tecnologias sem fio para dar suporte a aplicações verticais. Por exemplo, muitas destas tecnologias estão se tornando os principais facilitadores de aplicações especializadas em redes inteligentes. No entanto, aplicações críticas ainda estão em fase de avaliação e ainda não foram implantadas comercialmente. Por exemplo, o 5G ainda não é capaz de habilitar aplicações críticas que requerem baixa latência e alta confiabilidade. Suplir esta necessidade é o principal objetivo da presente dissertação de doutorado.

Esta dissertação de doutorado considera a norma IEC 61850 como *benchmark* de referência. Este padrão define a base de um protocolo amplamente utilizado em aplicações de smart grid, que atualmente é implantado majoritariamente em redes cabeadas.

Para permitir a aplicação do padrão IEC 61850, o canal de comunicação sem fio deve atender certos requisitos. Esses requisitos definem indicadores de desempenho especializados como latência, taxa de transferência e confiabilidade. Como a complexidade das funcionalidades para suportar o IEC 61850 KPIs vão além do design atual do 5G, nós propomos uma estrutura genérica para permitir e facilitar a identificação, implementação e integração entre as redes celulares sem fio com o padrão IEC 61850.

O guarda-chuva definido pelo framework proposto visa habilitar o RAN slicing, que é uma funcionalidade de rede celular adotada recentemente pela indústria sem fio para adicionar isolamento entre serviços que compartilham recursos de rádio. Esta dissertação de doutorado enfoca em funções especializadas de comunicação celular nas camadas PHY e MAC.

Na camada PHY, fornecemos um modelo matemático para avaliar a forma de onda GFDM sem a necessidade de extensas simulações. Com base nessa estrutura, as principais métricas, como BER, sum rate e probabilidade de outage, podem ser derivadas analíticamente.

Na camada MAC, propomos uma alocação dinâmica de RAN slicing usando DRL para habilitar mensagens específicas do IEC 61850. Aqui, o desempenho da solução é medido com base a cada SLA definido para cada RAN slice.

Para resumir, discutimos os principais resultados do estudo e seu potencial impacto no padrão 3GPP visando o 5G-advanced e 6G. Também destacamos o impacto da estrutura proposta em outras verticais industriais, como mineração, petróleo e gás.

Keywords: Conectividade em smart grid, RAN slicing, GFDM, deep reinforcement learning, sub-1GHz bands

Preface

Reality is merely an illusion, albeit a very persistent one.

— ALBERT EINSTEIN

This work was carried out in the LUT School of Energy Systems at Lappeenranta–Lahti University of Technology LUT, Finland and at the Department of Electrical Engineering at Campinas University (UNICAMP), Brazil. It is in fulfillment of the requirements for acquiring the double degree of Doctor of Science (Technology) in Finland and Doctor of Philosophy in Brazil.

This dissertation summarizes the scientific work carried out by the author during his doctoral studies between August, 2018 and July, 2022. The doctoral studies were supported by the Academy of Finland through: (a) ee-IoT project n.19009; (b) FIREMAN consortium n.326270 part of CHIST-ERA-17-BDSI-003; (c) EnergyNet Fellowship n.321265 / n.328869 / n.352654; and (d) X-SDEN project n.349965; and by Jane and Aatos Erkko Foundation through the STREAM project.

The doctoral dissertation provides a self-contained summary of five attached scientific articles, which have been peer-reviewed and published. While the research details are left to the specific publications at the end of the dissertation, the main body of the dissertation is conceived as a guide on how these scientific papers can be contextualized in the bigger picture of cellular networks enabling smart grid applications.

Acknowledgments

The beginning of knowledge is the discovery of something we do not understand.

— FRANK HERBERT

First of all, I would like to thank God because I got the chance to live in Finland and because this fantastic country became my family's home during the execution of this dissertation.

I want to express my deepest appreciation to my supervisors, Associate Professor (Tenure Track) Pedro Juliano Nardelli and Associate Professor Gustavo Fraidenraich for their invaluable guidance and consideration in giving me the opportunity to pursue a doctoral degree.

This endeavor would not have been possible without the reviewers of this dissertation; I am grateful to Associate Professor Jasmine Priscyla Leite de Araujo and Associate Professor Jimmy Jessen Nielsen for their valuable comments, suggestions, and effort in the preliminary examination process of the manuscript. These interactions were highly important for the successful accomplishment of this research work.

I would like to thank the co-authors of the publications presented in this dissertation for their valuable contribution and collaboration. Indeed, I would like to extend my special gratitude to Doctor Charalampos Kalalas for helping to arrange and host my research mobility at CTTC in Barcelona, Spain. I am proud that our collaboration resulted in extraordinary scientific outcomes. I also owe a lot to Associate Professor Demostenes R. Zegarra for his feedback and technical suggestions, which were essential for achieving significant milestones during the execution of this dissertation.

I would like to express my special thanks to Associate Professor Hanna Niemelä for improving the quality of presentation of several scientific publications written at LUT, including this doctoral dissertation.

During my doctorate studies, I received internal and external funding. I, therefore, acknowledge the important financial support I received from the LUT Research Foundation and Nokia Foundation to cover trips and event expenses.

I thank my colleagues in the Cyber-Physical Systems (CPS) research group at LUT and the Communication Department at Campinas University for the valuable discussions and

interchange of ideas. At LUT University, I owe my deepest thanks to Dr. Aleksei Mashlakov, Dr. Arun Narayanan, Dr. Arthur Sousa de Sena, Dr. Daniel Gutierrez-Rojas, Dr. Antti Pinomaa, Dr. Gonçalo Pinto Mendes, Doctoral Student Pedro Goria Silva, Doctoral Student Mehar Ullah, and Doctoral Student Mohamed Selim.

I owe my special gratitude to Dr. Majid Hussain and Doctoral Student Alejandro Ibañez Rioja, because beyond the academic interchange of ideas, we had the chance to play several amazing tennis matches. Furthermore, I want to express my special gratitude to Doctoral Student Iurii Demidov for the interchange of ideas on using ArchLinux and other interesting technological topics.

Thanks to LUT staff Ms. Päivi Nuutinen, Ms. Marika Hyrylä, Ms. Sofia Pyyhtiä, and Ms. Anu Honkanen for dealing with the bureaucratic issues on my behalf and patiently answering all my queries. A special thank to Ms. Saara Merrit and Ms. Sari Damsten-Puustinen, for guidance and support in the graduation process.

In Brazil, I would like to thank my father- and mother-in-law, Settimio Grassone and Nadir Fernandes; my sister-in-law Adriana, her husband Mauricio, and their kids Clarice and Fernando; and my brother-in-law Aldo, for your unwavering support.

A special thanks goes to my soul brother Luis Rurush, because he is a life witness of the momentousness of this doctoral dissertation and the hard road I had to go through to get here.

I would like to thank my family in Perú for being my constant inspiration of life and effort. Especially, I would like to thank my parents, Melania Melgarejo Gomero and Carmelo Carrillo Sanchez; my sisters Madeleyni, Jacqueline, and Marifrance; my uncles Elgar, Flavio, and Joaquín ; my cousins Jhosselin and Giomara; my nieces Sofia, Leandra, and Melani; and my nephew Nicolas for devoting their time, energy, and love to support my dreams.

I express my deepest gratitude to my core family, to my loved Sandra Grassone and my daughters Maria Luiza and Hanna. Without your patience and support, this work would definitely not have been completed.

Dick Carrillo Melgarejo
September 2023
Lappeenranta, Finland

Dedicated to my parents Melania and Carmelo

whose commitment inspires every second of my life and because my achievements are their achievements.

Contents

List of publications

This dissertation is based on the following papers. The rights have been granted by the publishers to include the papers in the dissertation. The author is identified as D. Carrillo or D.C. Melgarejo, both referring to the full name Dick Carrillo Melgarejo.

Publication I

D. Carrillo et al., "Boosting 5G on Smart Grid Communication: A Smart RAN Slicing Approach," *IEEE Wireless Communications*, early access, pp. 1–8, 2022.

Publication II

D. C. Melgarejo et al., "Optimizing Flying Base Station Connectivity by RAN Slicing and Reinforcement Learning," *IEEE Access*, vol. 10, pp. 53746–53760, 2022.

Publication III

D. Carrillo, S. Kumar, G. Fraidenraich, and L. L. Mendes, "Bit Error Probability for MMSE Receiver in GFDM Systems," *IEEE Communications Letters*, vol. 22, no. 5, pp. 942–945, May 2018.

Publication IV

D. Carrillo Melgarejo et al., "Dynamic Algorithm for Interference Mitigation Between Cells in Networks Operating in the 250 MHz Band," *IEEE Access*, vol. 10, pp. 33803–33815, 2022.

Publication V

D. Carrillo, S. Kumar, G. Fraidenraich, P. H. J. Nardelli, and D. B. d. Costa, "Achievable Sum Rate and Outage Capacity of GFDM Systems with MMSE Receivers," in *ICC 2020 - IEEE International Conference on Communications (ICC)*, 2020, pp. 1–6.

Author's contribution

Dick Carrillo Melgarejo is the principal author, investigator, and promoter in all the publications. The author's contributions to the appended publications are the following:

Publication I: The author provided the definition of the RAN slicing framework, mapped IEC 61850 messages on each RAN slice, and verified the deep reinforcement learning model by simulation. He also led the paper writing.

Publication II: The author provided the system-level definition of the proposed solution. He designed the machine learning model and fitted it to the wireless communication system model. Elaboration of the simulation campaigns was also part of the author's duties.

Publication III: The author conducted the analytical derivation using random matrix theory with the support of coauthors. He also produced the simulation results of GFDM in different scenarios and parameters and performed the literature review.

Publication IV: The author implemented the driving test used to calibrate the simulator. He also defined the benchmark setup on NS3 to run the system-level simulation. The author also contributed with the deep reinforcement learning model applied in the solution. Finally, he led the paper writing.

Publication V: The author developed an end-to-end simulation and an analytical model to obtain the sum rate and the outage capacity. He also led the publication writing. Furthermore, the author presented the publication at the conference.

Relevant publications (not included in the dissertation)

In the course of his doctoral studies, the author has been the main author or a coauthor in the following publications. They are, however, omitted from the dissertation because they are not directly related to the primary objective of the work, or they are partially covered by other papers included in this dissertation. The author is identified as D. Carrillo or D.C. Melgarejo, both referring to the full name Dick Carrillo Melgarejo.

Journal papers

1. D. Carrillo, K. Mikhaylov, P. J. Nardelli, S. Andreev, and D. B. da Costa, "Understanding UAV-Based WPCN-Aided Capabilities for Offshore Monitoring Applications," *IEEE Wireless Communications*, vol. 28, no. 2, pp. 114–120, April 2021.

2. D. Carrillo, S. Kumar, G. Fraidenraich, and P. Nardelli, "Analytical derivation of the SINR for GFDM signals on Rician fading channels with MMSE receiver," *IEEE Transactions on Vehicular Technology*. Submitted 2023.

3. D. Carrillo et al., "Containing Future Epidemics with Trustworthy Federated Systems for Ubiquitous Warning and Response," *Frontiers in Communications and Networks*, (2021), p. 11. 2021.

4. D. Zegarra Rodríguez, D. Carrillo, M. A. Ramirez, P. N. Nar, S. Moller, "Incorporating Wireless Communication Parameters into the E-Model Algorithm," *IEEE/ACM Transactions on Audio, Speech, and Language Processing (2021)*, pp. 1–1. 2021.

5. A. S. Sena, D. Carrillo, F. Fang, P. H. J. Nardelli, D. B. Costa, U. S. Dias, Z. Ding, C. B. Papadias, W. Saad, "What Role Do Intelligent Reflecting Surfaces Play in Multi-Antenna Non-Orthogonal Multiple Access?" *IEEE Wireless Communications*, (2020), pp. 24–31. 2020.

6. F.H.C Santos Filho, P.S. Dester, E.M.G. Stancanelli, P. Cardieri, D. Carrillo P.H.J. Nardelli, H. Alves, "Performance of LoRaWAN for Handling Telemetry and Alarm Messages in Industrial Applications," *Sensors*, 20.3061 (2020).

7. R. L. Rosa, M. J. De Silva, D. H. Silva, M. S. Ayub, D. Carrillo, P. H. J. Nardelli, D. Z. Rodríguez, "Event Detection System Based on User Behavior Changes in Online Social Networks: Case of the COVID-19 Pandemic," *IEEE Access*, (2020), pp. 158806–158825. 2020.

8. P. H. J. Nardelli, H. Alves, A. Pinomaa, S. Wahid, M. D. C. Tomé, A. Kosonen, F. Kühnlenz, A. Pouttu, D. Carrillo, "Energy Internet via Packetized Management: Enabling Technologies and Deployment Challenges," *IEEE Access* (2019), pp. 16909–16924. 2019.

9. Marielle Jordane Silva, Dick Carrillo Melgarejo, Renata Lopes Rosa, Demóstenes Zegarra Rodríguez, "Speech Quality Classifier Model based on DBN that Considers Atmospheric Phenomena," *Journal of Communications Software and Systems*, (2020).

10. A. Narayanan, A. S. D. Sena, D. Gutierrez-Rojas, D. Carrillo, H. M. Hussain, M. Ullah, S. Bayhan, P. H. J. Nardelli, "Key Advances in Pervasive Edge Computing for Industrial Internet of Things in 5G and Beyond," *IEEE Access*, (2020), pp. 206734–206754. 2020.

11. R. Cipriano M., P. H. J. Nardelli, M. Taynnan B., W. Saad, A. Hekmatmanesh, Pedro E. G. Silva, A. S. Sena, M. Dzaferagic, H. Siljak, W. Van Leekwijck, D. Carrillo M., S. Latré, "Neurosciences and Wireless Networks: The Potential of Brain-Type Communications and Their Applications," *IEEE Communications Surveys Tutorials*, (2021), pp. 1599–1621. 2021.

12. Ogobuchi Daniel Okey, Dick Carrillo Melgarejo, Muhammad Saadi, Renata Lopes Rosa, João Henrique Kleinschmidt, Demóstenes Zegarra Rodríguez, "Transfer Learning Approach to IDS on Cloud IoT Devices Using Optimized CNN," *IEEE Access* (2023), pp. 1023–1038. 2023.

13. Jouni Ikonen, Niklas Nelimarkka, Pedro H. J. Nardelli, Niko Mattila, Dick Carrillo Melgarejo, "Experimental Evaluation of End-to-End Delay in a Sigfox Network," *IEEE Networking Letters*, (2022), pp. 194–198. 2022.

Conference proceedings

1. D. C. Melgarejo, J. M. Moualeu, P. Nardelli, G. Fraidenraich, and D. B. da Costa, "GFDM-Based Cooperative Relaying Networks with Wireless Energy Harvesting," in *16th International Symposium on Wireless Communication Systems (ISWCS)*, 2019, pp. 416–421.

2. D. C. Melgarejo, C. Kalalas, A. S. de Sena, P. H. J. Nardelli, and G. Fraidenraich, "Reconfigurable Intelligent Surface-Aided Grant-Free Access for Uplink URLLC," in *2nd 6G Wireless Summit (6G SUMMIT)*, 2020, pp. 1–5.

3. A. Lana, I. Demidov, A. Pinomaa, D. Carrillo, O. Pyrhönen, "Energy Management Methodology for Fusion Grid," in *2019 IEEE PES Innovative Smart Grid Technologies Europe (ISGT-Europe)*, 2019.

4. D. C. Melgarejo, G. Fraidenraich, L. Quirino, A. Medeiros, P. Nardelli, "Performance of Multi-carrier Technology over VHF Channels for Rural Area Applications," in *2019 IEEE Wireless Communications and Networking Conference Workshop (WCNCW)*, 2019.

5. F. Polunin, D. C. Melgarejo, T. Lindh, A. Pinömaa, P. H. J. Nardelli, O. Pyrhönen, "Demonstrating the Impact of LTE Communication Latency for Industrial Applications," in *2019 IEEE 17th International Conference on Industrial Informatics (INDIN)*, 2019.

6. R. T. Caldeira, D. C. Melgarejo, R. Coutinho, "Application of LTE 450 MHz in the electric energy sector," in *2017 European Conference on Networks and Communications (EuCNC)*, 2017.

Technical report

1. 3rd Generation Partnership Project; Technical Specification Group Radio Access Network, "Study on Artificial Intelligence (AI)/Machine Learning (ML) for NR air interface," 3GPP TR 38.843 V0.2.0 (Release 18). 2023.

Nomenclature

Latin Alphabet

$d_{s,k}$	complex symbol block at the sth time and the kth subchannel
$x[n]$	GFDM signal representation
$g_{s,k}[n]$	circular time-frequency-shifted version of the prototype filter $g[n]$
$g[n]$	discrete prototype pulse shaping
$\sigma^2_{\mathbf{d}}$	variance of the transmit symbol block $\mathbf{d}$
σ^2_{ν}	variance of the AWGN noise $\boldsymbol{\nu}$
$\mathbf{A}$	self-interference matrix of the GFDM system
$\mathbf{H_{ch}}$	circular Toeplitz matrix channel representation
γ_n	SINR of the nth data symbol of a GFDM signal

Notation

$(.)^{\dagger}$	Hermitian conjugate operator
$[.]^T$	vector transpose operator
$*$	linear convolution operator

Acronyms

3GPP	3rd Generation Partnership Project
4G	4th generation of mobile network
5G	5th generation of mobile network
6G	6th generation of mobile network
ACSI	abstract communication service interface
AI/ML	artificial intelligence / machine learning
AI	artificial intelligence
AMI	advanced metering infrastructure
AWGN	additive white Gaussian noise
BER	bit error rate
BS	base station

CBM circuit breaker monitoring
CDC common data classes
CDMA code division multiple access
CHP combined heat and power
CPP critical peak pricing
CP cyclic prefix
CSI channel state information
CU centralized unit
DAP data aggregate unit
DER distributed energy resource
DPR digital protective relay
DRL deep-reinforcement learning
DR demand response
DSP digital signal processing
DTFT discrete-time Fourier transform
DU distributed unit
E2E-NSI end-to-end network slice instance
E2E end-to-end
EHV extra high voltage
eMBB enhanced mobile broadband
EPRI Electric Power Research Institute
EU European Union
FBMC filterbank multicarrier
FBS flying base station
FDD frequency division duplex
FDE frequency-domain equalization
FDMA frequency division multiple access
FFR fractional frequency reuse
FR frequency reuse
FSFC frequency selective fading channel
GAN generative adversarial network
GFDM generalized frequency division multiplexing
gNB next-generation NodeB
gNodeB 5G Node B
GOOSE generic object oriented substation event
GSE generic substation events
GSM global system for mobile communications
GSSE generic substation status event
GeSI Global e-Sustainability Initiative
HAN home area network

HMI human machine interface
HSR high-availability seamless redundancy
HV high voltage
ICIC intercell interference coordination
ICI intercarrier interference
ICT information and communication technology
IEC International Electrotechnical Commission
IED intelligent electronic device
IEEE Institute of Electrical and Electronics Engineers
IMT-2020 International Mobile Telecommunications-2020 standard
IRSS Intelligent RAN slicing scheduler
ISI intersymbol interference
ISO International Organization for Standardization
IS international standards
ITU-R Radiocommunication Sector of the International Telecommunication Union
IUC integrated utility communication
IoT Internet of Things
KPI key performance indicator
LN logical node
LTE-M LTE machine-type communication
LTE long-term evolution
MAC media access control
MDMS metering data management system
MEC mobile edge computing
MIMO multiple-input multiple-output
ML machine learning
MLP multi-level perspective
MMSE minimum mean squared error
MMS manufacturing message specification
mMTC massive machine-type communication
MSE mean-squared error
MTU master terminal unit
MU merging unit
NAN neighborhood-area networks
NB-IoT narrowband IoT
NLOS non-line-of-sight
NOMA non-orthogonal multiple access
NPN nonpublic networks
NR new radio
NSI network slice instance

NSP Northern States Power Company
NSSI network slice subnet instance
OFDMA orthogonal frequency-division multiple access
OFDM orthogonal frequency division multiplexing
OOB out-of-band
OSI open systems interconnection
PAPR peak-to-average power ratio
PDC phasor data concentrator
PDF probability density function
PHY physical layer
PMU phasor measurement unit
PRP parallel redundancy protocol
PTP precision time protocol
QAM quadrature amplitude modulation
QCI QoS class identifier
QoS quality of service
RANA RAN architecture
RAN radio access network
RAT radio access technology
RB resource block
RIL RAN isolation level
RIS reconfigurable intelligent surface
RL reinforcement learning
RQ research question
RRC root raised cosine
RSF RAN slicing function
RSM RAN slicing management
RSRP reference signal received power
RSSI received signal strength indication
RTP real-time pricing
RTU remote terminal unit
RU radio unit
SAS substation automation system
SC-FDE single carrier frequency domain equalization
SCADA supervisory control and data acquisition
SCL substation configuration language
SCSM specific communication service mapping
SDN software-defined network
SE spectral efficiency
SIC successive interference cancellation

SINR signal-to-interference-and-noise ratio
SIP session initiation protocol
SLA service-level agreement
SNR signal-to-noise ratio
SON self-organizing network
SST slice/service type
SV sampled value
TCP/IP transmission control protocol/Internet protocol
TCP Transmission Control Protocol
TDMA time division multiple access
TOU time of use
TR technical report
TS technical specifications
UAV unmanned aerial vehicle
UCA utility communication architecture
UDP User Datagram Protocol
UE user equipment
URLLC ultra-reliable low-latency communication
V2G vehicle to grid
V2I vehicle to infrastructure
VHF very high frequency
WAM wide-area measurement system
WAN wide area network
WLAN wireless Local Area Network
WRAN Wireless Regional Area Network
WiMAX worldwide interoperability for microwave access
XML extensible markup language
ZF zero-forcing

1 Introduction

Science may set limits to knowledge,
but should not set limits to
imagination.

— BERTRAND RUSSELL

Actions to mitigate climate change require effective operations in large-scale infrastructures, especially in the energy system. Recently, the European Union (EU) has set the goal of a digital green transition to make Europe the first climate-neutral continent by 2050. Following this objective, an intermediate target was defined to reduce net greenhouse gas emissions by at least 55% by 2030.

The Global e-Sustainability Initiative (GeSI) published the SMARTer2030 report, issued in June 2015 [1]. In the report, it is stated that the greenhouse gas emissions of the information and communication technology (ICT) sector are expected to decrease to 1.97% of the global greenhouse gas emissions by 2030. By the use of ICT, energy companies are also looking for more efficient and alternative ways to generate energy in a reliable manner and bring down emissions. ICT-enabled smart grids have the potential to generate significant efficiency improvements in existing grids to facilitate the integration of distributed and renewable energy. By 2030, ICT-enabled solutions have the potential to reduce global CO2e emissions by 1.8 Gt CO2e and save 6.3 billion MWh of energy by improving supply and demand management, grid efficiency gains, and integration of renewables. In this context, the most recent advances of ICT could support a more effective operation of electricity grids, creating a smart grid [1].

The smart grid is a modern electric power grid infrastructure that aims to enhance reliability and efficiency through high-power converters, automated control, sensing, modern communication infrastructure, metering, and demand response optimization. The smart grid represents a convergence of sensors, actuators, control technology, computers, and communication to improve the consumption efficiency of the electric power grid.

For a smooth operation of smart grids, the communication infrastructure should be scalable and pervasive. This connectivity is essential to improve the quality and reliability of the power supply and reduce the risk of an electricity blackout. Nowadays, wired connectivity is the most popular choice in the power system industry; however, wireless solutions are gaining popularity. Considerations between wired or wireless communication depend on several factors. These factors can involve, e.g., geographical topography, costs, and operational requirements. For instance, smart grids use a combination of wired and wireless communication technologies, depending on the infrastructure.

However, wireless communication alternatives have some advantages over wired com-

munication, such as a low cost and connectivity in inaccessible areas. For these reasons, many factors and requirements have to be considered for each case to decide which communication technology could be employed. For example, wireless communication is less costly to implement in a complex infrastructure and easier to install in some areas. On the other hand, wired connection will not necessarily suffer from interference issues like wireless solutions may do. For the above-mentioned reasons, both types of communication are necessary in a smart grid to support specialized requirements.

Importantly, the requirements that the smart grid sets for connectivity technologies consider essential features, such as ultra-low latency supporting 3 ms in critical applications; very high reliability with 99.999% of packet lost; a very high bandwidth and data rates up to 1 Gbps; and supporting an extremely high density of devices. In some cases, the communication device should consider a very low energy consumption to meet the targets of battery life duration [2].

Based on the above, we provide an overview of the main objectives and research questions in the next section.

1.1 Overall aim, objectives, and research questions

Based on the current scenario described above, our target is to focus on the design of wireless technologies to support smart grids. Thus, this doctoral dissertation aims to provide solid scientific foundations for radio access network techniques to support these vertical applications. For this purpose, an RAN framework is proposed to enable the usability of three key technologies, which are the main focus of this study.

- The first technology is RAN slicing, which aims to provide critical trade-offs between service isolation and efficiency in radio resource allocation.
- The second technology is generalized frequency division multiplexing (GFDM), which aims to be an alternative waveform in future wireless networks.
- Finally, the third technology is a machine learning approach supporting the physical layer of the cellular network based on DRL.

The study on GFDM is based on random matrix theory as a mathematical tool. The RAN slicing scenarios were studied by using Monte Carlo and complex system simulations. In the case of DRL, a system model simulator based on Python was integrated into a TensorFlow machine learning model to evaluate the RAN slicing scenarios. To assess the performance of the DRL, we considered a cellular network simulator based on C++ as a benchmark.

The scientific outputs of this study are achieved by using tools such as random matrix theory, Monte Carlo, and complex system simulations, which are integrated with machine learning platforms, such as TensorFlow. To serve readers and researchers, a public

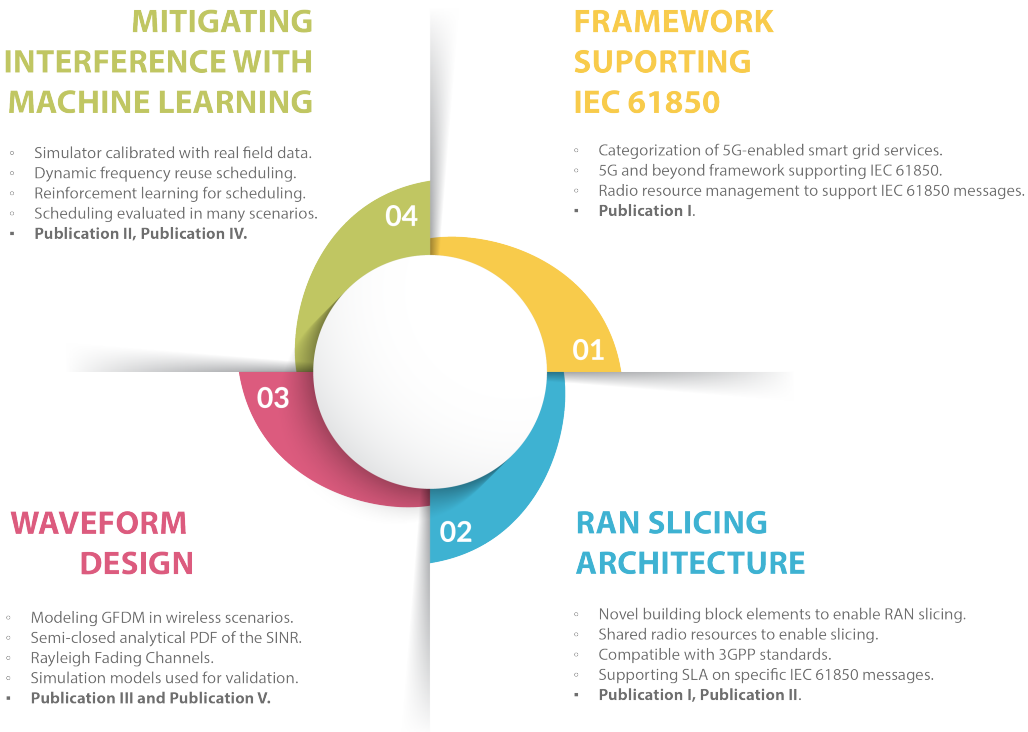

Figure 1.1: Overall description of the content and target of the dissertation, including the respective publications.

Github repository is shared in some contributions.

This doctoral dissertation aims to contribute to the ongoing trend in 5G/6G research, emphasizing technologies that focus on waveforms and radio resource management facilitated by machine learning to enable vertical applications. For this purpose, the framework proposed in this doctoral dissertation aims to integrate the essential elements that compose the RAN slicing framework following current 3GPP premises.

Based on this framework, this dissertation aims to provide scientific contributions in the PHY layer focusing on GFDM, which was a 5G waveform candidate with a high potential to become a 6G waveform candidate. Another PHY layer target is RAN slicing, which is an approach that is being discussed in the current evolution of the specification 3GPP Rel. 18 planned to be frozen at the end of 2023.

In the MAC layer, the contributions are not limited to the application of DRL to improve the scheduling of RAN slicing resources in challenging scenarios. The main aims of the dissertation are illustrated in Fig. 1.1.

To achieve the objectives described above, the following research questions (RQs) are formulated:

RQ1 *What are the limitations (if any) of existing wireless technologies for current cellular networks to serve smart grid communications, especially for protection / substation operation?*

This starting research question aims to explore and comprehensively define the state of the art in smart grid communication technologies to figure out the current requirements. In particular, this question focuses on current communication protocols, standards, use cases, and requirements for smart grid communications with the emphasis on critical applications as protection / substation operations. This question concerns the possibility to identify potential mismatches between cellular network protocols and widely used smart grid communication standards, which limit the employment of cellular technologies in critical applications.

Hypothesis: Currently, the widely used protocol is IEC 61850, which was designed to enable smart grid communications in wired Ethernet. There are studies introducing IEC 61850 in applications using wireless technologies. However, the limitations of current cellular standards enabling critical applications are not known. Our hypothesis is that there is a mismatch between the current cellular standard and the standard IEC 61850 for protection / substation operation.

Impact: By identifying those potential mismatches, new tailored cellular network protocols for dedicated critical smart grid communication could be proposed in standardization for future generations of cellular systems.

Novelty: Although similar studies can be found in the literature, none of them have constructed in a systematic way a method to assess the performance of smart grid communication protocols over wireless cellular networks. The novelty of this dissertation is that we propose such a method to analyze and evaluate the performance of the standard IEC 61850 with current cellular technology, demonstrating its feasibility.

Methodology: The methodology of this study is based on a top-down approach. It starts with an analysis and understanding of the smart grid industry. The analysis is used to identify some communication benchmarks, which are mostly related to popular wired communication technologies, such as fiber and copper communication. These technologies usually follow some requirements defined by specific standards or protocols. For instance, the standard IEC 61850 defines strict requirements for critical and non-critical messages. Furthermore, a test bed is used to evaluate the performance of a 4th generation of mobile network (4G)/5G network in a real scenario that aims to transport IEC 61850 messages. This output helps us to get an objective indicator of the current status of the state of the art of cellular networks supporting smart grid communications. Based on this outcome, a framework is proposed to complement the current 5G standard to enable IEC 61850 messages, all together in the same protocol solution.

RQ2 *In what conditions generalized waveforms—which are yet not part of current cellular standards—can outperform the existing solutions, potentially allowing new smart grid applications in indoor and outdoor environments?*

The current cellular technology is based on a waveform family employing orthogonal frequency division multiplexing (OFDM). This waveform is based on orthogonal spectrum allocation, which can be redesigned to achieve better performance, which may benefit the operation of smart grid communications for critical applications. In this respect, GFDM is a strong candidate for the next generation of cellular networks, including improved energy efficiency among other benefits, such as full legacy support to OFDM.

Hypothesis: To enable critical functionalities of smart grid applications, other waveforms beyond OFDM must be considered. For instance, GFDM has some features that outperform OFDM in scenarios, whose channel models are usually based on Rayleigh distributions.

Considering the new challenging applications for cellular networks, such as smart grid communications, our hypothesis is that GFDM is capable of outperforming OFDM under a diversity of scenarios.

Impact: If GFDM outperforms OFDM in terms of physical layer performance metrics, like peak-to-average power ratio (PAPR), then critical applications might be feasible to be supported by wireless communications. Therefore, we expect this to have a positive impact on the deployment of cellular networks for substation communications.

Novelty: Although many studies have been carried out on generalized waveforms, none of them have demonstrated that GFDM outperforms OFDM when the receiver is based on a minimum mean squared error (MMSE) decoder operating on non-line-of-sight (NLOS).

RQ3 *Is it possible to improve the performance of current cellular technology through machine learning techniques to better serve smart grid communications, specifically in supporting critical applications?*

The current 5G standard (3GPP Rel. 15/16/17) considers a specific machine learning technique in improving subnet orchestration in the core network. However, there are no machine learning applications in the radio interface or radio access network defined by the standard yet. Only at the beginning of the year 2022 a study item was initiated with the aim of evaluating the impact of machine learning on three representative use cases, namely beam management, channel state information (CSI) prediction, and enhanced positioning. This study is part of the ongoing standardization meetings related to 3GPP Rel. 18, which should be frozen in the first quarter of 2024.

In the specific case of smart grid communications operating in cellular networks, there are many critical applications that rely simultaneously on three classes or RAN slices, namely ultra-reliable low-latency communication (URLLC), massive

machine-type communication (mMTC), and enhanced mobile broadband (eMBB). These RAN slices carry a diversity of messages, some of them related to critical applications. As these slices share the same radio resources, machine learning techniques can be used to effectively solve the radio resource management as is done in similar problems in other domains.

Hypothesis: In the context of smart grid communication, our hypothesis is that DRL, which is a class of machine learning techniques, is effective to solve radio resource allocation for smart grid communication, as well as other types of applications.

Impact: machine learning can solve (in operational time) optimization/allocation problems in RAN slicing scenarios using DRL, providing better performance than traditional *computationally expensive distributed optimization*. The solution is flexible and adaptable compared with deterministic optimization.

Novelty: The machine learning approach to solve resource allocation of RAN slicing is novel and flexible to be used in different verticals including smart grid communications supporting critical applications, for which a suitable solution has not been found so far.

In summary, the scientific contributions of this work refer to the improvement of the operational strategies and methods to efficiently use wireless communication to support smart grid communications.

1.2 Outline of the doctoral dissertation

This doctoral dissertation is structured as a report of a collection of papers, introducing the main concepts that constitute the core of this study, providing the necessary background information, and summarizing the overall contributions of the publications developed throughout this doctoral study. Thus, the structure of this dissertation is as follows:

Chapter 1 presents the background of the research, terminology, methodology, research questions, and objectives of the dissertation. In addition, each research question is explained, placing special emphasis on the description of hypotheses, impacts, and novelty.

Chapter 2 provides some background information to facilitate a better understanding of the critical contributions explained in the next chapter.

Chapter 3 outlines the main contributions of **Publications I–V**. These contributions are mapped into some building elements that are part of the proposed RAN slicing framework.

Chapter 4 focuses on the main outcomes of this dissertation; a generic framework is proposed to support verticals. Finally, the main conclusions are highlighted and discussed.

2 Background information

The more original a discovery, the more obvious it seems afterwards.

— ARTHUR KOESTLER

In this chapter, background information of relevant topics is provided to enhance the explanation of the critical contributions of this study. Essential information of smart grids with the focus on substation automation systems (SASs) is presented in Section 2.1. Complementing the overview of smart grids, Section 2.2 includes highlights of communication technologies supporting smart grids. Section 2.3 focuses exclusively on a brief literature review of wireless communication technologies supporting IEC 61850. Complementing the previous section, a brief definition and features of the IEC 61850 protocol is included in Section 2.4. Section 2.5 introduces relevant technologies that are considered in the 5G standard supporting smart grids. To get a better understanding of network slicing, a short list of features is considered in Section 2.6. Complementing the previous information, a high-level description of waveforms beyond 5G is provided in Section 2.7 with the emphasis on GFDM. To finalize the background information, relevant concepts of machine learning and its application in cellular networks are addressed in Section 2.8.

2.1 Smart grid

A smart grid is an electrical grid that includes an advanced metering infrastructure, smart distribution boards and circuit breakers, renewable energy sources, energy-efficient resources, distribution of surplus electricity, and sufficient utility-scale broadband connectivity [3, 4, 5]. Smart grids are characterized by electronic power conditioning and control of the production and distribution of electricity [4].

In smart grids, substations play an essential role: they represent nodes connecting cables to power sources and power lines to distribute and transmit electricity. For instance, extra high voltage (EHV) lines are connected through transmission substations, which control the conversion of EHV into high voltage (HV) by using transformers and deliver a variety of voltage levels to distribution substations.

Specifically, the SAS aims to replace operators by performing automatic functions to guarantee safe and reliable service of electric power distribution and transmission. The typical SAS functions include data acquisition, control, protection, monitoring, and remote access communications.

Nowadays, in the context of the SAS, protective relays are intelligent electronic devices (IEDs), which are microprocessor-based electronic devices with a dedicated com-

mon communication interface. In practice, IEDs exchange information that can be saved locally or remotely for detailed log registration and processing. This information enables utilities to employ asset management programs (life extension, advanced planning, and predictive maintenance) and enhance reliability. It is important to remark that one important enabler of every SAS is a reliable and low-latency communication network.

The size of an SAS is usually larger in the EHV transmission substations than in the HV distribution substations. However, both share similar functionalities. For instance, the sensors measure very high voltage and current quantities, and the IEDs or protection relays perform the logical protection. These devices sense electrical voltage and current quantities to calculate measurement values that are monitored by the protection algorithm. For example, when a parameter exceeds a threshold or a setting value, the protection algorithm reacts according to a logical sequence. In such cases, a trip signal is usually sent to the associated circuit breaker to disconnect a bus or a line in the occurrence of a fault. For further detail on the SAS, see [6].

As the SAS supports a variety of functionalities, it is important to define a network architecture occupying a specific geographic area. A generic architecture can be based on the following three levels:

- **Station level:** At this level, the main target is to incorporate monitoring, supervision, and related operations. It is usually located in a shielded room to provide a high-level overview of the whole station. The main functionalities are installed in computers that have access to corporate data through a wide area network (WAN). At this level, human machine interfaces (HMIs) are used to monitor and send commands to the substation equipment and devices.

- **Bay level:** At this level, control and protection devices are scaled to perform specific functions. The devices are IEDs and protective relays, which are connected to local area network devices, such as Ethernet nodes. Here, the devices are able to perform power control and protection functions autonomously to receive data from the station level, as well as to handle faults at the process level. Many bays can be deployed in one substation; for this purpose, there is cooperation between devices located in adjacent bays or other substations.

- **Process level:** This is the level at which the EHV and HV power equipment (busbars and transformers) are installed and connected. This level also includes the connection of buses, lines, feeders, instrumentation, and transformers.

Further details of the three levels are given in [7]. The structure of an SAS representing the station, bay, and process levels is illustrated in Fig. 2.1.

In early substation automation systems, hardwired cables were used to connect power process types of equipment (e.g., instrument transformers and circuit breakers) with devices (e.g., protective relays and remote terminal units). Nowadays, modern communication

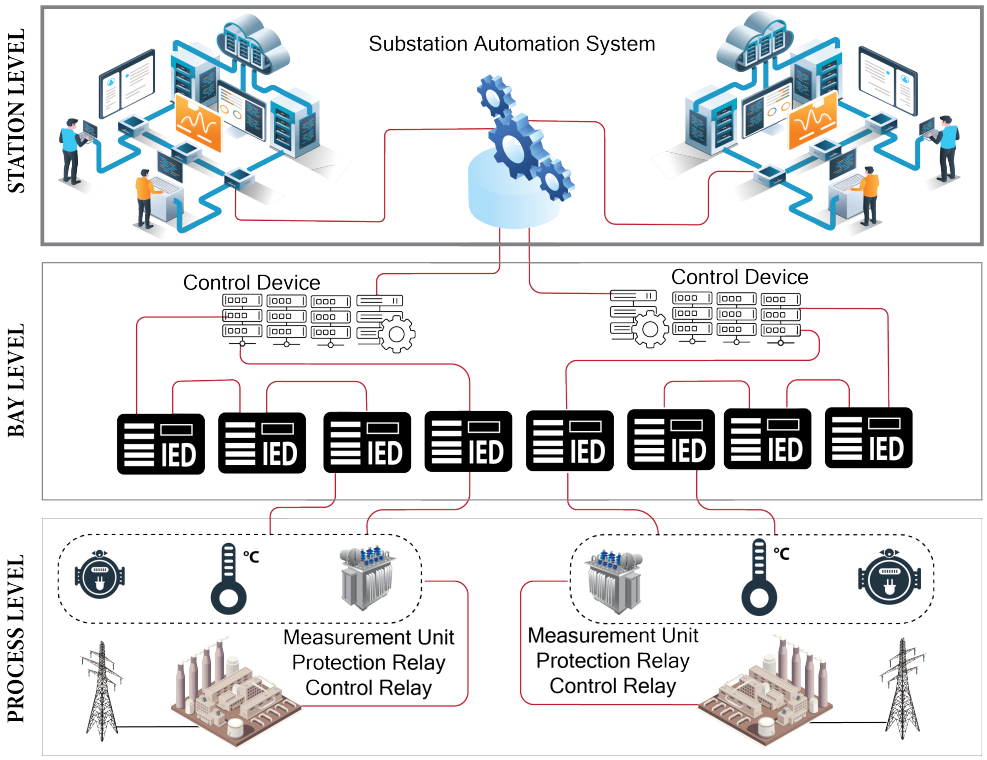

Figure 2.1: Structure of a substation automation system representing station, bay, and process levels.

technology enables the replacement of hardwired connections by using Ethernet ports. Thus, the transmission of physical parameters takes place via network message frames using specialized communication protocols to encapsulate and deliver these parameters. The use of Ethernet in the transport layer allowed the development and implementation of network application protocols in industrial control facilities. These protocols enabled substation manufacturers to integrate several functions into a single or several IEDs.

Many proprietary protocols have been developed to support and enable connectivity in SASs. These protocols are required to maintain data interoperability when a substation project involves multiple protocols, devices, and equipment from a diversity of suppliers. For instance, since 1986, the Electric Power Research Institute (EPRI) identified the issue of diverse protocols in substation installations without a common standard. Consequently, the EPRI released the protocol utility communication architecture (UCA) 1.0 at the end of 1991. The release of the UCA specified the use of the manufacturing message specification (MMS) and the integrated utility communication (IUC). Therefore, the EPRI organized a forum with Northern States Power Company (NSP) to discuss the implementation of the MMS across multiple communication platforms. UCA 2.0 was released in

1999 as a substation implementation document. It was published as the 1550 technical report (TR) of the Institute of Electrical and Electronics Engineers (IEEE). This TR was used as a foundation for the standard IEC 61850, which is the benchmark considered in this dissertation. Details of the evolution of this protocol are given in [8].

2.2 Communication technologies supporting smart grids

Ideally, a smart grid should have high-quality communication networks compared with the traditional power grid in terms of latency, reliability, and synchronization. To achieve this target, two fundamental milestones should be accomplished:

- Two-way communication capabilities between customers and utilities.
- Control and real-time monitoring of most of the power grid devices.

An improved two-way communication network is applied to control new renewable energy sources besides energy storage units. Moreover, an enhanced monitoring and control system can provide relevant information to prevent system failures or blackouts. Both fundamental features are mandatory, considering the complexity of the smart grid. Thus, to better understand the role of ICT in smart grids, a generic framework is defined.

The target of this framework is to provide a generic and clear overview of the entire communication network used on the smart grid. It also facilitates analysis of the integration between physical smart grid components. This framework reveals the information flow between smart grid entities, such as utilities, customers, and power stations. Moreover, it enables researchers and developers to propose and implement special features.

Another advantage of defining this ICT framework is that it facilitates the definition of requirements for technologies and equipment used in the implementation of applications. These requirements are fundamental inputs to be enabled by the wireless communication technologies studied and evaluated in this research work.

Moreover, with detachable microgrids [1] and renewable energy sources, which are difficult to control and predict, optimal control of the power grid is extremely hard and expensive to implement with only the information and computing resources from utilities. In this respect, the generic ICT framework would be the catalyst to highlight such problems. This is essential information for grid planners to add extra tools, such as cloud computing, machine learning applications, and data analytics.

[1] A microgrid is a small-scale electricity network connecting consumers to an electricity supply. A microgrid may have a number of connected distributed energy resources.

Generic ICT framework

This ICT framework, originally proposed in [9], aims to enable relevant inputs to system-level designers to address requirements in terms of efficiency and reliability of the smart grid. To make the illustration clearer, the generic ICT framework is described using demand response as the main use case. This ICT framework considers three types of networks:

- Local-area networks used to enable connectivity with households;
- Private networks, to provide connectivity to utilities and service providers;
- Internet, provided by a third-party Internet service provider (ISP).

The two-way communication is possible because of the convergence of these three types of networks. This ICT framework is systematized into four entities: internal data collectors (i.e., customers and grid monitoring sensors), a service provider or a utility company, power generators, and external information sources. These entities are illustrated in Fig. 2.2, where an overview of the proposed ICT framework is shown.
Between all elements of the ICT framework, the smart grid is directly related to the service provider, internal data collectors, and power generators. Likewise, external information sources provide insightful information to the smart grid operations.

Communication networks and technologies

Nowadays, communication in the smart grid is achieved through the convergence of private and public networks. Utilities maintain and deploy private networks. Public networks, such as cellular connections and the Internet, are offered by third-party service providers.

The wide-area measurement systems (WAMs) transmit monitoring data as phasor measurement unit (PMU) data by using private networks. The reasons for deploying private networks are security, reliability, and cost.

In the smart grid, the communication networks consist of home area networks (HANs), neighborhood-area networkss (NANs), and WAN. For example, in the case of advanced metering infrastructures (AMIs), an HAN is established within a household, linking a smart meter and smart appliances with actuators and sensors. Smart meters upload metering using the data aggregate units (DAPs), and the metering data management system (MDMS) provides storage, management, and processing of meter data.

Some other wireless technologies used in smart grids have been widely employed in HANs and NANs to cover the last-mile communication systems. HAN and NANs are considered in the smart grid because of their flexibility in deployment and environmental adaptiveness, especially in extreme situations. Numerous works have studied the HAN as

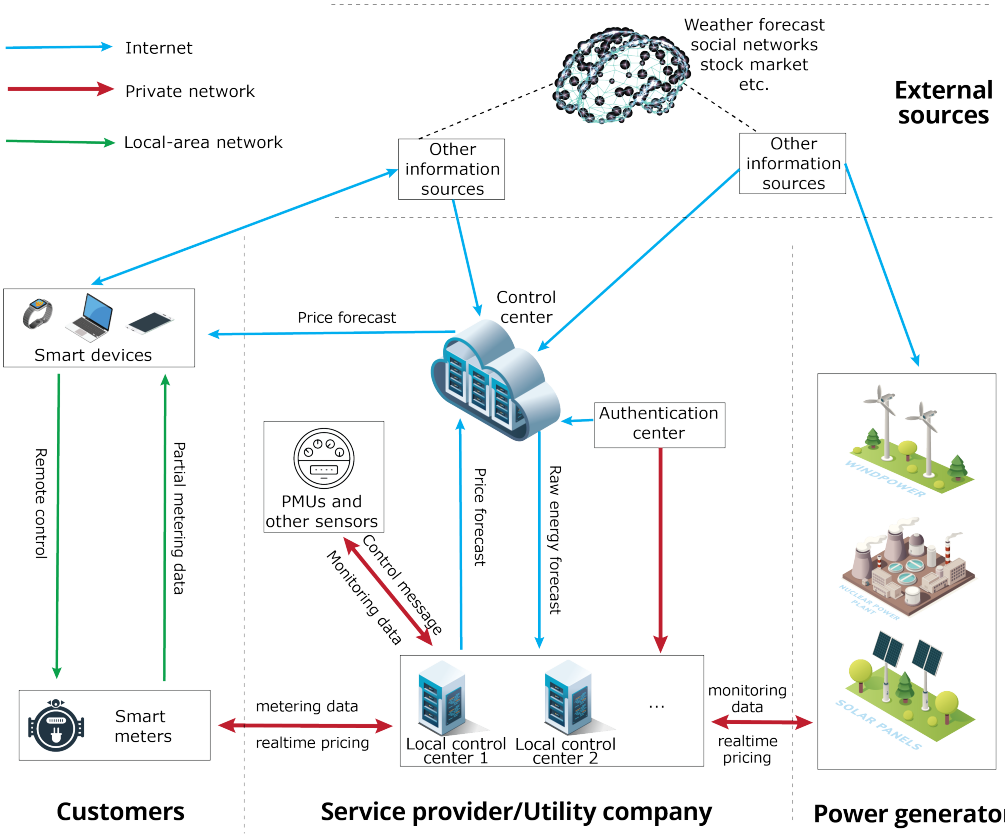

Figure 2.2: Generic ICT framework to support the smart grid connecting external sources, customers, service providers, utility companies, and power generators.

a network with a small coverage area and a low rate of data transmission, including a single smart meter as the collector and several smart appliances. Both wireless and wire-line technologies can be applied to HANs. The wireless transmission technologies include Wi-Fi, Bluetooth, ZigBee, and Z-Wave.

2.3 Wireless communication supporting IEC 61850

The promising standard IEC 61850 brings new features to SASs, and these features can be considered also in other micro grid scenarios. The standard provides fault event recording, flexibility of measurements, protection and control functionalities, supervision, and other interconnected functions within substations. The standard IEC 61850 enables interoperability among IEDs, protection relays, and equipment manufactured by different vendors in the substation automation market.

By default, the standard IEC 61850 is deployed on wired Ethernet networks because it supports critical applications with very strict requirements on latency and reliability in

the communication networks.

From the viewpoint of networking, the standard IEC 61850 is an application protocol that defines specific requirements for the lower open systems interconnection (OSI) layers. In the link-level layer, the User Datagram Protocol (UDP) and the Transmission Control Protocol (TCP) support the standard IEC 61850. As stated above, in the MAC and PHY layers, the popular networking technology is Ethernet, which is usually used in wired networks.

If a communication designer aims to switch from a wired to a wireless technology, it is important to use the requirements defined by the standard as a reference and evaluate them for the candidate communication technologies [10]. In the case of wireless technologies, there are a diversity of studies on evolving 4G and 5G networks. In most of these cases, the analysis is limited to noncritical messages and test scenarios with very ideal test bed scenarios. To provide an overview of the most relevant studies of IEC 61850 on wireless systems, the current state of the art is summarized in the following paragraphs.

For instance, [11] evaluated a wireless Local Area Network (WLAN) technology in a power distribution substation that interchanges information by using IEC 61850 messages. The study is based on the measurement of noise interference at 27.6 and 13.8 kV distribution substations, including circuit breaker switching operations. A high-level evaluation of the application performance was carried out for smart distribution substation monitoring, protection, and control setup. The results of this study indicated that IEC 61850 generic object oriented substation event (GOOSE) messages supporting a protection and control setup achieved a delay of 3.5 ms when the IEDs were separated by a distance of 45 m.

In [12], Gaouda et al. performed an experimental validation of a merging unit (MU) that transmits data measurements using the standard IEC 61850. A supervisory control and data acquisition (SCADA) system and the MU were communicated over Ethernet and a WiFi operating at 5 GHz. Thus, the capability of the MU to acquire real-time sampling was evaluated when the wireless network was used as media transmission. The laboratory experiment indicated that the wavelet-based digital signal processing (DSP) technique in the MU as a smart tool can monitor, control, and protect the power grid using the standard IEC 61850 over wireless networks.

An optimization framework was proposed in [13] to deploy a distributed algorithm using a local wireless network and a quasi-distributed approach on a wide-area Internet-based cloud. Here, the IEC 61850 interoperability protocol was adopted to achieve a certain delay performance. To perform the evaluation, a hardware-based prototype IED was developed using embedded systems. The experimental results indicated that the proposed framework meets the communication requirements.

A diversity of information models for vehicle to infrastructure (V2I) and vehicle to grid

(V2G) communication based on the standard IEC 61850 were proposed in [13]. The authors performed an end-to-end delay evaluation of the proposed communication network over different vehicular ad-hoc networks. The evaluation of the results carried out by simulation using the Riverbed modeler indicated that a lower overhead on different routing protocols enabled IEC 61850 messages to meet the delay requirements.

In [14], Hussain et al. proposed a backup protection scheme using a wireless communication channel operating in an unlicensed radio spectrum. Following some specific constraints, a radio cognitive network was considered to support the transportation of IEC 61850 messages. With a relative comparison, the proposed scheme will cut the costs of building backup protection systems in a substation. The reliability and time delay analysis performed in the study indicated an acceptable performance when healthy and fault conditions were evaluated.

An anti-islanding protection method called Loss of Mains was proposed in [15]. The application standard was based on the IEC 61850 MMS protocol over a global system for mobile communications (GSM) cellular network. The proposed methodology enables some advanced approaches employing a wide variety of information available in the smart grid. A lightweight IED was implemented using low-cost embedded systems and open-source libraries. The performance measurement on a wireless network indicated that the MMS message was transmitted with the expected reliability and latency defined in the standard IEC 61850.

Moreover, a study reported in [16] proposed the implementation of coordinated operation between a microgrid controller and a distributed energy resource (DER) using the standard IEC 61850 over a wireless network. Here, the reactive power management system was implemented using the standard IEC 61850 in the application layer and long-term evolution (LTE) in the transport layer. An LTE simulator was used considering a proper mapping between the LTE stack and the standard IEC 61850. In the simulation, specific QoS class identifier (QCI) classes were considered to prioritize the IEC 61850 messages (GOOSE, sampled value (SV), and MMS). The end-to-end delay estimated by a network simulator indicated that the wireless network using LTE brought extra advantages when compared with other technologies, such as WiFi and worldwide interoperability for microwave access (WiMAX).

An inclusive survey was conducted in [17] on time synchronization, which plays a key role in industrial Internet of Things (IoT) applications. The benchmark is based on IEEE 1588 precision time protocol (PTP), which was complemented with advanced features to improve the internal clock stability, transmission delay, processing delay, and PTP transported in wireless communications to support the standard IEC 61850 and another advanced application protocols. It was concluded that the clock synchronization protocol is still an open issue considering the necessity for an efficient symbol timing synchronization mechanism that allows exact timestamp message recognition and decryption.

The impact of communication on the performance of a microgrid was discussed in [18]. The approach was based on the definition of requirements for the network based on the response of three levels (primary, secondary, and tertiary) of a hierarchical control approach. This contribution identified standards, networking protocols, and communication technologies in which the cellular network and the standard IEC 61850 were extensively analyzed. After an analysis of the influence of wired and wireless connectivity on the microgrid performance, it was concluded that in the particular case of current cellular technologies, more robust schemes are required to reduce communication degradation when compared with wired communication. According to the study, further aspects, such as security, resilience, and interoperability, will require continued efforts in research and practical applications.

The feasibility of the implementation of IEC 61850 services in a public LTE infrastructure was evaluated in [19]. The authors provided a detailed description of the protocol stack defined by the 3GPP standard and concluded that a regular LTE cannot meet the stringent latency requirements of such services. Thus, they introduced a new LTE quality of service (QoS) class and a new LTE scheduler to prioritize and automate the traffic with respect to regular cellular users, such as human-centric traffic. The IEC 61850 messages that are part of the evaluation are MMS and GOOSE. The results are evaluated through a system simulator platform based on the achievable latency and throughput metrics. The authors concluded that a proper LTE scheduler is a strong requirement to meet the performance requirements of the standard IEC 61850.

An integration framework to enable the transmission of the IEC 61850 MMS in a wireless network operating in remote areas was proposed by Dehalwar et al. in [20]. The contribution is based on the integration of a cognitive radio based on IEEE 802.22 [2] and the standard IEC 61850. Considering that the superframe structure of IEEE 802.22 is capable of sending data on uplink, Dehalwar et al. analyzed the specifications and requirements of the standard IEC 61850. Based on the analysis, it was concluded that the performance classes of the standard IEC 61850 can use the MMS for transmitting synchrophasors and teleprotection over IEEE 802.22. Thus, the integration of the standards IEC 61850 and IEEE 802.22 can provide better communication facilities in a smart grid.

In a master's thesis [21], the performance of a private LTE network was evaluated to examine the readiness and applicability of the standard IEC 61850. The target of this work was to investigate the performance of phasor communication over a cellular network to evaluate metrics such as reliability, availability, throughput, and latency. The results indicated that the nonpublic LTE supporting the IEC 61850 stack is suitable only for noncritical applications. This is due to the fact that the latency and reliability obtained in the study were, on average, 45 ms and 99.7 %, respectively. According to the study, the worst performance was visible in periods of the day in which the network is being used

[2] It is a long-distance wireless specification for a Wireless Regional Area Network (WRAN) that can support long-distance wireless communication for low-latency, high-volume, reliable, and secure communication.

by other applications, such as web browsing, messaging, and other full buffer traffic.

The performance of the standard IEC 61850 over a WLAN for various smart distribution substation applications was investigated in a doctoral dissertation [22]. The initial objective was to measure the noise level of a variety of substations. The noise was modeled because of the PDF to simulate the substation environment employing OPNET. [3] Further, a hardware prototype was developed to enable the application of the standard IEC 61850 on WLAN. The results indicated that the average delay of IEC 61850 messages were in compliance with scenarios with high SINR values. The latency indicated the worst performance when the distance of the devices was extended to further 100 m. Finally, the test bed results and the simulation results were compared to highlight the accuracy of the simulation model considered in OPNET.

2.4 Definition and features of the IEC 61850 protocol

A technical committee released the first edition of the standard IEC 61850 around 2003 with core parts including TR, technical specifications (TS), and international standards (IS).

The first four parts cover definitions, general requirements, and system and project management. The fifth part addresses communication requirements for devices and function models. The sixth part provides some examples to illustrate the description languages, such as the substation configuration language (SCL) and the IED capability description with extensible markup language (XML)-based files. In the seventh part, the basic communication structures, abstract communication service, data classes, and logical nodes are explained. It also includes the mapping of the MMS communication service to the International Organization for Standardization (ISO)/IEC layer interface, i.e., ISO/IEC 8802-3 (Ethernet). In the ninth part, the standard emphasizes the SV mapping to a serial unidirectional multidrop point-to-point link and ISO/IEC 8802-3.

In 2012, the second edition of IEC 61850, entitled Communication Networks and Systems for Power Utility Automation, was released. In 2016, the standard added a new release that focused particularly on a time synchronization mechanism with a precision time protocol profile. In this edition, many parts were updated with an extension to other power system applications, including, e.g., communication between substations and network control centers, DER, and recommendations for redundant architectures. In the second release of this edition, communication redundancy recommendations were defined for the GOOSE and SV messages services. As indicated in [23], in this new release, the standard recommends the high-availability seamless redundancy (HSR) and the parallel redundancy protocol (PRP) as redundancy with a zero recovery time.

In relation to the SAS scenarios, the standard aims to enable interoperability among de-

[3] A popular industry-trusted communication networking simulator tool

vices. It also aims to integrate subsystems to build an overall SAS system.

The standard IEC 61850 is enabled by several devices that have certain features, such as data models with a logical node (LN) and common data classes (CDC); reporting of GOOSE and SV messages; support of XML based on IED capability description files; interoperable control, measurement, monitoring, and protection functions; substation devices that can be configured through the SCL language; and communication service interfaces.

The IED as a physical device has an interface linked to the communication network, and it has at least one network address. The standard incorporates one or more logical devices, enabling a single physical device to act as a gateway for multiple devices.

Messages and requirements of the standard IEC 61850

The IEC 61850 communication services exist in horizontal and vertical schemes. The transmission of messages in a vertical communication scheme is usually carried out between database archives, operation, and engineering at the station level and IEDs at the bay level. The horizontal communication scheme is usually found within substations, and it is carried out between IEDs.

The typical data transmitted from the process level to protection and control IEDs at the bay level are related to power values, such as voltage, current, and frequency. The standard IEC 61850 enables IEDs to behave according to specific rules from the network perspective through the definition of the abstract communication service interface (ACSI) models, detailed in [24].

The ACSI is an independent network interface that defines the semantics of service models emphasizing their attributes and identifying what these services provide. This abstraction is necessary to separate the SAS data models from the communication technology. In other words, ACSI provides compatibility with SAS devices with the latest communication technologies. This mapping is carried out through the specific communication service mapping (SCSM) that defines message encoding and syntax, such as GOOSE message transmission and peer-to-peer services for SV messages.

The standard IEC 61850 considers a multicast transmission of specific messages using the communication scheme of a publisher/subscriber without acknowledgment, such as GOOSE and SV. It also considers the connection-oriented association using client/server networking to transport the MMS, which is transmitted over a transmission control protocol/Internet protocol (TCP/IP). As many applications in SASs require real-time and low-latency performance, the Ethernet frames are encapsulated directly without overhead data of the middle layers. Important to consider from the communication point of view is the mapping of IEC 61850 messages as illustrated in Fig. 2.3.

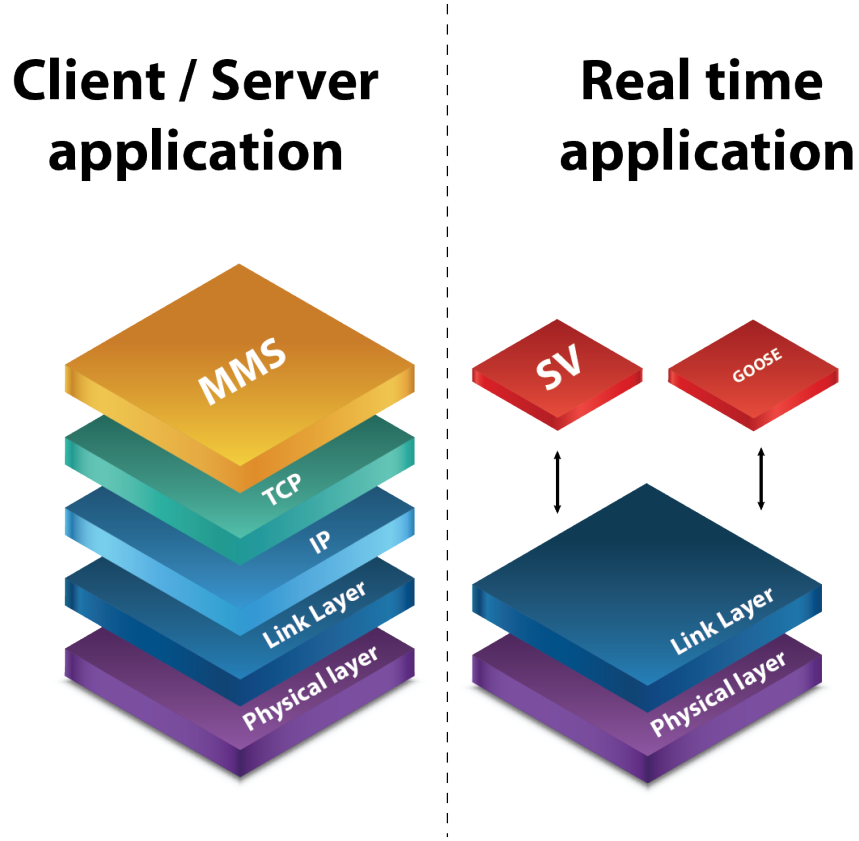

Figure 2.3: Communication services: direct mapping of real-time messages to the Ethernet layers.

- **Manufacturing message specification (MMS) specifications:** It is a public protocol that has a proven implementation track report in the field of process control. The standard IEC 61850 uses the MMS because it has a rich library of objects and services. The standard maps objects into MMS objects, and it easily supports naming and service models.

  For client/service mapping of the MMS protocol, the standard specifies the SCSM, which has a full TCP/IP stack above the Ethernet layer.

  The MMS is used to transmit noncritical data services embedded in reliable application (upper layer) protocols. The MMS is suitable for communication between station-level workstations and bay-level IEDs for many purposes, such as reporting, status polling, and sending commands.

  Inside the substation, many applications use MMS services, e.g., HMI, SCADA, and IEDs configuration.

- **Generic substation events (GSE):** These events are used to transmit information

between control and protection applications. The standard IEC 61850 defines this message in [25] as a peer-to-peer communication to transfer defined data objects when their attributes change.

GSE has two types of message services: GOOSE and the generic substation status event (GSSE), the latter being the backward compatibility for UCA GOOSE. The GOOSE carries long datasets, whereas the GSSE carries binary data that represent state changes. Both enable information exchange between the input data values of one IED and other IEDs by multicast communication.

In general, any IED can play a role of a publisher and a subscriber. GOOSE and GSSE messages are used to compute data for internal use, such as local interlocking condition processing comparing received switch positions.

For time-critical applications, GOOSE requires a real-time performance class. This low-latency communication requirement enforces directly embedding of a GOOSE dataset into an Ethernet frame, instead of using TCP or UDP as a transport layer.

At the substation bay level, IEDs exchange input and output statuses via multicast-GOOSE messages.

- **Measured sampled value (SV)**: The standard enables transmission of sampled values of current, voltage, and frequency, as well as other process values. This is possible because some communication interfaces are defined to include digital communications, such as the process switchgear with integrated electronics, and nonconventional current and voltage transformers with a digital communication interface.

  The transmission of SV messages is sensitive to transmission delays, as defined in [24]. For this reason, to avoid processing delay in the middle layers, the standard maps SV messages directly into the Ethernet layer. The information that is transmitted in the SV contains measured values, which are sampled and digitized by specialized sensors in the MU. These measurements are encapsulated into Ethernet frames by using a specialized mapping defined in [25, 24].

2.5 5G standards supporting smart grids

The 3GPP is the main standardization organization that defines the specifications shaping the technology that is developed by the communication industry. It relies on the participation of the main players in the wireless communication industry.

Compared with 4G, which was mostly focused on supporting human-to-human communication, one of the major drivers of 5G is to support industrial applications. Aligned with this target, the Radiocommunication Sector of the International Telecommunication Union (ITU-R) issued the International Mobile Telecommunications-2020 standard (IMT-2020) to set specific requirements and use cases to be considered in 5G. To achieve these targets, the 3GPP started to specify 5G since 3GPP Rel. 15 and its evolution named 5G-advanced since 3GPP Rel. 18. A brief description of the main features that are being

specified with a high impact on smart grid applications is given in the following.

Since 3GPP Rel. 15, the standard started to define the specifications of 5G. However, only after this release, fundamental features that are required by IEC 61850 messages were determined. For instance, in 3GPP Rel. 16 the URLLC, time-sensitive networking, private networks, and NR unlicensed spectrum were specified [26].

In 3GPP Rel. 17, new improvements were specified, such as a neutral host for private network enhancements, RedCap or new radio (NR)-light for industrial IoT, and network automation [27, 28, 29].

In 3GPP Rel. 18, a study on 5G smart energy and infrastructure is being completed, and the energy vertical is discussed in a technical report related to cyber-physical control applications. Other key features are developed in this release, such as RedCap, timing resiliency, and time synchronization [30].

It is important to remark that in the current 3GPP rel. 18 (5G Advanced), the target is to study and define the first use cases using artificial intelligence (AI)/machine learning (ML) at the radio access level. These studies will define the main foundations of the application of artificial intelligence to the upcoming 3GPP releases that will shape the 6G [31].

2.6 Network slicing

Network slicing provides a network-as-a-service model with unique allocation flexibility of resources based on dynamic demands. The slice-based 5G network has significant features to support the smart grid. These features are described in the following.

- **Service isolation:** Network resources of one service can be isolated from others without affecting each other. In addition, the security and reliability of each slice can be improved.
- **Tenant-oriented virtual network:** A network slice supports slice tenants to operate their own dedicated networks. The tenant could be an individual customer or a vertical industry company that rents and occupies network slice instances from network slice providers.
- **Guaranteed SLA:** Service assurance of supporting QoS expectations, which is driving end-users to negotiate a specific SLA.
- **Customization capabilities:** The 5G slicing architecture enables implementation of customized end-to-end networks according to the service requirements.
- **Mobile edge computing:** Edge computing moves network resources that are typically implemented in the cloud to closer/edge virtualized networks to enable a low end-to-end (E2E) delay access network.

- **Distributed architecture:** Distributed information processing and storage architecture is ideally suited for services requiring low latency and localized decision-making.

The stakeholders that are beneficiaries in the network slicing ecosystems are the network slice subnet instance (NSSI) provider, the intermediate-network slice instance (NSI) provider, the end-to-end network slice instance (E2E-NSI) provider, the network slice tenant, and the end customer.

This ecosystem enables new business use cases that have direct benefits for power system utilities and also for operators with a specialized value chain. This value chain has a direct dependence on the power system utilities, which are related to power system actors between generation, transmission, distribution, and prosumers.

The opportunities of this new business model will change the way in which utilities deploy the communication infrastructure, being in most of cases private networks using a variety of communication technologies that support individual use cases without any possibility to integrate them into a unified network. With network slicing, smart grid utilities can meet special requirements and also create additional business benefits through new cost savings and use cases.

The service business model forces operators to move beyond a fixed rental fee per device. Therefore, part of the charge cost should be defined based on the performance-based SLAs and KPIs, which could also be complemented by the added value on each power system utility requirement.

2.7 Waveforms beyond 5G: GFDM

Spectrum is a very important and expensive resource to operators, and therefore, it must be used as efficiently as possible to deliver increased system and user throughput. One obvious approach to increase the efficiency of using spectrum is to increase the bandwidth, which implies that not only the traditional licensed spectrum is used, but also unlicensed spectrum sharing is deployed [32]. Besides that, in the last few years, a new wave of research has focused on investigating the millimeter and terahertz wave spectrum [33, 34].

Another fundamental element used in wireless communication with a high impact on the efficient usage of spectrum is the waveform design. Here, the use of orthogonal multiple access techniques before 4G mostly relied on frequency division multiple access (FDMA), time division multiple access (TDMA), and code division multiple access (CDMA). However, to support the exponential system capacity and data rate in 4G, the LTE cellular system used OFDM to enable the use of orthogonal frequency-division multiple access (OFDMA), which provides the capability to assign different subcarriers to different users and enables a finite number of orthogonal resources. However, OFDM has certain disadvantages; for instance, using cyclic prefix (CP) overhead usually results

in a loss of spectral efficiency, sensitivity to frequency and timing offsets, high out-of-band emission, and high PAPR. Eventually, these drawbacks cause signal distortion and high energy consumption.

For 5G NR, the standard selected the OFDM-based waveform because it satisfies the requirements and properties such as simple channel estimation and low complexity equalization. However, new alternatives in the waveform design, such as filtered OFDM, windowed OFDM, and universal filtered OFDM, have been proposed to reduce the out-of-band (OOB) emission.

Future mobile systems, such as 6G, will be characterized by a wide variety of different use cases. It implies that flexible time–frequency allocation becomes necessary. In this respect, the other group of waveforms, consisting of filterbank multicarrier (FBMC) [35] and GFDM [36], completely discards the orthogonality to achieve better spectral and temporal characteristics.

To achieve ultra-low OOB emission, FBMC uses linear filtering and relies on the soft transition of its filter tail to combat multipath fading because it does not use a CP [35, 37]. In the case of GFDM, it uses circular filtering to ensure a block-based waveform with no filter tails. Using a single CP protects multisymbol transmission to enhance temporal efficiency. In this work, the focus is on GFDM; however, the proposed framework addressed in the contributions of this dissertation is not limited to it.

GFDM uses circular shifted filters for pulse shaping and reduces out-of-block leakage and is based on an independent modulation block consisting of a number of subcarriers and subsymbols. The subcarriers are filtered with a prototype filter circularly shifted in time and frequency. It allows reducing the OOB emissions. However, the subcarrier filtering causes nonorthogonal subcarriers and increases intersymbol interference (ISI) and intercarrier interference (ICI). On the receiver side, an efficient scheme such as matched filter with iterative interference cancellation is used, and it achieves the same performance as OFDM systems. It is important to remark that OFDM and single carrier OFDM can be regarded as special cases of GFDM.

Discrete signal model of GFDM

The GFDM system setup under consideration is set to transmit a complex symbol block $d_{s,k}$ at the sth time instant and the kth subchannel containing $S \times K$ data symbols ($s = 0, \ldots, S-1$; $k = 0, \ldots, K-1$). Assuming that the data symbols are independent and statistically identical ($x[n]$), the GFDM signal is written as

$$x[n] = \sum_{s=0}^{S-1} \sum_{k=0}^{K-1} d_{s,k}\, g_{s,k}[n] \tag{2.1}$$

where $g_{s,k}[n]$ denotes the circular time-frequency-shifted version of the prototype filter $g[n]$. The filter $g[n]$ is usually a root raised cosine (RRC) defined by the roll-off factor that represents the rate at which the lobes of the function (or ripples) decrease. Basically, if the bandwidth of the function is B when the roll-off is 0, then it becomes 2B when the roll-off is 1.

The discrete prototype pulse shaping $g[n]$ is expressed as

$$g_{s,k}[n] \triangleq g[(n - sK)_N]\, e^{j2\pi nk/K}, \tag{2.2}$$

where $N = S \times K$, and $(.)_N$ denotes a modulo-N operator with a rectangular window. To simplify the circular convolution, the transmitter filter $g[n]$ is usually designed as being circular with a period of n mod N. It is also noteworthy that in (2.2) the GFDM shifting step is K in the time domain and $1/K$ in the frequency domain.

In the case of asynchronous subcarriers, the design should employ continuous discrete-time Fourier transform (DTFT) of the prototype pulse shaping. Under the assumption of perfect synchronization, the pulse shape can be carried out in the frequency domain so that only the first and last S samples of (2.2) have nonzero values to ensure that the ICI is limited to adjacent subcarriers [38].

Transmitter block

Let us first use (2.1) to rewrite the elements of the transmit symbol block in a single vector as: $\mathbf{d} = [\mathbf{d}_0^T, \ldots \mathbf{d}_{s-1}^T]^T$ and $\mathbf{d}_s = [\mathbf{d}_{s,0}, \ldots \mathbf{d}_{s,K-1}]^T$ with the variance σ_{d}^2, where the operator $[.]^T$ represents the vector transpose.

The vector form of $x[n]$ ($n = 0, \ldots, N-1$) can be formulated as

$$\mathbf{x} = \mathbf{A}\mathbf{d}, \tag{2.3}$$

where $\mathbf{x} = [x[0], \ldots x[N-1]]^T \in \mathbb{C}^{N\times 1}$ and $\mathbf{A} \in \mathbb{C}^{N\times N}$, which denotes the modulation matrix or the self-interference matrix of the GFDM system. This matrix can be defined as $\mathbf{A} = [\mathbf{G}_0, \ldots \mathbf{G}_{S-1}]$ so that $\mathbf{G}_s$ represents the $N \times K$ matrix of $g_{s,k}[n]$ coefficients, i.e.,

$$\mathbf{G}_s = \begin{bmatrix} g_{s,0}[0] & g_{s,1}[0] & \cdots & g_{s,K-1}[0] \\ g_{s,0}[1] & g_{s,1}[1] & \cdots & g_{s,K-1}[1] \\ \vdots & \vdots & \ddots & \vdots \\ g_{s,0}[N-1] & g_{s,1}[N-1] & \cdots & g_{s,K-1}[N-1] \end{bmatrix}. \tag{2.4}$$

A CP of the length N_{cp} is added to the GFDM signal $\mathbf{x}$ to prevent interblock interference over a frequency selective fading channel (FSFC). Then, the transmitted signal is given by $\mathbf{x}_{\mathrm{cp}} = [\mathbf{x}(N - N_{\mathrm{cp}} + 1 : N);\ \mathbf{x}]$.

Receiver block

Without loss of generality, we assume a circular symmetric complex (CSC) channel $\mathbf{h} = [h_1, h_2, \cdots, h_L]^T$, where h_r denotes the complex baseband channel coefficient of the rth path ($1 \leq r \leq L$). We also consider that $N_{\text{cp}} \geq L$, which means that the CP length must be higher than the delay spread of the multipath channel [39]. Additionally, the channel coefficients related to distinct paths are assumed uncorrelated. Then, the received signal has the length $N_{\text{t}} = N_{\text{cp}} + N + L - 1$, and it can be modeled as

$$\mathbf{y}_{cp} = \mathbf{h} * \mathbf{x}_{\text{cp}} + \boldsymbol{\nu}_{\text{cp}}, \tag{2.5}$$

where the symbol $*$ denotes linear convolution operation, and $\boldsymbol{\nu}_{\text{cp}}$ is the additive white Gaussian noise (AWGN) signal with the variance σ_ν^2, and it is also represented by a vector of the length N_{t}.
Before starting the decoding process, the CP introduced at the transmitter has to be removed. Here, the frequency-domain equalization (FDE) properties can be employed so that the linear convolution in (2.5) becomes a circular convolution. Thus, the resulting received vector after the CP removal can be expressed as

$$\mathbf{y} = \mathbf{H}_{\text{ch}}\boldsymbol{A}\mathbf{d} + \boldsymbol{\nu}, \tag{2.6}$$

where the vector $\boldsymbol{\nu}$ represents the AWGN signal of the length N with the variance σ_ν^2, and $\mathbf{H}_{\text{ch}} \in \mathbb{C}^{N\times N}$ is the circular Toeplitz matrix based on the vector $\mathbf{h}$, and can be written as [40]:

$$\mathbf{H}_{\text{ch}} = \begin{bmatrix} h_1 & 0 & \cdots & 0 & h_L & \cdots & h_2 \\ h_2 & h_1 & \cdots & 0 & 0 & \cdots & h_3 \\ \vdots & & \ddots & & & \cdots & \vdots \\ h_L & h_{L-1} & \cdots & \cdots & \cdots & \cdots & 0 \\ 0 & h_L & \cdots & \cdots & \cdots & \cdots & 0 \\ \vdots & & \ddots & & & \cdots & \vdots \\ 0 & 0 & & h_L & \cdots & \cdots & h_1 \end{bmatrix}. \tag{2.7}$$

The matrix $\mathbf{H}_{\text{ch}}$ has a very special pattern. Each row is a circular shift of the first row. To estimate the transmitted complex data symbols $\hat{\mathbf{d}}$, we consider a matrix $\mathbf{G}$ by using the following equation:

$$\hat{\mathbf{d}} = \mathbf{G}\,\mathbf{y}, \tag{2.8}$$

The design of the demodulation prototype filter $\mathbf{G}$ depends on the demodulator selection, such as zero-forcing (ZF) and MMSE. The main contribution of this doctoral dissertation focuses on scenarios in which the MMSE is considered on the receiver side.

2.8 Machine learning-aided cellular networks

Machine learning is a tool that was popularized by a diversity of data science applications in a huge universe of applications in many verticals, such as self-driving cars, robotics, and smart grids. In the last years, image recognition based on machine learning methods

was supporting many end-user applications for security and entertainment purposes. In wireless communication networks, the most popular application of machine learning is related to orchestration in the network layer. Here, the target is to enhance the resource scheduling of complex systems [41, 42], which has traditionally relied on empirical solutions.

There are three machine learning categories using neural networks:

- Supervised learning: When the learning of the neural network depends on ground truth labeling or labeling data. The main application of supervised learning is to make inferences.
- Unsupervised learning: In contrast to supervised learning, here, the main task is to cluster samples without the necessity to use labeled or ground truth data. The goals of unsupervised learning are mainly clustering and reducing dimensionality to compress the data.
- Reinforcement learning (RL): Here, the task is to learn through trial and error. In this type of task, no one labels data, and no user collects or explicitly designs the collection of data. In simple words, the goal in reinforcement learning (RL) is to act.

In RL, the computer program that takes decisions is referred to as an agent. Agents learn through trial and error: they try something, observe, learn, try something else, and so on [43]. The environment, in turn, is represented by a set of variables related to a specific problem. Then, the set of decisions that the agent can take is mapped in the state space. The subset of a state that the agent can observe is known as an observation. It is important to note that tasks that have a natural ending, are called episodic tasks. Finally, agents may take several time steps and episodes to learn and solve a task.

In recent years, the application of machine learning in wireless cellular networks has gained in popularity. For example, machine learning models can extract sequential and spatial features from time-varying received signal strength indication (RSSI) [44]. An auto-encoder can be used to reduce the overhead of CSI reporting from the user equipment (UE) to the next-generation NodeB (gNB), when a massive multiple-input multiple-output (MIMO) setup is used in the cellular network [45]. Other machine learning models can closely approximate universal and complex functions with similar performance but with a much lower model and computational complexity. In addition, DRL supports the implementation of a self-organizing network (SON) with self-optimization capabilities to achieve specific KPIs as spectral efficiency [46].

3 Contributions

Not everything that can be counted
counts, and not everything that counts
can be counted.

— ALBERT EINSTEIN

In this chapter, the fundamental contributions of this dissertation are summarized. The contributions are organized into the following subtopics that are mapped onto their respective publications:

- RAN slicing enabling the standard IEC 61850 is summarized in Section 3.1. Here, a framework is proposed to enable the IEC 61850 by using a cellular network. This section addresses the main discoveries made in **Publication I**.
- Modeling GFDM in wireless scenarios is summarized in Section 3.2. Here, the main discoveries related to the analytical model proposed for the GFDM system are based on the contributions of **Publication III** and **Publication V**.
- Finally, the interference mitigation in wireless scenarios with machine learning is summarized in Section 3.3. Here, **Publication II** and **Publication IV** are the sources of discoveries.

To highlight the value of each contribution to the current state of the art that defines the 5G-NR, the main architecture elements of the RAN are mapped with the main contributions of each **Publication I–V**. This mapping is illustrated in Fig. 3.1.
In all subtopics, the focus is on the research questions defined in the first, introductory chapter, and on providing answers to them.

3.1 RAN slicing enabling the standard IEC 61850

RAN slicing technology can deliver tailored radio resources to smart grid communication. In this context, this contribution first studied the network demand of messages defined in the IEC 61850 protocol. These messages were classified and mapped according to their latency, reliability, and service priority requirements.

To support this contribution, a novel RAN slicing framework was proposed in the upcoming cellular network domain to support smart grid communication. A wireless network, based on the proposed framework, was used to enable connectivity in a substation protection and control scenario to evaluate the system spectrum efficiency. This framework is intended to inspire new opportunities for communication and power system industries.

In the context of the dissertation, this section aims to answer research questions **RQ1** and **RQ3**.

RQ1 *What are the limitations (if any) of existing wireless technologies for current cellular networks to serve smart grid communications, especially for protection / substation operation?*

RQ3 *Is it possible to improve the current cellular technology through machine learning techniques in order to better serve smart grid communications, specifically in supporting critical applications?*

Recently, many smart grid applications have gained popularity as a result of the evolution of communication network technologies. Usually, these smart grid applications rely on wired communication. However, wireless connectivity is becoming popular, especially in noncritical applications. On the other hand, the wireless communication industry is evolving to support services that require high throughput, a high density of users, and low-latency connectivity. It is the case of 5G, which is a key enabler of the current cellular wireless connectivity around the world.

Among the critical novelties brought by 5G and beyond systems, RAN slicing emerges as an enabling platform for the efficient integration of smart grid connectivity solutions over a shared radio interface, as proposed by network slicing. Thus, RAN slicing is a complement of network slicing in the radio resource domain. It splits the radio resources into logically isolated radio networks, in which one slot can be interpreted as an RAN slice.

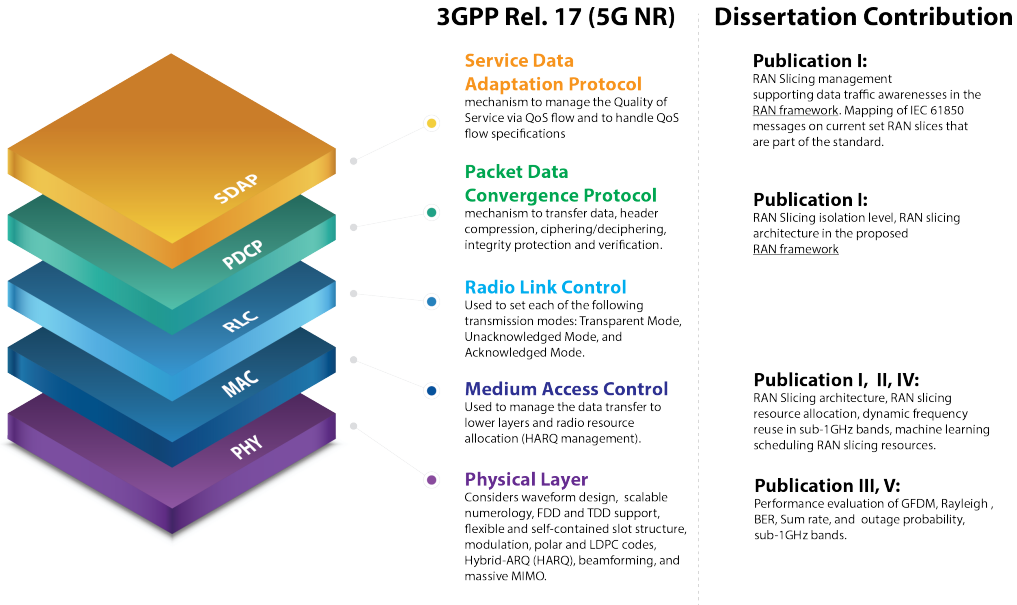

Figure 3.1: 5G New Radio protocol stack based on the current 3GPP Rel. 17 specification mapped with **Publications I–V**.

In clear contrast to previous mobile network generations, the 5G system-level design leverages cloud-native concepts to allow disaggregation and virtualization of network functions, which are well defined in TS 3GPP 23.501. For instance, network slicing constitutes a key enabler for integrating the segmented connectivity landscape of smart grid services over a common core and the RAN network. A slice-based network addresses efficiently the inherent smart grid service heterogeneity. It provides significant benefits, such as service isolation, a tenant-oriented virtual network, a guaranteed SLA, customization capabilities, mobile edge computing (MEC), and a distributed architecture.

The opportunities of this new business model are expected to change the way that utilities deploy communication infrastructure. In the most common scenario, such an infrastructure is comprised of private networks using a variety of communication technologies. For example, Ameren is a publicly traded utility providing energy services for approximately 2.4 million customers across 167,759 square kilometers in Illinois and Missouri [47]. Ameren used a private LTE network for AMI or AMI backhaul, substation backhaul, distribution and gas system sensors and controls, and monitoring and control of customer-owned distributed energy inverters. With this intention, Ameren strove to eliminate disparities in network solutions and standardize a single robust one for the field area network. Using a private LTE network, they aim to simplify the operation from over 15 network solutions to only two (LTE and mesh networks for metering) [47]. This example indicates the potential relevance of the 5G nonpublic networks (NPN) in the smart grid setting.

Nowadays, the service business model forces operators to move beyond subscription-based charges and fixed rental fees per device. As a result, part of the charging cost should be defined based on performance-based SLAs and KPIs, which could also be complemented by the value added on each power system utility requirement.

In the coming years, smart grid utilities will be able to address specialized requirements using a unique infrastructure based on network slicing premises. They will also have the chance to reap additional business benefits through cost savings and new use cases.

In the smart grid, wireless connectivity supports noncritical applications. However, these applications serve specific purposes with proprietary protocols and lower bandwidth, and are implemented in shared frequency bands. In addition, these wireless interfaces are not suitable for some of the new demands. For instance, in the case of distribution automation, an unlicensed 900 MHz mesh radio network is usually used between devices. Here, the data of these devices are aggregated using a backhaul in a separate licensed 900 MHz system [48]. As an alternative, this backhaul is replaced and extended by private LTE networks with very promising results [49]. These private LTE networks also assist users in the field, providing different QoS wireless services, such as voice and full buffer traffic. In remote areas, some LTE/WiFi gateways are used to provide a WiFi calling method using session initiation protocol (SIP)-trunking for smartphones. In some scenarios, such as the capacitor bank controller, a narrowband IoT (NB-IoT) 200KHz channel is considered [50]. Following the success of 4G private networks to support industrial markets, the

deployment of private 5G networks is expected to support critical verticals, such as the smart grid.

The target is to unify the above-mentioned radio access technologys (RATs) into a unique infrastructure. However, the proliferation of proprietary protocols, technologies operating in both licensed and unlicensed bands, and uncoordinated signal processing techniques disable the chance of a unique infrastructure. Therefore, 5G supports critical applications and also proposes network slicing to support different applications, such as eMBB, mMTC, and URLLC using end-to-end isolated networks in the same physical infrastructure. One important enabler of network slicing is RAN slicing [51], which is not yet specified by 3GPP. In this sense, the proposed framework aims to ease the integration of the standard IEC 61850, used as a communication protocol in smart grid applications, and RAN slicing. This integration provides important advantages over the current RATs used in the field in terms of local spectrum license, the overall cost of the system, easy reconfiguration, security, data-driven approach, control of essential infrastructure, and performance guarantees based on artificial intelligence / machine learning (AI/ML) techniques.

3.1.1 Categorization of 5G-enabled smart grid services

To better understand the impact of the proposed RAN slicing framework, it is important to point out that, in general, a smart grid has two parallel infrastructures: the power system with multidirectional power flow and the two-way communication system. Both infrastructures are enablers of the proposed categorization of the following 5G-enabled smart grid services:

- Smart distribution automation;
- Wide-area monitoring, control, and protection;
- Metering data acquisition;
- Integration of distributed generation;
- Volume and price balancing.

These services are detailed in brief to understand the critical role of the proposed RAN slicing framework. The role of RAN slicing is highlighted in each service, including the specific slice/service type (SST) indicator.

1. **Smart Distribution Automation:** Sophisticated, reliable, and low-latency communication forms the backbone of a smart distribution automation system. It allows power distribution systems to rearrange themselves when a fault occurs (for loss reduction, load balancing, and service restoration), restricting the problem to a smaller area without violating metrics, such as line power flow limits and bus voltage.

In this context, a smart distribution automation system enabled by the proposed 5G and beyond framework aims to achieve real-time situational awareness and quasi-real-time analysis of the grid behavior by supporting advanced functionalities [52], such as:

- Efficient load flow examination for balanced and unbalanced distribution systems.
- Short-circuit analysis, which is the process of estimating voltages and currents in the power system in undesired conditions.
- Automated feeder reconfiguration for loss reduction— in the network configuration, it is performed by closing (generally open) and opening (usually closed) switches in the network. The greater the number of switches is, the greater the possibilities for reconfiguration.
- Optimized service restoration in a distribution system, which is a task that aims to locate and isolate a fault that occurs in a feeder of a distribution system, and subsequently restore supply by appropriate switching actions.
- Automated feeder reconfiguration for load balancing, which is a key feature to ensure an adequate power supply to minimize the losses and avoid an excessive voltage drop. It is a critical application to enable demand response, distribution generation, decentralized renewable energy, microgrids, and demand-side management.
- Automated location of faults, which is a key tool to support the identification of faulted components, speed up restoration, improve system reliability, and reduce outage time.

Role of RAN slicing in smart distribution automation: As it is a critical service, it should be enabled by a URLLC slice to guarantee low latency and high reliability. As the majority of the messages are mostly related to automated commands, these messages will require a low bandwidth with a low density of users. However, the service priority should be very high. Based on the standard definitions of network slicing, this service should be enabled by SST value 2, which is related to the URLLC slice.

2. **Wide-Area Monitoring, Control, and Protection:** The main task of a transmission system operator is to accurately manage the high-voltage power system. The main mission is to guarantee quality, affordability, and safety. To execute this task, applications based on complex analysis and software are used. Usually, these applications require significant information to predict smart grid evolution in every operating condition. To supply this information, a wide area measurement system is required. Usually, it is implemented by using digital devices, such as PMUs, to record sensible information, such as geographical positioning and high sampling rate dynamic power system data. The wide area measurement system depends strongly on the communication between actuators, controllers, and sensors through a shared

communication network. These measurements are critical to provide alerts, especially during unexpected conditions. In addition, the monitoring system can also be used in enhancing equipment maintenance applications and replacements.

By exploiting a 5G and beyond communication infrastructure, wide-area monitoring systems aim to enhance traditional SCADA systems, offering advanced supervision features, such as:

- Supervisory control and data acquisition, which is based on three essential functions: supervisory control, alarm display and control, and data acquisition. This system includes a master terminal unit (MTU) in the control center, a remote terminal unit (RTU) as a stand-alone data acquisition and control unit, IED, which is a small industrial computer that operates devices such as relays, switches, and mechanical timers. All of these are connected through a communication system between the control center and the remote site.
- Synchronized phasor measurement system, which is driven by an advanced device that measures voltages and currents and computes the phase between them. This device is composed of a PMU that acquires the electrical waves in a power system, and a phasor data concentrator (PDC) that receives synchrophasors from a poll of PMUs or other PDC to create a coherent record of simultaneously recorded data. As synchrophasors transmit sensible information and are continuous stream data, they have strict communication system requirements in terms of low latency and bandwidth.
- Digital fault recorder to archive sensible and accurate waveforms related to fault events. It aims to get information in the prefault, postfault, and fault stages. The recorded information is used for offline processing.
- Digital protective relay (DPR), which is based on advanced microprocessor technology to distinguish faults in power systems by processing current and voltage waveforms.
- Circuit breaker monitoring (CBM) is an electronic device that keeps track of circuit breakers. It works in real-time to gather information in scenarios in which the breakers are operated manually or automatically by the control and protection equipment if necessary.

Role of RAN slicing in wide-area monitoring, control, and protection: As this service has a mix of requirements in terms of latency and reliability, it should be enabled by SST value 1 that supports eMBB, SST value 2 that supports URLLC, and finally, SST value 3 to support mMTC applications. As the target is to gather a massive number of sensor information, it will require a medium bandwidth with a medium density of users. In addition, the service priority should be very high or medium.

3. **Metering Data Acquisition:** The AMI, constitutes one of the critical components of the smart grid. Smart meters are continuously evolving into sophisticated com-

puting units, which should process, gather, and deliver user consumption information to data aggregation units for additional processing and analysis. In addition, AMI systems can take advantage of the distributed information processing and storage architecture of 5G and beyond core networks, supporting virtualized edge computing platforms for localized decision-making. They also enable a well-organized energy demand management system as well as precise forecasting and analysis of future energy needs. The smart grid uses smart meters for continuous monitoring and adjusting the consumption of electricity. The smart meter system transfers collected data to service providers at equal time intervals. This is done to enable customer billing, data reduction, work management, distribution planning, peak demand, quality of service monitoring, distribution network analysis, outage management, time-based demand data analysis, and service interruption. The AMI integrates several technologies, such as

- Smart devices comprise the end user device that enables data collection and measurements required in specific time intervals with the time stamping feature.
- Communication by a highly reliable network, because a large number of smart meters are required to transmit the gathered information to computers for analysis.
- Data management system is typically a centralized module that aims to manage the multimodular structure of the smart grid.

Role of RAN slicing in metering data acquisition: As this service requires a medium/low latency, it should be enabled by SST value 3 to enable mMTC applications in the AMI systems. As the target is to gather a massive amount of sensor information, it will require a medium/high bandwidth with a low/medium density of users. In addition, the service should be between low and medium priority.

4. **Integration of Distributed Generation:** With the increasing efforts worldwide to reduce carbon-intensive energy supply, a variety of different generation plants and equipment are connected to the electrical distribution networks, for instance, photovoltaic systems, combined heat and power (CHP), wind turbines, solar thermal, fuel cells, micro-CHP, flywheels in marine renewable technologies, and flow battery storages.

   The proposed 5G and beyond framework has the potential to provide safer and more reliable connectivity to the distributed generation units. It has a positive impact on smart grids, especially in using renewable energy sources and providing them with a higher fault tolerance. In this context, the proposed connectivity framework should be capable of supporting the advanced control techniques and networking schemes for a seamless process, particularly when the energy storage capacity is low.

   Role of RAN slicing in the integration of distributed generation: As this service requires a medium/low latency with high reliability, it is enabled by SST value 2 and SST value 3 to enable URLLC and mMTC applications, respectively. As

the target is to integrate sensor measurements between distributed generators with short package information, it will require a short bandwidth with the capacity of supporting a medium/high density of users. Furthermore, the service should be between medium and high priority.

5. **Volume and Price Balancing:** Demand response (DR) is one of the core elements of the smart grid. It embraces a diversity of electricity-pricing schemes, such as time of use (TOU) pricing, real-time pricing (RTP), and critical peak pricing (CPP), and a variety of algorithms for controlling appliances.

   In this use case, a reliable and extensive cellular network with capabilities offered by 5G networks and beyond can enable prosumers to collaborate in the production of energy on a peer-to-peer basis. This decentralized strategy aims to determine prices accurately.

   Role of RAN slicing in volume and price balancing: As this service requires a medium/high latency with a medium/low reliability, it is enabled by SST value 1 and SST value 3 to enable eMBB and mMTC applications, respectively. Considering that the data transmitted in the wireless communication network require considerable data rates, a medium/high bandwidth with a medium/high density of users is needed. However, the service is of low priority compared with other smart grid services.

3.1.2 5G and beyond RAN slicing framework supporting the IEC 61850 protocol

The application protocol defined in the standard IEC 61850 was originally defined considering that Ethernet supports lower protocol stack layers on a wired interface. Thus, in terms of physical layer communication, it is expected to provide a reliable and predictable channel because it is usually static without significant variability and usually offers a high bandwidth, as in the case of fiber optics. In the case of wireless channels, the chances of external impairments and different coherence bandwidths are higher than in the wired counterpart. Therefore, the 5G, which is specified by 3GPP since the release 15 until the current release 17, is based on key technologies such as:

- Legacy 4G waveform: OFDM aims to reduce intercarrier interference, which is a desired feature in multicarrier systems, such as 5G;
- New numerology for the radio frame to operate on different subcarrier bandwidth sizes to enable URLLC capabilities;
- Advanced channel coding;
- Antenna array technology to increase the spectral efficiency based on the spatial domain together with MIMO;
- Functional split of RAN to provide flexibility in the deployment of critical applications;

- High bandwidth capabilities on the mmWave spectrum;
- Usability of machine learning to manage the core network through software-defined network (SDN).

However, the standard has not yet specifications on RAN slicing, especially to support industrial vertical communication protocols, such as IEC 61850. The reality is that IEC 61850 messages and consumer applications could share the same resources, such as the frequency spectrum. However, IEC 61850 users and typical cellular network users do not share exactly the same network requirements. For instance, in the case of mobile network users, a high bandwidth and low costs are usually the best and suitable choices. In contrast, IEC 61850 users mostly require low-latency communications and a high reliability to enable specialized smart grid services. Thus, QoS awareness of device-specific aspects and traffic requirements is critical for their success.

In the state of the art there are many RAN slicing frameworks to enable vertical applications. However, most of them are generic realizations of preallocation resources at the network level and dynamic scheduling at the 5G Node B (gNodeB) level using traditional scheduling methodologies [53]. In other studies, RAN slicing uses artificial intelligence for scheduling radio resources [54]. However, they consider generic and noncompatible requirements with the standard IEC 61850 and fixed transmission power allocation.

The proposed RAN slicing framework to enable the standard IEC 61850:
The novelty of the proposed RAN slicing framework is that the QoS policies are defined based on the dynamic requirement of the IEC 61850 application protocol, and the building elements provide a high level of flexibility to support dynamic allocation, simultaneously supporting any SLA level.

In practice, there are two different approaches to model each RAN slice. RAN slicing approach A considers dedicated subchannels or subsets of the total bandwidth for each RAN slice as illustrated in Fig. 3.2. Another option is to consider RAN slicing approach B, which adds more sharing granularity to the front end of the RF module and also requires sophisticated methodologies, such as successive interference cancellation (SIC), to guarantee the performance in the highly resource sharing scenario.

In the proposed framework, we considered RAN slicing approach A because it is the most suitable deployment scenario. Thus, substantial interference is to be expected when two or more gNodeBs are providing connectivity. To mitigate the interference between gNodeBs, a deep reinforcement learning model schedules the subchannels across different gNodeBs focusing on a specific target, such as spectral efficiency maximization. We complement the traditional resource blocks (RBs) scheduling with individual power allocation on each UE.

The requirements introduced by the standard IEC 61850 are the main target of the proposed RAN slicing framework. This framework comprises five building elements, viz.

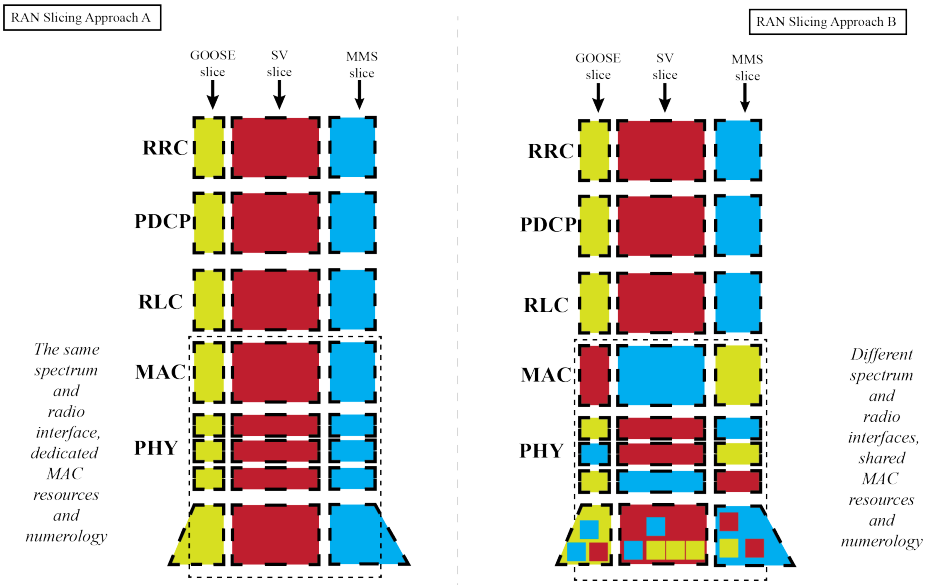

Figure 3.2: Illustration of both RAN slicing approaches in the physical layer mapped in the generic cellular network architecture specified by 3GPP Rel. 17. On the left, RAN slicing approach A, and on the right, RAN slicing approach B.

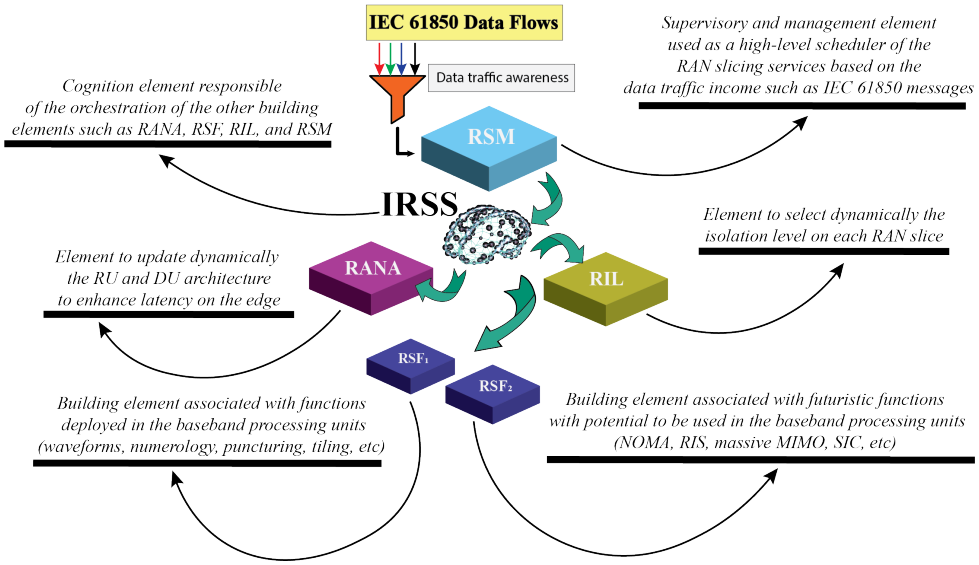

Figure 3.3: Illustration of the RAN slicing framework to enable the IEC 61850 data flow.

the RAN architecture (RANA), the RAN isolation level (RIL), the RAN slicing function (RSF), the RAN slicing management (RSM), and the Intelligent RAN slicing scheduler (IRSS). These elements are illustrated in Fig. 3.3 and summarized in the following:

1. **RANA:**

   It considers the fundamental RAN architecture elements such as the radio units (RUs), the distributed units (DUs), and the centralized unit (CU) can support the heterogeneous IEC 61850 requirements. These functional elements are determined and configured based on the RANA index value. For instance, when RANA=1, a centralized architecture is enabled to support IEC 61850 messages that match classes with end-to-end latency levels of $\geq$20 ms. Alternatively, a configuration with a higher RANA index enables an entirely distributed architecture that depends on the flexible deployment of combinations of DUs and RUs. In the former case, the IEC 61850 critical messages are transmitted using a functional split near the CU to achieve lower latency levels, e.g., IEC 61850 performance classes Type-1A and Type-4 messages with a $\leq$10 ms or $\leq$3 ms time requirement according to the standard IEC 61850-5.

2. **RIL:**

   Considering that isolation means that a slice does not interfere with other slices, this building element sets the required segregation level among slices, reflecting a trade-off between isolation and efficiency. In this context, this framework proposes a conservative isolation policy on base stations (BSs). Thus, each RAN slice defined by this framework is carried in one specific subchannel, which is orthogonal to other subchannels.

3. **RSF:** This building element is predominantly associated with functionalities performed in the baseband processing units. Two well-defined subelements carry out a partition of these functionalities.

   The RSF_1 comprises the 5G/NR features and involves the scalable 5G/NR frame structure and numerology. This subelement is associated with fundamental PHY and MAC layer functions, such as puncturing, scheduling, and tiling.

   Another subelement is the RSF_2, which consists of tailored baseband features to support vendor-specific operations or not yet specified technologies in the standard. It is associated with beyond-5G technical enhancements, preparing the next-generation connectivity enablers to be incorporated in the IEC 61850 RAN slicing framework.

4. **RSM:**

   This element monitors the necessary capabilities of the preceding RANA, RIL, and RSF elements. The RSM is a high-level scheduler of RAN slicing elements as part of its management and supervisory role. The role of the RSM needs to consider the different SLAs of IEC 61850 messages designated by upper layers and the core

network. As illustrated in Fig. 3.3, the RSM uses the *data traffic awareness* block to evaluate, analyze, and model the IEC 61850 data traffic.

5. **IRSS:**

   It is the cognitive element of the proposed framework. It has the task of acting as the scheduler of functionalities over the other framework elements. Thus, the IRSS guarantees the key network metrics that evaluate the system performance. This is done by assisting other elements with machine learning algorithms as RL to improve the system performance metrics, such as SINR and spectrum efficiency, which indirectly enhances critical network metrics, such as latency, reliability, and throughput. In the scope of RL, an agent learns to interact with its environment (radio channel impairments, such as interference, and fading).

3.1.3 Radio resource management proposed using machine learning

Every BS enables independent learning agents or ML models. However, the proposed learning scheme follows a multiagent strategy. Two policies are considered for each agent. One policy is to choose the associated RAN slice, and the other one is to set the power transmission level.
The DRL methodology considered the following components:

- **Agents:** the agents are deployed in the BSs.
- **Policies:** The design considers two policies: π_1 to select a specific RAN slice and π_2 to set an adequate transmission power for each user.
- **Actions:** Two sets of actions are considered; the first set has discrete actions related to the indication of RAN slices, and the second set has continuous action to select the transmission power for each individual user.
- **States:** A state is composed of a finite-order list of information related to the RAN slice allocation, the spectral efficiency (SE) and gain inference in each individual user.
- **Rewards:** In general, the reward value is proportional to the receiver spectral efficiency of each UE. The spectral efficiency of every UE is evaluated under the condition that neighborhood agents are not transmitting. As a consequence, if the SE value is considerable, then the target agent is penalized. On the opposite side, if the SE maintains a homogeneous value, then the BS is rewarded.

The solution considers two different policies. However, the DRL is not capable of exploring and exploiting both policies simultaneously. For this reason, the DRL makes use of two optimization approaches. The first is a Deep Q-network that optimizes a stochastic policy to enhance the RAN slice indication. The second is a Deep Q-network that optimizes a deterministic policy with the target to select a satisfactory power transmission. It

is important to note that the second deep Q-network depends on the decision of the first one to define its state inputs prior to setting the transmit power of the agent.
Finally, some implications and generality related to the existing knowledge, as well as future potential applications, are summarized in the following.

- **Implications of the results:** The results obtained in **Publication I** indicate that the current cellular networks can use the proposed RAN slicing framework. This RAN slicing definition enables the selection of the isolation level to support specific applications. In the case of the standard IEC 61850, a very conservative setup is advisable, as used in this work. However, the framework is flexible enough to avoid the need for another functional split setup.

- **Generality (limitations) of the results:** The present architecture is based on the current functional split defined in the 3GPP Rel. 17. However, some specific signalization with a high specification impact is expected but not considered in this dissertation.

3.1.4 Summary

In this contribution, we proposed a categorization of 5G-enabled smart grid services to identify and map standardized 5G slices in services like smart distribution automation; wide-area monitoring, control, and protection; metering data acquisition; distributed generation integration; and volume and price balancing. In addition, considering the key requirements defined in the standard IEC 61850, a 5G and beyond RAN slicing framework was proposed to enable a smooth integration between power system devices and wireless communication devices. Finally, based on the proposed RAN slicing framework, a solution for radio resource management was proposed using a deep reinforcement learning scheme.

3.2 Modeling GFDM in wireless scenarios

An analytical derivation of the SINR for GFDM signals on Rayleigh fading channels with MMSE receivers was the target of **Publications III and V** related to the modeling of GFDM. This research contribution aims to complement the RIL module defined in the RAN slicing framework proposed in the previous section. Specifically, enhancing the performance of the physical layer by using the GFDM's flexibility has a strong potential to enable sophisticated applications, which would enhance the operation of smart grids, especially in the most demanding cases in terms of reliability and latency. Thus, in the context of the dissertation, this section aims to answer research question **RQ2**.

RQ2 *In what conditions generalized waveforms—which are yet not part of current cellular standards—can outperform the existing solutions, potentially allowing new smart grid applications in indoor and outdoor environments?*

In the last decade, GFDM has arisen as a potential alternative to OFDM for current cellular networks and beyond [55]. OFDM relies on rectangular pulse shaping, which is the main source of sizeable OOB radiation. Moreover, the CP used in each OFDM block reduces the spectrum efficiency, which is more notorious in highly frequency selective channels [56]. In contrast, GFDM can carry data symbols in a well-localized prototype filter in both the frequency and time domains [57]. This characteristic reduces the CP percentage, and consequently, the OOB emission is mitigated [56].

In recent studies, GFDM has attracted great attention as a waveform to be used in future cellular networks. For instance, in the case of integration of satellite and terrestrial communication, the research community proposes a solution based on GFDM to support the expected demand considering a more compatible and robust physical layer waveform [58]. This integration is only feasible if a flexible waveform is compatible with OFDM. Because in GFDM there is great flexibility to set the number of subcarriers and subsymbols, GFDM is compatible with CP-OFDM and discrete-Fourier-transform-spread OFDM (DFT-S-OFDM) [59, 58]. In other words, GFDM covers the 5G standardized waveform OFDM and single carrier frequency domain equalization (SC-FDE), which represent GFDM corner cases [60, 61].

The main motivation of this study is to propose a mathematical framework to obtain an analytical model of the SINR through the semiclosed form of its PDF. **Publication III** contributes to fill a gap in the literature by deriving a semiclosed expression of such a distribution when the GFDM system employs MMSE receivers on Rayleigh channels.

The Rayleigh fading channel is used to model NLOS links, which is a popular wireless communication scenario for many applications. In this context, the proposed analytical model can be employed in a potential analysis that considers technologies related to 5G and beyond. This scenario could be applied to smart grid use cases that are deployed inside a substation, in which there are many cluttering elements that increase the chances of NLOS links.

The motivation to use the linear MMSE equalizer is based on the fact that it is a classic functional block and that it is ubiquitous in digital communications [62]. Another reason is that MMSE is also the building block of more advanced communication schemes. However, the existing performance analyses of GFDM and MMSE on Rayleigh channels are far from complete.

Another important contribution is based on **Publication V**. Here, the distribution of the PDF of the SINR was obtained to achieve the analytic calculation of important wireless metrics, such as outage probability, achievable sum rate, outage capacity, spatial diversity, BER, and channel hardening.

3.2.1 Semiclosed analytical PDF of the SINR obtained on fading channels

In wireless communication theory, the use of random variables is one of the most popular approaches to analytically model features, especially in the physical layer.
In the case of Rayleigh fading channels, a complex channel coefficient is represented by

$$h = h_r \, e^{-j\theta}, \tag{3.1}$$

where θ is a random variable defined by a uniform distribution between $-\pi$ and π, and h_r is a random variable defined by

$$h_r = |h|. \tag{3.2}$$

Here, in general, the real (h^{Re}) and imaginary (h^{Im}) parts of h have the same variance equal to σ_r^2 and nonzero mean values m_{Re} and m_{Im}, respectively, expressed by:

$$p_{h^{\text{Re}}}(h^{\text{Re}}) = \frac{1}{2\pi\sigma_r^2} \exp\left(-\frac{|h^{\text{Re}} - m_{\text{Re}}|^2}{2\sigma_r^2}\right), \tag{3.3}$$

$$p_{h^{\text{Im}}}(h^{\text{Im}}) = \frac{1}{2\pi\sigma_r^2} \exp\left(-\frac{|h^{\text{Im}} - m_{\text{Im}}|^2}{2\sigma_r^2}\right), \tag{3.4}$$

if $m_{\text{re}} = m_{\text{im}}$ and $m_{\text{re}} = \frac{\mathcal{V}}{\sqrt{2}}$, where $\mathcal{V}$ is the distance between the reference point and the center of the bivariate distribution. Thus, we obtain the PDF of the magnitude of h represented in (3.2), which is an independent and identically distributed Rician channel realization defined by

$$p_{h_r}(h_r)_{rice} = \frac{h_r}{\sigma_r^2} \exp\left(-\frac{h_r^2 + \mathcal{V}^2}{2\sigma_r^2}\right) I_o\left(\frac{h_r \mathcal{V}}{\sigma_r^2}\right). \tag{3.5}$$

A very important property is that the Rayleigh distribution is a corner case of the Rice distribution. Thus, when the Rician fading channel parameter $\mathcal{V}$ is zero, it becomes a Rayleigh random variable.

$$p_{h_r}(h_r) = \frac{h_r}{\sigma_r^2} \exp\left(-\frac{h_r^2}{2\sigma_r^2}\right). \tag{3.6}$$

This particular contribution considered the distribution of the Rayleigh fading channel to represent specific smart grid scenarios in the communication system model. This system model considers that a GFDM waveform is transmitted on a Rayleigh fading channel. However, it can be extended to Rician fading channels.

On the receiver side, it is common to consider linear receivers, such as MMSE. MMSE is used to maximize the SINR of the GFDM signal transmitted through the wireless channel.

Considering a generic system model, the GFDM signal is used as an input of the channel model block with the variable **x**. The output of the channel model block is represented by the variable **y**, and this signal is used as the input of the linear receiver MMSE. Following a similar sequence, the output of the MMSE receiver is represented by the random vari-

able **z**. The target of the contribution is to mathematically obtain the distribution of the random variable **z** when the fading channel is modeled by a Rayleigh distribution.

To better illustrate the above-mentioned scenario, an illustrative system model is shown in Fig. 3.4. In this particular system model, a variety of random variable transformations were considered using mathematical tools to approximate random variables with specific distributions by matching the first and second moments.

Finally, the distribution of the SINR of the random variable **z** was obtained analytically based on a semiclosed model, which is the primary outcome and contribution of **Publications III and V**.

3.2.2 Performance metrics obtained analytically by using the PDF of the SINR

Based on the previous contribution, in which the PDF of the SINR of the signal **z** was obtained, a variety of performance metrics can be found analytically.

Considering that MMSE is used on the receiver side, it can be shown that the SINR of the nth data symbol can be expressed as

$$\gamma_n = \frac{1}{\text{MMSE}_n} - 1 = \frac{1}{\left[(\mathbf{I}_N + \frac{p}{N}(\mathbf{H}_{\text{ch}}\mathbf{A})^{\dagger}\mathbf{H}_{\text{ch}}\mathbf{A})^{-1}\right]_{nn}} - 1. \tag{3.7}$$

where the operator $(.)^{\dagger}$ represents the Hermitian conjugate of a matrix, $\mathbf{I}_N$ is a $N \times N$ identity matrix, and p is the average signal-to-noise ratio (SNR), given by $p = \sigma_d^2/\sigma_\nu^2$. Note that (3.7) has the same form of [63, eq. (7.49)], being thus not restricted to binary signals, and its derivation is based on the second-order statistics of the input signals [64].

As it was stated in [65], the BER for the l-th probability (P_b) of error (E) given by a specific SINR (γ_n) of a $\mathcal{M}$-quadrature amplitude modulation (QAM) constellation can be expressed as

$$P_b(E|\gamma_n) = \frac{1}{\sqrt{\mathcal{M}}} \sum_{t=0}^{(1-2^{-l})\sqrt{\mathcal{M}}-1} \left\{ (-1)\left\lfloor \frac{t\,2^{l-1}}{\sqrt{\mathcal{M}}} \right\rfloor \times \left(2^{l-1} - \left\lfloor \frac{t\,2^{l-1}}{\sqrt{\mathcal{M}}} + \frac{1}{2} \right\rfloor \right) \times \text{erfc}\left((2t+1)\sqrt{\frac{3\log_2\mathcal{M}\,\gamma_n}{2(\mathcal{M}-1)}} \right) \right\}, \tag{3.8}$$

where γ_n is the postprocessing SINR for the nth received symbol given in (3.7). The γ_n random variable has a PDF ($p_\gamma(\gamma_n)$), which was already obtained analytically in Subsection 3.2.1. With all these elements, the BER is obtained analytically in **Publications III and V** by using the following generic model:

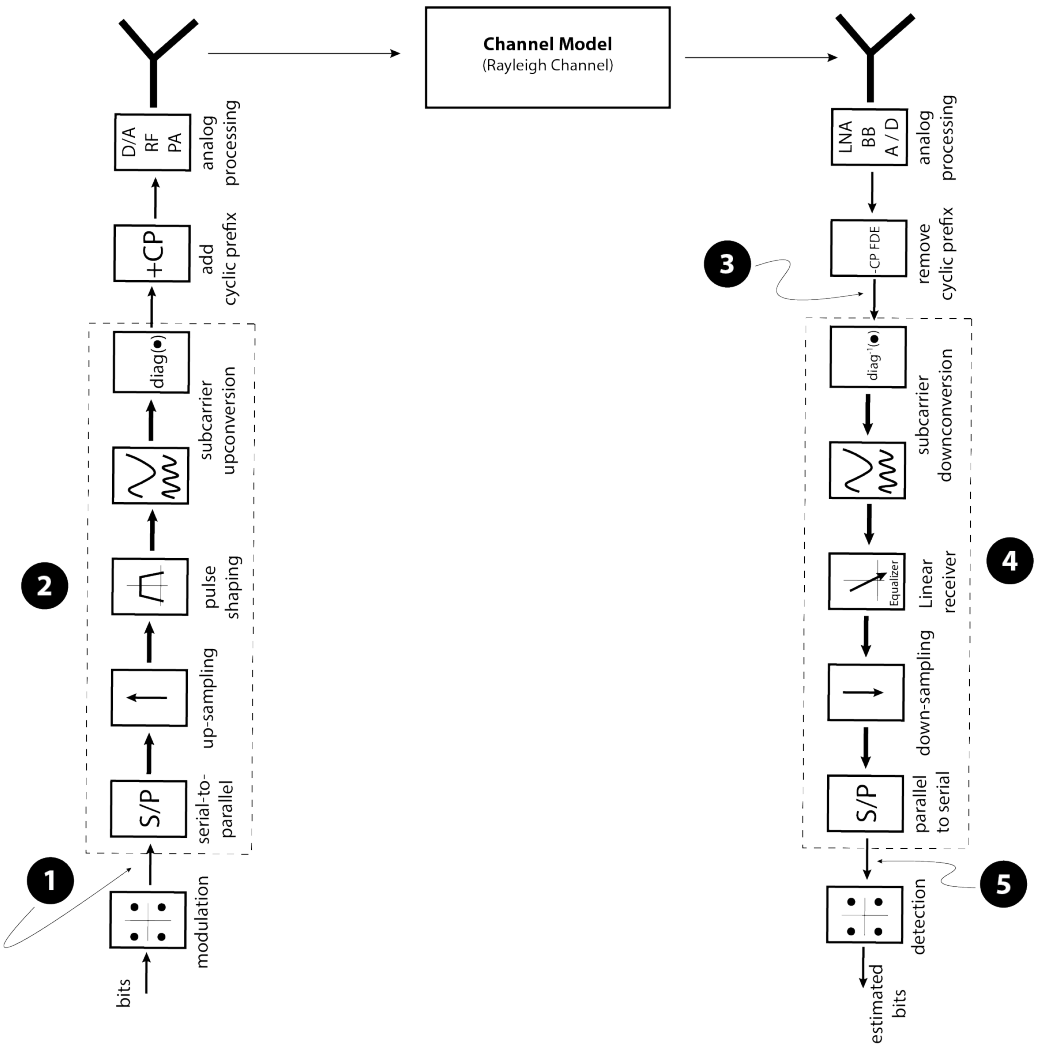

Figure 3.4: Illustration of the GFDM system model. Here, the numbers in black circles indicate the main signal points. In (1), we have the input signal after the mapping modulation represented by the variable $\mathbf{x}$. In (2), we have the GFDM modulation matrix represented by the variable $\mathbf{A}$. In (3), the discrete version of the channel output and after the CP is extracted, which is represented by the variable $\mathbf{y}$. In (4), the block represents the linear receiver, in this specific case the MMSE. Finally, in (5), the discrete output of the estimated symbols represented by the variable $\mathbf{z}$.

$$P_b(E) = \frac{1}{N} \times \sum_{n=0}^{N-1} \int_0^{\infty} P_b(E|\gamma_n)\, p_\gamma\left(\gamma_n\right) d\gamma_n \tag{3.9}$$

In the case of the achievable ergodic sum rate for the MMSE receiver is given by (3.10), which was already used in [66].

$$\begin{aligned} \mathcal{R}^{\text{mmse}}(\gamma_n, N) &= \sum_{n=1}^{N} E_{\gamma_n}[\log_2(1+\gamma_n)] \\ &= \sum_{n=1}^{N} \int_0^{\infty} [\log_2(1+\gamma_n)]\, p_\gamma(\gamma_n)\, d\gamma_n, \end{aligned} \tag{3.10}$$

Following a similar approach, the PDF of the SINR is also used to obtain analytically the outage capacity taking into consideration that the variable γ_n represents the SINR of the nth data symbol, and thus, it is possible to calculate the nonergodic capacity of the nth data symbol by $\log_2(1+\gamma_n)$ [67, 68]. However, to evaluate the outage capacity, it is important to note that there are $N = S \times K$ symbols. Afterward, we obtain the GFDM capacity by

$$C_{\gamma_n} = \sum_{r=1}^{N} \log_2(1+\gamma_n) = N\ \log_2(1+\gamma_n). \tag{3.11}$$

Thus, as we know the PDF of γ_n (already obtained in Subsection 3.2.1), it is possible to calculate the PDF $f_{C_{\gamma_n}}(C_{\gamma_n})$ of the random variable C_{γ_n} by traditional random variable transformation

$$f_{C_{\gamma_n}}(C_{\gamma_n}) = \frac{d}{d\gamma_n} p_\gamma(\gamma_n)\Big|_{\gamma_n = 2^{C_{\gamma_n}/N} - 1} \tag{3.12}$$

By definition, the outage indicates the probability that the random variable C_{γ_n} falls below an arbitrary data rate R_{out} Thus, the outage probability is

$$\begin{aligned} P_{\text{out}} &= P[C_{\gamma_n} < R_{\text{out}}] \\ &= F_{C_{\gamma_n}}(R_{\text{out}}) \end{aligned} \tag{3.13}$$

where $F_{C_{\gamma_n}}(C_{\gamma_n})$ is the cumulative distribution of the random variable C_{γ_n}. In our contribution, the cumulative distribution defined before calculates the outage probability for any arbitrarily R_{out}.

In summary, the previously mentioned mathematical formulations enable the analytic calculation of BER, outage probability, and sum rate for GFDM on Rayleigh fading channels.

3.2.3 Semiclosed approximation compared successfully with simulation in different scenarios

The PDF of γ_n (the SINR when the GFDM signal is transmitted on Rayleigh fading channels) has as the main target of approximating the Monte Carlo simulation as well as possible in different scenarios.

The Monte Carlo simulation is based on the generation of discrete samples of the GFDM signal. This data generation considers the GFDM modulation matrix, which contains important GFDM parameters, such as the roll-off (pulse shape), and the number of subcarriers and subsymbols. The generated GFDM signal is transmitted over a Rayleigh fading channel. The fading channel is simulated using a Rayleigh distribution. Assuming a circular symmetric complex (CSC) channel (Rayleigh), we also consider that the CP length must be higher than the delay spread of the multipath channel [39]. Additionally, the channel coefficients related to distinct paths are assumed uncorrelated.

Before starting the decoding process, the CP introduced at the transmitter is removed. Here, the FDE properties can be employed so that the linear convolution introduced by the CP becomes a circular convolution. Thus, the received vector is modeled as:

$$\mathbf{y} = \mathbf{H}_{\text{ch}}\boldsymbol{A}\mathbf{d} + \boldsymbol{\nu}, \tag{3.14}$$

where the vector $\boldsymbol{\nu}$ represents the AWGN signal of the length $N = K \times S$ with the variance σ_ν^2, S represents the number of subsymbols, K represents the number of subcarriers, **A** is the GFDM modulation matrix, **d** represents the transmitted complex data symbols, and $\mathbf{H}_{\text{ch}}$ is the $N \times N$ circular Toeplitz matrix.

To estimate the transmitted complex data symbols, we consider the MMSE received matrix. The received vector **y** is distorted by (i) self-interference coming from GFDM inherent nonorthogonality and (ii) frequency selectivity introduced by the channel impulse response. Thus, the SINR of the nth data symbol can be expressed as (3.7).

Equation (3.7) is used in the Monte Carlo simulation and in the analytical model to generate the simulated and analytical version of BER, sum rate, and outage probability.

For instance, in the case of BER, it is shown in Fig. 3.5 that the analytical version follows the tendency of the simulation. In this figure, the evaluation considered the following parameters: $K = 128$, $S = 9$, roll-off = 0.1. The multifading channel is based on the ITU Veh-A channel with paths [0 310 710 1090 1730 2510] ns with the chip rate 1 Mcps, and the average power of each path is [0 -1 -9.0 -10.0 -15.0 -20.0] dB.

Finally, in the case of outage probability, we obtained results presented in Fig. 3.6 for a sum rate outage of $R = 3$ b/s/Hz. Here, the GFDM signal considers the following parameters: for $N = 6$ with roll-off=0.1, and power delay profile $\sigma_m^2 = e^{-0.75m}$, $m = 1 \dots L$; $N = 40$ with roll-off=0.1, and power delay profile $\sigma_m^2 = e^{-0.1m}$, $m = 1 \dots L$; $N = 1152$

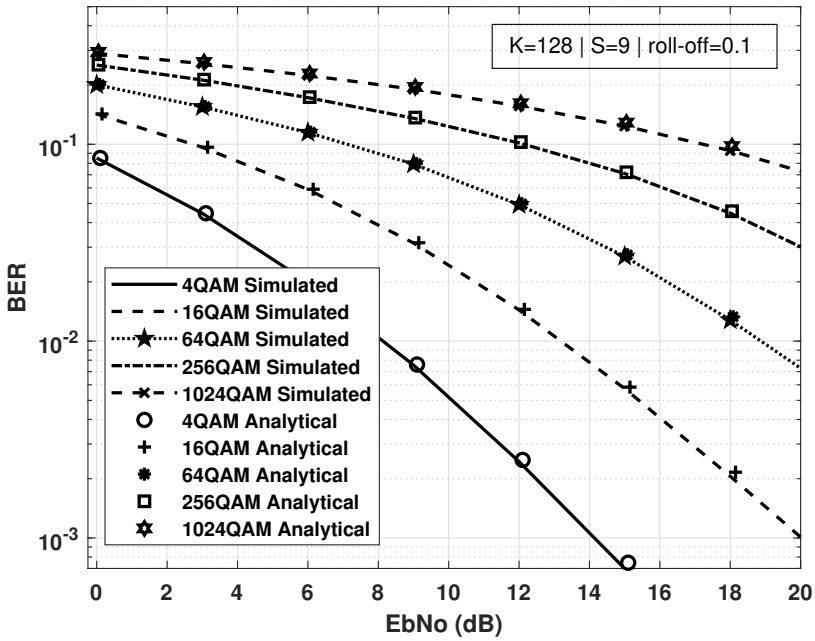

Figure 3.5: BER for different modulation schemes. Here, the simulated and analytical derivations are compared.

with roll-off=0.1, and power delay profile $\sigma_m^2 = e^{-0.48m},\ m = 1 \dots L$;. This metric is very important to evaluate different GFDM parameters in different channel models because it is directly related to the reliability of the communication network. As mentioned in the previous section, some IEC 61850 messages have strict requirements in this respect to guarantee the transmission of critical information between devices that constitute a specific smart grid application.

In the proposed GFDM framework, we introduced a semiclosed form of the SINR when the GFDM signal is transmitted on Rayleigh channels. The numerical analysis considered the key GFDM parameters, a Rayleigh fading channel, and FSFC parameters to evaluate the performance of the analytical and simulated models. In all cases, the semiclosed form indicated a high accuracy, even at lower and high SINR values. A negligibly small inaccuracy appears in the outage probability metric at higher SINR values.

To evaluate the accuracy of the proposed analytical semiclosed model of the BER, a mean-squared error (MSE) was calculated between the simulated and analytical approximation for three different scenarios. This analysis is shown in Fig. 3.7. In this evaluation, the following parameters were considered: $N = 6$, the number of channel delay taps $L = N$, and the power delay profile is defined by $\sigma_m^2 = e^{-0.48m},\ m = 1 \dots L$. Scenario 1 is defined by roll-off=0.1 . Scenario 2 is defined by roll-off=0.5 and Scenario 3 is defined

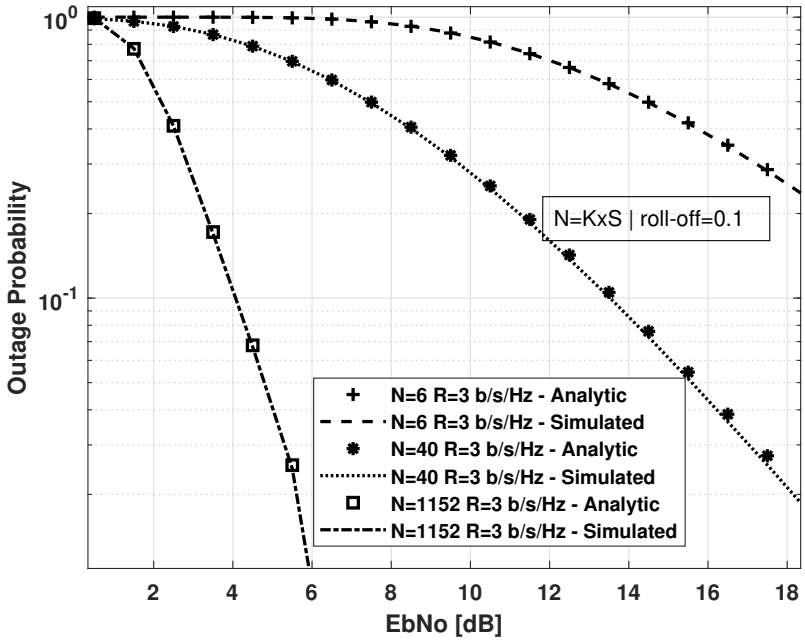

Figure 3.6: Probability of outage versus SNR for different values of sum rate outage (R) and $N = S \times K$.

.

by roll-off=0.9. In general, the accuracy is degraded when the roll-off is around 1.

In all scenarios, it is observed that the accuracy is lost when the modulation scheme is increased. For instance, in scenario 1, the 4QAM modulation gets an MSE of almost 10^{-9}, and the 1024QAM modulation obtains an MSE of 10^{-6}.

3.2.4 Summary

In this contribution, we proposed a semiclosed analytical model to represent the PDF of the SINR of GFDM signals when Rayleigh fading channel models was considered. Based on the analytical PDF, some important physical layer metrics were calculated, such as BER, achievable sum rate, and outage probability.

These channel models are typical in smart grid scenarios, which are characterized in some cases by NLOS links, especially in scenarios as substations, in which every element aims to transmit specialized IEC 61850 messages through high-density clutters or power system devices.

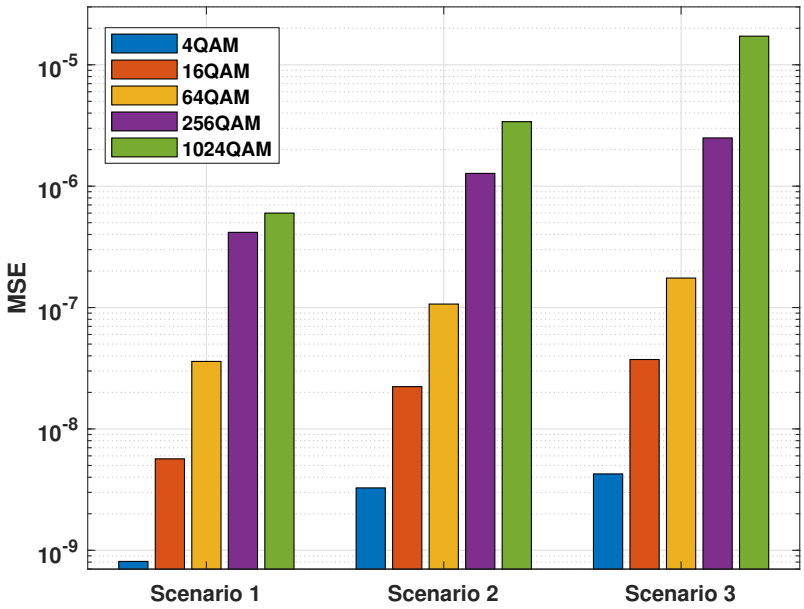

Figure 3.7: Accuracy analysis of the proposed semiclosed BER for three different scenarios. Scenario 1 is defined by roll-off=0.1, Scenario 2 defined by roll-off=0.5, and Scenario 3 defined by roll-off=0.9.

3.3 Mitigating interference with machine learning

In the last decade, the evolution of cellular networks has attracted attention in many industries, e.g., agribusiness, sheep transportation, and power systems. Some of these industries require a larger cell radius than regular commercial systems and usually do not require a highest throughput in most of the cases, especially to support IoT applications. Thus, using low frequency ranges to carry band base information becomes an interesting approach to increase the cell radius and maintain the band base functionality of the cellular network, which can be built on 4G or 5G technology. In contrast to the advantage of using low frequencies on cellular radio, there is a fundamental disadvantage that is related to the intercell interference, which is a challenging characteristic in smart grids because of the widespread measuring elements whose data need to be communicated to enable an improved operation of the electricity network. This problem is the target of this contribution, which aims to answer research question **RQ3**.

RQ3 *Is it possible to improve the current cellular technology through machine learning techniques in order to better serve smart grid communications, specifically in supporting critical applications?*

Using low frequencies in cellular networks is becoming a sustainable and lucrative option for vertical industries. For instance in Brazil, some verticals like agribusiness and

power systems are introducing cellular networks to support IoT applications for monitoring, controlling, and supervising devices using very high frequency (VHF) bands. These cellular systems operate at 250 MHz, 450 MHz, and 700 MHz frequencies to achieve a cell coverage between 10 and 50 km.

By using IoT, many vertical industries aim to connect every physical object to the Internet, as part of the digitalization process of regular procedures. Usually, digitalization requires connectivity in dense urban and rural areas. Urban areas are typically well supported by telecom operators. However, access can be difficult in rural areas, and long distances must be covered, which means that operators expect a low return on investment. For that reason, the use of private networks is becoming popular between industrial verticals and also between network vendors. For instance, the feasibility of LTE in the 800 MHz frequency band was tested to serve rural areas [69] and [70], respectively. In [71], LTE machine-type communication (LTE-M) and NB-IoT were evaluated with the network operating in the 800 MHz frequency band. In [72], a 4G network was investigated in the field to identify the opening features that are aimed to be bridged by 5G in rural scenarios.

One important drawback of using cellular networks is the ICI, which is effectively attenuated by using beamforming and massive arrays in current 5G networks. However, these approaches cannot be used in sub-1GHz bands. To address this issue, in [73], a flexible tool was provided to implement traditional frequency reuse (FR) schemes in the LTE. The FR evolves from a static to a dynamic procedure based on an intercell interference coordination (ICIC) algorithm. The complexity of this algorithm increases like in typical resource allocation algorithms [74], which in the specific case of a smart grid should deal, for example, with a diversity of QoS requirements in terms of latency, reliability, and transmission rate as defined by the standard IEC 61850. This has an impact in a rural scenario because coverage requirements and sparse user locations. As a consequence, the operational and capital expenditures (OPEX/CAPEX) of IoT network providers are not attractive to service providers [75, 76].

In this contribution, we proposed a solution that aims to schedule the FR allocation by using a DRL approach. The radio simulator was calibrated with real measurements obtained in the field from a network operating at 250 MHz. Further details in each contribution are discussed in the following.

3.3.1 Simulation and calibration with real field data

The band between 225 MHz and 270 MHz was allocated to the Private Limited Service (SLP) on a primary and nonexclusive basis [77] in 2010 in Brazil. In this context, a cellular network was developed and implemented using an LTE band base operating at 250 MHz to provide connectivity within a radius of 50 km. The cellular network operates in the frequency division duplex (FDD) mode within the 5 MHz bandwidth. The channeling used in this deployment followed the distribution defined in Table 3.1. The cellular system was deployed in a rural area with the radio parameters described in Table 3.2.

Table 3.1: Channeling used in the broadband system operating in the 250 MHz band.

Central Frequency (MHz)	Channels (Based on Res. 555 - ANATEL)	Band	Duplexing Type
228.75 (Uplink), 251.25 (Downlink)	1, 2, 3, 4, 5	A	FDD
237.50 (Uplink), 265.00 (Downlink)	7, 8, 9, 10, 11	B	FDD

Table 3.2: Key system parameters of the cellular network deployed in the field.

Element Name/Feature	**Quantity / Information**
BSs	3 units
UEs	10 units
Frequency band	Band A
Bandwidth	5 MHz (25 RBs)
Duplexing type	FDD
Antenna height in BS	40 m
Antenna Height in UE	3.5 m
Transmission power - UE	30 dBm
Transmission power - BS	43 dBm

The link-level evaluation achieved the expected physical layer KPIs. However, the system-level analysis in which many base stations were involved faced radio impairments because of intercell interference. This scenario motivated the study related to this scientific contribution.

To evaluate the intercell interference, we used a system-level simulator that is based on C++. This simulator provides an abstraction of the physical layer with a proper representation of the channel propagation that is suitable to be calibrated. Thus, the first step was to perform field measurements to build a dataset with information of reference signal received power (RSRP), throughput, SINR, and system coverage. For instance, at a cell radius of 40 km the system achieved a data rate up to 2 Mbps in downlink as shown in Fig. 3.8. In the same figure, a comparison is made between the prediction of coverage in the SINR obtained by simulation and the radio measurements obtained in the drive test after the calibration. Here, we can infer the capability of cellular networks operating in sub-1GHz bands to support typical applications on transmission or distribution lines, such as protection and control systems enabled by a wireless system with a large coverage and specialized schemes to enhance the cellular performance based on IEC 61850 messages and their respective requirements.

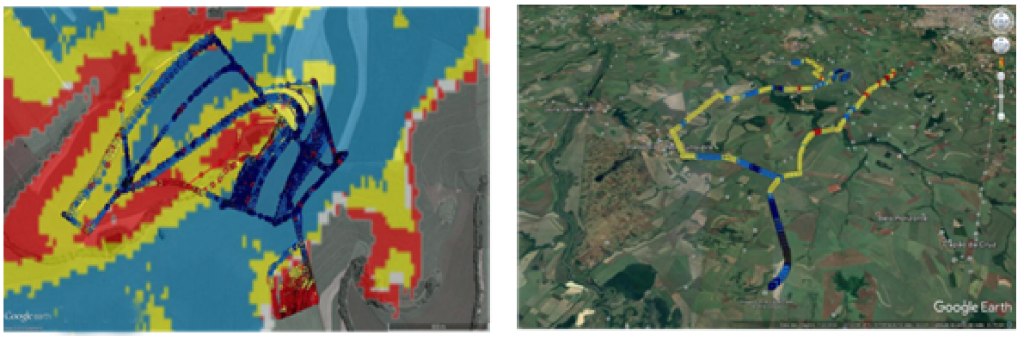

(a) (b)

Figure 3.8: (a) Comparison of the driving test in intense colors compared with the coverage prediction obtained by simulation with less intense colors. (b) A transmission rate of 2 Mbps was obtained in a range of 40 km.

The simulator was calibrated based on a modification of the evolved-UTRA absolute radio frequency number (EARFCN) configuration. With this setting we guarantee that the simulator will calculate the propagation in the correct VHF band. We also calibrated the large-scale model attenuation of the wireless channel in the simulator. It was done by modifying the parameters of the Okumura–Hata model [78].
After fitting and applying an MSE regression, the model parameters were modified to the following values

$$L = L_{\text{urban}} - 4,78(\log f)^2 + 18,33 \log f - \mathbf{15,94}, \tag{3.15}$$

and

$$\begin{aligned} L_{\text{urban}} =& 69,55 + 26,16 \log f - 13,82 \log h_t - A(h_r) + \\ & (\mathbf{20,9} - 6,55 \log h_t) \log d, \end{aligned} \tag{3.16}$$

This contribution was a key enabler of the next scientific evaluation because it guarantees that the simulation results are in compliance with the real scenarios. This is an important milestone because most of the state-of-the-art studies are limited to generic assumptions, which usually underrepresent some specific wireless scenarios.

3.3.2 Frequency reuse based on machine learning

To evaluate different frequency reuse schemes, a mathematical model was introduced in **Publication IV**. Here, the downlink is offered to a group of UEs in a geographical area $\mathcal{A}$, and the I BSs are part of the set $\mathcal{I}$. Each BS $i \in \mathcal{I}$ serves an area $\mathcal{A}_i$, such that $\cup_{\forall i \in \mathcal{I}} \mathcal{A}_i = \mathcal{A}$ and $\mathcal{A}_i \cap \mathcal{A}_k \neq \emptyset$ for any $i \neq k \in \mathcal{I}$. In other words, it is expected that there is a significant intersection between cells. The metric to be used to compare the different schemes is the throughput in the downlink. Thus, we defined the downlink spectral efficiency achieved by the frequency reuse at subchannel m, at the user n, in the

time slot t from the BS located at x_i to a UE located at $y \in \mathcal{A}_i$ is

$$\mathcal{C}_{n,m}^{(t)}(x_i, y) = \log_2 \left(1 + \gamma_{n,m}^{(t)}(x_i, y) \right), \tag{3.17}$$

where $\gamma_{n,m}^{(t)}(x_i, y)$ is the SINR at the user n, on the subchannel m, in the time slot t, which is defined in (3.18)

$$\gamma_{n,m}^{(t)}(x_i, y) = \frac{\left[\beta_{l,m}^{(t)} \, g_{l \to n,m}^{(t)}(x_l, y) \, p_l^{(t)} \right]_{l=n}}{\sum\limits_{v \neq l} \beta_{v,m}^{(t)} \, g_{v \to n,m}^{(t)}(x_v, y) \, p_v^{(t)} + \sigma_n^2}, \tag{3.18}$$

where $\beta_{v,m}^{(t)}$ indicates the subchannel selection m, which is transmitted from the BS v in the time slot t, $g_{v \to n,m}^{(t)}(x_v, y)$ indicates the downlink channel gain from the BS v to the user n on the subchannel m in the time slot t when the UE is located in the position y and the BS in the position x_v , $p_v^{(t)}$ is the transmit power of the BS v in the time slot t, and σ^2 is the additive white Gaussian noise power spectral density at the user receiver n

$$g_{v \to n,m}^{(t)}(x_v, y_n) = h_{v \to n}^{(t)}(x_v, y_n) \left| \alpha_{n \to l,m}^{(t)} \right|^2 , \; t = 1, 2, \cdots , \tag{3.19}$$

where $h_{v \to n}^{(t)}(x_v, y_n) = L$ is the path loss on a linear scale, which is calculated using the calibration done in the simulator with the drive test information, and finally, $\alpha_{n \to l,m}^{(t)}$ is the small-scale Rayleigh fading.

The proposed model is a generalization of different fractional frequency reuse (FFR) methodologies. These methodologies are differentiated with the binary variable $\beta_{v,m}^{(t)}$ to choose one specific subchannel m used by the BS v. The same framework considers power transmission in each BS, which is modeled with the variable $p_v^{(t)}$.

In **Publication IV** we presented a diversity of FR schemes. From this list of schemes, the main contribution comes from the machine learning approach that is based on DRL. It aims to schedule dynamically the subchannels used in the FR.

In this contribution, to improve the explanation of the radio optimization using DRL, we define a radio optimization problem. Here, the subchannels and power vectors in the time slot t are denoted by:

$$\boldsymbol{\beta}^{(t)} = \left[\beta_{1,1}^{(t)}, \beta_{1,2}^{(t)}, \cdots , \beta_{N,M}^{(t)} \right]^T \tag{3.20}$$

and

$$\boldsymbol{p}^{(t)} = \left[p_1^{(t)}, \cdots, p_N^{(t)}\right]^T \tag{3.21}$$

Using (3.17), we define the sum-rate maximization problem as

$$\begin{aligned} \max_{\boldsymbol{p}^{(t)}, \boldsymbol{\alpha}^{(t)}} \quad & \sum_{n=1}^{N} \mathcal{C}_n^{(t)}(x_i, y_n) \\ \text{s.t.} \quad & 0 \leq p_n^{(t)} \leq P_{\text{max}}, \forall n \in \mathcal{N}, \\ & \beta_{n,m}^{(t)} \in \{0,1\}, \forall n \in \mathcal{N}, \forall m \in \mathcal{M}, \\ & \sum_{m \in \mathcal{M}} \beta_{n,m}^{(t)} = 1, \forall n \in \mathcal{N}, \end{aligned} \tag{3.22}$$

where

$$\mathcal{C}_n^{(t)} = \sum_{m=1}^{M} \mathcal{C}_{n,m}^{(t)}(x_i, y_n) \tag{3.23}$$

The nonconvex problem in (3.22) is handled considering that it is a multiagent learning scheme where each transmitter, mounted in each BS, operates as an independent learning agent as described in Subsection 3.1.3.

An extended explanation of the algorithm is detailed in Algorithm 1. This type of architecture is similar to a generative adversarial network (GAN), where both a discriminator and a generator participate in a game [79]. The generator generates a fake subchannel selection, and the discriminator evaluates how good the fake information generated with its representation of the radio environment is. Over time, the generator can create fake information that cannot be distinguished from the discriminator. Similarly, an actor and a critic are participating in the game. However, both of them are improving over time, unlike GAN.

Actor–Critic is a method that allows tackling challenging problems. The actor can be seen as a policy gradient algorithm, and the value function that evaluates policies is considered to be a critic.

A similar approach used in **Publication IV** was applied in **Publication II**, in which the aim is to optimize the performance of a system of flying base stations (FBSs). Here, the BSs are considered to be deployed in unmanned aerial vehicles (UAVs). Thus, the wireless channel model is updated to prioritize a 3D model in which the height is evaluated with a probabilistic model. In this new contribution, we also consider an ideal backhaul, because our main target was the radio optimization of a cellular system supporting a diversity of services. The radio optimization was carried out by using a similar architecture of DRL. The performance in most of the scenarios was satisfactory.

Algorithm 1 Algorithm of the deep reinforcement learning approach.

▷ Main Loop
while Stop Criteria not met **do**
    SUBCHANNEL SELECTION()
    POWER CONTROL()

▷ Subchannel selection
function SUBCHANNEL SELECTION()
    ▷ Agent subchannel Selection
    State set design $\leftarrow s_{n,m}^{(t)}$ (setting base station and UE pairs for each specific state)
    Training by Critic and Actor Network
    Training by ACTOR NETWORK()
    Training by CRITIC NETWORK()
    Reward function design
    Update Policies: Ω, γ
    Repeat until optimal policies are achieved

▷ Power Control
function POWER CONTROL()
    ▷ Agent Selection
    agent $\leftarrow a_{n,a_n^{(t)}}^{(t)} \in \mathcal{A}_{\text{power}} = [0, 1]$
    State set design $\leftarrow s_{n,a_n^{(t)}}^{(t)}$
    Training by deep-Q Network
    Reward function design
    Update Policies: θ
    Repeat until optimal policy is achieved

▷ Actor Network
function ACTOR NETWORK()
    ▷ Action Selection
    agent $\leftarrow a_n^{(t)} \in \mathcal{A}_{\text{subchannel}} = \{1, \cdots, M\} = \mathcal{M}$ (frequency reuse selection)
    State set design $\leftarrow s_{n,a_n^{(t)}}^{(t)}$
    Learning based is based on policy gradient
    Update Policies: Ω

▷ Critic Network
function CRITIC NETWORK()
    ▷ Agent feedback
    Evaluation on $\longrightarrow a_n^{(t)}$
    adjustment on $\longrightarrow a_n^{(t)}$
    Evaluate the action produced by the Actor
    Update Policies: γ

3.3.3 Summary

In this contribution, we demonstrated the performance of an optimization based on DRL in a FR setup. This FR setup is a popular scheme to perform a static schedule of subchannels on the available bandwidth when the cellular system operates at sub-1GHz frequencies, such as VHF. In this particular study, the system operates at 250 MHz to achieve a radius of 50 km. As the main drawback of this approach is the intercell interference, we proposed a dynamic scheduling of the frequency reuse or subchannels by adopting a machine learning approach.

We considered deep reinforcement learning based on a conjunction of an actor network and a critic network, which are part of a continuous learning scheme used in machine learning. With this methodology, the system is capable of scheduling the radio resources dynamically over time. This means that there is no intermediate process that would modify the learning process, but it is updated online by itself.

A similar approach was considered in a different setup in which the BSs were mounted on a set of UAVs, named FBS by the state of the art. In this new application, a 3D channel model is considered to accurately model the new environment. However, similar machine learning was considered with satisfactory results in terms of throughput and latency performance.

In the scope of the smart grid, this wireless scenario is feasible in smart grid use cases that are based on a private network operating in sub-1GHz bands because of the large coverage to support critical applications on distribution or transmission power lines by using IEC 61850 messages.

4 Discussion and conclusions

Prediction is very difficult, especially about the future.

— NIELS BOHR

In this chapter, comments and forecasts are made on potential new approaches associated with the proposed RAN slicing framework. This is done considering each individual building element of the framework. Furthermore, an extension of this framework is proposed to support other vertical applications. Finally, the conclusion summarizes the main contributions of this dissertation.

4.1 Forecasting new approaches to support smart grids

The proposed RAN slicing framework, which aims to support the messages that are part of the standard IEC 61850, provides a diversity of elements. Each element represents specific wireless communication network functionalities that can enable the use of a diversity of cellular communication applications.

In the RANA, the system engineering design can take advantage of the distributed flexibility of DUs and the CU to support different IEC 61850 messages aligned to their specific requirements of latency, throughput, and reliability. In some cases, in the functionality that enables URLLC by specialized waveforms such as GFDM, the expectation is that resources deployed in the edge are used massively. In other cases where latency is not the main target, some radio network functions can be deployed through backhaul or fronthaul to support another features, such as reliability, a high user density, and throughput.
In the case of the RIL, isolation is a parameter that can be considered between a conservative and an optimistic range. In particular, messages that require high reliability can consider the use of orthogonal radio resources to reduce the chances of interference. Some messages can be transmitted over shared radio resources. However, it is necessary to use specialized technologies that are capable of operating in scenarios even with interference. For instance, non-orthogonal multiple access (NOMA) is a strong candidate to support this specific level of isolation.

The RSF is probably the building element with a direct impact on the physical layer technologies that are not limited to the waveform design. It can also consider technologies that are nowadays discussed on the research edge, such as cell-free massive MIMO to move from a cellcentric communication to a usercentric approach; reconfigurable intelligent surface (RIS) to control the radio propagation through transceivers that are capable of modifying the phase and gain of reflected surfaces; energy harvesting communication to support energy efficiency, especially in IoT devices or with reduced capabilities; finally, it can consider the semantic communication, regarded by the academy as the breakthrough

beyond the Shannon paradigm.

In the current proposal of the RAN slicing framework, the IRSS considered a centralized DRL to enhance and schedule the available radio resources. This implies that in real deployment, there is a strong dependence on fronthaul and backhaul to enable connectivity between base stations (agents), which can represent an expensive infrastructure to operators. Another approach can consider application of the DRL in a decentralized manner. In other words, a distributed learning process supported by federated learning can enhance the performance of the system based on a decentralized scheduling system.

4.2 Present and future transition in wireless communication and power systems

During the elaboration of this dissertation, the author had the chance to interact with experts in the field on both industries, power systems, and wireless communication. Based on this interaction, some important heuristic takeaways on the integration of both industries were raised.

To formalize some of these speculative thoughts, the multi-level perspective (MLP) methodology was used to explain the present and future of wireless communication and power systems. For this specific MLP evaluation, It is important to note that the smart grids are within the context of the power system industry, and wireless communication is mostly represented by cellular networks. Another important remark is that the focus of this analysis is on the application of wireless communication technologies supporting critical smart grid applications. The MLP is represented by three levels: niche innovations, sociotechnical regimes, and sociotechnical landscapes. Details of each level definition are described in [80].

Technological niches or niche innovations are mostly related to the micro level, where radical novelties usually emerge. These novelties are initially unstable and act as incubation rooms. They are conducted and advanced by small networks of dedicated actors, such as outsiders or marginal actors.

The sociotechnical regimes refer to shared cognitive routines in an engineering community and explain patterned development along technological trajectories. Policymakers, scientists, users, cultural habits, and special-interest groups contribute to the process of patterning it.

The sociotechnical landscape is composed of an exogenous environment beyond the direct influence of niche and regime actors, such as deep cultural patterns, macroeconomics, and macropolitical developments. Rotation at this level usually takes place slowly.

An illustrative description of the present and future of both industries is given in Fig. 4.1. In the sociotechnical dimension, the wireless communication industry rarely achieves sta-

bilizing trajectories because of its continuous evolution, especially in the last decades—since 4G, the current research and development of 5G, until the current academic research on 6G. In contrast, the power system industry is represented by a regime that is stabilized and rigid, usually with resistance to new innovations on using wireless communication for critical applications because of its conservative nature.

In the technological niches, both industries are always generating new innovations and research outcomes. However, the power industry is usually locked in because of the stabilized and conservative sociotechnical regime. On the other hand, the wireless communication industry is influenced by the expectation of the sociotechnical landscape and the sociotechnical regime to remain a series of new generations, such as 5G in 2010 and 6G in 2022 and beyond.

Finally, in the case of the sociotechnical landscape, the power system industry is characterized by a slowly evolving landscape in the medium/long term. The landscape of the wireless communication industry is opposite to the power system industry because it is usually represented by a turbulent sociotechnical landscape, driven mostly by the digitalization of verticals and new user experiences that require low-latency and high-reliability data communication.

Our personal expectation in the future is that the current effort in the research and development of 6G in the wireless industry will have an impact on the power system landscape around 2035 or before. This disruptive change of scenario in the power system will represent an inflection point that will generate new user experiences, new policies, and especially new markets and user preferences.

4.3 Proposing a generic framework supporting verticals

In this research work, our main motivation is the power system vertical. However, the same framework can be applied to a diversity of industrial verticals. For example, the mining industry requires connectivity in remote and sometimes uninhabitable scenarios. In some cases, connectivity is required in underground mines, which usually involves high personnel costs. Thus, solutions that aim to increase safety and reduce human errors call for the utilization of special machines, which require specialized and flexible connectivity. In the case of oil and gas industry, connectivity is usually required in both onshore plants and offshore operations. Here, the impact of the RAN slicing framework is relevant, especially to provide flexibility in the selection of the isolation level in the RIL element to discriminate a diversity of applications in scenarios in which backhaul and fronthaul are limited.

In the last few years, the COVID-19 pandemic has been a catalyst that highlighted the fundamental role of connectivity in the lives of citizens and also in the communication networks supporting hospitals. In this context, the proposed framework may enhance specialized radio slices in specialized medical applications requiring low-latency com-

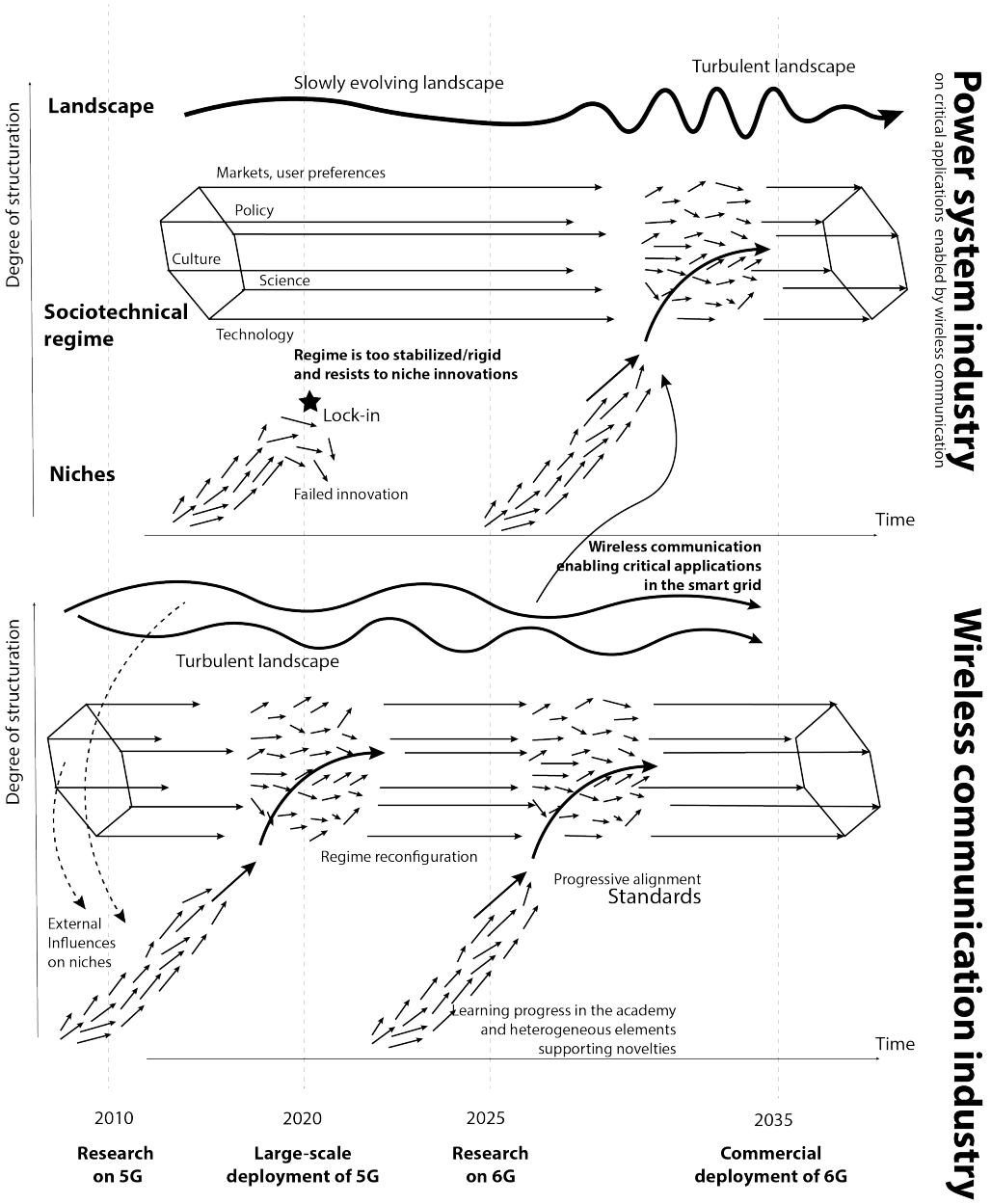

Figure 4.1: MLP representation in the time and degree of structure domains for both industries: power systems and wireless communication. Here, the analysis is based on critical applications in power systems enabled by wireless communication systems.

munication for remote operations and high-density user communication for full-buffer applications.

Other industrial verticals that can be supported by the proposed framework are, e.g., the chemical industry, the steel production industry, the heavy-duty trucking industry, the maritime shipping industry, and the aviation industry.

In all cases there is a lack of mapping between current communication networks (in some cases still using wired technologies) and the cellular network is not yet specified, at least not in the 3GPP forum.

4.4 Conclusions

Achieving the goals of the digital green transition to make Europe the first climate-neutral continent by 2050 depends on mitigation actions in large-scale infrastructures, such as energy systems. Here, the use of cutting-edge communication technologies plays a fundamental role in connecting all elements in the smart grid. For this purpose, a RAN slicing framework was proposed to enable the standard IEC 61850 supporting smart grid applications.

The proposed RAN slicing framework provides flexibility and adaptability based on the use of all building elements, such as RANA, RIL, RSF, RSM, and IRSS. This framework can be used in future standardization efforts to create interfaces and maps between the current IEC 61850 standards and 3GPP standard evolution.

Based on the proposed framework, two building elements were the main focus of the study. The first is the RSF; here, we considered the GFDM as a waveform with high chances to complement current OFDM systems. In this context, our contribution was related to an analytical methodology that enables the evaluation of the GFDM system in Rayleigh channels. Here, we obtained a semiclosed form of the SINR on Rayleigh distribution. This mathematical model enabled us to obtain key KPIs, such as BER, achievable sum rate, and outage probability.

Another building element of the proposed RAN slicing framework is the IRSS. Here, a DRL approach was adopted to efficiently schedule the RAN slices. Here, the SLA was evaluated following the system requirements established by the standard IEC 61850.

In summary, the current cellular network cannot support critical applications in the smart grid industry. However, an alternative is the RAN slicing framework that provides a set of building blocks or elements to enable low-latency and reliability requirements with specialized improvements in the scheduling of the radio resources with a DRL approach.

It is expected that before 2035, critical smart grid applications will be enabled by 6G and disruptive technologies, such as machine learning applied to radio interface functionalities, such as RAN slicing to support a diversity of vertical industries.

References

[1] A. GeSI, "SMARTer2030-ICT solutions for 21st century challenges," *Executive Summary*, 2015.

[2] S. F. Bush, S. Goel, and G. Simard, "Ieee vision for smart grid communications: 2030 and beyond roadmap," *IEEE Vision for Smart Grid Communications: 2030 and Beyond Roadmap*, pp. 1–19, 2013.

[3] J. Hu and A. Lanzon, "Distributed finite-time consensus control for heterogeneous battery energy storage systems in droop-controlled microgrids," *IEEE Transactions on Smart Grid*, vol. 10, no. 5, pp. 4751–4761, 2019.

[4] M. Lee, O. Aslam, B. Foster, D. Kathan, J. Kwok, L. Medearis, R. Palmer, P. Sporborg, and M. Tita, "Assessment of demand response and advanced metering," *Federal Energy Regulatory Commission, Tech. Rep*, 2013.

[5] M. S. Saleh, A. Althaibani, Y. Esa, Y. Mhandi, and A. A. Mohamed, "Impact of clustering microgrids on their stability and resilience during blackouts," in *2015 International Conference on Smart Grid and Clean Energy Technologies (ICSGCE)*. IEEE, 2015, pp. 195–200.

[6] J. C. Das, *Power system protective relaying*, ser. Power Systems Handbook. Boca Raton: Taylor Francis, a CRC title, part of the Taylor Francis imprint, a member of the Taylor Francis Group, the academic division of TF Informa, plc, 2018.

[7] "*Communication Networks and Systems in Substations – Part 5: Communication Requirements for Functions and Device Models*," IEC-61850, Standard, 2003.

[8] V. Skendzic and A. Guzma, "Enhancing Power System Automation Through the Use of Real-Time Ethernet," in *2006 Power Systems Conference: Advanced Metering, Protection, Control, Communication, and Distributed Resources*, 2006, pp. 480–495.

[9] F. Ye, *Smart Grid Communication Infrastructures*, 1st ed. Wiley-IEEE Press, 2018.

[10] P. Bishop and N. K. C. Nair, *IEC 61850 Principles and Applications to Electric Power Systems*. Springer, 2023.

[11] P. P. Parikh, T. S. Sidhu, and A. Shami, "A Comprehensive Investigation of Wireless LAN for IEC 61850–Based Smart Distribution Substation Applications," *IEEE Transactions on Industrial Informatics*, vol. 9, no. 3, pp. 1466–1476, 2013.

[12] A. M. Gaouda, A. Abdrabou, K. B. Shaban, M. Khairalla, A. M. Abdrabou, R. El Shatshat, and M. M. A. Salama, "A Smart IEC 61850 Merging Unit for Impending Fault Detection in Transformers," *IEEE Transactions on Smart Grid*, vol. 9, no. 3, pp. 1812–1821, 2018.

[13] E. Harmon, U. Ozgur, M. H. Cintuglu, R. de Azevedo, K. Akkaya, and O. A. Mohammed, "The Internet of Microgrids: A Cloud-Based Framework for Wide Area Networked Microgrids," *IEEE Transactions on Industrial Informatics*, vol. 14, no. 3, pp. 1262–1274, 2018.

[14] S. M. S. Hussain, T. S. Ustun, P. Nsonga, and I. Ali, "IEEE 1609 WAVE and IEC 61850 Standard Communication Based Integrated EV Charging Management in Smart Grids," *IEEE Transactions on Vehicular Technology*, vol. 67, no. 8, pp. 7690–7697, 2018.

[15] M. Mekkanen and K. Kauhaniemi, "Wireless Light-Weight IEC 61850 Based Loss of Mains Protection for Smart Grid," *Open Engineering*, vol. 8, no. 1, pp. 182–192, 2018. [Online]. Available: https://doi.org/10.1515/eng-2018-0022

[16] S. M. S. Hussain, M. A. Aftab, and T. S. Ustun, "Performance Analysis of IEC 61850 Messages in LTE Communication for Reactive Power Management in Microgrids," *Energies*, vol. 13, no. 22, 2020. [Online]. Available: https://www.mdpi.com/1996-1073/13/22/6011

[17] Z. Idrees, J. Granados, Y. Sun, S. latif, L. Gong, Z. Zou, and L. Zheng, "IEEE 1588 for Clock Synchronization in Industrial IoT and Related Applications: A Review on Contributing Technologies, Protocols and Enhancement Methodologies," *IEEE Access*, vol. 8, 2020. [Online]. Available: https://doi-org.ezproxy.cc.lut.fi/10.1109/ACCESS.2020.3013669

[18] I. Serban, S. Céspedes, C. Marinescu, C. A. Azurdia-Meza, J. S. Gómez, and D. S. Hueichapan, "Communication Requirements in Microgrids: A Practical Survey," *IEEE Access*, vol. 8, pp. 47 694–47 712, 2020.

[19] C. Kalalas, L. Gkatzikis, C. Fischione, P. Ljungberg, and J. Alonso-Zarate, "Enabling IEC 61850 communication services over public LTE infrastructure," in *2016 IEEE International Conference on Communications (ICC)*, 2016, pp. 1–6.

[20] V. Dehalwar, A. Kalam, M. L. Kolhe, A. Zayegh, and A. K. Dubey, "Integration of IEC 61850 MMS and IEEE 802.22 for Smart Grid Communication," in *Networking Communication and Data Knowledge Engineering*, G. M. Perez, K. K. Mishra, S. Tiwari, and M. C. Trivedi, Eds. Singapore: Springer Singapore, 2018, pp. 79–88.

[21] L. Eriksson, "Performance Evaluation of IEC 61850-90-5 Over a Non-Commercial 4G LTE Network," Master's thesis, 2017.

[22] P. P. Parikh, "Investigation of Wireless LAN for IEC 61850 based Smart Distribution SubstationsDistribution Substations," Ph.D. dissertation, 2012.

[23] A. Khavnekar, S. Wagh, and A. More, "Comparative analysis of IEC 61850 Edition-I and II standards for substation automation," in *2015 IEEE International Conference on Computational Intelligence and Computing Research (ICCIC)*, 2015, pp. 1–6.

[24] "*Basic communication structure- ASCI*," IEC-61850, Standard, 2003.

[25] "*Introduction and Overview*," IEC-61850, Standard, 2003.

[26] T.-K. Le, U. Salim, and F. Kaltenberger, "An overview of physical layer design for ultra-reliable low-latency communications in 3gpp releases 15, 16, and 17," *IEEE Access*, vol. 9, pp. 433–444, 2021.

[27] A. Rico-Alvariño, I. Bouazizi, M. Griot, P. Kadiri, L. Liu, and T. Stockhammer, "3GPP Rel-17 Extensions for 5G Media Delivery," *IEEE Transactions on Broadcasting*, vol. 68, no. 2, pp. 422–438, 2022.

[28] G. Medina-Acosta, L. Zhang, J. Chen, K. Uesaka, Y. Wang, O. Lundqvist, and J. Bergman, "3GPP Release-17 Physical Layer Enhancements for LTE-M and NB-IoT," *IEEE Communications Standards Magazine*, vol. 6, no. 4, pp. 80–86, 2022.

[29] M. M. Saad, M. A. Tariq, J. Seo, and D. Kim, "An Overview of 3GPP Release 17 & 18 Advancements in the Context of V2X Technology," in *2023 International Conference on Artificial Intelligence in Information and Communication (ICAIIC)*, 2023, pp. 057–062.

[30] X. Lin, "An Overview of 5G Advanced Evolution in 3GPP Release 18," *IEEE Communications Standards Magazine*, vol. 6, no. 3, pp. 77–83, 2022.

[31] W. Chen, X. Lin, J. Lee, A. Toskala, S. Sun, C. F. Chiasserini, and L. Liu, "5G-Advanced Toward 6G: Past, Present, and Future," *IEEE Journal on Selected Areas in Communications*, vol. 41, no. 6, pp. 1592–1619, 2023.

[32] H. Zhang, S. Leng, Y. Wei, and J. He, "A Blockchain Enhanced Coexistence of Heterogeneous Networks on Unlicensed Spectrum," *IEEE Transactions on Vehicular Technology*, vol. 71, no. 7, pp. 7613–7624, 2022.

[33] P. Wang, B. Di, and L. Song, "Cellular Communications Over Unlicensed mmWave Bands With Hybrid Beamforming," *IEEE Transactions on Wireless Communications*, vol. 21, no. 8, pp. 6064–6078, 2022.

[34] I. F. Akyildiz, C. Han, Z. Hu, S. Nie, and J. M. Jornet, "Terahertz Band Communication: An Old Problem Revisited and Research Directions for the Next Decade," *IEEE Transactions on Communications*, vol. 70, no. 6, pp. 4250–4285, 2022.

[35] M. Bellanger, D. Le Ruyet, D. Roviras, M. Terré, J. Nossek, L. Baltar, Q. Bai, D. Waldhauser, M. Renfors, T. Ihalainen *et al.*, "FBMC physical layer: a primer," *PHYDYAS, January*, vol. 25, no. 4, pp. 7–10, 2010.

[36] N. Michailow, M. Matthé, I. S. Gaspar, A. N. Caldevilla, L. L. Mendes, A. Festag, and G. Fettweis, "Generalized Frequency Division Multiplexing for 5th Generation Cellular Networks," *IEEE Transactions on Communications*, vol. 62, no. 9, pp. 3045–3061, 2014.

[37] A. Aminjavaheri, A. Farhang, A. RezazadehReyhani, and B. Farhang-Boroujeny, "Impact of timing and frequency offsets on multicarrier waveform candidates for 5G," in *2015 IEEE Signal Processing and Signal Processing Education Workshop (SP/SPE)*, 2015, pp. 178–183.

[38] M. Vaezi, Z. Ding, and H. V. Poor, *Multiple access techniques for 5G wireless networks and beyond*. Springer, 2019, vol. 159.

[39] C. Shin, R. W. Heath, and E. J. Powers, "Non-Redundant Precoding-Based Blind and Semi-Blind Channel Estimation for MIMO Block Transmission With a Cyclic Prefix," *IEEE Transactions on Signal Processing*, vol. 56, no. 6, pp. 2509–2523, June 2008.

[40] S. Tiwari, S. S. Das, and K. K. Bandyopadhyay, "Precoded Generalized Frequency Division Multiplexing System to Combat Intercarrier Interference: Performance Analysis," *IET Communications*, vol. 9, no. 15, pp. 1829 – 1841, May 2015.

[41] C. V. Nahum, L. De Novoa Martins Pinto, V. B. Tavares, P. Batista, S. Lins, N. Linder, and A. Klautau, "Testbed for 5G Connected Artificial Intelligence on Virtualized Networks," *IEEE Access*, vol. 8, pp. 223 202–223 213, 2020.

[42] J. Malik, A. Akhunzada, I. Bibi, M. Imran, A. Musaddiq, and S. W. Kim, "Hybrid Deep Learning: An Efficient Reconnaissance and Surveillance Detection Mechanism in SDN," *IEEE Access*, vol. 8, pp. 134 695–134 706, 2020.

[43] Z. Lu, C. Zhong, and M. C. Gursoy, "Dynamic Channel Access and Power Control in Wireless Interference Networks via Multi-Agent Deep Reinforcement Learning," *IEEE Transactions on Vehicular Technology*, vol. 71, no. 2, pp. 1588–1601, 2022.

[44] A. A. S. AlQahtani and N. Choudhury, "Machine learning for location prediction using rssi on wi-fi 2.4 ghz frequency band," in *2021 IEEE 12th Annual Information Technology, Electronics and Mobile Communication Conference (IEMCON)*, 2021, pp. 0336–0342.

[45] Y. Wang, Y. Zhang, J. Sun, G. Gui, T. Ohtsuki, and F. Adachi, "A novel compression csi feedback based on deep learning for fdd massive mimo systems," in *2021 IEEE Wireless Communications and Networking Conference (WCNC)*, 2021, pp. 1–5.

[46] O. Iacoboaiea, B. Sayrac, S. Ben Jemaa, and P. Bianchi, "Coordinating son instances: Reinforcement learning with distributed value function," in *2014 IEEE 25th Annual International Symposium on Personal, Indoor, and Mobile Radio Communication (PIMRC)*, 2014, pp. 1642–1646.

[47] J. Hughes *et al.*, "With the Future in Mind, Ameren Charts a New Course with its Private Comms Networks," *Utilities Technology Council Journal*, vol. 1, no. 1, 2020 [On line].

[48] K. C. Budka *et al.*, *Communication Networks for Smart Grids*. Springer, 2016.

[49] SNS Telecom & IT. (2019) The Private LTE and 5G Network Ecosystem: 2020 - 2030 - Opportunities, Challenges, Strategies, Industry Verticals Forecasts. [Online]. Available: https://www.snstelecom.com/private-lte

[50] FCC, "PDV Spectrum Holding Company - 0945-EX-CN-2018," FCC, Tech. Rep., 2018.

[51] C. Sexton *et al.*, "Customization and Trade-offs in 5G RAN Slicing," *IEEE Commun. Mag.*, vol. 57, no. 4, pp. 116–122, 2019.

[52] B. Das, *Power Distribution Automation*. Institution of Engineering and Technology (IET), 2016.

[53] J. Li, W. Shi, P. Yang, Q. Ye, X. S. Shen, X. Li, and J. Rao, "A Hierarchical Soft RAN Slicing Framework for Differentiated Service Provisioning," *IEEE Wireless Commun.*, vol. 27, no. 6, pp. 90–97, 2020.

[54] J. Mei, X. Wang, K. Zheng, G. Boudreau, A. B. Sediq, and H. Abou-Zeid, "Intelligent Radio Access Network Slicing for Service Provisioning in 6G: A Hierarchical Deep Reinforcement Learning Approach," *IEEE Transactions on Communications*, vol. 69, no. 9, pp. 6063–6078, 2021.

[55] G. Wunder, P. Jung, M. Kasparick, T. Wild, F. Schaich, Y. Chen, S. T. Brink, I. Gaspar, N. Michailow, A. Festag, L. Mendes, N. Cassiau, D. Ktenas, M. Dryjanski, S. Pietrzyk, B. Eged, P. Vago, and F. Wiedmann, "5GNOW: non-orthogonal, asynchronous waveforms for future mobile applications," *IEEE Communications Magazine*, vol. 52, no. 2, pp. 97–105, February 2014.

[56] B. Farhang-Boroujeny and H. Moradi, "OFDM Inspired Waveforms for 5G," *IEEE Communications Surveys Tutorials*, vol. 18, no. 4, pp. 2474–2492, 2016.

[57] D. Zhang, A. Festag, and G. P. Fettweis, "Performance of Generalized Frequency Division Multiplexing Based Physical Layer in Vehicular Communications," *IEEE Transactions on Vehicular Technology*, vol. 66, no. 11, pp. 9809–9824, 2017.

[58] Y. Yang, L. Zhu, X. Mao, Q. Tan, and Z. He, "The Spread Spectrum GFDM Schemes for Integrated Satellite-terrestrial Communication System," *China Communications*, vol. 16, no. 12, pp. 165–175, 2019.

[59] Y. Yang, L. Zhu, and Z. He, "An Interference-Free GFDM Transmission Scheme for Integrated Satellite-Terrestrial Communication," in *2018 IEEE Global Communications Conference (GLOBECOM)*, 2018, pp. 1–6.

[60] L. Mendes, N. Michailow, M. Matthé, I. Gaspar, D. Zhang, and G. Fettweis, "GFDM: Providing Flexibility for the 5G Physical Layer," *Opportunities in 5G Networks: A Research and Development Perspective*, pp. 325–390, 2016.

[61] D. Zhang, M. Matthé, L. L. Mendes, and G. Fettweis, "A Study on the Link Level Performance of Advanced Multicarrier Waveforms Under MIMO Wireless Communication Channels," *IEEE Transactions on Wireless Communications*, vol. 16, no. 4, pp. 2350–2365, 2017.

[62] J. G. Proakis, *Digital Communications*, 3rd ed. McGraw-Hill, 1995.

[63] A. Paulraj, R. Nabar, and D. Gore, *Introduction to Space-time Wireless Communications*. Cambridge university press, 2003.

[64] P. Li, D. Paul, R. Narasimhan, and J. Cioffi, "On the Distribution of SINR for the MMSE MIMO Receiver and Performance Analysis," *IEEE Trans. Inf. Theory*, vol. 52, no. 1, pp. 271 – 286, Jan 2006.

[65] K. Cho and D. Yoon, "On the general BER expression of one-and two-dimensional amplitude modulations," *IEEE Trans. on Commun.*, vol. 50, no. 7, pp. 1074–1080, Jul 2002.

[66] C. Zhong, M. Matthaiou, A. Huang, and Z. Zhang, "On the sum rate of MIMO Nakagami-m fading channels with MMSE receivers," in *2012 IEEE 7th Sensor Array and Multichannel Signal Processing Workshop (SAM)*, June 2012, pp. 49–52.

[67] A. Maaref and S. Aissa, "Closed-form expressions for the outage and ergodic Shannon capacity of MIMO MRC systems," *IEEE Transactions on Communications*, vol. 53, no. 7, pp. 1092–1095, July 2005.

[68] P. Wijesinghe, U. Gunawardana, and R. Liyanapathirana, "An Efficient Algorithm for Capacity and Outage Probability Estimation in MIMO Channels," *IEEE Communications Letters*, vol. 15, no. 6, pp. 644–646, June 2011.

[69] A. Jha and D. Saha, "Techno-economic assessment of the potential for LTE based 4G mobile services in rural India," in *2015 IEEE International Conference on Advanced Networks and Telecommuncations Systems (ANTS)*, Dec 2015, pp. 1–6.

[70] C. Ovando, J. Pérez, and A. Moral, "LTE techno-economic assessment: The case of rural areas in Spain," *Telecommunications Policy*, vol. 39, no. 3-4, pp. 269–283, 2015.

[71] M. Lauridsen, I. Z. Kovacs, P. Mogensen, M. Sorensen, and S. Holst, "Coverage and Capacity Analysis of LTE-M and NB-IoT in a Rural Area," in *2016 IEEE 84th Vehicular Technology Conference (VTC-Fall)*, Sep. 2016, pp. 1–5.

[72] M. Lauridsen, L. C. Gimenez, I. Rodriguez, T. B. Sorensen, and P. Mogensen, "From LTE to 5G for Connected Mobility," *IEEE Communications Magazine*, vol. 55, no. 3, pp. 156–162, 2017.

[73] P. Gawlowicz, N. Baldo, and M. Miozzo, "An Extension of the Ns-3 LTE Module to Simulate Fractional Frequency Reuse Algorithms," in *Proceedings of the 2015 Workshop on Ns-3*, ser. WNS3 '15, 2015, pp. 98–105.

[74] S. Sadr, A. Anpalagan, and K. Raahemifar, "Radio Resource Allocation Algorithms for the Downlink of Multiuser OFDM Communication Systems," *IEEE Communications Surveys Tutorials*, vol. 11, no. 3, pp. 92–106, rd 2009.

[75] C. Feijóo, J. Gómez-Barroso, and S. Ramos, "An analysis of next generation access networks deployment in rural areas," in *2011 50th FITCE Congress - "ICT: Bridging an Ever Shifting Digital Divide"*, Aug 2011, pp. 1–18.

[76] Y. Wei and S.-H. Hwang, "Investigation of spectrum values in rural environments," *ICT Express*, vol. 4, no. 4, pp. 234 – 238, 2018.

[77] Agência Nacional de Telecomunicacões (ANATEL), "Resolucão n 555, de 20 de dezembro de 2010," Dec. 2010.

[78] A. Medeisis and A. Kajackas, "On the use of the universal Okumura-Hata propagation prediction model in rural areas," in *VTC2000-Spring. 2000 IEEE 51st Vehicular Technology Conference Proceedings (Cat. No.00CH37026)*, vol. 3, 2000, pp. 1815–1818.

[79] M. Morales, *Grokking deep reinforcement learning*. Manning Publications, 2020.

[80] F. W. Geels and J. Schot, "Typology of sociotechnical transition pathways," *Research policy*, vol. 36, no. 3, pp. 399–417, 2007.

Publication I

Carrillo, D., Kalalas, C., Raussi, P., Michalopoulos, D., Zegarra, D., Hokkoniemi-Tarkkanen, H., Ahola, K., Nardelli, P., Fraidenraich, G., and Popovski, P.
Boosting 5G on Smart Grid Communication: A Smart RAN Slicing Approach

Reprint with permission from
IEEE Wireless Communications
Early access, pp. 1–8, 2022. (in press)

Boosting 5G on Smart Grid Communication: A Smart RAN Slicing Approach

Dick Carrillo, Charalampos Kalalas, Petra Raussi, Diomidis S. Michalopoulos, Demóstenes Z. Rodríguez, Heli Kokkoniemi-Tarkkanen, Kimmo Ahola, Pedro H. J. Nardelli, Gustavo Fraidenraich, and Petar Popovski

***Abstract*—Fifth-generation (5G) and beyond systems are expected to accelerate the ongoing transformation of power systems towards the smart grid. However, the inherent heterogeneity in smart grid services and requirements pose significant challenges towards the definition of a unified network architecture. In this context, radio access network (RAN) slicing emerges as a key 5G enabler to ensure interoperable connectivity and service management in the smart grid. This article introduces a novel RAN slicing framework which leverages the potential of artificial intelligence (AI) to support IEC 61850 smart grid services. With the aid of deep reinforcement learning, efficient radio resource management for RAN slices is attained, while conforming to the stringent performance requirements of a smart grid self-healing use case. Our research outcomes advocate the adoption of emerging AI-native approaches for RAN slicing in beyond-5G systems, and lay the foundations for differentiated service provisioning in the smart grid.**

***Index Terms*—RAN slicing, smart grid, smart substations, 5G, IEC 61850.**

I. Introduction and Motivation

In recent years, the ongoing modernization of the aging power systems towards the smart grid has mainly relied on three prevailing trends: (i) *large-scale information acquisition*, with the massive deployment of smart meters to keep track of energy consumption; (ii) *reliable monitoring, protection, and control*, where intelligent electronic devices (IEDs) offer situational awareness and rapid fault detection; and (iii) *integration of distributed energy resources (DERs)*, which results in high power system dynamics and a growing need for real-time grid supervision to ensure stability. On top of the drivers mentioned above, the deregulation of energy markets and the need for advanced security against hostile cyberattacks have a significant impact on the transformation of power systems.

Instrumental to this paradigm shift is the underlying communication infrastructure deployed for robust, scalable, and reliable connectivity among the power system components [1]. Connectivity in power systems currently involves a plethora of technologies, ranging from optical fibers and power line communication to wireless technologies and satellite networks. Among those, wired connectivity schemes have been extensively used in power systems for localized mission-critical applications. Notwithstanding, wireless solutions exploit the advantages of lower deployment/maintenance cost and their intrinsic scalable characteristics to offer enhanced grid functionalities [2]. For example, in distribution automation, IEDs need to timely exchange protection-related messages for fast decision-making to avoid extensive disturbances to the entire grid. On the other hand, advanced metering installations require highly scalable network deployments to manage meter readings from consumers located at disparate spatial locations.

The advent of fifth-generation (5G) and beyond communication networks is expected to revolutionize traditional power systems by supporting a wide range of real-time and autonomous operations [3]. Unlike previous mobile network generations, 5G systems are designed to enable three key generic services with broadly diverging operational requirements, i.e., enhanced mobile broadband (eMBB), massive machine-type communication (mMTC), and ultra-reliable low-latency communication (uRLLC). Cellular networks are progressively becoming ubiquitous with omnipresent applicability in vertical industries. Thus, the business potential of 5G in the smart grid domain can be remarkably high with the realization of unprecedented use cases, such as millisecond-level precise load control, decentralized fault detection and self-healing operation, and predictive maintenance of grid infrastructure [4]. Among the pivotal 5G novelties, radio access network (RAN) slicing allows the partition of radio resources into logically isolated radio networks, each one interpreted as a RAN slice. RAN slicing is recently gaining momentum as an enabling platform for the integration of vertical services over a shared physical infrastructure.

One of the key challenges for the realization of RAN slicing relates to the efficient resource management among RAN slices, each of them customized to meet diverse quality-of-service (QoS) requirements. A RAN soft-slicing approach based on network-level resource pre-allocation is proposed in [5] to enable opportunistic resource sharing among slices and support instantaneous service demands. With the aim of improving resource utilization efficiency, the RAN slicing control strategy in [6] adopts multiple time-resource granularities, where radio resources can be dynamically shared between slices. However, the potential of RAN slicing on addressing the inherent smart grid service heterogeneity has not yet been adequately explored in the literature. Focusing on smart grid service provisioning, this article introduces a beyond-5G RAN slicing framework using the IEC 61850 standard to define smart grid communication requirements. In summary, our contribution is threefold:

1) We present a comprehensive categorization of 5G-enabled smart grid services, highlighting the role of RAN slicing on their efficient integration.
2) We propose a novel RAN slicing framework empowered by artificial intelligence (AI) for the accommodation of IEC 61850 services in beyond-5G systems.
3) We demonstrate the feasibility of our approach in a smart

TABLE I
CATEGORIZATION OF 5G-ENABLED SMART GRID SERVICES AND THEIR RELATIONSHIP WITH NETWORK SLICES

Service category	Latency	Reliability	Bandwidth	Node density	Service priority	SST value
Smart distribution automation	Low	High	Low	Medium/Low	High	2 (uRLLC)
Wide-area monitoring, control, and protection	Low/Medium	High/Medium	Medium/Low	Medium	Medium/High	1 (eMBB), 2 (uRLLC), 3 (mMTC)
Metering data acquisition	Medium/High	Medium/Low	Medium/High	High	Low/Medium	3 (mMTC)
Distributed generation integration and microgrids	Low/Medium	High	Low	Medium/High	Medium/High	2 (uRLLC), 3 (mMTC)
Volume and price balancing	Medium/High	Medium/Low	Medium/High	Medium/High	Low	1 (eMBB), 3 (mMTC)

grid self-healing use case, where efficient radio resource allocation is achieved while conforming to peculiar QoS requirements.

The rest of the paper is organized as follows: Section II presents a classification of smart grid services enabled by 5G systems and their associated slices. Section III describes key aspects of RAN slicing and highlights the major benefits for smart grid communication from technological and business perspective. Section IV introduces our proposed RAN slicing framework for IEC 61850 services, with a comprehensive description of its building blocks. Section V outlines our AI-based methodology and presents a performance assessment pertaining to a smart grid communication scenario. Finally, concluding remarks are summarized in Section VI.

II. CLASSIFICATION OF 5G-ENABLED SMART GRID SERVICES

Two interdependent domains form the smart grid infrastructure: *i)* a hierarchical power system, covering multi-directional power flow steps from generation to final consumption; and *ii)* a two-way communication system, enabling extensive information exchange. In what follows, we provide a categorization of 5G-enabled smart grid services and we highlight the relationship with 5G network slices based on their requirements.

A. Smart Distribution Automation

Distribution automation allows power distribution systems to reconfigure themselves when a fault occurs, restricting the problem to a smaller area [2]. Rapid fault location, isolation, and service restoration offered by IEDs and other controllable units reduce the total outage time and the number of interruptions. 5G-enabled distribution automation aims to achieve real-time situational awareness and quasi-real-time analysis of the grid behaviour by supporting advanced functionalities, e.g., automated feeder switching and optimized restoration dispatch. Such operations are often linked to stringent performance requirements, i.e., very low end-to-end latency and ultra-high reliability, falling under the uRLLC network slice.

B. Wide-Area Monitoring, Control, and Protection

Power system operators install sensors on critical grid components, such as power lines and transformer banks, to measure equipment status parameters. Such measurements provide real-time alerts for abnormal conditions and outage information to support utilities in predicting equipment maintenance and replacement. By exploiting 5G and beyond communication infrastructure, wide-area monitoring systems aim to enhance traditional supervisory control and data acquisition (SCADA) systems, offering advanced supervision capabilities [3]. Since the characteristics of the monitoring elements vary, this service category requires a synergistic mix of uRLLC, mMTC, and eMBB slices.

C. Metering Data Acquisition

The massive deployment of smart meters for large-scale information acquisition constitutes one of the principal components of next-generation power systems [7]. Smart meters continuously evolve to sophisticated computing units, which gather, process, and transmit user consumption information to data aggregation units for further processing and analysis. The advanced mMTC capabilities of beyond-5G systems are instrumental for generating unprecedented volumes of metering information. In addition, advanced metering systems can leverage the distributed information processing and storage architecture of 5G and beyond core networks, supporting fog computing platforms for localized decision-making.

D. Distributed Generation Integration and Microgrids

By providing higher fault tolerance and islanding detection, 5G-enabled smart grids enable safer and more reliable connections of distributed generation units, e.g., solar photovoltaic panels, wind turbines, and natural-gas-powered fuel cells. The increasing penetration of renewable energy sources gives rise to the microgrid paradigm, which acts as a single controllable entity concerning the grid, i.e., operation in either a grid-connected or island mode. Integrating intermittent renewable sources and microgrid management require advanced control techniques and networking schemes for seamless operation, especially when the energy storage capacity is low. The diverse requirements introduced by this service category are a combination of traditional uRLLC and mMTC network slices.

E. Volume and Price Balancing

The introduction of smart grid has pushed the roll-out of demand response programs with flexible management of energy consumption at consumer ends in response to supply conditions regulated by the utility providers [4]. Through extensive information exchange provided by 5G networks, energy consumers can be transformed into prosumers, who interact and collaborate by producing, consuming, storing, and exchanging energy on a peer-to-peer basis. Such decentralized energy optimization strategies, performed locally, allow markets to determine prices accurately, resulting in cost savings. Considering a high number of prosumers and market

information exchanges with historical load data, this service category requires a combination of mMTC and eMBB.

Table I summarizes the categorization of 5G-enabled smart grid services with their associated network slice(s), indicated by the standardized slice/service type (SST) index. It is worth noting that each SST may be linked to diverse requirements within the same slice, with the aid of a slice differentiator parameter which builds customized fine-grained slices.

III. RAN Slicing for the Smart Grid

This section highlights key aspects of RAN slicing, underlying the benefits of integrating the multi-faceted connectivity landscape of smart grid services, from both technological and business perspectives.

A. Key Features

In stark contrast to previous mobile network generations, the 5G architecture leverages cloud-native concepts to allow the disaggregation and virtualization of network functions [8]. By leveraging virtualized network function management, smart grid services can be instantiated in a flexible manner, following a network-as-a-service model. This architectural shift towards network softwarization allows differentiated handling of smart grid traffic types, and ensures their harmonic coexistence with proper allocation of storage, computing, processing and radio resources. A slice-based 5G RAN can efficiently address the inherent smart grid service heterogeneity, as illustrated in Fig. 1, and offers significant benefits summarized as follows:

1) Service isolation: Network resources of a smart grid service can be isolated from other service resources in a resilient manner without violating the agreed service-level agreements (SLAs). In addition to increased security/privacy, service isolation offers a higher reliability potential owing to the guaranteed resources required to achieve stringent performance requirements, e.g., ultra-high reliability for protection-related functions in substation communication.

2) Tenant-oriented virtual network: RAN slice tenants are able to operate their own dedicated network and manage the provisioning of customized network components based on the adopted business models. The tenant can be an individual energy consumer or a power system utility that leases and occupies RAN slice instances. By allowing partial/full control of the virtualized end-to-end networks to tenants, RAN slicing clearly differentiates from other network sharing techniques, offering new roles to energy players.

3) Guaranteed SLA: RAN slicing offers differentiated service provisioning with QoS guarantees based on negotiated SLAs. A management and orchestration entity is responsible for mapping the requirements established in SLAs into the functional elements of RAN slices. Due to the mission-critical nature of certain smart grid services, SLA monitoring needs to be predictive while ensuring efficient radio resource utilization. In this context, the exploitation of emerging AI techniques holds the promise of conforming to SLAs by exploiting slice state information.

4) Customization capabilities: The implementation of customized functions is a key RAN slicing feature, given the highly diverse service ecosystem in smart grids. By leveraging edge computing, decision-making and intelligence can be shifted closer to the network endpoints, achieving faster response times and targeted operational actions. Agile function placement facilitates the support of new use cases and often results in reduced installation/operational cost for utilities.

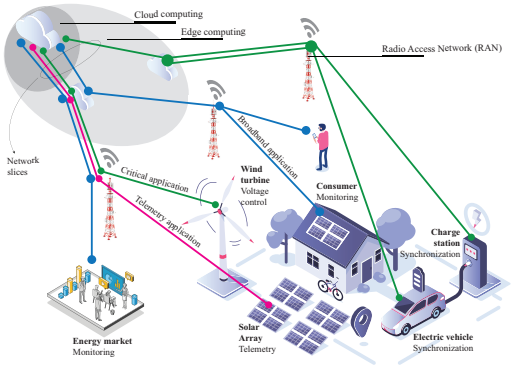

Fig. 1. RAN slicing supports a variety of smart grid services, creating multiple isolated logical networks on top of an underlying physical infrastructure.

5) Distributed architecture: RAN slicing promotes a decentralized structure of the smart grid against the traditional model, in which non-cooperative systems are deployed and managed independently in a hierarchical manner. On-demand deployment of virtual functions facilitates the seamless integration of DERs and paves the way towards a *prosumer-centric* vision of future power systems. Smart grid protection services requiring low latency can be performed autonomously rather than being delegated to a central management unit [3].

B. Business Potential

The support of 5G-enabled smart grid services via RAN slicing comes along with a continuously rising number of subscriptions and traffic demand, giving rise to significant business opportunities. The stakeholders, i.e., the beneficiaries in the network slicing ecosystem, consist of the network slice subnet instance (NSSI) provider, the intermediate-network slice instance (NSI) provider, the end-to-end network slice instance (E2E-NSI) provider, the slice tenant, and the end customer. In some cases, multiple network slice providers may coexist to provide an E2E slice, while in other business scenarios a single mobile network operator (MNO) may undertake the role of E2E slice provider. The service-based business model promoted by RAN slicing, motivates MNOs to move beyond traditional subscription-based schemes with fixed rental fees to more flexible pricing policies and direct value propositions to the smart grid utilities, e.g., revenue split schemes and incentive strategies. As a result, the new electricity business models on ownership, operation, maintenance as well as usage, will be defined according to performance-based SLAs and relevant key performance indicators of the electrical infrastructure, which could be complemented by the added value on each utility.

From the perspective of power system utilities, service provisioning and cost efficiency empowered by RAN slicing, in conjunction with the deregulation of the energy sector,

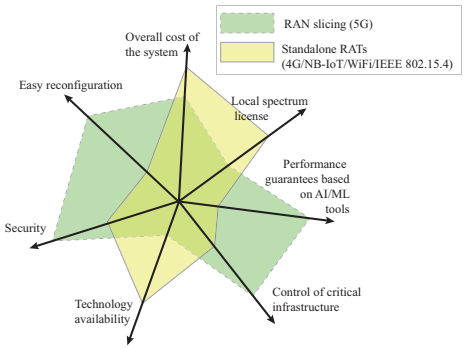

Fig. 2. Comparison between a RAN slicing framework and wireless RATs, such as LTE, NB-IoT, Wi-Fi, and IEEE 802.15.4, when applied as standalone connectivity solutions for smart grid services.

reinforce new business practices. The opportunities of this evolving market context are expected to alter the way transmission/distribution system operators use connectivity technologies in the grid. Leveraging RAN slicing, novel use cases and diversified requirements can be supported using a unique communication infrastructure with significant cost savings.

A qualitative comparison between RAN slicing and existing radio access technologies (RATs) for the smart grid is illustrated in Fig. 2. It is worth noting that in terms of technology availability, existing RATs have an essential advantage compared with RAN slicing, related to the maturity of communication standards and the already well-established ecosystems adopting such technologies. The same applies when local spectrum licenses are in force. Nonetheless, enhanced security mechanisms, reconfiguration capabilities, overall system cost, control of the critical infrastructure, and incorporation of artificial intelligence are some of the aspects where RAN slicing demonstrates clear superiority.

IV. The Proposed Framework

The diverse QoS requirements in the smart grid provide a fertile ground for the application of an agile RAN slicing approach. Our methodology is devised to cope with the rising complexity of supporting 5G-enabled smart grid services, achieving not only more manageable RAN slices but also conforming to the business propositions sought by network operators and smart grid utilities. The proposed framework complements the RAN slicing enhancements introduced in [9], by bridging the gap between IEC 61850 services and the 3GPP-standardized radio resource sharing strategies.

A. The IEC 61850 Standard

In terms of power industry communication standards, the IEC 61850 standard is of particular note. Originally defined to cover the stringent requirements for automation within electrical substations, IEC 61850 emerges as a versatile interoperable standard that can be applied beyond the substation boundaries to facilitate intersubstation message exchange, wide-area transmission of synchrophasor information and DERs' communication. IEC 61850 promotes abstract and application-specific data models and services that are decoupled from the underlying communication technologies. As the applicability of the standard expands continuously, there is growing research interest to integrate IEC 61850 services with wireless protocols and overcome the physical limitations and high installation costs of the default Ethernet technology.

The IEC 61850 standard defines the performance classes and communication requirements for various message types exchanged between power system components. In this context, the IEC 61850 message classification can be intrinsically associated with the RAN slicing concept. In particular, Type-1 and Type-6 messages impose requirements that fall under the uRLLC slice, as they are linked to real-time substation protection actions and time synchronization, respectively. For instance, in line phase comparison for analog protection, Type-1 messages must be delivered with ultra-high reliability levels, i.e., a packet loss rate in the order of 10^{-5} [10]. Other message types, related to continuous IED data streams (or large file transfers) and sporadic medium-speed event reports, can be mapped to eMBB and mMTC slices, respectively.

B. RAN Slicing for IEC 61850 Services

Our RAN slicing framework aims to accommodate IEC-61850 services over a single shared infrastructure and lays the foundation for a fine-grained service management in the smart grid. As illustrated in Fig. 3, it is primarily composed of a number of interworking functional components with programmable capabilities, aiming at a flexible instantiation of IEC 61850 services. In what follows, we provide a concise description of the building elements defined for RAN slicing.

1) RAN architecture (RANA): The next-generation NodeB (gNodeB) is a key component in the RAN slicing architecture. It provides RAN slice subnets which consist of the centralized unit (CU), multiple distributed units (DUs) and multiple radio units (RUs). Heterogeneous IEC 61850 requirements can be supported by appropriate RAN operating principles that involve different functional roles among the RUs, the DUs and the CU. Such roles are determined based on the RANA index value, offering QoS flexibility to MNOs to select the appropriate deployment option. For certain RANA values, the transmission of IEC 61850 message types follows a centralized (i.e., client/server) architecture to support traffic types with moderate end-to-end latency levels. On the other hand, proper RANA configurations may also enable a (fully) distributed architecture that relies on a disaggregated functional split to DUs and/or RUs. In this case, processing functions are primarily located closer to the DUs and/or RUs, achieving lower latency levels for critical IEC 61850 messages, e.g., IEC 61850 traffic types with $\leq$10ms or $\leq$3ms latency budgets [10].

2) RAN isolation level (RIL): Considering that isolation represents the state in which the performance degradation of one slice does not impact the performance of other slices [11], the RIL functional element defines the required isolation level among slices, which reflects a trade-off between isolation and system efficiency. In an inter-slice sharing strategy, radio resource management for IEC 61850 messages reduces the associated slice tenant costs. On the other hand, a conservative

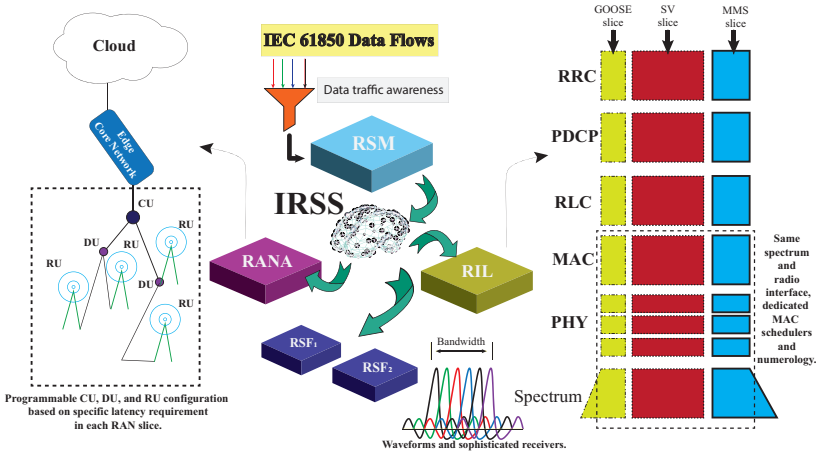

Fig. 3. A functional RAN slicing framework to support wireless connectivity for IEC 61850 services.

isolation policy employs dedicated radio resource assignments, conforming to stringent security and privacy enforcements.

3) RAN slicing function (RSF): This building element is mainly associated with the functionalities performed in the DUs. To ensure a future-proof element design, a partition of these functionalities is carried out into two well-defined subelements. The RSF_1 comprises the already standardized 5G/NR functionalities and involves the scalable 5G/NR numerology on the frame structure [11]. This subelement is associated with fundamental RAN functions, such as tiling, scheduling and puncturing. Tiling refers to the assignment of radio resources into different tiles defined in the time/frequency space, which can be individually configured according to the IEC 61850 service requirements and the respective SLAs. Scheduling refers to the allocation of radio resources, while traffic puncturing allows efficient multiplexing of various IEC 61850 services by prioritizing the transmission of time-sensitive message types. On the other hand, the RSF_2 subelement consists of customized baseband functionalities to support vendor-specific operations or features not yet specified by standards. It considers beyond-5G technical enhancements, paving the way for next-generation connectivity enablers to be incorporated in the RAN slicing framework.

4) RAN slicing management (RSM): This component monitors the necessary capabilities of the aforementioned RANA, RIL and RSF elements. With a supervisory and management role in the RAN domain, the RSM handles RAN slice instantiation and lifecycle management of IEC 61850 services. The RSM interacts with the *data traffic awareness* module, a specialized function used to process, analyze and evaluate the IEC 61850 data flows. Its intent-driven operation needs to rigorously consider the diversified SLAs of IEC 61850 services designated by the core network. The fundamental hallmark of RSM element is therefore to guarantee a harmonic coexistence of multiple RAN slices and their respective SLAs.

5) Intelligent RAN slicing scheduler (IRSS): This element adds cognition to the proposed framework. The key operation of IRSS lies in the knowledge extraction from the aggregated IEC 61850 traffic for RAN slice scheduling and radio resource assignment. The exploitation of advanced AI techniques by the IRSS holds the promise of achieving a high degree of automation and operational efficiency for RAN slicing. Radio resource allocation in IRSS needs to ensure an efficient multiplexing of IEC 61850 services by prioritizing the transmission of time-sensitive message types. To ensure such contextual decision-making, the IRSS interacts with all aforementioned elements of the framework for RAN slice awareness, e.g., SLA monitoring and resource isolation.

V. Performance Assessment

A. Network Scenario

To evaluate the feasibility of the proposed RAN slicing framework, we consider the smart grid self-healing scenario in [12], where automatic reconfiguration occurs after a short-circuit fault. The IEDs, smart substation controllers (SSCs), and merging units (MUs) are equipped with 5G interfaces to transmit IEC 61850 messages in a multicell network topology. As illustrated in Fig. 4, connectivity is provided by gNodeBs deployed to provide coverage in the different segments of the power system delimited by the IEDs and SSCs. Three RAN slices are considered, corresponding to the generic object oriented substation event (GOOSE), sampled value (SV), and manufacturing message specification (MMS) services in IEC 61850. In particular:

1) **GOOSE** slice, supporting uRLLC-type information exchange between IEDs, to isolate the fault and restore power supply in other power system segments. Short transmission latency of GOOSE messages is critical to minimize the impact on power system stability.
2) **SV** slice, supporting uRLLC-type information exchange between MUs and IEDs. SV messages contain current

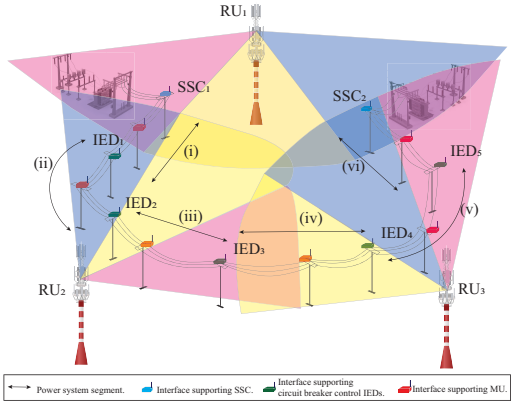

Fig. 4. Smart grid self-healing use case with a cellular network deployment supporting IEC 61850 services. The gNodeBs provide connectivity to different segments of the power system denoted as (i)-(vi). The smart substation controllers (SSCs), intelligent electronic devices (IEDs), and merging units (MUs) are equipped with 5G interfaces, and exchange system-related information by sharing available radio resource blocks.

and voltage measurements with accurate timestamp data. Similar to GOOSE, stringent latency requirements apply.

3) **MMS** slice, supporting mMTC-type information exchange between IEDs and SCADA centers, to monitor the power system segments. Such messages have relatively moderate latency requirements compared to GOOSE and SV slices.

Path loss model, radio configurations and simulation assumptions follow the 3GPP specifications in [13]. Radio resource blocks are shared among the active IEC 61850 communication links; thus, each smart grid device suffers from co-channel interference caused by other devices sharing the same resource blocks. Dynamic scheduling for RAN slices is necessary to efficiently manage resource allocation, minimize interference, and prioritize specific IEC 61850 messages according to SLAs.

B. IRSS Implementation

To address the joint radio resource assignment and power control problem for smart grid devices, the IRSS employs two deep reinforcement learning (DRL) algorithms which collaboratively aim to maximize the achieved spectral efficiency of all active IEC 61850 communication links. DRL models sequential decision-making problems with an agent and an environment interacting and exchanging information in the form of *states*, *actions*, and *rewards* [14]. With the aid of deep neural networks for function approximation, smart grid devices successively learn two *policies* to determine their assigned radio resources and transmit power levels, and maximize the expected sum of rewards. The reward function, common for both algorithms, takes into account *i*) the achieved spectral efficiency of each smart grid device and *ii*) the interference level caused to other devices. As illustrated in Fig. 5a, IRSS employs the following two learning layers:

- A deep Q-network (DQN) algorithm is considered for resource assignment to the different RAN slices. DQN

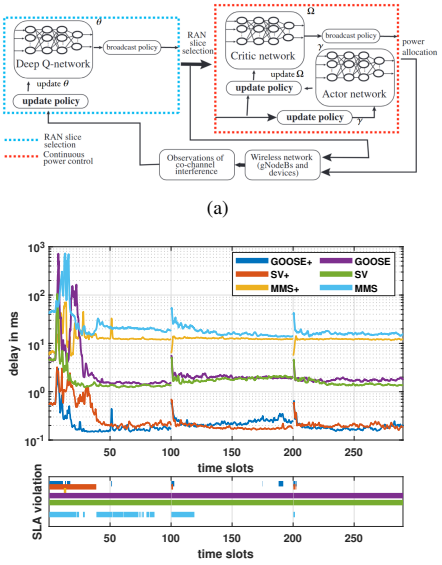

Fig. 5. (a) DRL-based IRSS implementation for radio resource assignment and power control of smart grid devices. The DQN layer provides the resource assignment decision to the actor-critic algorithm, which, in turn, determines the transmit power levels. (b) RAN slice performance assessment for three IEC 61850 services in terms of latency and SLA violation rate in a smart grid self-healing use case. For slices labeled with symbol +, DRL-based IRSS takes into account the beyond-5G configuration options for RANA, RIL and RSF elements. Latency requirement for time-sensitive GOOSE and SV services is set to 0.3 ms and 0.5 ms, respectively, whereas a latency budget of 40 ms is specified for MMS services [10].

is a value-based algorithm, applicable to environments with discrete action space. To strike a balance between exploring state-action pairs and exploiting knowledge, we adopt a Boltzmann policy to steer exploration towards more promising actions off the Q-value-maximizing path, instead of selecting all actions with equal probability [14]. During training, experiences gathered by older policies are stored in a replay memory, and are reused to improve sample efficiency.

- An actor-critic algorithm is applied to manage the continuous action space for transmit power allocation. In actor-critic schemes, two components are learned jointly; an actor, which learns a parameterized policy, and a critic which learns a value function to evaluate state-action pairs. The actor first receives as input the resource block assignment decision from the DQN layer. Using a learned value function, the critic provides a reinforcing signal to the actor which can be more informative for a policy than the rewards from the environment. In our method, we learn an *advantage* function as the reinforcing signal, which measures the extent to which an action is better or worse than the policy's average action in a state. The estimation of advantage function is performed using an exponentially weighted average of a number of advantage

estimators with different bias and variance [15].

C. Results

The top plot in Fig. 5b illustrates the latency performance for GOOSE, SV and MMS slices for two different simulation setups. In particular, the transmission latency for each IEC 61850 communication link is measured as the ratio of the packet size (prescribed in [10]) over the achieved throughput. In the first setup (i.e., slices labeled with symbol +), the DRL-based IRSS element takes into consideration the beyond-5G configuration options for RANA, RIL and RSF elements, as described in Section IV. In this case, the augmented state-action space for each smart grid device opens up the possibility of discovering better states and ways of acting in the quest for the optimal resource and power decisions. In the second setup, the DRL-based IRSS element uses default 5G configurations for resource assignment and power control according to [13]. It can be observed that IRSS achieves superior latency performance in the first setup compared to the second one, while conforming to the SLA requirements for GOOSE, SV and MMS slices as specified by the RSM element. The considered SLAs refer to the latency requirements for IEC 61850 services, and an SLA violation occurs when the achieved latency level becomes higher than the threshold value [10]. In addition, IRSS learns to prioritize time-sensitive GOOSE and SV services, resulting in significant latency reduction compared to the default 5G configuration. This, in turn, leads to fewer SLA violations, as illustrated in the bottom plot of Fig. 5b.

We note that the transient latency behavior for all RAN slices identified in the first time slots is attributed to the exploration phase of the DRL-based IRSS, which may result in suboptimal actions by each smart grid device. However, as training progresses, the rate of exploration gradually decays, and smart grid devices learn better policies for their assigned resources and transmit power levels.

VI. Concluding Remarks

The smart grid paradigm undoubtedly represents an essential showcase for 5G and beyond systems, mainly because of the heterogeneous connectivity landscape and the wide range of service requirements. In this context, RAN slicing poses elevated merit for a fine-grained smart grid service management with a shared communication infrastructure. At the same time, the proliferation of AI techniques for sequential decision-making problems offers remarkable benefits in RAN slice management. This article introduced an AI-native RAN slicing framework for the integration of IEC 61850 services in beyond-5G systems. Our proposed framework comprises multiple functional elements which interoperate towards intent-driven RAN slice management. The feasibility of our approach was demonstrated with the aid of a smart grid self-healing scenario with diversified QoS requirements. By resorting to two DRL-based algorithms, the joint resource allocation, interference minimization, and IEC 61850 message prioritization can be efficiently handled, while conforming to SLAs.

In the path forward, we will direct our efforts towards the design of traffic forecasting modules for IEC 61850 services, and their incorporation in our RAN slicing framework. This will facilitate predictive slice provisioning by ensuring traffic-aware admission control policies. The introduced signaling overhead for RAN slicing control will also be quantified.

Acknowledgment

This paper is partly supported by Academy of Finland via: (a) FIREMAN consortium CHIST-ERA/n.326270; (b) EnergyNet Research Fellowship n.321265/n.32886/n.352654; (c) X-SDEN project n.349965; (d) 6G Flagship (n.346208). This research is also supported by the joint Baltic-Nordic Energy Research programme project "Guidelines for Next Generation Buildings as Future Scalable Virtual Management of MicroGrids [Next-uGrid]" (n.117766), and Finnish public funding agency for research, Business Finland under projects 5GVIIMA and IFORGE, the projects are parts of 5G Test Network Finland (5GTNF) and Smart Otaniemi ecosystems. The work of Charalampos Kalalas was supported by FIREMAN project CHIST-ERA-17-BDSI-003 funded by the Spanish National Foundation (PCI2019-103780). The work of Petar Popovski was, in part, supported by the Villum Investigator Grant "WATER" from the Velux Foundation, Denmark.

References

[1] V. Gungor *et al.*, "Smart Grid Technologies: Communication Technologies and Standards," *IEEE Trans. Ind. Informat.*, vol. 7, no. 4, pp. 529–539, Nov. 2011.

[2] Q.-D. Ho *et al.*, "Challenges and research opportunities in wireless communication networks for smart grid," *IEEE Wireless Commun.*, vol. 20, no. 3, pp. 89–95, Jun. 2013.

[3] M. Cosovic *et al.*, "5G Mobile Cellular Networks: Enabling Distributed State Estimation for Smart Grids," *IEEE Commun. Mag.*, vol. 55, no. 10, pp. 62–69, 2017.

[4] P. Ahokangas *et al.*, "Business Models for Local 5G Micro Operators," *IEEE Trans. Cogn. Commun. Netw.*, vol. 5, no. 3, pp. 730–740, 2019.

[5] J. Li, W. Shi, P. Yang, Q. Ye, X. S. Shen, X. Li, and J. Rao, "A hierarchical soft ran slicing framework for differentiated service provisioning," *IEEE Wireless Commun.*, vol. 27, no. 6, pp. 90–97, 2020.

[6] J. Mei, X. Wang, K. Zheng, G. Boudreau, A. B. Sediq, and H. Abou-Zeid, "Intelligent radio access network slicing for service provisioning in 6g: A hierarchical deep reinforcement learning approach," *IEEE Transactions on Communications*, vol. 69, no. 9, pp. 6063–6078, 2021.

[7] W. Meng *et al.*, "Smart grid neighborhood area networks: a survey," *IEEE Netw.*, vol. 28, no. 1, pp. 24–32, Jan. 2014.

[8] 3GPP, "Technical Specification Group Services and System Aspects; System architecture for the 5G System (5GS); Stage 2," Technical Specification (TS) 23.501, Mar. 2020, version 16.4.0.

[9] ——, "Technical Specification Group RAN; NR; Study on enhancement of Radio Access Network (RAN) slicing," 3rd Generation Partnership Project (3GPP), Technical Specification (TS) 38.832, Jun. 2021, version 17.0.0.

[10] "*Communication Networks and Systems in Substations – Part 5: Communication Requirements for Functions and Device Models*," IEC-61850, Standard, 2004.

[11] S. E. Elayoubi *et al.*, "5G RAN Slicing for Verticals: Enablers and Challenges," *IEEE Commun. Mag.*, vol. 57, no. 1, pp. 28–34, 2019.

[12] R. Ricart-Sanchez, A. C. Aleixo, Q. Wang, and J. M. Alcaraz Calero, "Hardware-Based Network Slicing for Supporting Smart Grids Self-Healing over 5G Networks," in *2020 IEEE International Conference on Communications Workshops (ICC Workshops)*, 2020, pp. 1–6.

[13] 3GPP, "Technical Specification Group Radio Access Network; Evolved Universal Terrestrial Radio Access (E-UTRA); Radio Frequency (RF) requirements for LTE Pico Node B," 3rd Generation Partnership Project (3GPP), Technical Report 36.931, 03 2022, version 17.0.0.

[14] R. S. Sutton and A. G. Barto, *Reinforcement learning: An introduction*. MIT press, 2018.

[15] J. Schulman, P. Moritz, S. Levine, M. Jordan, and P. Abbeel, "High-dimensional continuous control using generalized advantage estimation," 2015. [Online]. Available: https://arxiv.org/abs/1506.02438

Dick Carrillo [S'01, M'06] (dick.carrillo.melgarejo@lut.fi) received the B.Eng. degree (Hons.) in electronics and electrical engineering from San Marcos National University, Lima, Perú, and the M.Sc. degree in electrical engineering from Pontifical Catholic University of Rio de Janeiro, Rio de Janeiro, Brazil, in 2004 and 2008, respectively. Between 2008 and 2010, he contributed to WIMAX (IEEE 802.16m) standardization. From 2010 to 2018, he worked with the design and implementation of cognitive radio networks and projects based on 3GPP technologies. Since 2018 he is a researcher at Lappeenranta–Lahti University of Technology, where he is also pursuing the doctoral degree in electrical engineering. His research interests are mobile technologies beyond 5G, energy harvesting, intelligent meta-surfaces, cell-free mMIMO, and RAN Slicing. Since 2022, he is a Senior Standardization Specialist at Nokia Bell Labs, where he is contributing on shaping the 3GPP release 18 standard (5G-Advanced).

Charalampos Kalalas [S'15, M'18] (ckalalas@cttc.es) received the Ph.D. degree (Cum Laude) in Signal Theory and Communications from the Technical University of Catalonia (UPC) in 2018. He holds an Electrical and Computer Engineering degree (2011) from the National Technical University of Athens (NTUA), Greece, and a M.Sc. degree in Wireless Systems (2014) from the Royal Institute of Technology (KTH), Sweden. He is currently a Researcher with the Sustainable Artificial Intelligence research unit at the Centre Tecnològic de Telecomunicacions de Catalunya (CTTC/CERCA).

Petra Raussi (petra.raussi@vtt.fi) received the M.Sc. degree in electrical engineering from LUT University, Lappeenranta, Finland in 2018. She is currently a doctoral candidate at the Department of Electrical Engineering and Automation, School of Electrical Engineering, Aalto University, Espoo, Finland. In 2016, she was a Research Assistant with the School of Energy Systems, LUT University, Lappeenranta, Finland. Since 2017, she has been first a Research Trainee, a Research Scientist, and currently a Senior Scientist with the VTT Technical Research Centre of Finland, Espoo, Finland. Her research interest includes power system communication and automation, 5G and beyond for critical data exchange, distributed control, and real-time systems.

Diomidis Michalopoulos [S'05, M'10, SM'15] (diomidis.michalopoulos@nokia-bell-labs.com) is Department Head of Device Standardization Research, Nokia, Germany. He and his team conduct research on 5GAdvanced/6G networks and devices, with emphasis on physical layer and radio access aspects. Prior to joining Nokia he was employed by the University of British Columbia, Canada, and the University of Erlangen-Nuremberg, Germany. Diomidis obtained the Engineering and PhD degree from the Aristotle University of Thessaloniki, Greece. He received the Marconi Young Scholar award from the Marconi Society and various prizes for academic excellence, including the Banting fellowship in Canada. Diomidis is currently the industry-academia collaboration coordinator within the IEEE EMEA region.

Demóstenes Z. Rodríguez (M'12-SM'15) received the B.S. degree in electronic engineering from the Pontifical Catholic University of Peru, and his M.Sc. and Ph.D. degree from the University of São Paulo in 2009 and 2013, respectively. He is currently an Adjunct Professor with the Department of Computer Science, Federal University of Lavras, Brazil. He has a solid knowledge in Telecommunication Systems based on 15 years of professional experience. His research interest includes QoS-QoE in multimedia services and new generation networks.

Heli Kokkoniemi-Tarkkanen (heli.kokkoniemi-tarkkanen@vtt.fi) received the M.Sc. in applied mathematics and computer science from the University of Jyväskylä, Jyväskylä, Finland in 1995. Since 1992, she has been working at VTT Technical Research Centre of Finland in several positions, currently as a Senior Scientist. She has over 28 years of experience in commercial, military, and research projects covering various aspects of wireless communication from radio wave propagation modeling and network simulation to early-phase product development. In recent years, she has been focusing on QoS, latency, and reliability aspects by piloting and testing 5G services in new mission-critical vertical use cases such as protection and control of smart energy grids and harbor automation.

Kimmo Ahola (kimmo.ahola@vtt.fi) received the M.Sc. degree from the University of Jyväskylä, Jyväskylä, Finland in 1997. From 1996 to 1997, he was a Research Trainee with VTT Technical Research Centre of Finland. From 1997 to 2001, he worked as a Research Scientist with VTT Technical Research Centre of Finland. Since 2001, he has been working as a Senior Scientist and between 2006 and 2013 as a Team Leader in Adaptive Networks team. He has participated and led software development in several national and European projects. Lately, his research interests have focused on 5G networks, software defined networking (SDN), network functions virtualization (NFV), cloud infrastructures, and security in network and cloud infrastructures.

Pedro H. J. Nardelli [M'07, SM'19] (pedro.nardelli@lut.fi) is Associate Professor (tenure-track) at LUT University and also Academy of Finland Research Fellow. He is also the coordinator of the Strategic Research Area for Energy Vertical of the 6G Flagship at University of Oulu.

Gustavo Fraidenraich (gf@decom.fee.unicamp.br) graduated in Electrical Engineering from the Federal University of Pernambuco, UFPE, Brazil, in 1997. He received his M.Sc. and Ph.D. degrees from the State University of Campinas, UNICAMP, Brazil, in 2002 and 2006, respectively. From 2006 to 2008, he worked as a Postdoctoral Fellow at Stanford University (Star Lab Group) - USA. Currently, Dr. Fraidenraich is Assistant Professor at UNICAMP - Brazil and his research interests include Multiple Antenna Systems, Cooperative systems, Radar Systems and Wireless Communications in general. He has been associated editor of the ETT journal for many years. Dr. Fraidenraich was a recipient of the FAPESP (Fundação de Amparo à Pesquisa do Estado de São Paulo) young researcher Scholarship in 2009.

Petar Popovski [S'97, A'98, M'04, SM'10, F'16] (petarp@es.aau.dk) is a Professor at Aalborg University, where he heads the section on Connectivity and a Visiting Excellence Chair at the University of Bremen. He received his Dipl.-Ing and M. Sc. degrees in communication engineering from the University of Sts. Cyril and Methodius in Skopje and the Ph.D. degree from Aalborg University in 2005. He is currently an Editor-in-Chief of IEEEE JOURNAL ON SELECTED AREAS IN COMMUNICATIONS. His research interests are in the area of wireless communication and communication theory. He authored the book "Wireless Connectivity: An Intuitive and Fundamental Guide", published by Wiley in 2020.

Publication II

Carrillo, D., Pokorny, J., Seda, P., Narayanan, A., Nardelli, P., Rasti, M., Hosek, J., Seda, M., Zegarra, D., Koucheryavy, Y., and Fraidenraich, G.

Optimizing Flying Base Station Connectivity by RAN Slicing and Reinforcement Learning

Reprint with permission from
IEEE Access
Vol. 10, pp. 53746–53760, 2022 (in press)

IEEE Access
Multidisciplinary ⋮ Rapid Review ⋮ Open Access Journal

Date of publication xxxx 00, 0000, date of current version xxxx 00, 0000.

Digital Object Identifier 10.1109/ACCESS.2017.DOI

Optimizing Flying Base Station Connectivity by RAN Slicing and Reinforcement Learning

DICK CARRILLO MELGAREJO[1,2,3], JIRI POKORNY[4,5], PAVEL SEDA[4], ARUN NARAYANAN[1], PEDRO H. J. NARDELLI[1], MEHDI RASTI[1], JIRI HOSEK[4], MILOS SEDA[6], DEMÓSTENES Z. RODRÍGUEZ[7], YEVGENI KOUCHERYAVY[5], GUSTAVO FRAIDENRAICH[2]

[1]Department of Electrical Engineering, School of Energy Systems, Lappeenranta-Lahti University of Technology (LUT), Lappeenranta, Finland. (e-mail: name.lastname@lut.fi).
[2]School of Electrical and Computer Engineering, State University of Campinas, Brazil.
[3]Nokia Bell Labs, Espoo, Finland.
[4]Department of Telecommunications, Faculty of Electrical Engineering and Communication, Brno University of Technology. (e-mail: @vut.cz).
[5]Unit of Electrical Engineering, Tampere University, Korkeakoulunkatu 7, 337 20 Tampere, Finland. (e-mail: evgeny.kucheryavy@tuni.fi).
[6]Institute of Automation and Computer Science, Faculty of Mechanical Engineering, Brno University of Technology.
[7]Department of Computer Science, Universidade Federal de Lavras (UFLA), Lavras, Minas Gerais, Brazil.

Corresponding author: Dick Carrillo Melgarejo (e-mail: dick.carrillo.melgarejo@lut.fi).

This paper is partly supported by Academy of Finland via: (a) FIREMAN consortium CHIST-ERA-17-BDSI-003/n.326270, and (b) EnergyNet Research Fellowship n.321265/n.328869; and by Jane and Aatos Erkko Foundation via STREAM project.

ABSTRACT The application of flying base stations (FBS) in wireless communication is becoming a key enabler to improve cellular wireless connectivity. Following this tendency, this research work aims to enhance the spectral efficiency of FBSs using the radio access network (RAN) slicing framework; this optimization considers that FBSs' location was already defined previously. This framework splits the physical radio resources into three RAN slices. These RAN slices schedule resources by optimizing individual slice spectral efficiency by using a deep reinforcement learning approach. The simulation indicates that the proposed framework generally outperforms the spectral efficiency of the network that only considers the heuristic predefined FBS location, although the gains are not always significant in some specific cases. Finally, spectral efficiency is analyzed for each RAN slice resource and evaluated in terms of service-level agreement (SLA) to indicate the performance of the framework.

INDEX TERMS Flying Base Stations, UAVs, Location Optimization, Wireless Communication, Deep-reinforcement Learning.

I. INTRODUCTION

Extensive developments in the field of unmanned aerial vehicles (UAVs) have opened many opportunities for new applications in both private and public domains, such as surveillance, transportation, environmental monitoring, industrial monitoring, agriculture services, and disaster relief [1], [2]. Recently, the increasing number of use cases employ UAVs as wireless hotspots or relays to extend network coverage in areas where it is required. Moreover, nowadays, there are UAV applications used as a tool for communications at the application level, for example, information sharing in social media or searching for missing persons. Another example is the recent floods in Germany [3], which showed that the infrastructure is still quite vulnerable. Therefore, it is worth pursuing solutions to overcome problems when the regular communication infrastructure stops working. Thus, the use of UAVs provides an essential resource for allowing the continuity of communications and supporting human operators to continue to communicating in search and rescue operations, thereby guaranteeing efficient operation [4]. In such scenarios, the option of rapidly and efficiently deploying a fleet of drones is crucial in quickly establishing a communication network capable of saving lives, especially as it might be difficult to use terrestrial means comprising temporary networking equipment, such as a cell on wheels in natural disasters. This feature makes UAVs unique and crucial for deployment in such use cases [5].

In addition, deploying UAVs as flying base stations

(FBS) has also recently emerged as a feasible response to highly localized traffic demands in next-generation cellular networks [6], [7]. Using UAVs in such a way provides an opportunity to exploit their agility of motion to improve the air-to-ground link capacity by optimal air placement [8], [9]. Typically, the above-mentioned use cases consider significantly large areas where multiple UAVs must be used. However, this leads to two major problems. First, the UAVs must be positioned to optimally cover as many users as possible [10], [11]. Second, the intracell and intercell interference must be mitigated [12]. The first problem can be effectively approached by using heuristic algorithms. These algorithms can provide a solution with a low computational time and good results, as shown in [13], for example. In the case of intracell interference, the system performance can be improved with a variety of multiple access techniques, such as orthogonal frequency-division multiple access (OFDMA). When intercell interference is taken into account, some popular schemes, such as frequency reuse, graph theory, and cooperative multi-point (CoMP) [9], [14]–[18], can be employed.

In our previous work [13], we addressed the UAVs position optimality using an heuristic methodology. However, the radio channel interference problem was not addressed in detail. The present work extends [13] by employing a representative wireless channel model. In addition, we proposed a radio access network (RAN) slicing framework that enables the allocation of radio resources (slices) carrying specific data services. Our proposed framework aims to accommodate a diversity of services over a single shared fifth generation (5G) infrastructure and lays the foundation for fine-grained service management in FBS networks. We have considered that an agile RAN slicing framework is an appropriate solution to achieve the performance requirements introduced by verticals on 5G communication networks. The RAN slicing framework comprises several interworking functional components, aiming at a flexible instantiation of radio services, that can cope with the increasing complexity of supporting FBS services. In our work, we consider three slices: enhanced mobile broadband (eMBB), ultra-reliable low-latency communication (URLLC), and massive machine-type communications (mMTC).

The allocation of these slices is achieved by optimizing a cost function that is directly related to the spectral efficiency (SE) of the downlink data transmission, which is constrained by the maximum power transmission and the number of RAN slices. A cellular network based on subchannels usually has a high probability of intercell interferences in the edge cell. To solve this intricate allocation problem, we introduce an intelligent component in the framework—i.e., a deep reinforcement learning (DRL) model—that improves the system performance and manages the radio resource allocation minimizing the interference. By using our proposed interference management methodology to optimize the SE on each RAN slice, specific service-level agreement (SLA)[1] can be achieved between the network service provider and the customer.

To facilitate readers comprehension of this paper, the main contributions of this paper are summarized as follows:

- enhancement of the UAV location distribution algorithm proposed in [13], using a proper air-to-ground channel model to enable aa appropriate interference analysis.
- a novel RAN slicing framework is proposed to enable the use of advanced machine learning techniques, such as DRL.
- we propose a distributed DRL approach to mitigate the downlink interference, in which each FBS operates as an independent learning agent.
- three representative scenarios of FBSs are described and analyzed in detail to compare the SLA performance between the DRL and the benchmark.
- a multiagent learning technique is proposed to optimize a nonconvex problem in the FBS system model.

The rest of the paper is organized as follows. The model finding optimal placement of UAVs in a given area, used as benchmark in this research work, is presented in Section II. In Section III, the RAN slicing framework is defined, including the system model and the DRL methodology to allocate the radio resources. A detailed description of the optimization sequence is given in Section IV. The simulation setup is presented in Section V. Numerical results together with a thorough comparative performance analysis are discussed in Section VI. Our concluding remarks and future work are presented in Section VII.

II. UAV LOCATION OPTIMIZATION

The effective deployment of UAVs across a selected area is a difficult task that falls into the category of $\mathcal{NP}-$complete class of problems [19]. To address this task, we enhance the model presented in [13] for location covering of the UAV deployment in on-demand connectivity scenarios. The enhancement focuses in the elimination of interference for all pairs of newly added centres and for new and existing centres. The proposal in [13] did an extended explanation of the UAV location methodology. The main idea of this deployment was to select a feasible locations where UAVs can be located by this heuristic methodology. Based on that, the optimization algorithm selected the suitable UAV location to compose a list of UAVs and their respective locations.

A. DEPLOYMENT MODEL

To facilitate the understanding of the model, we provide the terminology used in the rest of this paper adapted to the terms used in the literature in Table 1. To localize the suitable positions for the FBS deployment, location optimization problems is taken as inspiration. Currently, there exist several

[1]SLAs establish customer expectations regarding the service provider's performance and overall quality. It is a contract between the network service (NS) provider and the customer.

TABLE 1. Mapping mathematical terminology to communication networks terminology.

Mathematical Terminology	Wireless Networks Terminology
Facility	UAV or FBS node.
Demand	A user demanding certain level of network connectivity in a given area.
Capacity	Throughput that is requested by the sum of user requirements in a given area to be covered.
Multiple service	A user requires to be potentially covered by the x UAV or FBSs.
Existing service	Usually FBS nodes that already exist in the area to be covered and should remain after the reconfiguration or deployment phase.

facility location problems dealing with many real-world use cases. Simply, they can be divided into location set covering problems (LSCPs) [20], and maximal covering location problems (MCLPs) [21]. The LSCP targets the minimization question in which the number of facilities that satisfy the network requirements and the need to be located is minimized. On the other hand, in the MCLP, a predefined number of resources tries to maximize its coverage. The main division is based on the available resources. Because these models have been used for a wide range of applications, they are not tied to telecommunication network deployment only. Hence, to the best of our knowledge, there is a gap in the literature that [13] aims to bridge for these models and the use case of UAV deployment. As a gap, we see the following factors (or their combination in one model):

(i) Separating the capacity of facilities or locations covering both downlink and uplink. This may differ for each location or facility.
(ii) Consideration of the existing services; for the use case of UAVs, it is essential to consider the existing infrastructure that can serve at least some demand from the locations to be covered ad hoc.
(iii) Splitting capacity requirements from one location to only one facility at a given moment.
(iv) Covering some locations with zero or a higher number of facilities. This is crucial for the must-have locations where it is not acceptable to lose the connectivity.
(v) The oversimplified wireless interference is based on the overlaps between cellular cells. We eliminate the interference by Eq. (8) and (9).

In [13], it is assumed that coverage availability is guaranteed. Capacity considerations are critical in the 5G-and-beyond deployments that expect a significant increase in network traffic. This is due to the growth of services that have considerably higher network throughput requirements, such as the growth of high-definition videos, augmented reality (AR) / virtual reality (VR), machine-to-machine communication, and other very intensive or demanding services in terms of network requirements. In particular, we have to deal with a high density of users that are simultaneously connected. For the existing facilities E_f and their corresponding decision variables x_i, where $i \in E_f$, we set this parameter to 1, which means that all the existing facilities are taken into account. The allocation of capacity requirements between uploads and downloads represents a split of 100 Mbps to 80 Mbps for download (more extensive) and 20 Mbps for upload. In addition, we still need to satisfy the requirement that the demand j both for download and upload must be assigned to the same facility i.

To derive a mathematical model, let us set the following notation:

- I = a set of facility sites (UAV or FBS) $1, 2, \ldots, m$;
- J = a set of demand areas (customers) $1, 2, \ldots, n$;
- d_{ij} = the shortest distance between facility i and demand j;
- D_{max} = maximum distance which will be accepted for operation between the facilities and demands;
- l_j = number of facilities required for servicing demand j;
- $x_i \in \{0, 1\}$, where $x_i = 1$ means that facility i is selected, while $x_i = 0$ means that it is not selected.
- $N_j = \{i | d_{ij} \leq D_{max}\}$ = the set of facilities i that can cover the demand location j;
- C_i^u = upload capacity of facility i;
- C_i^d = download capacity of facility i;
- a_j^u = upload amount of demand at j;
- a_j^d = download amount of demand at j;
- $y_{ij} \in \{0, 1\}$ = nonfragmented demand from location j is assigned (1) or is not assigned (0) to facility i.

Now, we set out the following model extracted from [13] to minimize the number of required FBSs and maximize the cellular coverage area.

$$\min \sum_{i \in I} x_i, \tag{1}$$

subject to

$$\forall j \in J : \sum_{i \in N_j} x_i \geq l_j \tag{2}$$

$$\forall j \in J : \sum_{i \in N_j} y_{ij} = 1 \tag{3}$$

$$\forall i \in N_j : C_i^u x_i \geq \sum_{j \in J} y_{ij} a_j^u \tag{4}$$

$$\forall i \in N_j : C_i^d x_i \geq \sum_{j \in J} y_{ij} a_j^d \tag{5}$$

$$(\forall i \in I)(\forall j \in J) : y_{ij} \leq x_i \tag{6}$$

$$\forall i \in E_f : x_i = 1 \tag{7}$$

$$(\forall i \in I - E_f)(\forall j \in I - E_f)(i \neq j) : d_{ij} \geq (x_i + x_j - 1) d_{\min} \tag{8}$$

$$(\forall i \in I - E_f)(\forall j \in E_f) : d_{ij} > d_{\min} x_i \tag{9}$$

$$\forall i \in I : x_i \in \{0, 1\} \tag{10}$$

$$(\forall i \in I)(\forall j \in J) : y_{ij} \in \{0, 1\} \tag{11}$$

Constraint (3) guarantees that the demand j is assigned to only one facility at a given moment. All selected facilities must have a sufficient sum of their capacities for uploads and downloads to cover all upload and download demands (in practice, this is an ideal case that network operators are trying to reach with the available resources), this is guaranteed by constraints (4) and (5). If a facility is selected to be removed from the network infrastructure, none of the demand should be assigned to it; this constraint is given by (6). In [13], the interference is simplified to minimize the coverage overlaps defined by the cells. Finally, consider the following: if d_{ij}, $i \in I$, $j \in I$ is the distance between the facilities i and j, then we can set that for all pairs of selected facilities, the facilities will have a distance greater or equal than a certain threshold, which is guaranteed by constraint (8).

Further, as it is typical in the state of the art dealing with location coverage with model enhancements, authors in [13] provided an alternative maximization model that considers a predefined number of new facilities (not yet optimized) to be located and covered as much area as possible:

$$\max \sum_{i \in N_j} \sum_{j \in J} y_{ij}(a_j^u + a_j^d), \tag{12}$$

subject to the same constraints as in the minimization model, but with the addition of the following constraint for a predefined number of new facilities.

$$\sum_{i \notin E_f} x_i = p \tag{13}$$

Note that this model targets the localization of FBS nodes, which defines the benchmark. This information is used as input in the optimization of FBS based on (RAN) slicing framework, which is detailed in Section III-E.

The brief explanation of the algorithm implementing the model is detailed in Algorithm 1. The *GetInputData* part represents the list existing facilities, expected/existing demands with coordinates, and additional important metadata. For the *CoveringModel* computation part the heuristics needs to implement repair operator satisfying all the model constraints (e.g., adding new UAVs or FBSs to the list of solution to satisfy the capacity requirements).

B. CONSIDERATIONS OF THE COMPUTATIONAL COMPLEXITY MODEL

The size of the search space is determined by the number of all possible selections of facilities. For m facilities, according to the binomial theorem, it is equal to

$$\binom{m}{1} + \binom{m}{2} + \cdots + \binom{m}{m} = (1+1)^m - 1 = \mathcal{O}(2^m). \tag{14}$$

Furthermore, we need to find the most complex condition in extended models for $m < n$ (where n is the number of demand areas) to find the resulting computational complexity. In the minimization model, these are (6) and (11) in the corresponding equations of the maximization model, which require $m \cdot n$ operations. This is based on the fact that the resulting time complexity of these models is $\mathcal{O}(2^m mn)$ [13].

Algorithm 1 Algorithm that optimizes the UAVs or FBSs location.

▷ Main part
function FINDLOCATIONS
    GetInputData
    Generate theoretical possible UAVs locations
    Apply CoveringModel() with these data
▷ Covering model
function COVERINGMODEL()
    Generate possible solutions
    Apply repair operator providing feasible solutions
    Apply selected heuristics to find optimal solution
Suitable locations for the UAV deployment

III. RAN SLICING FRAMEWORK

To complement the benchmark described in Section II, in this section we describe the proposed RAN slicing framework. We employ the standardized definitions of RAN slicing in 5G, the system channel model, the radio optimization problem formulation, and our proposed approach using DRL.

A. FRAMEWORK DESCRIPTION

The diverse performance requirements introduced by 5G communication networks are fertile ground for the application of an agile RAN slicing framework. Our proposed framework aims to accommodate a diversity of services over a single shared 5G infrastructure and lays the foundation for fine-grained service management in FBS networks. This RAN slicing framework primarily comprises several interworking functional components, aiming at a flexible instantiation of radio services. The proposed architecture is devised to cope with the rising complexity of supporting FBS services, achieving not only more manageable RAN slices but also conforming the business propositions sought by network operators and service provider stakeholders.

This framework comprises orthogonal physical resources that split the available bandwidth to support a specific number of network slices. In this specific work, we consider three slices: eMBB, URLLC, and mMTC. In a cellular network based on subchannels, the RAN slicing framework is exposed to a high probability of intercell interference, specially in the edge cell. To address this issue, we incorporate an intelligent component in the framework to manage the radio resource allocation using DRL. This interference management aims to achieve specific SLA policies between the network service provider and the customer by optimizing the SE on each RAN slice.

A graphical description of the concept of the proposed framework is shared in Fig. 1. The system model and the DRL methodology are detailed in the following section.

B. SYSTEM MODEL

Consider a set $\mathcal{I}$ of I FBS providing downlink wireless service to a group of user equipments (UEs) in a geographical area $\mathcal{A}$. Each FBS $i \in \mathcal{I}$ serves an area $\mathcal{A}_i$, such that $\cup_{\forall i \in \mathcal{I}} \mathcal{A}_i = \mathcal{A}$ and $\mathcal{A}_i \cap \mathcal{A}_k \neq \emptyset$ for any $i \neq k \in \mathcal{I}$. In other words, we consider that when UAVs are allocated by the optimization algorithm presented in Section II, it is possible that some cells have a significant intersection between them.

The path loss of the air-to-ground communication link from a typical FBS located at $x_i \in \mathbf{R}^3$ to a typical ground UE that is located at $y \in \mathbf{R}^3$ is given as follows [22]:

$$h^{(t)}_{v\to n}[dB](x_i, y) = 20\log_{10}\left(\frac{4\pi f_c \|x_i - y\|}{c}\right) + \xi(x_i, y), \tag{15}$$

where f_c is the carrier frequency of FBS downlink communications, $\|x_i - y\|$ is the FBS–UE distance, c is the speed of light, and $\xi(x_i, y)$ is the additional path loss of the air-to-ground channel, compared with the free space propagation. The value of $\xi(x_i, y)$ can be modeled as a Gaussian distribution with different parameters $(\mu_{\text{LOS}}, \sigma^2_{\text{LOS}})$ and $(\mu_{\text{NLOS}}, \sigma^2_{\text{NLOS}})$ for line-of-sight (LOS) and non-line-of-sight (NLOS) links, respectively. Then, the downlink spectral efficiency achieved by the RAN slice m, the user n, at the time slot t from the FBS located at x_i to a UE located at $y \in \mathcal{A}_i$ is

$$\mathcal{C}^{(t)}_{n,m}(x_i, y) = \log_2\left(1 + \gamma^{(t)}_{n,m}(x_i, y)\right), \tag{16}$$

where $\gamma^{(t)}_{n,m}(x_i, y)$ is the signal-to-interference-plus-noise (SINR) at the user n, on the RAN slice m, at the time slot t, which is defined by (17)

$$\gamma^{(t)}_{n,m}(x_i, y) = \frac{\left[\beta^{(t)}_{l,m}\, g^{(t)}_{l\to n,m}(x_l, y)\, p^{(t)}_l\right]_{l=n}}{\sum\limits_{v\neq l} \beta^{(t)}_{v,m}\, g^{(t)}_{v\to n,m}(x_v, y)\, p^{(t)}_v + \sigma^2_n}, \tag{17}$$

where $\beta^{(t)}_{v,m}$ is the binary variable that indicates the RAN slicing selection m transmitted from the UAV v at time t, $g^{(t)}_{v\to n,m}(x_v, y)$ indicates the downlink channel gain from the FBS v to the user n on the RAN slice m in the time slot t when the UE is located in the position y and the FBS in the position $x_v \in \mathbf{R}^3$, $p^{(t)}_v$ is the transmit power of the UAV v in the time slot t, and σ^2 is the additive white Gaussian noise power spectral density at the user receiver n.

$$g^{(t)}_{v\to n,m}(x_v, y_n) = h^{(t)}_{v\to n}(x_v, y_n)\left|\alpha^{(t)}_{n\to l,m}\right|^2,\ t = 1, 2, \cdots, \tag{18}$$

where $h_{v\to n}(x_v, y_n)$ is the path loss in a linear scale, which is calculated in (15), and $\alpha^{(t)}_{n\to l,m}$ is the small-scale Rayleigh fading.

The probability of having an LOS link between the FBS j located at x_j and the UE located at y is given by [22]:

$$P_{\text{LOS}}(x_j, y_i) = \frac{1}{1 + a\exp\left(-b\left[\frac{180}{\pi}\sigma(x_j, y) - a\right]\right)}, \tag{19}$$

where a and b are constant values that depend on the communication environment, $\sigma(x_j, y) = \sin^{-1}\left(\frac{H_j}{\|x_j - y\|}\right)$ is the elevation angle, and H_j is the altitude of the FBS j. Then, the average downlink SE between an FBS i and the UE at n located in $y_n \in \mathcal{A}_i$ will be:

$$\begin{aligned}\bar{\mathcal{C}}^{(t)}_{n,m}(x_i, y_n) =& P_{\text{LOS}}(x_i, y_n)\mathcal{C}^{(t)\text{LOS}}_{n,m}(x_i, y_n) \\ &+ (1 - P_{\text{LOS}}(x_i, y_n))\mathcal{C}^{(t)\text{NLOS}}_{n,m}(x_i, y_n).\end{aligned} \tag{20}$$

C. RAN SLICING IN 5G

A simplified 5G logical architecture is composed of a core cloud, an edge cloud, and an RAN. The core cloud provides generic control plane signalization, slice management, mobility management, and authentication. The edge cloud performs some user plane functions as a packet/service gateway (P/S-GW) to improve latency communication on critical applications. It also enables data forwarding, control plane functions, and mobile edge computing platforms, such as content storage servers. In the radio access plane, the 3rd Generation Partnership Project (3GPP) defines the next-generation RAN (NG-RAN), which is comprised of next-generation NodeBs (gNBs) connected to the core network. This architecture is used to support the network slicing approach proposed in 5G. In this aspect, there are two types of subnets in the 5G slicing architecture: core network slice subnets and RAN slice subnets.

In the core network slice subnets, the network slicing operation used in the core network is controlled by the network slicing management. It is composed of the virtualized network function management (VNFM), the software-defined network (SDN) controller, the management and orchestration unit, and the virtualized infrastructure management (VIM). The VNFM maps the physical network functions to virtual machines (VMs); the SDN controller manages and operates the entire virtual network; the VIM allocates virtualized resources to VMs; and the management and orchestration unit creates, activates, and deletes network slices based on the service requirements.

In the RAN slice subnets, the gNB is a crucial enabler of network slices. It provides RAN slice subnets that are composed of a centralized unit (CU), multiple distributed units (DUs), and multiple radio units (RUs). The gNB functionalities are distributed in a flexible manner between

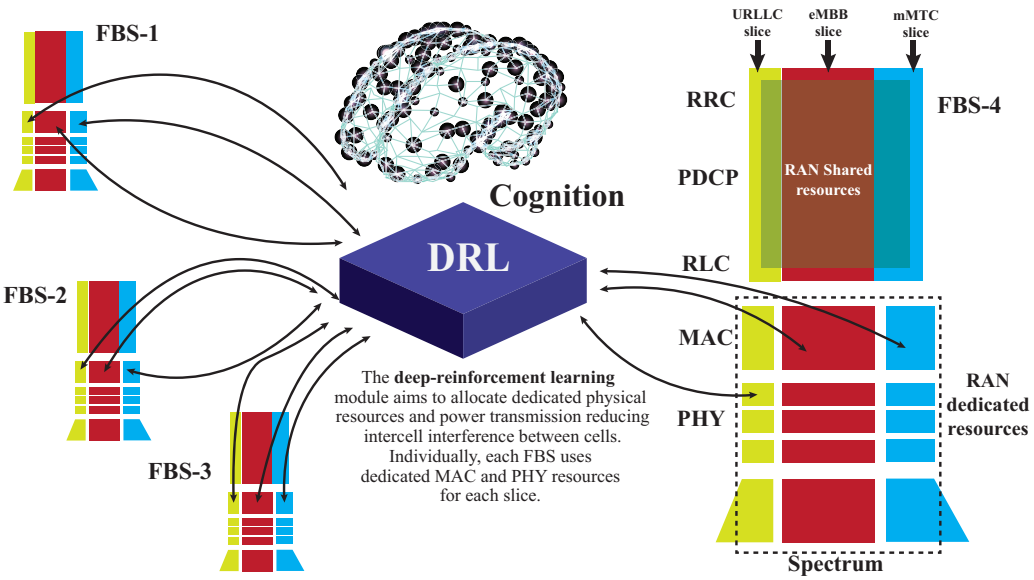

FIGURE 1. The RAN Slicing framework emphasizing the role of the DRL module. In this particular case we consider that each slice uses dedicated physical resources in each FBS. Thus, the cognition element optimizes the interference reduction using the deep-reinforcement learning approach.

the CU, DUs, and RUs. To manage their life cycles, the standard specifies the RAN network slice subnet template (NSST) and two management entities, such as the RAN network slice subnet management function (NSSMF) and the network function management functions (NFMFs) [23].

The core network slice subnets have been studied and developed in the current 5G with outstanding results. However, the RAN slicing is still an open topic, and it is not yet standardized. The RAN slicing aims to improve the efficient usage of available physical radio resources and simultaneously guarantees the SLA policies imposed in each slice.

D. REINFORCEMENT LEARNING AIDED UAVS

Machine learning is an approach that has become increasingly popular for sequential decision-making on wireless communication networks with applications in many diverse areas, such as smart grids, self-driving cars, and robotics. There are three machine learning categories, depending on the nature of the information or feedback available to the learning system: (i) supervised learning; (ii) unsupervised learning; and (iii) reinforcement learning (RL). In this paper, we use RL as the primary approach for optimizing the cost function based on spectral efficiency. RL is a technique that is concerned with how agents should determine the sequences of actions in an environment that will maximize cumulative rewards [24], [25]. It is a trial-and-error process where an agent interacts with an unknown environment in a sequence of discrete time steps to achieve a task. At time t, the agent first observes the current state of the environment, which is a tuple of relevant environment features and is denoted as $S^{(t)} \in \mathcal{S}$, where S is a set of possible states. It then takes an action $a^{(t)} \in \mathcal{A}$ from an allowed set of actions $\mathcal{A}$ according to a policy that can be either stochastic, i.e., π with $a^{(t)} \sim \pi(.|\mathcal{S}^{(t)})$ or deterministic, i.e., μ with $a(t) = \mu(\mathcal{S}^{(t)})$. Because the interactions are often modeled as a Markov decision process, the environment moves to a next state $S^{(t+1)}$ following an unknown transition matrix that maps state–action pairs onto a distribution of successive states, and the agent receives a reward $S^{(t+1)}$. Overall, the above process is described as an experience at $t+1$ denoted as $e^{(t+1)} = (S^{(t)}, a^{(t)}, r^{(t+1)}, s^{(t+1)})$.

The goal is to learn a policy that maximizes the cumulative discounted reward at time t, defined as follows:

$$R^{(t)} = \sum_{\tau=0}^{\infty} \gamma^{\tau} r^{(t+\tau+1)}, \tag{21}$$

where $\gamma \in (0; 1]$ is the discount factor.

RL has been growing in popularity because it does not require an extensive network model. Instead, its learning process is based on the interactions with the environment that produces its optimal strategies. Owing to the possibility of combining RL with deep learning [26], DRL is a highly suitable method for solving problems with a high number

of states and low prior knowledge, which is the case of the resource allocation scenario in RAN slicing.

DRL has recently been used in problems related to UAVs [27]–[31]. Moreover, the DRL approach has been exploited and applied to the problem of UAV position and resource allocation. In [30], the authors proposed a DRL algorithm based on echo state network (ESN) cells for optimizing the UAV path, cell association to minimize the intercell interference level, transmission delay, and transmit power level. In [32], the ESN algorithm was used based on a multiagent Q-learning approach, which was employed to predict the future positions of UEs and determine the positions of UAVs. However, this work did not consider UAV cooperation and capacity limitations of fronthaul links between UAVs and regular base stations. Further, for the optimization of FBS placement, the studies in [27], [28], [33] used an RL algorithm. In this work, we present an RAN slicing framework based on a DRL methodology that complements the location optimization model obtained in [13] by adding a radio channel model and optimizing the RAN slice resources between multiple FBSs covering an arbitrary area.

E. RADIO OPTIMIZATION PROBLEM FORMULATION

To apply the DRL methodology explained in the previous subsection, we define the radio optimization problem that this paper aims to optimize. Thus, details of the cost function and its constraints are defined in the following.

Denoting RAN slices and power vectors in the time slot t as $\boldsymbol{\beta}^{(t)} = \left[\beta_{1,1}^{(t)}, \beta_{1,2}^{(t)}, \cdots, \beta_{N,M}^{(t)}\right]^T$ and $\boldsymbol{p}^{(t)} = \left[p_1^{(t)}, \cdots, p_N^{(t)}\right]^T$ respectively, we define the sum-rate maximization problem as

$$\begin{aligned} \max_{\boldsymbol{p}^{(t)}, \boldsymbol{\alpha}^{(t)}} \quad & \sum_{n=1}^{N} \bar{\mathcal{C}}_n^{(t)}(x_i, y_n) \\ \text{s.t.} \quad & 0 \leq p_n^{(t)} \leq P_{\text{max}}, \forall n \in \mathcal{N}, \\ & \beta_{n,m}^{(t)} \in \{0,1\}, \forall n \in \mathcal{N}, \forall m \in \mathcal{M}, \\ & \sum_{m \in \mathcal{M}} \beta_{n,m}^{(t)} = 1, \forall n \in \mathcal{N}, \end{aligned} \tag{22}$$

where $\bar{\mathcal{C}}_n^{(t)} = \sum_{m=1}^{M} \bar{\mathcal{C}}_{n,m}^{(t)}(x_i, y_n)$.

The nonconvex problem in (22) requires a highly complex approach that could also increase the computational complexity. To handle this nonconvex problem, we consider a multiagent learning scheme, where each transmitter, mounted in each FBS, operates as an independent learning agent. Each agent successfully executes two policies to determine its associated RAN slice and transmission power level. The proposed multiagent approach is easily scalable to more extensive networks and can operate with local information after training.

The components of the DRL methodology considered based on the system model described before is composed by:

- **Agents:** in the multiple learning approach, the FBSs represent the agents.
- **Policies:** two well defined policies are considered. π_1 to choose an specific RAN slice, and the π_2 to select a proper power level for each user.
- **Actions:** we consider two well defined group of actions. The discrete actions related to the selection of RAN slices, and the continuous action to choose the power transmission for each individual user.
- **States:** It is composed by a tuple of information related to the RAN slice allocation, the SE, interference in each individual user, gain and interference in each user.
- **Rewards:** a proportional value of the SE in each receiver (UE) is used as reward. It considers the following criteria: the SE is evaluated in every user with the condition of one neighbourhood base station (BS) or agent is not transmitting. Thus, if the SE value is significant, then the BS being evaluated is penalized. In contrast, if the SE remains, then the BS is rewarded.

At the beginning of each time slot, each agent successively executes two policies to determine its associated transmission power level and RAN slice selection. For this purpose, the DRL considers two optimization approaches. The first considers a Deep Q-network to optimize a stochastic policy that aims to improve the RAN slice selection. A second Deep Q-network optimizes a deterministic policy to select a suitable power transmission value. The agent of the second Deep Q-network requires the RAN slice decision of the first approach to determine its state input before setting the transmit power of the agent. A brief explanation of this approach is done in Algorithm 2.

IV. DESCRIPTION OF THE PROPOSED SOLUTION

This paper aims to complement and enhance the output obtained in [13], which is not optimal if evaluated in a real scenario. Thus, the resource allocation that we propose is conditioned to the prelocation of each FBS obtained using the methodology presented in Section II. As the benchmark does not consider any channel model to evaluate the intracell and intercell interference, it can get suboptimal results in practical wireless scenarios. In particular, we aim to address the following research questions that arise during the FBS network deployment in a real scenario:

- What can be the potential improvements based on the FBSs prelocation defined in [13]?,
- What is the performance of the simulation setup when different services are supported by the FBS network?,
- Is it possible to develop a practical optimization method that is capable of improving the performance of FBSs?.

To address these questions, we use a standard simulation model defined by 3GPP and a RAN slicing framework proposed in Section III, which is proposed to analyze the network performance using a DRL methodology to optimize the radio resources.

The whole optimization process is divided into three phases— data matrix generation, FBS location minimization,

Algorithm 2 Algorithm of the DRL approach.

▷ Main Loop
while Stop Criteria not met **do**
  RAN SLICE SELECTION()
  POWER CONTROL()

▷ RAN slice selection
function RAN SLICE SELECTION()
  ▷ Action Selection
  action $\leftarrow a_n^{(t)} \in \mathcal{A}_{\text{RAN-Slice}} = \{1, \cdots, M\} = \mathcal{M}$
  State set design $\leftarrow s_{n,m}^{(t)}$
  Training by a deep-Q Network
  Reward function design
  Update Policies: π_1

▷ Power Control
function POWER CONTROL()
  ▷ Action Selection
  action $\leftarrow a_{n,a_n^{(t)}}^{(t)} \in \mathcal{A}_{\text{power}} = [0, 1]$
  State set design $\leftarrow s_{n,a_n^{(t)}}^{(t)}$
  Training by a deep-Q Network
  Reward function design
  Update Policies: π_2

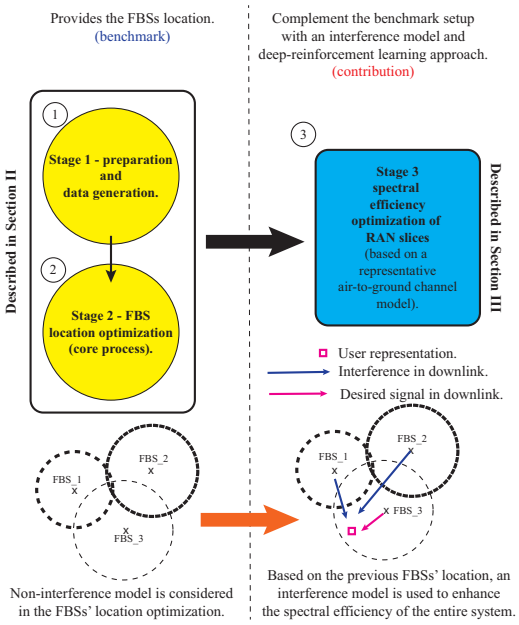

FIGURE 2. Optimization flow diagram showing major steps and stages. Here, we emphasis the optimization done in the benchmark (in yellow) and highlight the DRL approach (blue).

and RAN slicing optimization—as shown in Fig. 2. Here, Stages 1 and 2 have already been applied and verified in the original publication [13]. Details of each stage are described in the following paragraphs.

A. STAGE 1—DATA MATRIX GENERATION

In this stage, users are generated randomly and uniformly in one specific and fixed area. The FBSs are generated according to the desired radius. The larger the radius is, the lower the number of FBSs is required. A larger radius causes a higher percentage of overlaps. Note that Stages 1 and 2 do not take interference into consideration. Thus, interference has to be avoided by limiting the radio overlapping. The users are given random data rate requirements according to the traffic mix. The output of this stage is a matrix whose rows represent all FBSs and columns represent all users. The matrix is filled with zeros if the user is inside the specific FBS cell radius, and otherwise, it is filled with ones. This matrix is completed and used as the input for Stage 2.

B. STAGE 2—FBS LOCALIZATION

This stage is composed of a software service that uses the output of Stage 1. This stage aims to optimize the rows of the generated matrix so that the customer requirements are met. In this stage, we apply the optimization model from Section II-A. Because the complexity of selecting the optimal rows (FBSs) from the matrix is $\mathcal{O}(2^m)$, heuristic algorithms are applied. As a consequence, we use the differential evolution and cuckoo search algorithms with repair operators presented in [13]. The output of the computation is a set of FBSs (with their locations from the previous stage) that should be used in the network deployment. Further, the location of each FBS is used as an input to Stage 3, considering a representative interference channel model.

C. STAGE 3—OPTIMIZATION OF RAN SLICES

We add an interference model based on the 3GPP standard to complement the previous stages to analyze and mitigate downlink interference. Then, we calculate the SINR, defined in (17), for each user considering the signal strength coming from the serving UAV and from the FBSs that are interfering with that specific user n. Using (22), our simulation model calculates an optimal spectral efficiency for each user n following the proposed DRL approach on the RAN slicing framework defined in Section III.

V. SIMULATION SETUP

Two scenarios were designed to emphasize the gain of the optimization models that were previously explained. In both cases, 1000 users were deployed following a uniform distribution in a specific area. Subsequently, in accordance with the constraints in each scenario, the FBSs location optimizer determined the coordinates of each FBS. The constraints are mostly related to the cell radius, that depends on the radio frequency operation, and throughput demand of each user or group of users.

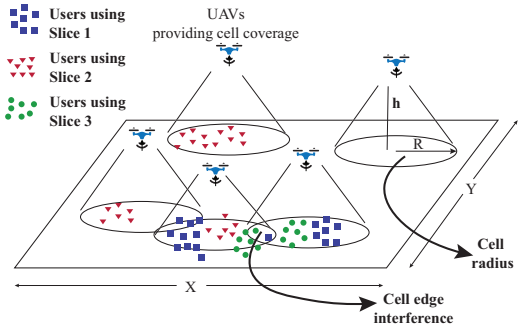

FIGURE 3. Generic simulation system model, considering the key constraints to be solved by the deep reinforcement learning approach.

Using the predetermined FBSs location, we consider a specific wireless system model. This system model considers an infinity backhaul capacity on each FBS. However, the offered bandwidth is limited in each FBS. The wireless system simulation considers that only a specific number of users are capable of getting the access stratum (AS)[2] interface. Thus, most of the users are in the RRC_IDLE and RRC_INACTIVE states, as defined in the 5G new radio (NR) standard. The remaining users that passed the random access procedure at the medium access control (MAC) layer are in the RRC_CONNECTED state.

To facilitate the analysis, we consider that each FBS is capable of supporting a fixed number of users N in the RRC_CONNECTED state. Based on this assumption, the cellular network is simulated with L FBSs, and each FBS supports K RAN slices. As we consider only downlink transmission, the interference that each user suffers from nonserving FBSs is calculated following the assumptions defined in the 3GPP TR 36.931 Ver. 16 specifications. The height altitude for all FBSs is 20 m.

The DRL and the wireless system model are deployed in Python. The machine learning implementation is done using TensorFlow libraries to implement the deep Q-network setup. The deep neural network used in the simulation has 3 hidden layers with 200, 100, 50 fully connected neurons. The batch size is 128. The epsilon-Greedy Algorithm, used in this work, considers a maximum ϵ equal to 0.1 and an ϵ_{decay} of 0.9995. The implementation and further hyper-parameters are available in the following Github URL *http://www.github.com/TBD*.

Three different scenarios were defined, considering aspects such as a fixed number of FBSs (Scenario 1), and coverage maximization with a fixed number of users in the desired coverage area and in each cell (Scenarios 2 and 3, respectively).

[2]AS is a functional interface that is responsible for transporting data over the wireless connection and managing radio resources.

TABLE 2. Comparison of parameters used in Scenarios 2 and 3.

Number of Users (N) – Scenario 2	Number of Users (N) – Scenario 3	Number of FBS (L)	Cell Radius in meters
114	152	38	50
114	76	19	75
114	44	11	100
114	32	8	120
114	24	6	140
114	16	4	160
114	16	4	180
114	12	3	200
114	8	2	300

A. SCENARIO 1—FIXED NUMBER OF AVAILABLE FBSs

This scenario considers $L = 20$ FBSs covering a specific area and supporting $N = 100$ users. To facilitate the analysis, it is considered that each FBS has $N/L = 5$ attached users. This scenario aims to identify an optimal cell radius supporting N users in the RRC_CONNECTED state. A graphical description of this scenario is shown in Fig. 4.

B. SCENARIO 2—MAXIMIZING THE NETWORK COVERAGE I

In this case, the number of FBSs (L) is defined by the optimization outputs of Stages 1 and 2, which were described in Section IV. Using Fig. 3 as a reference, the values of X and Y are 400 m. Thus, the number of FBSs is a function of cell radius; e.g., the larger the cell radius is, the smaller the number of FBSs needs to be deployed. In this scenario, the number of users N in the RRC_CONNECTED state is always the same in the area defined by X and Y. This scenario is illustrated in Fig. 5.

C. SCENARIO 3—MAXIMIZING THE NETWORK COVERAGE II

In this case, the number of UAVs (L) is defined by the optimization outputs of Stages 1 and 2, which were described in Section IV. Based on Fig. 3, the value of X and Y is fixed at 400 m. In this scenario, the number of N users in the RRC_CONNECTED state varies when the number of FBSs changes, as it is stated in Table 2. Each cell radius has a fixed number of N users in the scenario. Fig. 6 depicts this scenario.

VI. ANALYSIS AND RESULTS

A. ANALYSIS OF SCENARIO 1

The spectral efficiency obtained in Scenario 1 is presented in Fig. 7. Here, different cell radii between 50 m and 300 m are evaluated. In the same figure, the first 500 iterations of the first episode[3] (between 1 and 10000 iterations) are compared with the first 500 iterations of the second episode (between 10001 and 20000 iterations). The policy, defined in Subsection III-D, is almost null in the first iterations; the

[3]With *episode* we refer to a complete sequence of interactions, from start to finish. In our simulations, one episode is completed after 10 000 iterations.

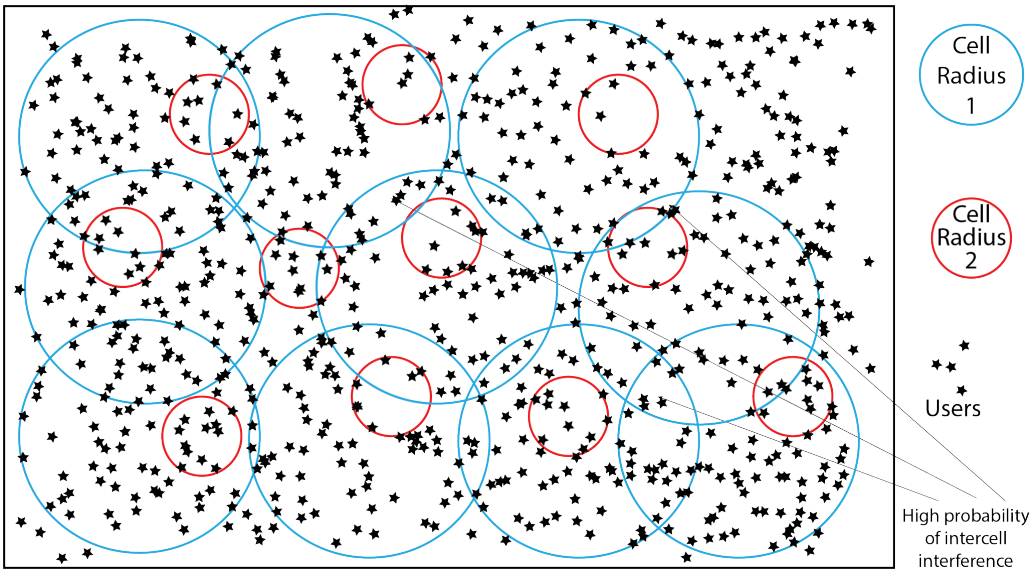

FIGURE 4. Visual description of Scenario 1. Here, the number of FBSs is a fixed, e.g., in this figure there are 11 UAVs. When the cell radius has a relatively high value with respect to the area of interest, the chances to have intercell interference is increased (cell radius 1). However, when the cell radius is small (cell radius 2), the chances of cell interference are reduced.

spectral efficiency is very low, similar to a random allocation of RAN slicing resources. At the beginning of episode 2, the spectral efficiency improves quickly despite that a new user deployment is considered.

To facilitate the interpretation of the simulation results, the average spectral efficiency in each scenario is calculated. For instance, Fig. 8 presents the results of Scenario 1 before and after applying the RAN slicing resource allocation. Before applying the resource allocation, the maximum spectral efficiency is almost 1.5 bps/Hz for the cell radius of 50 m. The spectral efficiency decreases for the other cell radii when the cell radius is increased. This output represents the network performance when only Stages 1 and 2, described in Section IV, are considered. However, the performance is improved in all cell radii after applying the DRL approach. In all cases, the spectral efficiency is improved. For instance, the cell radius of 75 m achieves a spectral efficiency of more than 3.5 bps/Hz, representing a gain of 2 bps/Hz compared with the setup without optimization.

B. ANALYSIS OF SCENARIO 2

In Fig. 9, the spectral efficiencies of six different cell radii were obtained after 30 000 iterations. In contrast to Scenario 1, the reinforcement learning approach yields a moderate improvement in the SE when compared with the original benchmark scenario. The best performance is obtained by the small cell radius of 50 m.

In Fig. 10, the lowest interference for Scenario 2 is for the cell with the radius equal to 100 m. However, this cell radius does not get the highest spectral efficiency because FBSs are deployed in such a way that the desired signal is not so strong when compared with cell radii of 50 and 75 m.

C. ANALYSIS OF SCENARIO 3

In this scenario, the SE indicates that the cell with a radius equal to 160 m obtains an SE of 4.5 bps/Hz, which is the best performance when compared with the previous scenarios. The interference in Fig. 10 indicates that in all cell radii of this scenario, the interference is above -100 dBm, which represents a less aggressive scenario in terms of interference when compared with the previous scenarios.

D. ANALYSIS OF THE RAN SLICING NETWORK PERFORMANCE

The proposed RAN slicing framework enables the analysis of the SE performance of individual RAN slices. We considered that the cellular network supports three different RAN slices following the 5G requirements defined in [34]. One slice supports eMBB, the second supports URLLC, and the third supports mMTC. To show the performance of this RAN

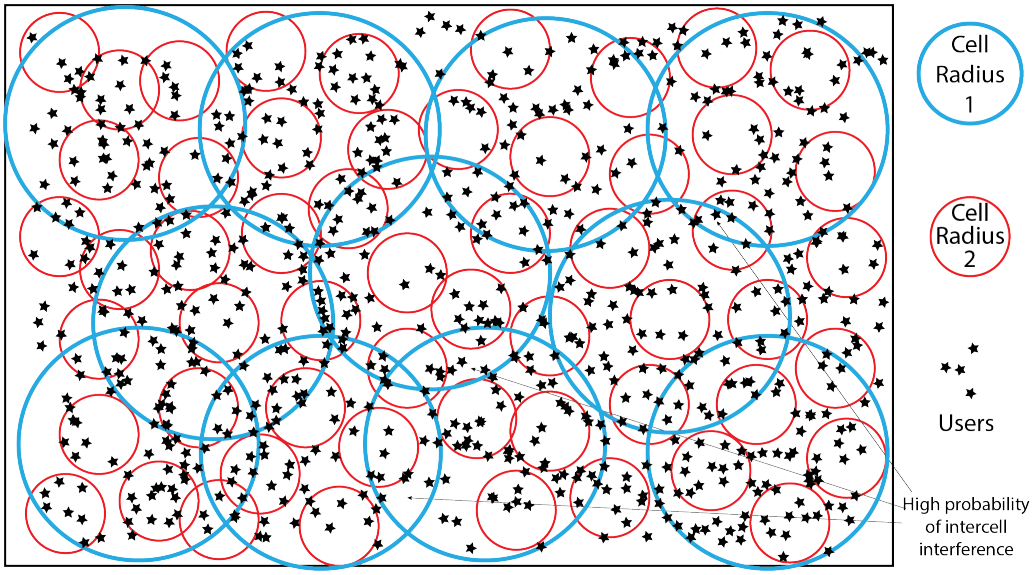

FIGURE 5. Visual description of Scenario 2. Here, the number of FBSs is not fixed. For instance, in this figure there are 11 UAVs for cell radius 1, and 75 UAVs for cell radius 2. When the cell radius has a relatively high value with respect to the area of interest, the chances to have intercell interference are increased (cell radius 1). However, when the cell radius is small (cell radius 2), the chances of cell interference are reduced. Here, the number of users (UEs) is fixed for both cell radius in the area of interest.

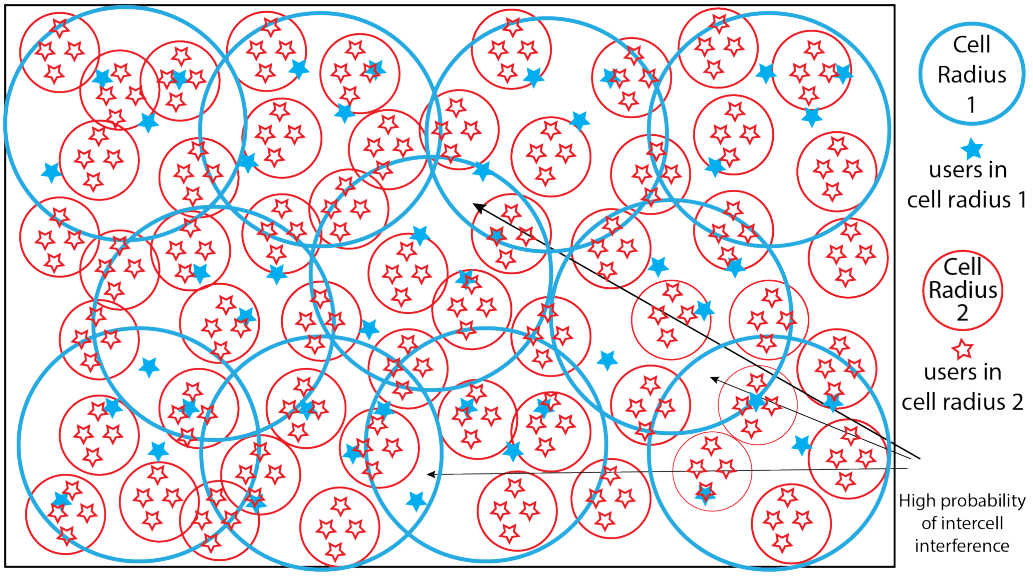

FIGURE 6. Visual description of Scenario 3. Here, the number of FBSs is not fixed. For instance, in this figure there are 11 UAVs for cell radius 1, and 75 UAVs for cell radius 2. Here, the number of users (UEs) is the same in every cell; in this illustrative representation every cell has four users. When the cell radius has a relatively high value with respect to the area of interest, the chances to have intercell interference are not significant (cell radius 1). However, when the cell radius is small (cell radius 2), the chances of cell interference are increased because the number of users in the area of interest is increased.

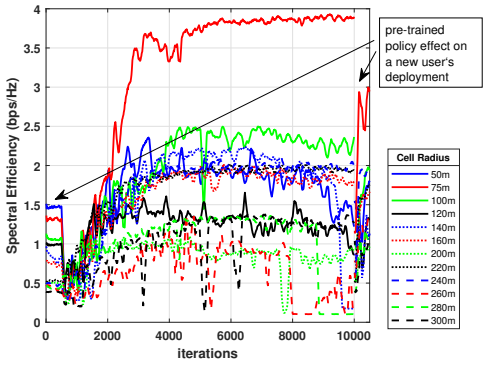

FIGURE 7. Spectral efficiency versus number of iterations obtained in Scenario 1 considering a diversity of radio cells. The first 500 iterations do not consider any pretrained DRL policy; after iteration 500 the policy gets a better understanding of the radio channel environment with a small degradation followed by a continuous improvement in most of the cells, especially in cells with small radius.

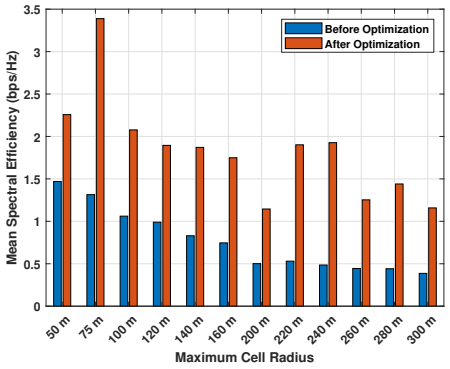

FIGURE 8. Mean of spectral efficiency of Scenario 1 comparing a diversity of cell radius before and after the RAN slicing resource allocation.

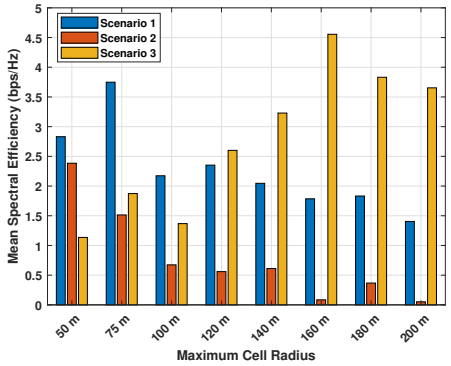

FIGURE 9. Mean spectral efficiency performance of different cell radii deployed for Scenarios 1, 2, and 3.

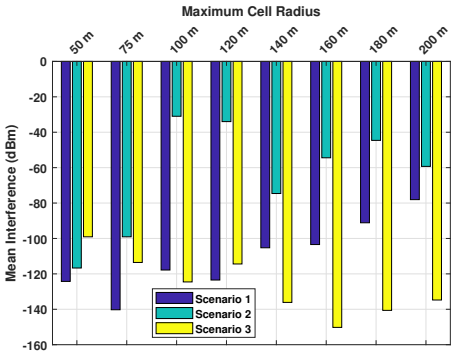

FIGURE 10. System interference of different cell radii deployed for Scenarios 1, 2, and 3.

slicing framework, we considered the cell radius equal to 50 m in Scenario 2.

In Fig. 11, we show the improvement in the time domain of the policy generated by the DRL model to prioritize the slice that supports URLLC data transmission over the other RAN slices. Based on the spectral efficiency of the previous figure, Fig. 12 shows the performance of each RAN slice in terms of delay. Here, the performance is improved only after the time slot 400, which means that the DRL policy has enough understanding of the RAN slicing environment. In the same Fig. 12, we present another way to visualize the performance of each RAN slice though SLA violation. Here, we can verify that the SLA violation of the URLLC slice only happens when the DRL model is starting to improve the policies defined by the optimizer. The other RAN slices still present frequent SLA violation, especially the slice related to mMTC, which is mainly used for noncritical applications. However, this SLA violations can be improved if the RAN slicing target is relaxed, which is feasible in non-critical applications.

VII. CONCLUSIONS

In this paper, we have proposed a RAN slicing framework that enables the allocation of radio resources (slices) carrying specific data services since it can achieve the diverse performance requirements introduced by 5G wireless systems. Our proposed framework aims to accommodate a diversity of services over a single shared 5G infrastructure and lays the foundation for fine-grained service management in FBS networks. In particular, we have demonstrated that the DRL model with the proposed RAN slicing approach

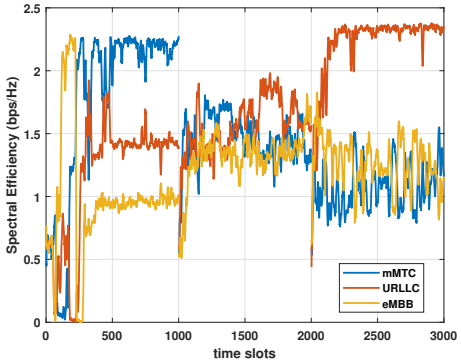

FIGURE 11. Spectral efficiency performance of three RAN slices deployed in the cell with a radius of 50 m in Scenario 2.

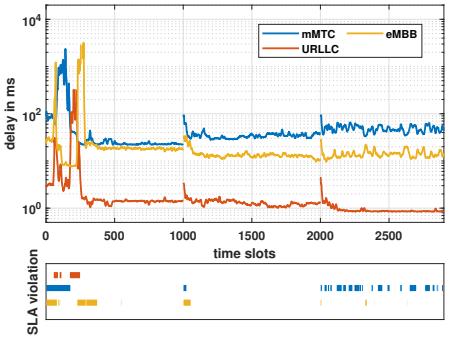

FIGURE 12. Delay of three RAN slices in the scenario with a cell radius of 50 m in Scenario 2.

is suitable for improving the SE of a predefined location distribution of FBSs. Three scenarios were considered to evaluate the performance of the proposed framework. These scenarios were generated by modifying key parameters, such as the number of FBSs and cell radius, and the optimization target of the predefined FBSs location. In all cases, the SE performance was improved when compared with the benchmark performance. However, the proposed methodology was more suitable for Scenario 3 because it presented a wireless network setup with low intercell interference.

The SE performance obtained in Scenarios 2 and 3 indicates that the deployment of the proposed framework in real scenarios can consider both approaches, and the specific cell radius should be chosen based on the network scenario. For instance, when there is a high density of users, Scenario 2 with a cell radius of 50 m is the most suitable setup to improve the SE system performance. On the other hand, if there is a moderate or low user density, Scenario 3 with a cell radius of 160 m will yield a better performance.

Potential future work that we have identified after the elaboration of this paper could include but is not limited to running a simulation on a setup with different radii on each FBS; adding another dimension to the analysis, based on the flying level or altitude of each FBS; and generating a full optimization of FBS location considering a cost function based on the system SE.

REFERENCES

[1] R. Shakeri, M. A. Al-Garadi, A. Badawy, A. Mohamed, T. Khattab, A. K. Al-Ali, K. A. Harras, and M. Guizani, "Design Challenges of Multi-UAV Systems in Cyber-physical Applications: a Comprehensive Survey and Future Directions," IEEE Communications Surveys & Tutorials, vol. 21, no. 4, pp. 3340–3385, 2019.

[2] M. Mozaffari, W. Saad, M. Bennis, and M. Debbah, "Mobile Unmanned Aerial Vehicles (UAVs) for Energy-Efficient Internet of Things Communications," IEEE Transactions on Wireless Communications, vol. 16, no. 11, pp. 7574–7589, 2017.

[3] A. Fekete and S. Sandholz, "Here Comes the Flood, but Not Failure? Lessons to Learn after the Heavy Rain and Pluvial Floods in Germany 2021," Water, vol. 13, no. 21, p. 3016, 2021.

[4] A. F. Ganazhapa, N. Palmieri, and M. I. C. Pushug, "Drones for Connectivity Support in Disaster Recovery," in Unmanned Systems Technology XXII, volume=11425. International Society for Optics and Photonics, 2020, p. 114250M.

[5] M. Mozaffari, A. Taleb Zadeh Kasgari, W. Saad, M. Bennis, and M. Debbah, "Beyond 5G With UAVs: Foundations of a 3D Wireless Cellular Network," IEEE Transactions on Wireless Communications, vol. 18, no. 1, pp. 357–372, 2019.

[6] G. Amponis, T. Lagkas, M. Zevgara, G. Katsikas, T. Xirofotos, I. Moscholios, and P. Sarigiannidis, "Drones in B5G/6G Networks as Flying Base Stations," Drones, vol. 6, no. 2, 2022. [Online]. Available: https://www.mdpi.com/2504-446X/6/2/39

[7] P. Mach, Z. Becvar, and M. Najla, "Joint Association, Transmission Power Allocation and Positioning of Flying Base Stations Considering Limited Backhaul," in 2020 IEEE 92nd Vehicular Technology Conference (VTC2020-Fall), 2020, pp. 1–7.

[8] J. Plachy, Z. Becvar, P. Mach, R. Marik, and M. Vondra, "Joint Positioning of Flying Base Stations and Association of Users: Evolutionary-Based Approach," IEEE Access, vol. 7, pp. 11 454–11 463, 2019.

[9] M. S. Hossain and Z. Becvar, "Soft Frequency Reuse With Allocation of Resource Plans Based on Machine Learning in the Networks With Flying Base Stations," IEEE Access, vol. 9, pp. 104 887–104 903, 2021.

[10] J. Qin, Z. Wei, C. Qiu, and Z. Feng, "Edge-Prior Placement Algorithm for UAV-Mounted Base Stations," in 2019 IEEE Wireless Communications and Networking Conference (WCNC), 2019, pp. 1–6.

[11] T. Kimura and M. Ogura, "Distributed Collaborative 3D-Deployment of UAV Base Stations for On-Demand Coverage, year=2020, volume=, number=, pages=1748-1757, doi=10.1109/INFOCOM41043.2020.9155283," in IEEE INFOCOM 2020 - IEEE Conference on Computer Communications.

[12] H. Wang, H. Zhao, W. Wu, J. Xiong, D. Ma, and J. Wei, "Deployment Algorithms of Flying Base Stations: 5G and Beyond With UAVs," IEEE Internet of Things Journal, vol. 6, no. 6, pp. 10 009–10 027, 2019.

[13] J. Pokorny, P. Seda, M. Seda, and J. Hosek, "Modeling Optimal Location Distribution for Deployment of Flying Base Stations as On-demand Connectivity Enablers in Real-world Scenarios," Sensors, vol. 21, no. 16, p. 5580, 2021.

[14] J. Yao and J. Xu, "Joint 3D Maneuver and Power Adaptation for Secure UAV Communication With CoMP Reception," IEEE Transactions on Wireless Communications, vol. 19, no. 10, pp. 6992–7006, 2020.

[15] M. Mozaffari, A. Taleb Zadeh Kasgari, W. Saad, M. Bennis, and M. Debbah, "Beyond 5G With UAVs: Foundations of a 3D Wireless Cellular Network," IEEE Transactions on Wireless Communications, vol. 18, no. 1, pp. 357–372, 2019.

[16] M. Kenyeres and J. Kenyeres, "Average Consensus over Mobile Wireless Sensor Networks: Weight Matrix Guaranteeing Convergence without Reconfiguration of Edge Weights," Sensors, vol. 20, no. 13, p. 3677, 2020.
[17] B. Wang, R. Zhang, C. Chen, X. Cheng, L. Yang, H. Li, and Y. Jin, "Graph-Based File Dispatching Protocol With D2D-Enhanced UAV-NOMA Communications in Large-Scale Networks," IEEE Internet of Things Journal, vol. 7, no. 9, pp. 8615–8630, 2020.
[18] M. Kenyeres and J. Kenyeres, "Distributed Mechanism for Detecting Average Consensus with Maximum-Degree Weights in Bipartite Regular Graphs," Mathematics, vol. 9, no. 23, p. 3020, 2021.
[19] M. R. Garey and D. S. Johnson, Computers and intractability. freeman San Francisco, 1979, vol. 174.
[20] C. ReVelle, C. Toregas, and L. Falkson, "Applications of the Location Set-covering Problem," Geographical analysis, vol. 8, no. 1, pp. 65–76, 1976.
[21] R. Church and C. ReVelle, "The Maximal Covering Location Problem," in Papers of the regional science association, vol. 32, no. 1. Springer-Verlag, 1974, pp. 101–118.
[22] Q. Zhang, W. Saad, M. Bennis, X. Lu, M. Debbah, and W. Zuo, "Predictive Deployment of UAV Base Stations in Wireless Networks: Machine Learning Meets Contract Theory," IEEE Transactions on Wireless Communications, vol. 20, no. 1, pp. 637–652, 2021.
[23] 3GPP, "Technical Specification Group Services and System Aspects; Management and orchestration; Architecture framework," 3rd Generation Partnership Project (3GPP), Technical Specification (TS) 28.533, March 2020, version 16.3.0.
[24] V. François-Lavet, P. Henderson, R. Islam, M. G. Bellemare, and J. Pineau, "An Introduction to Deep-reinforcement Learning," arXiv preprint arXiv:1811.12560, 2018.
[25] M. Kenyeres and J. Kenyeres, "Comparative Study of Distributed Consensus Gossip Algorithms for Network Size Estimation in Multi-Agent Systems," Future Internet, vol. 13, no. 5, p. 134, 2021.
[26] M. Morales, Grokking Deep Reinforcement Learning. Manning Publications, 2020.
[27] E. Krijestorac, S. Hanna, and D. Cabric, "UAV Access Point Placement for Connectivity to a User With Unknown Location Using Deep RL," in 2019 IEEE Globecom Workshops (GC Wkshps). IEEE, 2019, pp. 1–6.
[28] J. Qiu, J. Lyu, and L. Fu, "Placement Optimization of Aerial Base Stations with Deep Reinforcement Learning," in ICC 2020-2020 IEEE International Conference on Communications (ICC). IEEE, 2020, pp. 1–6.
[29] Q. V. Do, Q.-V. Pham, and W.-J. Hwang, "Deep Reinforcement Learning for Energy-Efficient Federated Learning in UAV-Enabled Wireless Powered Networks," IEEE Communications Letters, 2021.
[30] U. Challita, W. Saad, and C. Bettstetter, "Interference Management for Cellular-connected UAVs: A Deep Reinforcement Learning Approach," IEEE Transactions on Wireless Communications, vol. 18, no. 4, pp. 2125–2140, 2019.
[31] P. Luong, F. Gagnon, L.-N. Tran, and F. Labeau, "Deep Reinforcement Learning Based Resource Allocation in Cooperative UAV-Assisted Wireless Networks," IEEE Transactions on Wireless Communications, 2021.
[32] X. Liu, Y. Liu, Y. Chen, and L. Hanzo, "Trajectory Design and Power Control for Multi-UAV Assisted Wireless Networks: A Machine Learning Approach," IEEE Transactions on Vehicular Technology, vol. 68, no. 8, pp. 7957–7969, 2019.
[33] T. Bai, C. Pan, J. Wang, Y. Deng, M. Elkashlan, A. Nallanathan, and L. Hanzo, "Dynamic Aerial Base Station Placement for Minimum-Delay Communications," IEEE Internet of Things Journal, vol. 8, no. 3, pp. 1623–1635, 2020.
[34] M. J. Marcus, "5G and "IMT for 2020 and beyond" [Spectrum Policy and Regulatory Issues]," IEEE Wireless Communications, vol. 22, no. 4, pp. 2–3, 2015.

DICK CARRILLO MELGAREJO (M'06) received the B.Eng. degree (Hons.) in electronics and electrical engineering from San Marcos National University, Lima, Perú, and the M.Sc. degree in electrical engineering from Pontifical Catholic University of Rio de Janeiro, Rio de Janeiro, Brazil, in 2004 and 2008, respectively. Between 2008 and 2010, he contributed to WIMAX (IEEE 802.16m) standardization. From 2010 to 2018, he worked with the design and implementation of cognitive radio networks and projects based on 3GPP technologies. Since 2018 he is a researcher at Lappeenranta–Lahti University of Technology, where he is also pursuing the doctoral degree in electrical engineering. His research interests are mobile technologies beyond 5G, energy harvesting, intelligent meta-surfaces, cell-free mMIMO, and RAN Slicing. Since 2022, he is a Senior Standardization Specialist at Nokia Bell Labs, where he is contributing on shaping the 3GPP release 18 standard (5G-Advanced).

JIRI POKORNY is a Ph.D. candidate in a double degree program at the Department of Telecommunications, Brno University of Technology (BUT), Czech Republic, and at Tampere University, Finland. He received his M.Sc. in communications and informatics (2016) from BUT. His research focuses on wireless communication networks and unmanned aerial vehicles. Currently, his main task is the location optimization of flying base stations in crowded scenarios. His past experience involves research on LPWA networks, mainly on the NB-IoT technology. He has published five journal papers and more than ten papers in international conferences.

ARUN NARAYANAN (M'14) received his B.E. degree in Electrical Engineering from Visvesvaraya National Institute of Technology, Nagpur, India and M.Sc. in Energy Technology from Lappeenranta University of Technology (LUT), Finland, in 2002 and 2013, respectively. He subsequently completed his doctoral degree from the School of Energy Systems, LUT University, in 2019.

He is currently a postdoctoral researcher with LUT University, Lappeenranta, Finland, in the Cyber-Physical Systems Group. His research interests include renewable energy-based smart microgrids, electricity distribution and markets, demand-side management, energy management systems, and information and communications technology. He focuses on applying optimization, computational concepts, and artificial intelligence techniques to renewable electrical energy problems.

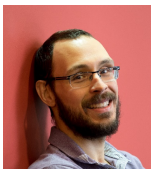

PEDRO H. J. NARDELLI received the B.S. and M.Sc. degrees in electrical engineering from the State University of Campinas, Brazil, in 2006 and 2008, respectively. In 2013, he received his doctoral degree from the University of Oulu, Finland, and the State University of Campinas following a dual degree agreement. He is currently Associate Professor (tenure track) in IoT in Energy Systems at LUT University, Finland, and holds a position of Academy of Finland Research Fellow with a project called Building the Energy Internet as a large-scale IoT-based cyber-physical system that manages the energy inventory of distribution grids as discretized packets via machine-type communications (EnergyNet). He leads the Cyber-Physical Systems Group at LUT and is Project Coordinator of the CHIST-ERA European consortium Framework for the Identification of Rare Events via Machine Learning and IoT Networks (FIREMAN). He is also Adjunct Professor at the University of Oulu in the topic of "communications strategies and information processing in energy systems". His research focuses on wireless communications particularly applied in industrial automation and energy systems. He received a best paper award of the IEEE PES Innovative Smart Grid Technologies Latin America 2019 in the track "Big Data and Internet of Things". He is also an IEEE Senior Member. More information: https://sites.google.com/view/nardelli/

MEHDI RASTI (S'08-M'11-SM'21) is currently an Associated Professor at the Department of Computer Engineering, Amirkabir University of Technology, Tehran, Iran and is a visiting researcher at the Lappeenranta-Lahti University of Technology (LUT), Lappeenranta, Finland. From November 2007 to November 2008, he was a visiting researcher at the Wireless@KTH, Royal Institute of Technology, Stockholm, Sweden. From September 2010 to July 2012 he was with Shiraz University of Technology, Shiraz, Iran. From June 2013 to August 2013, and from July 2014 to August 2014 he was a visiting researcher in the Department of Electrical and Computer Engineering, University of Manitoba, Winnipeg, MB, Canada. He received his B.Sc. degree from Shiraz University, Shiraz, Iran, and the M.Sc. and Ph.D. degrees both from Tarbiat Modares University, Tehran, Iran, all in Electrical Engineering in 2001, 2003 and 2009, respectively. His current research interests include radio resource allocation in IoT, Beyond 5G and 6G wireless networks.

PAVEL SEDA received his M.Sc. degree in communications and informatics from the Brno University of Technology and also M.Sc. in Applied Informatics from Masaryk University. From 2014 to 2018 Pavel worked as a Java Developer at IBM. Currently, Pavel focuses on research topics on cybersecurity, technologies, optimization, and cybersecurity education.

JIRI HOSEK received his M.S. and Ph.D. degrees in electrical engineering from the Faculty of Electrical Engineering and Communication at Brno University of Technology (BUT), Czech Republic, in 2007 and 2011, respectively. He is currently working as an Associate Professor and Deputy Vice-head for R&D and international relations at the Department of Telecommunications, BUT. His research work has concentrated on industry-oriented R&D projects in the area of future mobile networks, the Internet of Things, and home automation services. He has (co-)authored more than 130 research works on networking technologies, wireless communications, quality of service, user experience, and IoT applications.

MILOS SEDA received the M.Sc. and Ph.D. degrees in cybernetics from the Brno University of Technology and the M.Sc. degree in mathematical computer science from Masaryk University. From 1976 to 1986, he was a System Designer with První brněnská strojírna. He is currently a Professor and a Senior Researcher with the Institute of Automation and Computer Science, BUT. His current research interests include meta-heuristic algorithms, stochastic systems, and graph algorithms. He has (co)-authored over 150 research works on those topics.

DEMÓSTENES Z. RODRÍGUEZ (M'12-SM'15) received the B.S. degree in electronic engineering from the Pontifical Catholic University of Perú, the M.S. degree and Ph.D. degree from the University of São Paulo in 2009 and 2013. He is currently an Adjunct Professor with the Department of Computer Science, Federal University of Lavras, Brazil. He has a solid knowledge in Telecommunication Systems and Computer Science based on 15 years of professional experience in major companies. His research interest includes QoS and QoE in Multimedia services, architect solutions in Telecommunication Systems, artificial intelligence algorithms, and online social networks.

YEVGENI KOUCHERYAVY received the Ph.D. degree from the Tampere University of Technology (TUT), Finland. He is currently a Professor at the unit of Electrical Engineering, Tampere University. He is the author of numerous publications in the field of advanced wired and wireless networking and communications. His current research interests include various aspects in heterogeneous wireless communication networks and systems, the Internet of Things and its standardization, and nanocommunications.

GUSTAVO FRAIDENRAICH was born in Pernambuco, Brazil in 1977. He graduated in Electrical Engineering from the Federal University of Pernambuco (UFPE), Brazil. He received his M.Sc. and Ph.D. degrees from the State University of Campinas, UNICAMP, Brazil, in 2002 and 2006, respectively. From 2006 to 2008, he worked as Postdoctoral Fellow at Stanford University (Star Lab Group) - USA. Currently, Dr. Fraidenraich is Assistant Professor at UNICAMP - Brazil and his research interests include Multiple Antenna Systems, Cooperative systems, Radar Systems and Wireless Communications in general. He has been associated editor of the ETT journal for many years. Dr. Fraidenraich was a recipient of the FAPESP (Fundação de Amparo à Pesquisa do Estado de São Paulo) young researcher Scholarship in 2009. He has published more than 50 international journal papers and more than a hundred conference papers of the first line. He is the president of the technical board of Venturus Company, a branch from Ericsson Company.

Publication III

Carrillo, D., Kumar, S., Fraidenraich, G., and Mendes, L.
Bit Error Probability for MMSE Receiver in GFDM Systems

Reprinted with permission from
IEEE Communications Letters
Vol. 22, no. 5, pp. 942–945, May 2018 (in press)

Bit Error Probability for MMSE Receiver in GFDM Systems

Dick Carrillo, Santosh Kumar, Gustavo Fraidenraich, and Luciano Leonel Mendes

***Abstract*—In this paper, we consider the minimum mean-square error (MMSE) receiver for the generalized frequency division multiplexing system (GFDM) over frequency selective fading channels (FSFC). We derive an approximate probability density function (PDF) for the signal-to-interference-plus-noise ratio (SINR). This expression allows us to obtain a new approximate, but rather accurate formulation for the bit error probability (BER) for a $\mathcal{M}$-QAM modulation scheme. Our results resort on the pivotal properties exhibited by eigenvalues of a circulant matrix. Since the entries of the channel matrix $\mathbf{H}_{\text{ch}}$ are complex Gaussian distributed, and the eigenvalues are given as a weighted sum of its entries, the joint eigenvalue distribution is also Gaussian. Comparisons of the simulated and analytical results validate our formulation and allow a quick and efficient tool to compute the bit error rate for the GFDM system.**

***Index Terms*—GFDM, Gamma approximation, MMSE, SINR.**

I. Introduction

Several important waveforms have been recently proposed for fifth generation of mobile network (5G). One of these technologies that is being proposed for low latency and high throughput is called Generalized Frequency Division Multiplexing (GFDM) [1]. It employs circular filtering in order to keep the signal well localized in time and frequency domains [2]. GFDM uses a single cyclic prefix (CP) for several time-slots, increasing the spectral efficiency even for Ultra Reliable Low Latency (URLL) applications. This waveform can also cover Orthogonal Frequency Division Multiplexing (OFDM) and Single Carrier Frequency Domain Equalization (SC-FDE) as corner cases, making it compatible with legacy technologies [3]. GFDM has proven to be flexible enough to be tailored for the different 5G scenarios [4]. The main drawback presented by GFDM is the self-interference when Matched filter (MF) is employed at the receiver side. This disadvantage can be mitigated by using zero-forcing (ZF) or minimum mean square error (MMSE) receivers, but with performance loss when compared with orthogonal waveforms. In [1] and [2], analytical expressions for the signal-to-interference-and-noise ratio (SINR) over additive white Gaussian noise (AWGN) channel, assuming MF and ZF receivers were provided. A similar study is performed in [5] for MMSE receiver over AWGN channel.

However, an analytical expression for the SINR, assuming a MMSE receiver over frequency-selective channel (FSC) has hitherto remained unavailable. In this paper, we derive an approximate probability density function (PDF) for the SINR, which can be used to derive a new closed-form expression for the bit error rate (BER), assuming a quadrature amplitude modulation (QAM) constellation. The proposed model is compared with computational simulations, showing that the expression proposed in this paper agrees with the Monte Carlo simulations in all investigated scenarios.

To the best of our knowledge, no similar results have been published in the literature before.

A. Transmitter

GFDM is a generic circular filtering multicarrier system that could be represented using matrix notation and can be rewritten as in [5]. So, $\mathbf{x} = \mathbf{A}\mathbf{d}$, where $\mathbf{A}$ is the modulation matrix GFDM and the vector $\mathbf{d}$ represents the complex data symbols $\mathbf{d} = [d_0\ d_1 \cdots\ d_{N-1}]^T$ with variance σ_{d}^2. A cyclic prefix (CP) of length N_{cp} is added to the GFDM signal $\mathbf{x}$ to prevent inter-block interference over FSC. Therefore, the transmitted signal is given by $\mathbf{x}_{\text{cp}} = [\mathbf{x}(N - N_{\text{cp}} + 1 : N);\ \mathbf{x}]$.

B. Receiver

Let $\mathbf{h} = [h_1, h_2, \cdots, h_L]^T$ be the channel impulse response vector where h_r, for $1 \leq r \leq L$, represents the complex baseband channel coefficient of the rth path, which we assume to be zero-mean circular symmetric complex Gaussian (ZMCSC). We also assume that the channel coefficients related to different paths are uncorrelated, and that $N_{\text{cp}} \geq L$. The received vector of length $N_{\text{t}} = N_{\text{cp}} + N + L - 1$ is given by $\mathbf{y}_{cp} = \mathbf{h} * \mathbf{x}_{\text{cp}} + \boldsymbol{\nu}_{\text{cp}}$, where the symbol $(*)$ denotes the linear convolution, $\boldsymbol{\nu}_{\text{cp}}$ is the AWGN vector of length N_{t} with variance σ_ν^2. After removing the CP on the receiver side, the linear convolution in (1) resumes to circular convolution, which means that frequency-domain equalization (FDE) can be exploited. After the CP removal, the received vector can be written as,

$$\mathbf{y} = \mathbf{H}_{\text{ch}}\mathbf{A}\mathbf{d} + \boldsymbol{\nu}, \tag{1}$$

where $\boldsymbol{\nu}$ is the AWGN vector of length N with variance σ_ν^2 and $\mathbf{H}_{\text{ch}}$ is a circulant Toeplitz matrix based on vector h given as [5]

$$\mathbf{H}_{\text{ch}} = \begin{bmatrix} h_1 & 0 & \cdots & 0 & h_L & \cdots & h_2 \\ h_2 & h_1 & \cdots & 0 & 0 & \cdots & h_3 \\ \vdots & & \ddots & & & \cdots & \vdots \\ h_L & h_{L-1} & \cdots & \cdots & \cdots & \cdots & 0 \\ 0 & h_L & \cdots & \cdots & \cdots & \cdots & 0 \\ \vdots & & \ddots & & & \cdots & \vdots \\ 0 & 0 & & h_L & \cdots & \cdots & h_1 \end{bmatrix} \tag{2}$$

The received vector $\mathbf{y}$ is distorted due to (i) self-interference coming from GFDM inherent non-orthogonality, and (ii) frequency selectivity introduced by the channel impulse response.

D. Carrillo and G. Fraidenraich are with the Department of Communications, Unicamp, Campinas, Brazil. e-mail: {dickm, gf}@decom.fee.unicamp.br

S. Kumar is with the Department of Physics, Shiv Nadar University, Gautam Buddha Nagar, Uttar Pradesh 201314, India. e-mail: {skumar.physics}@gmail.com

L. Mendes is with Inatel, Sta. Rita Sapucaí, Brazil. e-mail: {luciano}@inatel.br

At this point, MMSE equalization is used to estimate the transmitted complex data symbols.

The authors in [6] have presented an expression for the SINR of the nth data symbol given as,

$$\gamma_n = \frac{1}{\text{MMSE}_n} - 1 = \frac{1}{\left[(\mathbf{I}_N + \frac{p}{N}(\mathbf{H}_{\text{ch}}\mathbf{A})^\dagger \mathbf{H}_{\text{ch}}\mathbf{A})^{-1}\right]_{nn}} - 1, \tag{3}$$

in which the operator $(.)^\dagger$ represents the Hermitian-conjugate of a matrix, and p is the average SNR given as $p = \sigma_d^2/\sigma_\nu^2$.

II. Approximate Distribution for γ_n

The representation in (3) of the SINR allows to use the known results of the eigenvalue distribution of circulant matrices. Unfortunately, all the known results in the literature consider that the elements of the columns of $\mathbf{H}_{\text{ch}}$ are non-zero. Our approach presents the particularity that only L elements are different from zero. In order to address this constraint, we consider a matrix $\mathbf{H}$ given as [7]

$$\mathbf{H} = \begin{bmatrix} h_1 & h_N & \cdots & h_2 \\ h_2 & h_1 & \cdots & h_3 \\ \vdots & \vdots & \cdots & \vdots \\ h_N & h_{N-1} & \cdots & h_1 \end{bmatrix}, \tag{4}$$

where h_r $(r = 1, ..., N)$ is complex Gaussian distributed with zero mean and variance σ_r^2, and therefore with probability density function

$$p_{h_r}(h_r) = \frac{1}{2\pi\sigma_r^2} \exp\left(-\frac{|h_r|^2}{2\sigma_r^2}\right). \tag{5}$$

To obtain $\mathbf{H}_{\text{ch}}$ from $\mathbf{H}$, we can consider the limit $\sigma_r \to 0$ for $r = L + 1$ to N. As a consequence, in this limit the joint probability density of h_1 to h_N would be

$$p_{\mathbf{h}}(h_1, ..., h_N) = \prod_{r=1}^{L} \frac{1}{2\pi\sigma_r^2} \exp\left(-\frac{|h_r|^2}{2\sigma_r^2}\right) \cdot \prod_{s=L+1}^{N} \delta(h_s). \tag{6}$$

Here $\delta(\cdot)$ represents the Dirac delta function and for a complex argument it represents the product of two delta functions involving the real and imaginary parts, respectively.

Consider the matrix defined in (4). It, being a circulant matrix, possesses the normalized eigenvectors given by [7]

$$\boldsymbol{\phi_j} = \frac{1}{\sqrt{N}} \left[1, \omega_j, \omega_j^2, \ldots, \omega_j^{N-1}\right]^T, \quad j = 1, ..., N, \tag{7}$$

where $$\omega_j = \exp\left(i\frac{2\pi(j-1)}{N}\right), \quad j = 1, ..., N \tag{8}$$

are the Nth roots of unity, and i represents the imaginary unit. The corresponding eigenvalues are given by [7]

$$\lambda_j = \sum_{r=1}^{N} h_r\, \omega_j^{N-r+1}. \tag{9}$$

These complex eigenvalues have joint probability density given by

$$p_{\boldsymbol{\lambda}}(\lambda_1, ..., \lambda_N) = \prod_{j=1}^{N} \frac{1}{2\pi\Phi^2} \exp\left(-\frac{|\lambda_j|^2}{2\Phi^2}\right), \tag{10}$$

where $\Phi^2 = \sum_{r=1}^{N} \sigma_r^2$. Thus, the eigenvalues are i.i.d. Gaussians with zero mean and variance Φ^2 for both the real and imaginary parts. The unitary matrix $\mathbf{U}$ that diagonalizes $\mathbf{H}$ is described by

$$\mathbf{U}_{jl} = \frac{1}{\sqrt{N}}\omega_j^{l-1}, \quad l, j = 1, ..., N, \tag{11}$$

and is nothing but the normalized DFT matrix [8]. We now consider the limit $\sigma_r \to 0$ for $r = L + 1$ to N, in order to obtain the joint probability density of eigenvalues appropriate to $\mathbf{H}_{\text{ch}}$. This results in the same expression as (10), and now we may write $\Phi^2 = \sum_{r=1}^{L} \sigma_r^2$.

Although we have derived the joint eigenvalue density of $\mathbf{H}_{\text{ch}}$, we actually need that of $\mathbf{H}_{\text{ch}}\mathbf{A}$. In this case, the product $\mathbf{H}_{\text{ch}}\mathbf{A}$ is not a circulant matrix in general, and therefore it does not seem feasible to obtain a closed-form expression for the joint density of eigenvalues. However, we try below to obtain some approximate results, which turn out to be rather good for roll-off factors between 0 and 1. Owing to the Hermiticity of matrix $p\,(\mathbf{H}_{\text{ch}}\mathbf{A})^\dagger\mathbf{H}_{\text{ch}}\mathbf{A}$, we can write down its eigenvalue decomposition as $\widetilde{\mathbf{U}}^\dagger\mathbf{D}\widetilde{\mathbf{U}}$, where $\widetilde{\mathbf{U}}$ is a unitary matrix, not in general a DFT matrix $\mathbf{U}$, and $\mathbf{D}$ is a diagonal matrix with eigenvalues of $p\,(\mathbf{H}_{\text{ch}}\mathbf{A})^\dagger\mathbf{H}_{\text{ch}}\mathbf{A}$. We should note that this is equivalent to considering the singular value decomposition $\sqrt{p}\,\mathbf{H}_{\text{ch}}\mathbf{A} = \mathbf{V}\mathbf{M}\widetilde{\mathbf{U}}^\dagger$, where $\mathbf{V}$ is another unitary matrix and $\mathbf{M} = \text{diag}(\mu_1, ..., \mu_N)$ contains the singular values. This then yields $p\,(\mathbf{H}_{\text{ch}}\mathbf{A})^\dagger\mathbf{H}_{\text{ch}}\mathbf{A} = \widetilde{\mathbf{U}}\mathbf{M}^\dagger\mathbf{M}\widetilde{\mathbf{U}}^\dagger$ and therefore, $\mathbf{D} = \mathbf{M}^\dagger\mathbf{M}$. Consequently, the MMSE_n is given by

$$\begin{aligned} \alpha_n &= \left[\left(\mathbf{I} + \frac{p}{N}(\mathbf{H}_{\text{ch}}\mathbf{A})^\dagger\mathbf{H}_{\text{ch}}\mathbf{A}\right)^{-1}\right]_{nn} \\ &= \left[\widetilde{\mathbf{U}}\left(\mathbf{I} + \frac{1}{N}\mathbf{M}^\dagger\mathbf{M}\right)^{-1}\widetilde{\mathbf{U}}^\dagger\right]_{nn} \\ &= \sum_{r,s=1}^{N} \widetilde{\mathbf{U}}_{nr}\left(1 + \frac{1}{N}|\mu_r|^2\right)^{-1}\delta_{rs}\widetilde{\mathbf{U}}_{ns}^* \\ &= \sum_{r=1}^{N}\left(1 + \frac{1}{N}|\mu_r|^2\right)^{-1}|\widetilde{\mathbf{U}}_{nr}|^2 \end{aligned} \tag{12}$$

where δ_{rs} is the Kronecker delta. At this point we observe that if $\mathbf{A}$ had been a circulant matrix, then $\widetilde{\mathbf{U}}$ would be same as the DFT matrix given by (11), for which $|\mathbf{U}_{nr}|^2 = 1/N$. Moreover, in this case $\{\mu_j\}$ will be equal $\sqrt{p}$ times the product of eigenvalues of $\mathbf{H}_{\text{ch}}$ and $\mathbf{A}$, giving us

$$\alpha_n = \sum_{r=1}^{N} \frac{1}{N + |\mu_r|^2}. \tag{13}$$

For the roll-off factors between 0 and 1, as a leading approximation, we use this expression for a general modulation matrix $\mathbf{A}$. We also notice that for this approximation, α_n is same for all n. Within this assumption eigenvalues of $\mathbf{H}_{\text{ch}}\mathbf{A}$ are approximately the product of eigenvalues of $\mathbf{H}_{\text{ch}}$ and $\mathbf{A}$. As will be seen in the simulations, this assumptions holds very well for roll-off factors between 0 and 1. The symmetrized joint probability density of $\{\mu_j\}$ is this case is given by

$$p_{\boldsymbol{\mu}}(\mu_1, ..., \mu_N) \approx \frac{1}{N!}\sum_{\{q(j)\}}\left[\prod_{j=1}^{N}\frac{1}{2\pi p\Phi^2|\chi_{q(j)}|^2} \times \exp\left(-\frac{|\mu_j|^2}{2p\Phi^2|\chi_{q(j)}|^2}\right)\right]. \tag{14}$$

Here the sum involves all $N!$ permutations of $\{q(1), q(2), ..., q(N)\}$ over $\{1, 2, ..., N\}$. We should point

out that this expression would be exact if $\mathbf{A}$ happens to be a circulant matrix, and would describe the eigenvalues of $\sqrt{p}\,\mathbf{H}_{\text{ch}}\mathbf{A}$, the latter being also circulant.

For $N = 1$, exact PDF's of α_n and γ_n can be readily obtained using (13), (14), or directly using (3), as there is just one element in the matrix. Dropping the index '1', for simplicity, we find the PDF's of α and γ to be, respectively,

$$p_\alpha(\alpha) = \frac{1}{2p\Phi^2|\chi|^2\alpha^2}\exp\left(-\frac{(1-\alpha)}{2p\Phi^2|\chi|^2\alpha}\right),\ 0<\alpha\leq 1, \tag{15}$$

$$p_\gamma(\gamma) = \frac{1}{2p\Phi^2|\chi|^2}\exp\left(-\frac{\gamma}{2p\Phi^2|\chi|^2}\right),\ 0\leq\gamma<\infty. \tag{16}$$

However, for general N, it does not seem feasible to derive the PDF of α_n, and that of γ_n, in an exact manner. Therefore, we aim for an approximation using the mean (μ) and variance (σ^2) of α_n, which can be found using the joint PDF (14) as

$$\mu = \mathbb{E}[\alpha_n] = -\sum_{j=1}^{N}\left[\frac{1}{\Psi_j^2}\exp\left(\frac{N}{\Psi_j^2}\right)\text{Ei}\Big(-\frac{N}{\Psi_j^2}\Big)\right], \tag{17}$$

$$\begin{aligned}\sigma^2 &= \mathbb{E}[\alpha_n^2] - (\mathbb{E}[\alpha_n])^2\\ &= \sum_{j=1}^{N}\left[\frac{1}{N\Psi_j^2} + \frac{1}{\Psi_j^4}\exp\left(\frac{N}{\Psi_j^2}\right)\text{Ei}\Big(-\frac{N}{\Psi_j^2}\Big)\right.\\ &\quad\left. - \frac{1}{\Psi_j^4}\exp\left(\frac{2N}{\Psi_j^2}\right)\text{Ei}^2\Big(-\frac{N}{\Psi_j^2}\Big)\right],\end{aligned} \tag{18}$$

where $\text{Ei}(x)$ represents exponential integral function and

$$\Psi_j^2 = 2p\Phi^2|\chi_j|^2. \tag{19}$$

Note that since $\text{Ei}(x) = -\Gamma(0,x)$ for $x>0$, we may write the result in terms of the incomplete Gamma function $\Gamma(0,x)$. The derivations of (17) and (18) rely on exploiting the symmetry among eigenvalues in (14) and then switching over to polar coordinates. The desired expressions then follow on using the following integrals (with $a, b > 0$):

$$\int_0^\infty \frac{\rho}{a+\rho^2}e^{-b\rho^2}d\rho = -\frac{1}{2}e^{ab}\,\text{Ei}(-ab), \tag{20}$$

$$\int_0^\infty \frac{\rho}{(a+\rho^2)^2}e^{-b\rho^2}d\rho = \frac{1}{2a} + \frac{1}{2}be^{ab}\,\text{Ei}(-ab). \tag{21}$$

With the information of mean and variance, we propose a Gamma approximation for the PDF of α_n as

$$p_\alpha(\alpha_n) \approx \frac{1}{\Gamma(k)\,\theta^k}\,\alpha_n^{k-1}\exp\Big(-\frac{\alpha_n}{\theta}\Big), \tag{22}$$

where the parameters k and θ are found using the mean and variance of α_n as $\theta = \sigma^2/\mu$ and $k = \mu^2/\sigma^2$. So, the PDF of SINR, which is given as a function of α_n as $\gamma_n = \frac{1}{\alpha_n} - 1$, turns out to be

$$p_\gamma(\gamma_n) \approx \frac{1}{\Gamma(k)\,\theta^k}\,(1+\gamma_n)^{-1-k}\exp\left(-\frac{1}{(1+\gamma_n)\theta}\right). \tag{23}$$

Fig. 1 shows the mean error between (17), calculated using our approximate joint eigenvalue distribution given in (14), and the exact value, computed by simulation of the mean value of (12). The roll-off factors varies from 0.1 to 0.9. As it can be seen, the error is always less than 3%, which validates our approximation.

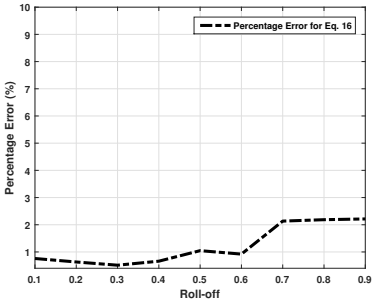

Fig. 1. Percentage error between (17), calculated using the approximate eigenvalue distribution given in (14), and the exact value computed by simulation of the mean value of (12), for roll-off factors varying from 0.1 to 0.9. This scenario considers 64 sub-carriers and 3 sub-symbols

III. Analytical derivation of the BER

As it was stated in [9], the BER for the lth bit error probability of $\mathcal{M}$-QAM constellation can be expressed as

$$P_b(E|\gamma_n) = \frac{1}{log_2\sqrt{\mathcal{M}}}\sum_{l=1}^{log_2\sqrt{\mathcal{M}}}\frac{1}{\sqrt{\mathcal{M}}}\sum_{t=0}^{(1-2^{-l})\sqrt{\mathcal{M}}-1}\left\{(-1)^{\left\lfloor\frac{t\,2^{l-1}}{\sqrt{\mathcal{M}}}\right\rfloor}\right. \tag{24}$$
$$\left.\times\left(2^{l-1} - \left\lfloor\frac{t\,2^{l-1}}{\sqrt{\mathcal{M}}} + \frac{1}{2}\right\rfloor\right)\times\text{erfc}\left((2t+1)\sqrt{\frac{3\log_2\mathcal{M}\,\gamma_n}{2(\mathcal{M}-1)}}\right)\right\},$$

where γ_n is the post-processing SINR for the nth received symbol given in (3). The average bit error probability can be written as

$$P_b(E) = \frac{1}{N}\times\sum_{n=0}^{N-1}\int_0^\infty P_b(E|\gamma_n)\;p_\gamma(\gamma_n)\,d\gamma_n. \tag{25}$$

Applying (23) and (24) into (25) leads to

$$P_b(E) \approx \frac{1}{N}\sum_{n=0}^{N-1}\int_0^\infty \frac{1}{log_2\sqrt{\mathcal{M}}}\sum_{l=1}^{log_2\sqrt{\mathcal{M}}}\frac{1}{\sqrt{\mathcal{M}}}\sum_{t=0}^{(1-2^{-l})\sqrt{\mathcal{M}}-1}\left\{(-1)^{\left\lfloor\frac{t\,2^{l-1}}{\sqrt{\mathcal{M}}}\right\rfloor}\right. \tag{26}$$
$$\left.\times\left(2^{l-1} - \left\lfloor\frac{t\,2^{l-1}}{\sqrt{\mathcal{M}}} + \frac{1}{2}\right\rfloor\right)\times\text{erfc}\left((2\,t+1)\sqrt{\frac{3\log_2\mathcal{M}\,\gamma_n}{2(\mathcal{M}-1)}}\right)\right\}$$
$$\times\frac{1}{\Gamma(k)\,\theta^k}\,(1+\gamma_n)^{-1-k}\exp\left(-\frac{1}{(1+\gamma_n)\theta}\right)d\gamma_n.$$

Using the Taylor series expansion for $e^x = \sum_{u=0}^{\infty}x^u/u!$, we can get a series representation to this integral, as expressed in (27), where ${}_1\tilde{F}_1$ is the regularized Confluent Hypergeometric function, and $\eta = (2r+1)\sqrt{\frac{3\log_2\mathcal{M}}{2(\mathcal{M}-1)}}$ where r is the index of the second sum in (27).

IV. Performance Analysis

The subsequent results are obtained through BER simulation using the GFDM parameters K (subcarriers), M (subsymbols), Root Raised Cosine (RRC) as prototype filter, roll-off factor, and power delay profile $\sigma_m^2 = e^{-0.2m},\ m = 1,\ldots,N$.

A. Simulation Results

Figure 2 compares the analytical and simulated Cumulative Density Function (CDF) with roll-off factor 0.1, assuming

$$P_b(E) \approx \frac{1}{log_2\sqrt{\mathcal{M}}} \sum_{l=1}^{log_2\sqrt{\mathcal{M}}} \sum_{r=0}^{(1-2^{-l})\sqrt{\mathcal{M}}-1} \sum_{t=0}^{\infty} \frac{\theta^{-t-k}(-1)^{\left\lfloor \frac{2^l-1_r}{\sqrt{\mathcal{M}}} \right\rfloor + t}}{2\sqrt{\mathcal{M}}t!(t+k)\Gamma(k)\Gamma(t+k+1)} \left(2\sec(\pi(t+k))\left\lfloor \frac{1}{2}\left(\frac{2^l r}{\sqrt{\mathcal{M}}}+1\right)\right\rfloor \left(\pi\eta(-t-k)\,{}_1\tilde{F}_1\right.\right.$$
$$\left.\left. \times \left(\frac{1}{2}; -t-k+\frac{3}{2}; \eta^2\right) + \Gamma(t+k+1)\left(\sqrt{\pi}\eta^{2(t+k)}\,{}_1\tilde{F}_1\left(t+k; t+k+\frac{1}{2}; \eta^2\right) - \cos(\pi(t+k))\right)\right) + 2^k\Gamma(t+k+1)\right) \quad (27)$$

three different signal-to-noise ratios (SNRs) (0 dB, 5 dB, and 10 dB). In all cases, the analytical model agrees with the simulated CDF of γ_n, which means that the approximation presented in (23) can be used to estimate the SINR.

Figure 3 shows the results with exponential power delay profile considering only the first $L = 2$ elements and nulling the others, $M = 3$, and $K = 32$ for the scenario 1, and $M = 5$, and $K = 64$ for scenario 2. In both cases, the modulations 4-QAM and 16-QAM are considered. The simulation and theoretical curves show an excellent agreement. These results validate our analytical approximation for the BER and show that they can be used to analyze the performance over FSC channels.

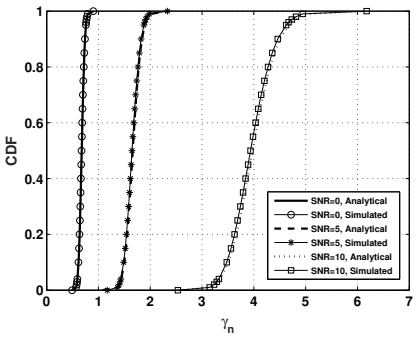

Fig. 2. Simulated and analytical CDF of γ_n obtained using the distribution of SINR_n given in (23), with $M = 32$, $K = 5$, roll-off factor of 0.1 for different values of SNR.

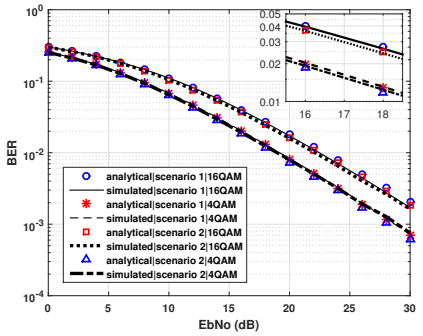

Fig. 3. Simulated and analytical BER for scenario 1 ($M = 3$, $K = 32$, $L = 2$, Roll-off= 0.9), scenario 2 ($M = 5$, $K = 64$, $L = 2$, Roll-off= 0.5), with modulation 4-QAM and 16-QAM, and exponential power delay profile.

V. Conclusion

In this paper, we have employed an analytical approach to calculate the SINR for GFDM waveform using the MMSE receiver, considering the influence of frequency selective fading channels. The pivotal properties exhibited by eigenvalues of a circulant matrix form the basis of the mathematical model used to obtain the sought-after SINR statistics. Our approach relies on finding a gamma-distribution approximation for the MMSE variable α_n. Subsequently, the corresponding approximate distribution for SINR variable γ_n has been derived based on the relationship $\gamma_n = 1/\alpha_n - 1$. This distribution then allowed us to obtained a series representation for the BER for a general $\mathcal{M}$-QAM constellation. The proposed mathematical model has been evaluated in several scenarios: using modulation schemes such as 4QAM and 16-QAM, and also varying the SNR between 0 dB and 30 dB. In all cases considered, the analytical predictions have agreed extremely well with the simulated CDF and BER, thereby validating the efficacy our results to analyze BER behavior for MMSE receiver in GFDM and similar systems.

Acknowledgments

We would like to thank the editor, Prof. Yue Xiao, and the anonymous reviewers for their constructive comments, which helped us to improve the manuscript.

References

[1] N. Michailow, M. Matthe, I. Gaspar, A. Caldevilla, L. Mendes, A. Festag, and G. Fettweis, "Generalized Frequency Division Multiplexing for 5th Generation Cellular Networks," *IEEE Trans. on Commun.*, vol. 62, no. 9, pp. 3045 – 3061, Sep 2014.

[2] M. Matth, N. Michailow, I. Gaspar, and G. Fettweis, "Influence of Pulse Shaping on Bit Error Rate Performance and Out of Band Radiation of Generalized Frequency Division Multiplexing," in *2014 IEEE International Conference on Communications Workshops (ICC)*, Jun 2014, pp. 43 – 48.

[3] I. Gaspar, L. Mendes, M. Matthe, N. Michailow, A. Festag, and G. Fettweis, "LTE-compatible 5G PHY based on Generalized Frequency Division Multiplexing," in *11th International Symposium on Wireless Communications Systems (ISWCS)*, Aug 2014, pp. 209 – 213.

[4] D. Zhang, M. Matthe, L. Mendes, and G. Fettweis, "A Study on the Link Level Performance of Advanced Multicarrier Waveforms under MIMO Wireless Communication Channels," *IEEE Trans. Wireless Commun.*, vol. 16, no. 4, pp. 2350 – 2365, Apr 2017.

[5] S. Tiwari, S. S. Das, and K. K. Bandyopadhyay, "Precoded Generalized Frequency Division Multiplexing System to Combat Intercarrier Interference: Performance Analysis," *IET Communications*, vol. 9, no. 15, pp. 1829 – 1841, May 2015.

[6] P. Li, D. Paul, R. Narasimhan, and J. Cioffi, "On the Distribution of SINR for the MMSE MIMO Receiver and Performance Analysis," *IEEE Trans. Inf. Theory*, vol. 52, no. 1, pp. 271 – 286, Jan 2006.

[7] R. M. Gray, "Toeplitz and circulant matrices: A review," *Commun. Inf. Theory*, vol. 2, no. 3, pp. 155–239, Aug. 2005.

[8] J. McClellan and T. Parks, "Eigenvalue and eigenvector decomposition of the discrete fourier transform," *IEEE Transactions on Audio and Electroacoustics*, vol. 20, no. 1, pp. 66–74, March 1972.

[9] K. Cho and D. Yoon, "On the general BER expression of one-and two-dimensional amplitude modulations," *IEEE Trans. on Commun.*, vol. 50, no. 7, pp. 1074–1080, Jul 2002.

Publication IV

Carrillo, D., Quirino, L., Machado de Medeiros, Á., Lorena, C., Lira, F., and Zegarra, D.
Dynamic Algorithm for Interference Mitigation Between Cells in Networks Operating in the 250 MHz Band

Reprinted with permission from
IEEE Access
Vol. 10, pp. 33803–33815, 2022 (in press)

IEEE Access
Multidisciplinary ⋮ Rapid Review ⋮ Open Access Journal

Date of publication xxxx 00, 0000, date of current version xxxx 00, 0000.

Digital Object Identifier 10.1109/ACCESS.2017.DOI

Dynamic Algorithm for Interference Mitigation Between Cells in Networks Operating in the 250 MHz Band

DICK CARRILLO MELGAREJO[1,2], LUIZ Q. R. DA COSTA FILHO[3], ALVARO A. M. DE MEDEIROS[3,4], CARLOS L. NETO[5], FABRICIO L. FIGUEIREDO[6], and DEMÓSTENES Z. RODRÍGUEZ[7].

[1]Department of Electrical Engineering, School of Energy Systems, Lappeenranta-Lahti University of Technology (LUT), Lappeenranta, Finland. (e-mail: dick.carrillo.melgarejo@lut.fi).
[2]School of Electrical and Computer Engineering, State University of Campinas (UNICAMP), Brazil.
[3]Department of Electrical Engineering, Federal University of Juiz de Fora University (UFJF), Juiz de Fora, MG, Brazil. (e-mail: [luiz.quirino, alvaro]@engenharia.ufjf.br).
[4]Department of Computer Science, Munster Technological University (MTU), Cork, Ireland.
[5]Tropico Systems and Telecommunications, Campinas, SP, Brazil. (e-mail: carlos.lorena@tropiconet.com).
[6]Research and Development Center in Telecommunications (CPqD), Campinas, SP, Brazil. (e-mail: fabricio@cpqd.com.br).
[7]Department of Computer Science, Universidade Federal de Lavras (UFLA), Lavras, MG, Brazil. (email: demostenes.zegarra@ufla.br).

Corresponding author: Dick Carrillo Melgarejo (e-mail: dick.carrillo.melgarejo@lut.fi).

This paper is partly supported by the Academy of Finland via: (a) FIREMAN consortium CHIST-ERA-17-BDSI-003/n.326270, and (b) EnergyNet Research Fellowship n.321265/n.328869; and by Jane and Aatos Erkko Foundation via the STREAM project

ABSTRACT The growing demand for Internet of Things (IoT) applications in agribusiness increases the necessity of reliable and secure connectivity in rural areas. Thus, in the particular case of Brazil, some initiatives aim to take advantage of frequency bands dedicated to limited private services. For instance, cellular networks based on orthogonal frequency-division multiple access (OFDMA) in 250 MHz bands require specialized adaptations because the interference between cells increases when these systems operate in the Very High Frequency (VHF) band. This work presents an analysis based on a reliable simulation of interference mitigation in OFDMA systems at 250 MHz using a network simulator. The simulator is calibrated with data obtained in the field by an extensive and rigorous drive test. Therefore, the analysis is based on a comparison of traditional frequency reuse schemes with a machine learning approach based on deep reinforcement learning (DRL) to reduce inter-cell interference. The numerical results indicate that the DRL approach outperforms the traditional frequency reuse (FR) schemes in four different typical agribusiness scenarios.

INDEX TERMS Frequency reuse, Internet of things, deep reinforcement learning, customized cellular networks, 250 MHz.

I. INTRODUCTION

THE Internet of Things (IoT) is an emerging and promising technology that aims to revolutionize the world through the connection of every physical object to the Internet. Although the IoT concept is generic, involving Internet connections in highly dense urban areas for a diversity of applications, many solutions are being developed for use in rural areas to support applications that today are being prioritized by the pandemic [1] (remote education, remote working, and remote healthcare), and also the agribusiness market [2]. Thus, relevant characteristics of rural regions, such as difficult access and long distances involved, have a direct impact on the development of IoT solutions for pandemic [3] and agribusiness scenarios [4]. Unfortunately, most of the technologies offered by telecom operators in urban areas are not available in remote areas, which makes it difficult to use adequate transport layer technologies to support IoT applications. Therefore, the use of very high frequency (VHF) bands is emerging as a technical solution to improve the propagation and optimize the coverage of wireless communication systems [5].

The increasing connectivity demand in rural areas has driven several research and development projects into designing cellular network solutions for this specific

scenario. Several wireless technologies are compared in [6] to provide Internet access in rural areas. Long-Term Evolution (LTE) arises as a solution that can provide a variety of services for rural IoT environments. For instance, the feasibility of an LTE network in the 800 MHz frequency band to serve rural areas in India and Spain is presented in [7] and [8]. The details of planning an LTE network operating in the 900 and 1800 MHz frequency bands in Indonesia are presented in [9]. In [10], the coverage and capacity of LTE IoT technologies, namely LTE machine-type communication (LTE-M) and narrowband IoT (NB-IoT), are analyzed in Denmark through an intensive drive test with the network operating in the 800 MHz frequency band. In [11], a Fourth Generation (4G) network is analyzed in the field in order to identify gaps that aim to be supported by Fifth Generation (5G) in rural scenarios.

One important drawback of using cellular networks in sub-1GHz bands, such as 250 MHz, is the inter-cell interference. To address this issue, in [12], a flexible tool was provided to implement traditional FR schemes in the LTE. Details of these FR techniques are described in a comprehensive survey of inter-cell interference coordination (ICIC) techniques in [13]. These techniques aim to improve the basic FR concept to mitigate or avoid interference between cells. As the FR evolves from a static to a dynamic procedure, the ICIC algorithm complexity increases such as typical resource allocation algorithms [14]. Such an increase in complexity requires higher processing capabilities of the base station, thereby having an impact on the final cost. This may not be an issue when a dense urban scenario is considered, where cells become smaller in order to meet the increasing demands of the traffic of a large number of users [15]–[17]. However, when it comes to a rural scenario, the extensive coverage requirements and the sparse user occupation of the cell discourage the cellular network deployment. Thus, there is a demand for simple and cheaper solutions that will not bring a significant increase in the operational and capital expenditures (OPEX/CAPEX) of IoT network providers [5], [18].

Recently, artificial intelligence methodologies for cellular network optimization have been gaining popularity. Especially in radio resource management, the allocation of resources is a difficult task. For instance, in [19], a deep reinforcement learning-based decentralized multiagent power control algorithm was proposed to improve the sum rate of a cellular network. In [20], multiagent deep reinforcement learning-based autonomous channel selection and transmission power selection were used to reduce the co-channel interference in a cellular network. However, to the best of author's knowledge, there is no similar approach with a proper comparison of traditional FR schemes with this deep reinforcement learning approach, especially in 250 MHz bands.

One of the primary motivations of this study is to compare the performance of traditional FR schemes with radio resource scheduling allocation based on deep reinforcement learning.

To establish the framework of our study, we provide a brief contextualization of the problem and a description of the particular scenario in Brazil and highlight the main contributions of this paper in the following subsections.

A. PROBLEM CONTEXTUALIZATION

As the rural scenario requires an extensive area cell coverage, the operation in a lower frequency band can make the provision of IoT services feasible for many agribusiness applications, such as precision farming, livestock control, storage monitoring, and automation of agricultural processes. However, the usage of lower frequency bands also implies higher inter-cell interference. An advanced solution is the use of directional antennas aimed at narrowing the radiation lobe of each sector and reducing the secondary lobes [21]. However, because of the low availability of off-the-shelf directional antennas for this frequency range, spectrum allocation and channel reuse control techniques, such as ICIC techniques, stand out as a viable solution for performance improvement in a VHF propagation scenario.

As the orthogonal frequency division multiplexing access (OFDMA) allows more specific occupation of the spectrum on a shorter time basis, the allocation management of resources for each user in the cell can be optimized in order to reduce the interference between cells. In such a way, a minimum quality of service (QoS) can be reached in different regions of the cell after applying techniques such as FR. Following this assumption, each resource block (RB) can be assigned with a specific transmission power to cell users in different time and space domains to reuse the neighbor cells.

B. THE PARTICULAR SCENARIO IN BRAZIL

In 2010, the Brazilian National Agency of Telecommunications (ANATEL) released Resolution 555 [22], which allocates 225 MHz to 270 MHz to the private limited service (SLP) on a primary and nonexclusive basis, aiming to modernize the radios that occupy this band. In this context, this paper presents a broadband system based on the LTE protocol stack, which was adapted and developed to operate in VHF bands. The target is to provide broadband IoT services to the agribusiness markets, because the coverage of large areas of plantations or pastures is favored by the best propagation in the range of VHF. This broadband technology has shown satisfactory results in terms of the radius of cell coverage and the ability to support several IoT solutions. As the 250 MHz frequency band is not available worldwide for such purposes, there is a lack of studies that analyze the performance of an LTE network in this scenario.

C. CONTRIBUTION

The main contributions of this study are the following:

- An open-source simulator is calibrated with data obtained in a driving test on a real scenario of the

network operating in 250 MHz in Brazil. Thus, our results provide a strong representation of what is expected in real scenarios.
(https://gitlab.com/aikonbrasil/freuse250mhz).
- A novel FR is proposed based on a deep reinforcement learning scheme to schedule sub-bands and power transmission simultaneously.
- The performance of typical FR schemes is evaluated and compared with the proposed approach in a cellular network operating in 250 MHz.
- An open source simulator is calibrated with data obtained by a drive test on a real scenario of the network operating in 250 MHz in Brazil. Thus, our results provide a strong representation of what is expected in real scenarios.

With the network simulator already calibrated to simulate real scenarios, we execute a performance analysis of ICIC techniques, presenting improvements in the system, especially in scenarios with high interference. Furthermore, we propose an algorithm that can be easily implemented in the deployed base stations in order to reduce interference considering performance for different scenarios.

The paper is organized as follows. Section II describes the cellular network developed for agribusiness applications that are used to obtain field measurements in 250 MHz. The adaptation of the ns-3 simulator to the field test network is detailed in Section III. Section IV gives a summary of the FR algorithms considered in this study. In Section IV-D, the algorithm proposed in this work is described. Section V provides details of the simulation campaign. In Section VI, the simulation results are presented and discussed. Conclusions and future work are addressed in Section VII.

II. DEPLOYMENT IN A REAL SCENARIO

Resolution 555 of the National Agency of Telecommunications (ANATEL) of Brazil, which allocates the 225 MHz to 270 MHz band to the Private Limited Service (SLP) on a primary and non-exclusive basis [22], was published in 2010 with the intent to modernize the radios operating in this band. In this context, a broadband system was developed based on the LTE to operate at this frequency band to provide broadband IoT services to the agribusiness market because the best propagation range of VHF favors the coverage of large areas of plantations or pastures.

The developed system is based on the protocol stack defined by the 3GPP LTE Release 8[1] [23] for the base station (BS) and cellular terminal (User Equipment or UE) software. The developed LTE system operates in the FDD (Frequency Division Duplex) mode, with a 5 MHz bandwidth, within the Resolution 555 bands described in Table 1.

The broadband system operating in the 250 MHz band was installed in a rural area of the interior of São Paulo belonging to a sugarcane plantation. The characteristics of the elements used to assemble this cellular network are described in Table 2.

[1]The same approach also applies to 5G new radio, since it is also based on OFDMA as stated in [11].

TABLE 1. Channeling used in the broadband system operating in the 250 MHz band.

Central Frequency (MHz)	Channels (Based on Res. 555 - ANATEL)	Band
228.75 (Uplink), 251.25 (Downlink)	1,2,3,4,5	A
237.50 (Uplink), 265.00 (Downlink)	7,8,9,10,11	B

TABLE 2. Key features of the broadband system operating in the deployed 250 MHz band.

Element Name/Feature	Quantity / Information
Base station	3 units
UE's (Terminal)	10 units
Frequency Band	Band A
Bandwidth	5 MHz (25 RBs)
Type of duplexing	FDD
BS Antenna Height	40 m
UE Antenna Height	3,5 m
Transmission power of each UE	30 dBm
Transmission power of each BS	43 dBm

A. DEPLOYED BROADBAND SYSTEM ARCHITECTURE

The field installation of the broadband system operating in the 250 MHz band was performed according to the architecture described in Fig. 1. In this Figure, it is possible to differentiate the main components of a cellular network, e.g., the evolved packet core (EPC), which is responsible for managing each user's features, such as charging, QoS, connectivity with external networks, IP packet addressing (Internet Protocol), paging processes, and user authentication. The other elements, installed in the field and taking care of the air interface, are part of the access network. The access network consists of the BS and the user terminal (UE). Note also in Fig. 1 that the UEs were installed on machines that participate in the sugarcane process. It is also possible to identify the network used as backhaul, called point-to-point (P2P) radio, in addition to other technologies used in IoT applications.

B. FIELD MEASUREMENTS

Field measurements were performed considering the topology shown in Fig. 2. In this Figure, it is observed that the distance between the base stations varies between 20 and 24 km. Fig. 2 also indicates the region to most likely present interference between cells.

A field measurement procedure was developed to collect data regarding throughput, signal to interference plus noise ratio (SINR), and system coverage. The system achieved a cell radius up to 40 km with an acceptable SINR value that enabled a data rate up to 2 Mbps (downlink).

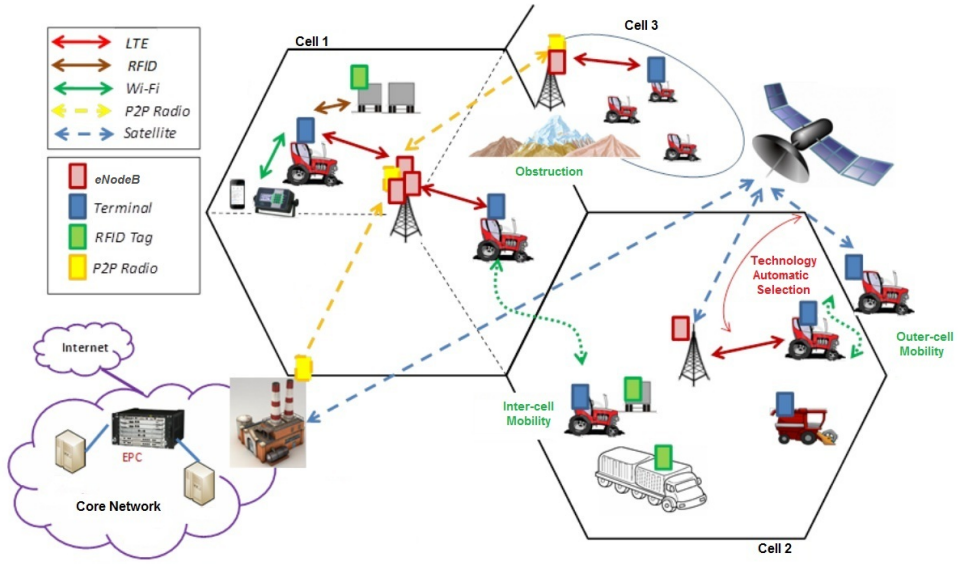

FIGURE 1. Agribusiness architecture deployed in the field using a broadband wireless network based on an OFDMA network, such as the LTE.

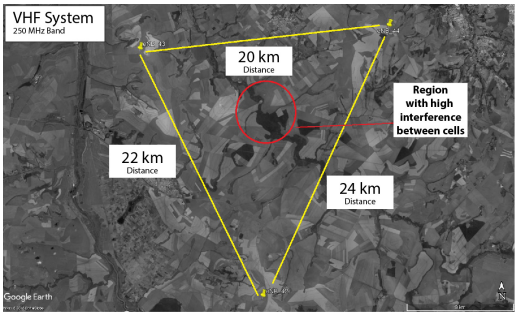

FIGURE 2. Topology of the broadband system operating in the 250 MHz band used for field measurements.

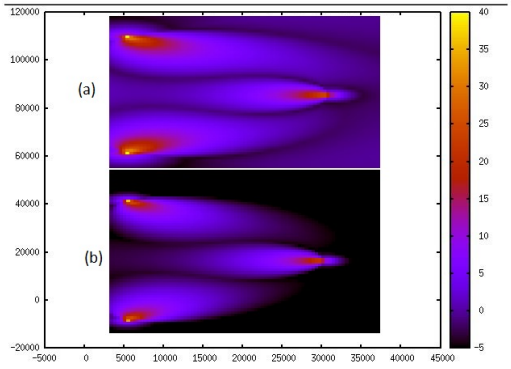

FIGURE 3. Adaptation of the configuration of the ns-3 LTE module to support the 250 MHz band. (a) Signal strength obtained in the ns-3 with EARFCN = 12 modified to operate in the 250 MHz band. (b) Signal strength obtained in the ns-3 with the original EARFCN = 12 operating in the 700 MHz band. The color bar represents the measured signal strength in dBm.

III. CALIBRATION OF SIMULATION TOOLS

Because the ns-3 simulator only supports some bands defined by the LTE standard, it was necessary to adapt the EARFCN (evolved-UTRA absolute radio frequency number) configuration so that the protocol stack of the simulator considers the propagation calculations of the VHF band. Fig. 3 shows the addition of the coverage of each cell when the system operates in the 250 MHz band in comparison with the operation at 700 MHz (EARFCN=12).

Using the values of the received signal strength indicator (RSSI), SINR, and throughput measured in the field, a calibration was made in the model of large-scale attenuation of the wireless channel used in the simulator. Among the large-scale models defined for the ns-3 simulator, the one that best adapted to the values measured in the field was the Okumura–Hata model [24]. The calibration process consists of altering the parameters of the Okumura–Hata empirical

formula so that the values of simulated RSSI, SINR, and throughput are very similar to measurements obtained in the field.

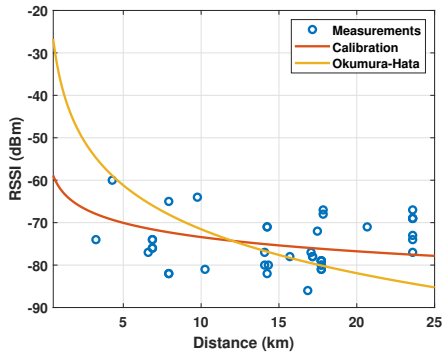

FIGURE 4. Calibration of the modified Okumura–Hata path loss model based on RSSI field measurements.

Signal attenuation in open rural areas in the classical Okumura–Hata formula is given by

$$L = L_{\text{urban}} - 4,78(\log f)^2 + 18,33 \log f - 40,93, \quad (1)$$

where f is the frequency of the transmitted carrier and L_{urban} is the loss given in the urban environment, which, in turn, is calculated by

$$L_{\text{urban}} = 69,55 + 26,16 \log f - 13,82 \log h_t - A(h_r) + (44,9 - 6,55 \log h_t) \log d, \quad (2)$$

where h_t and h_r are the heights of the transmitting and receiving antennas, respectively, $A(h_r)$ is a correction factor as a function of h_r and the size of the city, and d is the distance between the transmitter and the receiver.

Thus, (1) and (2) were altered to fit the values obtained by the field measurements, resulting in

$$L = L_{\text{urban}} - 4,78(\log f)^2 + 18,33 \log f - \mathbf{15,94}, \quad (3)$$

and

$$L_{\text{urban}} = 69,55 + 26,16 \log f - 13,82 \log h_t - A(h_r) + (\mathbf{20,9} - 6,55 \log h_t) \log d, \quad (4)$$

respectively. Table 3 shows the SINR values measured at points of the drive test and those obtained with the ns-3 simulator after the change of the model proposed in (3) and (4).

TABLE 3. Comparison of the measured values with the values obtained by the simulator after calibration.

Location	SINR Measured	SINR in Simulator
Spot 1	25,5 dB	26,5 dB
Spot 2	23 dB	25 dB
Spot 3	27,8 dB	25 dB

IV. SYSTEM MODEL AND FREQUENCY REUSE ALGORITHMS

Consider a set $\mathcal{I}$ of I BSs providing downlink wireless service to a group of user equipments (UEs) in a geographical area $\mathcal{A}$. Each BS $i \in \mathcal{I}$ serves an area $\mathcal{A}_i$, such that $\cup_{\forall i \in \mathcal{I}} \mathcal{A}_i = \mathcal{A}$ and $\mathcal{A}_i \cap \mathcal{A}_k \neq \emptyset$ for any $i \neq k \in \mathcal{I}$. In other words, it is possible that some cells have a significant intersection between them. Then, the downlink spectral efficiency achieved by the subchannel m, the user n, at the time slot t from the BS located at x_i to a UE located at $y \in \mathcal{A}_i$ is

$$\mathcal{C}_{n,m}^{(t)}(x_i, y) = \log_2 \left(1 + \gamma_{n,m}^{(t)}(x_i, y)\right), \quad (5)$$

where $\gamma_{n,m}^{(t)}(x_i, y)$ is the SINR at the user n, on the subchannel m, at the time slot t, which is defined in (6)

$$\gamma_{n,m}^{(t)}(x_i, y) = \frac{\left[\beta_{l,m}^{(t)}\, g_{l\to n,m}^{(t)}(x_l, y)\, p_l^{(t)}\right]_{l=n}}{\sum\limits_{v \neq l} \beta_{v,m}^{(t)}\, g_{v\to n,m}^{(t)}(x_v, y)\, p_v^{(t)} + \sigma_n^2}, \quad (6)$$

where $\beta_{v,m}^{(t)}$ is the binary variable that indicates the subchannel selection m transmitted from the BS v at the time slot t, $g_{v\to n,m}^{(t)}(x_v, y)$ indicates the downlink channel gain from the BS v to the user n on the subchannel m in the time slot t when the UE is located in the position y and the BS in the position x_v , $p_v^{(t)}$ is the transmit power of the BS v in the time slot t, and σ^2 is the additive white Gaussian noise power spectral density at the user receiver n

$$g_{v\to n,m}^{(t)}(x_v, y_n) = h_{v\to n}^{(t)}(x_v, y_n) \left|\alpha_{n\to l,m}^{(t)}\right|^2, \; t = 1, 2, \cdots, \quad (7)$$

where $h_{v\to n}^{(t)}(x_v, y_n) = L$ is the path loss on a linear scale, which is calculated in (1), and $\alpha_{n\to l,m}^{(t)}$ is the small-scale Rayleigh fading.

It is important to note that based on this framework, the possibility of using fractional frequency reuse (FFR) is based on the proper definition of the binary variable $\beta_{v,m}^{(t)}$ to choose one specific subchannel or band m, which is used by BS v. Another important parameter considered in FFR schemes is the proper consideration of the power transmission in each BS, which is modeled with the variable $p_v^{(t)}$.

In this work, we implement five methodologies, one methodology based on a deep reinforcement learning approach to define the FR dynamically, and four static algorithms derived from [12].

Based on the system model described before, we define these five methodologies of FR in the following.

A. HARD FREQUENCY REUSE

As in traditional cell reuse, the band is divided into N subchannels, and each of the neighboring N BSs uses one of

them. Such division ensures less interference between BSs, at the cost of less intelligent resource allocation. A didactical representation of this scheme is shown in Fig. 5. Using (6) as a reference, each BS v transmits into one specific subchannel m.

B. STRICT FREQUENCY REUSE

The band is divided into $N+1$ subchannels used by all BSs. In each cell-edge, the BSs use a different sub-band to avoid interference. A representation of this scheme is shown in Fig. 6.

Here, the inter-cell interference comes from disjoint sets of the interior subchannel, which is reused by all BSs.

C. SOFT FREQUENCY REUSE

The band is divided into N subchannels; each neighboring BS uses a different subchannel at the edge and center of each cell; thus, the entire band can be used.

Here, a power control $\beta \geq 1$ is considered for the transmit power to generate two different classes: $P_{\text{int}} = p_v^{(t)}$ and $P_{\text{edge}} = \beta p_v^{(t)}$, where P_{int} is the transmit power of the base station if the user y is an interior user, and P_{edge} is the transmit power of the base station if y is a cell-edge user.

The interfering base stations are also divided into two classes: $\mathcal{I}_{\text{int}}$, which consists of all interfering base stations transmitting to cell-interior users on the same subchannel of one specific user with a transmission power of P_{int}, and $\mathcal{I}_{\text{edge}}$, which consists of all interfering base stations transmitting to cell-edge users on the same subchannel with the power transmission P_{edge}.

A heuristic approach proposed in [25] concluded that a typical value of subchannels is between 2 and 20. To accomplish this, a power control factor $\beta \geq 1$ is introduced to the transmit power to create two different classes, P_{int} and P_{edge}, where P_{int} is the transmit power of the base station if the user is an interior user, and P_{edge} is the transmit power of the BS if the user is in the cell-edge network.

A didactic representation of this scheme is shown in Fig. 7.

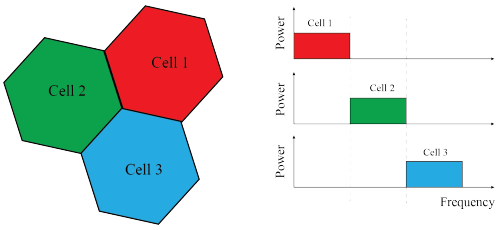

FIGURE 5. Hard FR scheme.

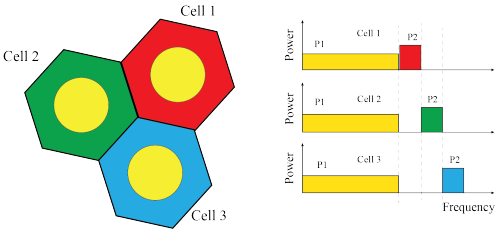

FIGURE 6. Strict FR scheme.

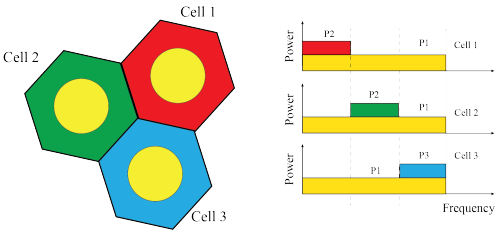

FIGURE 7. Soft FR scheme.

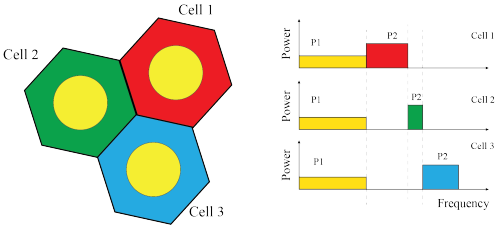

FIGURE 8. Dynamic Strict FR scheme.

D. DYNAMIC STRICT REUSE

The algorithm proposed in this Section is based on the Strict FR. Here, the band is also divided into $N+1$ subchannels, but the size of each subchannel is proportional to the number of UEs within the region that each subchannel is serving. Thus, we will refer to this algorithm as Dynamic Strict FR.

To calculate the size of each subchannel, the BSs must communicate with each other in order to discover how many UEs are serving. A representation of this scheme is shown in Fig. 8.

The size ω_i of the edge subchannel of BS i and the size θ of the subchannel in the center of each BS are given by

$$\omega_i = \frac{a_i}{\left(\sum_{i=1}^{n} a_i\right) + b}, \tag{8}$$

and

$$\theta = \frac{b}{\left(\sum_{i=1}^{n} a_i\right) + b}, \tag{9}$$

where a_i is the number of UEs at the edge of BS i, and b is the maximum number of UEs at the center of all BSs. .

Algorithm 1 Algorithm used in Dynamic Strict FR scheme.

▷ Defining the subchannel bandwidth in the edge and in the cell center.
while Stop Criteria not met **do**
  for i=1 **do** i=i+1
    $b \leftarrow$ number of Users at the center of the cell
    $a_i \leftarrow$ number of Users at the edge
  ▷ Calculating bandwidth for users near the cell center and users in the edge. Iteration in each BS i.
    $\omega_i \leftarrow$ a bandwidth based on the number of users in the edge using Eq. 8.
    $\theta \leftarrow$ a bandwidth based on the number of users in the center of the cell using Eq. 9.
  end for
end while

E. DYNAMICS BASED ON DEEP REINFORCEMENT LEARNING APPROACH

To improve the understanding of this methodology, we expand the explanation into a description of deep reinforcement learning and the particular cost function that is used to maximize the throughput in the following.

1) Deep Reinforcement Learning

In machine learning there are three categories; depending on the nature of the information or feedback available to the learning system, these categories are:

- supervised learning;
- unsupervised learning;
- reinforcement learning (RL).

In this paper, we use RL as the approach for optimizing a specific cost function with specific constraints to optimize the system throughput [26], [27]. It is a trial-and-error process where an agent interacts with an unknown environment in a sequence of discrete time steps to achieve a specific target or task. At time t, the agent first observes the current state of the environment, which is a tuple of relevant environment features and denoted by $S^{(t)} \in \mathcal{S}$, where S is a set of possible states. It then takes an action $a^{(t)} \in \mathcal{A}$ from an allowed set of actions $\mathcal{A}$ according to a policy that can be either stochastic, i.e., π with $a^{(t)} \sim \pi(.|\mathcal{S}^{(t)})$ or deterministic, i.e., μ with $a(t) = \mu(\mathcal{S}^{(t)})$. The interactions are modeled as a Markov decision process. For this reason, the environment moves to a next state $S^{(t+1)}$ following an unknown transition matrix that maps state–action pairs onto a distribution of successive states, and the agent receives a reward $S^{(t+1)}$. Overall, the above process is described as an experience at $t+1$ denoted by $e^{(t+1)} = (S^{(t)}, a^{(t)}, r^{(t+1)}, s^{(t+1)})$.

The goal is to learn a policy that maximizes the cumulative discounted reward $R^{(t)}$ at time t, defined as follows:

$$R^{(t)} = \sum_{\tau=0}^{\infty} \gamma^{\tau} r^{(t+\tau+1)}, \quad \text{and } \gamma \in (0;1] \tag{10}$$

Owing to the possibility of combining RL with deep learning [28], deep reinforcement learning (DRL) is a highly suitable method for solving problems with a high number of states and low prior knowledge, which is the case of the FR allocation scenario in the available subchannels.

2) Cost Function Definition

Here, we define the radio optimization problem to be optimized. To this end, details of the cost function and its constraints are defined in the following.

The subchannels and power vectors in the time slot t are denoted by $\boldsymbol{\beta}^{(t)} = \left[\beta_{1,1}^{(t)}, \beta_{1,2}^{(t)}, \cdots, \beta_{N,M}^{(t)}\right]^T$ and $\boldsymbol{p}^{(t)} = \left[p_1^{(t)}, \cdots, p_N^{(t)}\right]^T$, respectively. Using (5), we define the sum-rate maximization problem as

$$\begin{aligned} \max_{\boldsymbol{p}^{(t)}, \boldsymbol{\alpha}^{(t)}} \quad & \sum_{n=1}^{N} \mathcal{C}_n^{(t)}(x_i, y_n) \\ \text{s.t.} \quad & 0 \le p_n^{(t)} \le P_{\max}, \forall n \in \mathcal{N}, \\ & \beta_{n,m}^{(t)} \in \{0,1\}, \forall n \in \mathcal{N}, \forall m \in \mathcal{M}, \\ & \sum_{m \in \mathcal{M}} \beta_{n,m}^{(t)} = 1, \forall n \in \mathcal{N}, \end{aligned} \tag{11}$$

where $\mathcal{C}_n^{(t)} = \sum_{m=1}^{M} \mathcal{C}_{n,m}^{(t)}(x_i, y_n)$.

The nonconvex problem in (11) requires a highly complex approach that could also increase the computational complexity. To handle this nonconvex problem, we consider a multiagent learning scheme, where each transmitter, mounted in each BS, operates as an independent learning agent. Each agent successfully executes two policies to determine its associated subchannel and transmission power level. The proposed multiagent approach is easily scalable to more extensive networks and can operate with local information after training.

At the beginning of each time slot, each agent successively executes two policies to determine its associated transmission power level and subchannel. The agents are represented by the BSs, and the environment is the wireless communication channel model in which every agent or BS aims to optimize the network performance based on UEs's location. The DRL considers two different optimizations. The first case, enclosed in the red dotted square in Fig. 9, considers a Critic network and an Actor network [29] (both based on a Deep Q-network) to optimize the stochastic policy that aims to improve the subchannel selection. In the same Figure, a second Deep Q-network, enclosed in the blue dotted square, aims to optimize a second policy; a deterministic policy is used to select a suitable power transmission value. The agent of the second Deep Q-network requires the subchannel decision of the first approach to determine its state input before setting the transmit power of the agent. A brief explanation of the algorithm is detailed in Algorithm 2.

V. SIMULATION

In order to evaluate the traditional FFR algorithms in the OFDMA system operating in 250 MHz, we use the ns-3

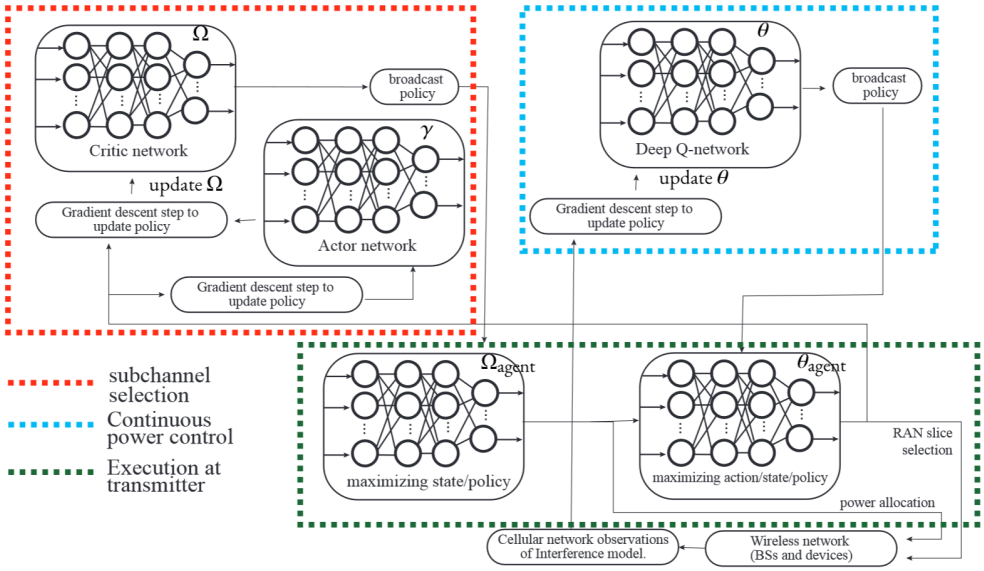

FIGURE 9. Architecture used by the deep reinforcement learning approach in the Monte Carlo simulation. The reinforcement learning policies Ω, θ, and γ are obtained by using a deep learning gradient descent.

Algorithm 2 Algorithm of the DRL approach.

▷ Main Loop
while Stop Criteria not met **do**
  SUBCHANNEL SELECTION()
  POWER CONTROL()
end while

▷ Subchannel selection
function SUBCHANNEL SELECTION()
  ▷ Agent Selection
  agent $\leftarrow a_n^{(t)} \in \mathcal{A}_{\text{subchannel}} = \{1, \cdots, M\} = \mathcal{M}$
  State set design $\leftarrow s_{n,m}^{(t)}$
  Training by Critic and Actor Network
  Reward function design
  Update Policies: Ω, γ
end function

▷ Power Control
function POWER CONTROL()
  ▷ Agent Selection
  agent $\leftarrow a_{n,a_n^{(t)}}^{(t)} \in \mathcal{A}_{\text{power}} = [0, 1]$
  State set design $\leftarrow s_{n,a_n^{(t)}}^{(t)}$
  Training by deep-Q Network
  Reward function design
  Update Policies: θ
end function

simulator, which is widely known and tested by the scientific community [30]. The ns-3 simulator is a discrete event simulator written in open-source C++. In this work, the cellular network module known as LENA [31] is adopted. This ns-3 module was chosen in this work because it produces accurate results when compared with commercial devices [32]. To evaluate the DRL model, we use Python and TensorFlow, which is a free and open-source software library for machine learning and artificial intelligence.

Both simulators are adjusted to the parameters described in Table 2 to reflect a real scenario as accurately as possible. The BSs are positioned as shown in Fig. 2, following the same topology as that used in the field. Here, each simulation has a duration of 2.5 s of network time.

The simulations are configured to evaluate the total downlink capacity. Thus, the generated traffic is a constant bit rate (CBR) over the user datagram protocol (UDP) transport protocol.

In order to evaluate the FR algorithms, the UEs are positioned in four different representative scenarios in agribusiness industry:

(I) **UEs on the edge** – Twenty simulations are performed with the UEs positioned at the edge of the cell. Starting with only one UE, each simulation adds a UE for each BS.
(II) **UEs on the center** – The UEs are positioned in the center of the cell in an area of low interference. In the

same way as Scenario (I), the number of UEs for each simulation is increased until the number of twenty UEs.

(III) **UEs near to one BS** – Twenty simulations are performed, where eighty UEs are positioned randomly in a region close to only one BS and connected in that BS.

(IV) **UEs randomly positioned** – One hundred simulations are performed with eighty UEs in the coverage area at random positions and connected to the BS with the best signal.

Scenarios (I), (II), and (III) reflect a situation where the UEs are all positioned close to each other. In the specific application of sugarcane cultivation, this type of scenario reflects a situation in which transport trucks connected to the Internet move together to receive or deliver sugarcane. Such scenarios may reflect other crop and livestock farming applications, such as cattle monitoring in limited pasture areas [33] or precision rotational grazing techniques [34], among other cases.

Scenario (IV) simulates a more generic case with random positioning that aims to analyze the behavior of the system with a large number of UEs.

A graphical representation of these scenarios is given in Fig. 10. Here, we emphasize the radio coverage of the cell radius in each BS. The main aspect of this Figure is the location of users, which is reflected on the final system throughput for each FR scheme.

The performance metrics used to compare these FR methodologies are the following:

- throughput per UE for Scenarios (I), (II), and (III);
- throughput per BS and cumulative distribution function (CDF) for Scenario (IV).

VI. RESULTS

In this Section, the results obtained in all defined scenarios are presented in terms of spectral efficiency to show the learning curve of the methodology based on DRL. After that, the average throughput is obtained for all scenarios defined before.

A. DEEP REINFORCEMENT LEARNING APPROACH

Considering a setup defined by Scenario I, the FR based on DRL is evaluated and presented in Fig. 11. The first iterations indicate that the performance of each subchannel is very low. However, when the number of iterations is increased, the deep-Q network and the policies provide better resource allocation, with a gain of 5 compared with the spectral efficiency in iteration 10 and iteration 25000.

It is important to remark that the spectral efficiency is combined with the bandwidth defined in Table 2 to obtain the throughput, which is used in the next results.

B. SCENARIO I

Fig. 12 shows the results of the simulations for the throughput per UE in Scenario (I). In this case, the high interference limits the performance of the system, reducing the throughput of the UEs. When all UEs are in a region of high interference, the FR based on DRL achieves a better performance when compared with the traditional FR schemes. However, the *Hard FR algorithm* presents the best performance when there are two or fewer users to be served. Because the methodology *based on DRL* optimizes the subchannel and power transmission allocation per UE, it has a better performance when the number of UEs is greater than 2. This performance remains until the number of UEs is lower than 14 simultaneous users. Because the *Hard FR* divides the spectrum for each BS, this algorithm is the second best methodology that guarantees less interference but with no flexibility for changes in spectrum allocation. The *Soft FR* technique performs very close to *Hard FR* because the UEs are located on the border of the cell, and the division of the subchannels is done in the same way as the *Hard FR*. However, the *Soft FR* algorithm has the advantage of greater flexibility in the allocation of RBs, in case the UEs are in a situation of lower interference. The *Dynamic Strict FR* algorithm also divides the subchannels like the other two algorithms after some parameter calculation defined in (8) and (9). However, its performance is close to the *Soft FR* technique. The *Strict FR* technique presents a less satisfactory performance because it reserves only part of the available band to the UEs on the edge of the cell. Finally, as expected, using no algorithm is the worst choice because resources are not being used efficiently under the high interference scenario.

C. SCENARIO II

When all UEs are in a situation of less interference (Scenario (II)), the results indicate that there is no need for any FR algorithm. In this scenario, not using any algorithm is the alternative that guarantees the highest throughput, because the UEs can transmit over the entire band with a very low probability of inter-cell interference, as it is shown in Fig. 13. We also note that the *Soft FR* technique outperforms similarly because it allows the BSs to use the entire band in the middle of the cell. By reserving a subchannel for the UEs with more significant interference, the algorithm of *Strict FR* shows a poor performance. The *Hard FR* algorithm divides the band between BSs, reducing its performance. The *Dynamic Strict FR* technique presents an intermediary performance because of its time for calculating the proper quantity of RBs for each BS. The methodology *based on DRL* achieves a similar performance to the *Dynamic Strict FR* when the number of simultaneous UEs is smaller than eight. However, when the number of UEs is increased, the performance tends to improve the average throughput.

D. SCENARIO III

When all UEs are connected to the same BS (Scenario (III)), the result is similar to Scenario (II), i.e., a scenario with a very low probability of interference. As the *Hard FR* and the *Strict FR* algorithms reserve a specific subchannel in each BS

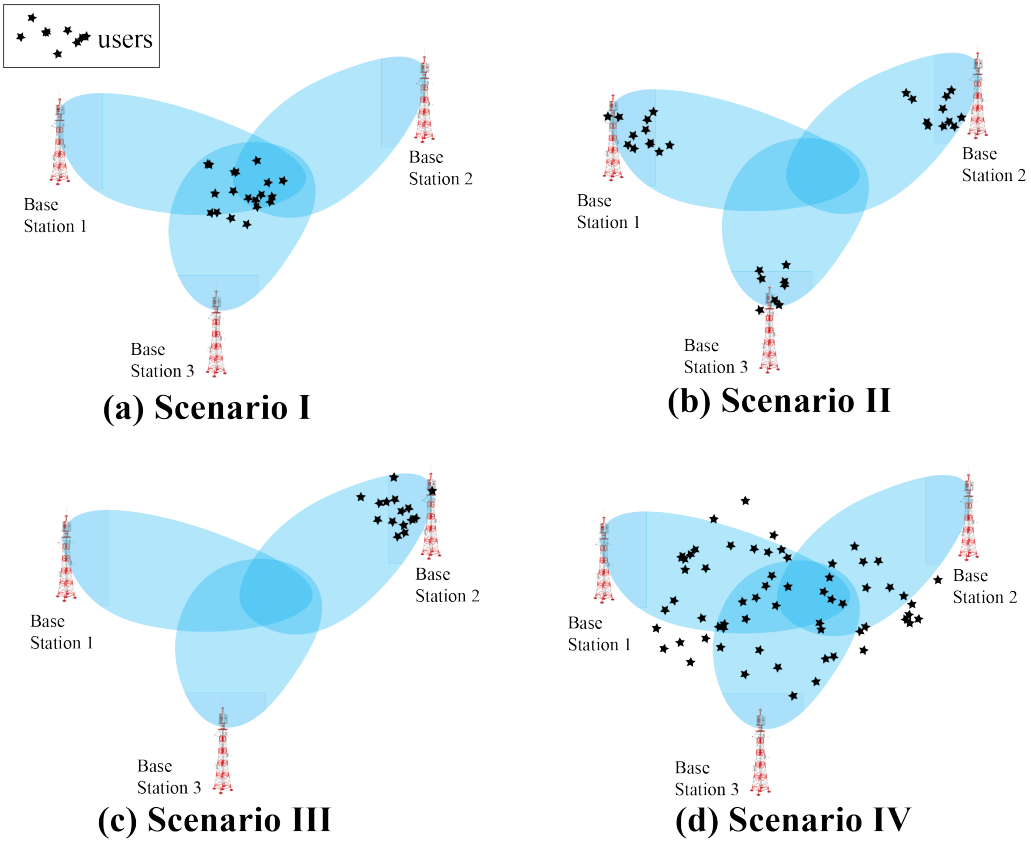

FIGURE 10. Four scenarios evaluated for each FR methodology; in each case, the user distribution is modified based on agribusiness applications.

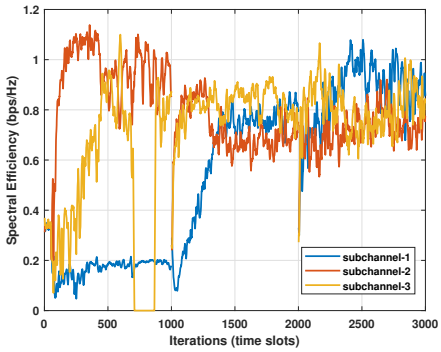

FIGURE 11. Spectral efficiency result in Scenario I when the DRL approach is considered to carry out the FR between three subchannels in the 250 MHz band.

that is not serving any user, both show an inefficient use of the available resources, which explains their poor performance. As presented in Fig. 14, the *Soft FR*, the *Dynamic Strict FR*, the no-algorithm use case, and the FR based on DRL achieve a better performance without any significant difference.

E. SCENARIO IV

The results of the simulation campaign for Scenario (IV) are shown in Figs. 15 and 16 to represent the throughput and the cumulative distribution function of the UE throughput per BS, respectively. In general, in this scenario it is always convenient to use some FR methodology. However, as the UEs are positioned randomly using a uniform distribution, the FR based on DRL outperforms the other traditional methodologies.

We can see in Fig. 15 that in the 60% percentile of the measurements, the hard FR and the methodology based on DRL achieves a better throughput than the other traditional

methodologies. However, as we analyze Fig. 16, we observe that the great part of UEs (almost 60%) have a throughput very close to zero (less than 0.1 Mbps). The *Hard FR* and the *Dynamic Strict FR* algorithms provide a minimum throughput of 0.1 Mbps for almost all UEs. As the *Soft FR* algorithm allows all cells to use the entire band in the center, the interference increases for UEs in the transition region between the cell center and the cell border. A result of this is that approximately 70% of the UEs have an average throughput below 0.1 Mbps. It can be verified that the average throughput of 40% of the UEs is below 0.1 Mbps when the Strict FR technique is adopted. The *Dynamic Strict FR* algorithm provides a higher fairness between the UEs, as approximately 90% of the UEs have an average throughput between 0.1 and 0.2 Mbps. Finally, the CDF indicates that the performance of the algorithm, which is based on DRL, outperforms the other traditional methodologies.

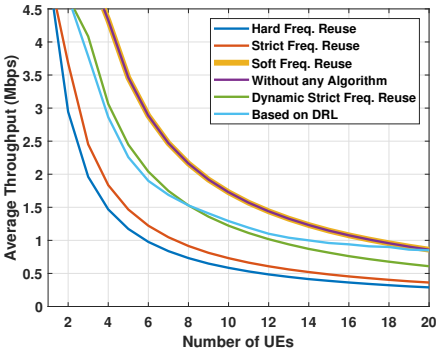

FIGURE 13. Average UE throughput in Scenario (II).

VII. CONCLUSIONS

The need for IoT applications in agribusiness has driven the development of cellular broadband systems using sub-1GHz bands owing to the long-range transmission required by connectivity in rural areas. However, the propagation in such bands implies an increase in interference, which usually degrades the system performance.

This work compared the performance of a cellular network using traditional FR schemes with a data-driven approach based on DRL when the system is operating in 250 MHz, which is a band not yet standardized and which has received limited attention in the literature so far. The simulation tools were calibrated using data gathered in drive test sessions using a real cellular network operating in the 250 MHZ band. Thus, the results of this work provide a strong ground because they are obtained considering a real setup as a benchmark.

Four scenarios were defined to represent typical agribusiness setups in terms of UE distribution. In Scenarios I and IV, the approach based on DRL achieves a better performance than the traditional FR schemes. In Scenarios II and III, the cellular system performance reaches a better performance when no FR methodology is considered. However, the approach based on DRL improves its performance when the number of simultaneous connected UEs is increased.

A. FINAL REMARKS

The importance of using machine learning schemes on FR allocation is an attractive approach, especially in methodologies that aim to maximize the allocation of resources in high-interference scenarios. A widespread scenario in agribusiness applications is the grouping of UEs in a cell region, either at the edge or center of the cell. The gain of using fractional reuse techniques is apparent when the analysis is performed with UEs located at the edges of the cells (Scenario (I)). For instance, in a system with four UEs per cell in Scenario I, the average throughput per UE

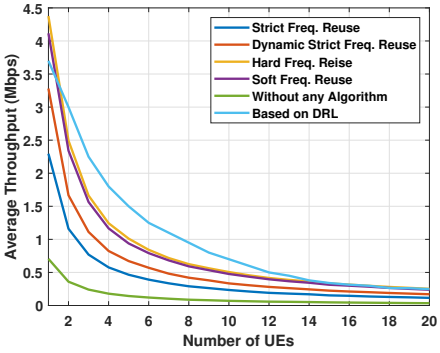

FIGURE 12. Average UE throughput for Scenario (I).

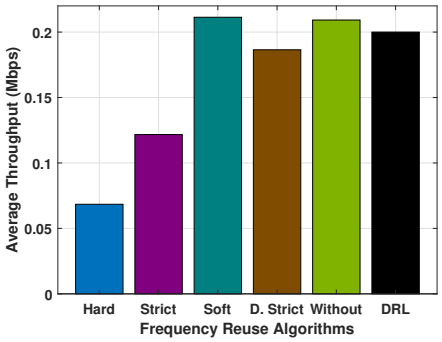

FIGURE 14. Average UE throughput for Scenario (III).

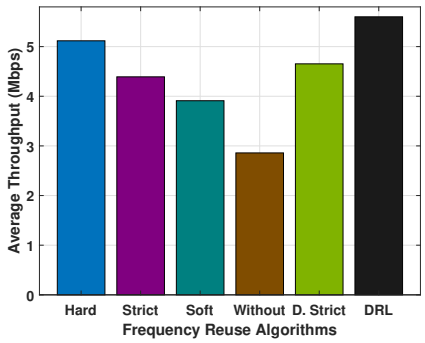

FIGURE 15. Average throughput for Scenario (IV).

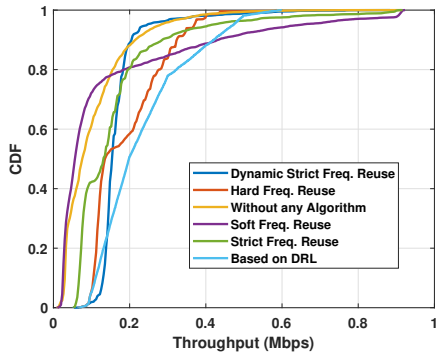

FIGURE 16. CDF of throughput for Scenario (IV).

increased from 0.15 Mbps to 1.13 Mbps when using the *Hard FR* or *Soft FR* algorithm when compared with a scenario that did not use any FR scheme. A similar comparison between the methodology based on DRL and not using any algorithm indicates that the average throughput is increased from 0.15 Mbps to 1.83 Mbps. In practice, it means that the UE can support video services (throughput over 800 kbps) instead of just supporting telemetry services (over 100 kbps) when any FR scheme is used.

When the agribusiness application requires fairness, i.e., all UEs with a minimum throughput, the FR based on DRL is the most acceptable alternative in high-interference scenarios, such as Scenario (IV). The methodology performs satisfactorily in low-interference scenarios when the number of simultaneous users is increased, such as in Scenario (III).

B. FUTURE WORK

The paper suggests that a similar approach can be handled on 5G New Radio operating in sub-1GHz because it is also based on OFDMA, specifically in the evolution of 5G-Advanced, which is standardized by the 3GPP Rel. 18.

Other interesting topic of future work would be to analyze beyond 5G networks to compare the performance of cell-free massive MIMO [35] in rural scenarios with the schemes proposed in this paper.

REFERENCES

[1] Y. Siriwardhana, C. De Alwis, G. Gür, M. Ylianttila, and M. Liyanage, "The Fight Against the COVID-19 Pandemic With 5G Technologies," IEEE Engineering Management Review, vol. 48, no. 3, pp. 72–84, 2020.
[2] A. M. Cavalcante, P. H. Gomes, M. V. Marquezini, I. Bonomini, and L. L. Mendes, "Applicability of IoT Technologies for 5G Use Cases in Brazil," in 2019 IEEE 2nd 5G World Forum (5GWF), 2019, pp. 53–57.
[3] M. S. Hossain, G. Muhammad, and N. Guizani, "Explainable AI and Mass Surveillance System-Based Healthcare Framework to Combat COVID-I9 Like Pandemics," IEEE Network, vol. 34, no. 4, pp. 126–132, 2020.
[4] D. Carrillo and J. Seki, "Rural area deployment of internet of things connectivity: LTE and LoRaWAN case study," in 2017 IEEE XXIV International Conference on Electronics, Electrical Engineering and Computing (INTERCON), 2017, pp. 1–4.
[5] Y. Wei and S.-H. Hwang, "Investigation of spectrum values in rural environments," ICT Express, vol. 4, no. 4, pp. 234 – 238, 2018.
[6] V. S. Anusha, G. K. Nithya, and S. N. Rao, "Comparative Analysis of Wireless Technology Options for Rural Connectivity," in 2017 IEEE 7th International Advance Computing Conference (IACC), Jan 2017, pp. 402–407.
[7] A. Jha and D. Saha, "Techno-economic assessment of the potential for LTE based 4G mobile services in rural India," in 2015 IEEE International Conference on Advanced Networks and Telecommuncations Systems (ANTS), Dec 2015, pp. 1–6.
[8] C. Ovando, J. Pérez, and A. Moral, "LTE techno-economic assessment: The case of rural areas in Spain," Telecommunications Policy, vol. 39, no. 3-4, pp. 269–283, 2015.
[9] A. S. Yogapratama, U. K. Usman, and T. A. Wibowo, "Analysis on 900 MHz and 1800 MHz LTE network planning in rural area," in 2015 3rd International Conference on Information and Communication Technology (ICoICT), May 2015, pp. 135–139.
[10] M. Lauridsen, I. Z. Kovacs, P. Mogensen, M. Sorensen, and S. Holst, "Coverage and Capacity Analysis of LTE-M and NB-IoT in a Rural Area," in 2016 IEEE 84th Vehicular Technology Conference (VTC-Fall), Sep. 2016, pp. 1–5.
[11] M. Lauridsen, L. C. Gimenez, I. Rodriguez, T. B. Sorensen, and P. Mogensen, "From LTE to 5G for Connected Mobility," IEEE Communications Magazine, vol. 55, no. 3, pp. 156–162, 2017.
[12] P. Gawlowicz, N. Baldo, and M. Miozzo, "An Extension of the Ns-3 LTE Module to Simulate Fractional Frequency Reuse Algorithms," in Proceedings of the 2015 Workshop on Ns-3, ser. WNS3 '15, 2015, pp. 98–105.
[13] A. S. Hamza, S. S. Khalifa, H. S. Hamza, and K. Elsayed, "A Survey on Inter-Cell Interference Coordination Techniques in OFDMA-Based Cellular Networks," IEEE Communications Surveys Tutorials, vol. 15, no. 4, pp. 1642–1670, Fourth 2013.
[14] S. Sadr, A. Anpalagan, and K. Raahemifar, "Radio Resource Allocation Algorithms for the Downlink of Multiuser OFDM Communication Systems," IEEE Communications Surveys Tutorials, vol. 11, no. 3, pp. 92–106, rd 2009.
[15] V. Fernández-López, K. I. Pedersen, and B. Soret, "Interference characterization and mitigation benefit analysis for LTE-A macro and small cell deployments," EURASIP Journal on Wireless Communications and Networking, vol. 2015, no. 1, pp. 1–12, 2015.
[16] B. Bojović, E. Meshkova, N. Baldo, J. Riihijärvi, and M. Petrova, "Machine learning-based dynamic frequency and bandwidth allocation in self-organized LTE dense small cell deployments," EURASIP Journal on Wireless Communications and Networking, vol. 2016, no. 1, pp. 1–16, 2016.
[17] S. Gimenez, D. Martín-Sacristán, D. Calabuig, and J. F. Monserrat, "Self-configurable Coordinated Scheduling for Ultra-dense Small Cell Deployments," in 2017 13th International Wireless Communications and Mobile Computing Conference (IWCMC), June 2017, pp. 512–517.

[18] C. Feijóo, J. Gómez-Barroso, and S. Ramos, "An analysis of next generation access networks deployment in rural areas," in 2011 50th FITCE Congress - "ICT: Bridging an Ever Shifting Digital Divide", Aug 2011, pp. 1–18.
[19] Z. Wang, J. Zong, Y. Zhou, Y. Shi, and V. W. Wong, "Decentralized Multi-Agent Power Control in Wireless Networks with Frequency Reuse," IEEE Transactions on Communications, pp. 1–1, 2021.
[20] J. Zhao, Y. Zhang, Y. Nie, and J. Liu, "Intelligent Resource Allocation for Train-to-Train Communication: A Multi-Agent Deep Reinforcement Learning Approach," IEEE Access, vol. 8, pp. 8032–8040, 2020.
[21] E. B. Perri and L. C. Trintinalia, "Secondary lobe level control in antenna arrays," in Proceedings of the 2003 SBMO/IEEE MTT-S International Microwave and Optoelectronics Conference - IMOC 2003. (Cat. No.03TH8678), vol. 2, Sept 2003, pp. 845–850 vol.2.
[22] Agência Nacional de Telecomunicações (ANATEL), "Resolução nº 555, de 20 de dezembro de 2010," Dec. 2010.
[23] 3GPP TS 36.300, "Technical Specification Group Radio Access Network; E-UTRA and E-UTRAN; Overall description," 2010.
[24] A. Medeisis and A. Kajackas, "On the use of the universal Okumura-Hata propagation prediction model in rural areas," in VTC2000-Spring. 2000 IEEE 51st Vehicular Technology Conference Proceedings (Cat. No.00CH37026), vol. 3, 2000, pp. 1815–1818.
[25] T. D. Novlan, R. K. Ganti, A. Ghosh, and J. G. Andrews, "Analytical Evaluation of Fractional Frequency Reuse for OFDMA Cellular Networks," IEEE Transactions on Wireless Communications, vol. 10, no. 12, pp. 4294–4305, 2011.
[26] V. François-Lavet, P. Henderson, R. Islam, M. G. Bellemare, and J. Pineau, An Introduction to Deep Reinforcement Learning, 2018.
[27] M. Kenyeres and J. Kenyeres, "Comparative Study of Distributed Consensus Gossip Algorithms for Network Size Estimation in Multi-Agent Systems," Future Internet, vol. 13, no. 5, p. 134, 2021.
[28] M. Morales, Grokking Deep Reinforcement Learning. Manning Publications, 2020.
[29] Q. Wei, L. Wang, Y. Liu, and M. M. Polycarpou, "Optimal Elevator Group Control via Deep Asynchronous Actor–Critic Learning," IEEE Transactions on Neural Networks and Learning Systems, vol. 31, no. 12, pp. 5245–5256, 2020.
[30] NS-3, "Network Simulator-3." [Online]. Available: https://www.nsnam.org/ (acessado em Abril de 2018).
[31] N. Baldo, M. Miozzo, M. Requena-Esteso, and J. Nin-Guerrero, "An Open Source Product-oriented LTE Network Simulator Based on Ns-3," in Proceedings of the 14th ACM International Conference on Modeling, Analysis and Simulation of Wireless and Mobile Systems, ser. MSWiM '11, 2011, pp. 293–298.
[32] A. Marinescu, I. Macaluso, and L. A. DaSilva, "System Level Evaluation and Validation of the Ns-3 LTE Module in 3GPP Reference Scenarios," in Proceedings of the 13th ACM Symposium on QoS and Security for Wireless and Mobile Networks, pages = 59–64, numpages = 6, keywords = lte, system level simulator, validation, ns-3, location = Miami, Florida, USA, series = Q2SWinet '17. New York, NY, USA: Association for Computing Machinery, 2017. [Online]. Available: https://doi.org/10.1145/3132114.3132117
[33] M. Chizzotti, F. Machado, E. Valente, L. Pereira, M. Campos, T. Tomich, S. Coelho, and M. Ribas, "Technical note: Validation of a system for monitoring individual feeding behavior and individual feed intake in dairy cattle," Journal of Dairy Science, vol. 98, no. 5, pp. 3438 – 3442, 2015. [Online]. Available: http://www.sciencedirect.com/science/article/pii/S0022030215001794
[34] D. P. Eaton, S. A. Santos, M. do Carmo Andrade Santos, J. V. B. Lima, and A. Keuroghlian, "Rotational Grazing of Native Pasturelands in the Pantanal: An Effective Conservation Tool," Tropical Conservation Science, vol. 4, no. 1, pp. 39–52, 2011. [Online]. Available: https://doi.org/10.1177/194008291100400105
[35] E. Björnson and L. Sanguinetti, "Making Cell-Free Massive MIMO Competitive With MMSE Processing and Centralized Implementation," IEEE Transactions on Wireless Communications, vol. 19, no. 1, pp. 77–90, 2020.

DICK CARRILLO MELGAREJO (M'08) received the B. Eng. degree (Hons.) in electronics and electrical engineering from San Marcos National University, Lima, Perú, and the M.Sc. degree in electrical engineering from Pontifical Catholic University of Rio de Janeiro, Brazil, in 2004 and 2008, respectively. Since 2018 he has been a researcher at LUT University where he is also pursuing a doctoral degree in electrical engineering. His research interests are mobile technologies beyond 5G, RAN slicing, Machine Learning in wireless communication.

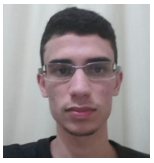

LUIZ QUIRINO REZENDE DA COSTA FILHO is pursuing his B. Eng. degree in Electrical Engineering at the Federal University of Juiz de Fora. His research interests are wireless networks, sensor networks, and network simulation.

ÁLVARO AUGUSTO MACHADO DE MEDEIROS received the B. Sc. degree in electrical engineering from the Federal University of Rio Grande do Norte (UFRN), Brazil, in 2000, and the M.Sc. and Ph.D. degrees in electrical engineering from the State University of Campinas (UNICAMP), Brazil, in 2002 and 2007, respectively. From 2007 to 2010, he was a Research Specialist at Nokia Institute of Technology (INDT), Brazil, and Research and Development Center (CPqD), Brazil. Since 2010, he has been with Federal University of Juiz de Fora (UFJF), Brazil, where he is currently an Associate Professor. In 2021, he joined as a Post Doc Researcher at Munster Technological University (MTU), Cork, Ireland. His research interests include wireless communications, wireless channel modeling, medium access control and wireless system dimensioning and performance analysis.

CARLOS LORENA NETO was born in Campinas, Brazil, in 1973. He received the B.S. degree in electrical engineering from Universidade Estadual de Campinas - UNICAMP, Campinas, Brazil, in 1996. Since 1996, he has been working as professional engineer in the areas of telecommunications, wireless communications and machine learning. He is currently the Senior System Engineer - Wireless and Machine Learning at Tropico Sistemas e Telecomunicacoes SA.

FABRICIO LIRA FIGUEIREDO received the Ph.D. in Wireless Communications area from the State University of Campinas (UNICAMP), in 2008, the M.Sc. in Electrical Engineering from the State University of Campinas (UNICAMP), in 1999, and graduated in Electronics Engineering at the Federal University of Pernambuco (UFPE), in 1995. He is currently Smart Agribusiness Manager in CPqD, leading CPqD business and innovation strategy targeting rural and remote areas. He has been the manager of the Wireless Communications Division in CPqD from 2008 to 2017. His major research interests comprise: mobile broadband networks, IoT connectivity, intelligent antennas, cognitive radio, self-organizing networks, machine learning, and speech recognition.

DEMÓSTENES ZEGARRA RODRÍGUEZ (M'12-SM'15) received the B.Sc. degree in electronic engineering from the Pontifical Catholic University of Peru, the M.S. degree and Ph.D. degree from the University of São Paulo in 2009 and 2013. He is currently an Adjunct Professor with the Department of Computer Science, Federal University of Lavras, Brazil. He has a solid knowledge in Telecommunication Systems and Computer Science based on 15 years of professional experience in major companies. His research interests include QoS and QoE in Multimedia services, architect solutions in Telecommunication Systems, artificial intelligence algorithms, and online social networks.

Publication V

Carrillo, D., Kumar, S., Fraidenraich, G., Nardelli, P., and Da Costa, D.
Achievable Sum Rate and Outage Capacity of GFDM Systems with MMSE Receivers

Reprinted with permission from IEEE
In 2020 IEEE International Conference on Communications (ICC)
pp. 1–6, virtual conference, 2020 (in press)

Achievable Sum Rate and Outage Capacity of GFDM Systems with MMSE Receivers

Dick Carrillo[1], Santosh Kumar[2], Gustavo Fraidenraich[3], Pedro H. J. Nardelli[1], and Daniel B. da Costa[4]
[1]School of Energy Systems, LUT University, Finland
[2]Department of Physics, Shiv Nadar University, India
[3]School of Electrical and Computer Engineering, State University of Campinas, Brazil
[4]Department of Computer Engineering, Federal University of Ceará, Brazil

***Abstract*—This paper investigates the achievable sum rate and the outage capacity of generalized frequency division multiplexing systems (GFDMs) with minimum mean-square error (MMSE) receivers over frequency-selective Rayleigh fading channels. To this end, a Gamma-based approximation approach for the probability density function of the signal-to-interference-plus-noise ratio is presented, based on which accurate analytical formulations for the achievable sum rate and outage capacity are proposed. The accuracy of our analysis is corroborated through Monte Carlo simulation assuming different GFDM parameters. Illustrative numerical results are depicted in order to reveal the impact of the key system parameters, such as the number of subcarriers, number of subsymbols, and roll-off factors, on the overall system performance.**

***Index Terms*—Achievable sum rate, GFDM systems, outage capacity, MMSE receivers.**

I. Introduction

Along the last years, Generalized Frequency Division Multiplexing (GFDM) has arisen as a potential alternative to Orthogonal Frequency Division Multiplexing (OFDM) for beyond 5G systems due to its promising bandwidth efficiency improvements [1]. Specifically, GFDM filters each subcarrier with a well-localized prototype filter and has low out-of-band (OOB) emission [2]. GFDM is also designed with a cyclic prefix (CP) that can be used by a large number of transmitted symbols instead of appending a CP per symbol, as in the OFDM case [3]. It has also been shown that GFDM can be harmoniously integrated with multiple-input multiple-output (MIMO) channels [2].

Despite of the above attractive features, GFDM has some deficiencies. In particular, it leads to self-interference among the transmitted symbols, which needs be equalized using, for instance, linear receivers as minimum mean square error (MMSE) to recover individual input samples from channel output. In this case, MMSE has the advantage of having low complexity compared to other non-linear receivers. However, fundamental performance limits of such an interesting combination, i.e., GFDM and MMSE receivers, are still unknown. Moreover, the current available literature dealing with GFDM systems only provides a handful of studies dealing with the sum rate of these systems. For instance, Seungyul *et al.* in [4] derived the data rates of GFDM systems for two types of channels: additive additive white Gaussian noise (AWGN) channel and Long-Term Evolution (LTE) Pedestrian B channel. However, such results relied on numerical approaches that were only valid for specific scenarios, limiting their generalization and practical usefulness.

Aiming to fill partly the gap that exists in the literature, this paper investigates the achievable sum rate and outage capacity of GFDM systems employing MMSE receivers and undergoing frequency-selective Rayleigh fading. To this end, a Gamma-based approximation approach for the probability density function (PDF) of the signal-to-interference-and-noise ratio (SINR) is presented, based on which, accurate analytical formulations are attained. The idea behind the proposed approximation relies on the framework proposed in [5]. The accuracy of our analysis is corroborated through Monte Carlo simulation assuming different GFDM parameters. Illustrative numerical results are depicted in order to reveal the impact of the key system parameters, such as number of subcarriers, number of subsymbols, and roll-off factors, on the overall system performance. To the best of the authors' knowledge, our theoretical results have not been reported in the literature yet and they can be used as a benchmark for future wireless communication studies.

The remainder of the paper is organized as follows. Section II describes the system model along with specific details for the transmitter and receiver blocks. Section III extends the description of the Gamma-based approximation approach proposed in [5], and applies it subsequently in Sections IV and V to derive closed-form accurate approximations for the achievable sum rate and the outage capacity, respectively. Section VI presents illustrative numerical results, which are corroborated by means of Monte Carlo simulations. Finally, Section VII concludes the paper.

II. System Model

The considered GFDM system setup is designed to transmit a complex symbol block $d_{s,k}$ at the sth time instant and kth subchannel containing $S \times K$ data symbols ($s = 0, \ldots, S-1$; $k = 0, \ldots, K-1$). Assuming that the data symbols are independent and identical, the GFDM signal can be written as

$$x[n] = \sum_{s=0}^{S-1} \sum_{k=0}^{K-1} d_{s,k}\ g_{s,k}[n], \tag{1}$$

where $g_{s,k}[n]$ denotes the circular time-frequency shifted version of the prototype filter $g[n]$, being expressed as

$$g_{s,k}[n] \triangleq g[(n - sK)_N]\ e^{j2\pi nk/K}, \tag{2}$$

where $N = S \times K$ and $(.)_N$ stands for modulo operator. To simplify the circular convolution, the transmitter filter $g[n]$ is usually designed as being circular with a period of n mod N. Also, it is noteworthy that in (2) the GFDM shifting step is K in time domain and $1/K$ in frequency domain. Next, the transmitter and receiver blocks of the considered GFDM system setup will be described.

A. Transmitter Block

Let us first use (1) to rewrite the elements of the transmit symbol block in a single vector as: $\mathbf{d} = [\mathbf{d}_0^T, \dots \mathbf{d}_{s-1}^T]^T$ and $\mathbf{d}_s = [\mathbf{d}_{s,0}, \dots \mathbf{d}_{s,K-1}]^T$, with variance σ_{d}^2. The vector form of $x[n]$ $(n = 0, \dots, N-1)$ can be formulated as

$$\mathbf{x} = \mathbf{A}\mathbf{d}, \tag{3}$$

where $\mathbf{x} = [x[0], \dots x[N-1]]^T$ and $\mathbf{A}$, with dimension $N \times N$, denotes the modulation matrix or self-interference matrix of the GFDM system. This matrix can be defined as $\mathbf{A} = [\mathbf{G}_0, \dots \mathbf{G}_{S-1}]$ so that $\mathbf{G}_s$ represents the $N \times K$ matrix of $g_{s,k}[n]$ coefficients, i.e.,

$$\mathbf{G}_s = \begin{bmatrix} g_{s,0}[0] & g_{s,1}[0] & \cdots & g_{s,K-1}[0] \\ g_{s,0}[1] & g_{s,1}[1] & \cdots & g_{s,K-1}[1] \\ \vdots & \vdots & \ddots & \vdots \\ g_{s,0}[N-1] & g_{s,1}[N-1] & \cdots & g_{s,K-1}[N-1] \end{bmatrix}. \tag{4}$$

A CP of length N_{cp} is added to the GFDM signal $\mathbf{x}$ to prevent inter-block interference over frequency selective fading channel (FSFC). Then, the transmitted signal is given by $\mathbf{x}_{\mathrm{cp}} = [\mathbf{x}(N - N_{\mathrm{cp}} + 1 : N);\ \mathbf{x}]$.

B. Receiver Block

Without any loss of generality, we assume a zero-mean circular symmetric complex (ZMCSC) Gaussian channel $\mathbf{h} = [h_1, h_2, \cdots, h_L]^T$, where h_r denotes the complex baseband channel coefficient of the rth path $(1 \le r \le L)$. Consider also that $N_{\mathrm{cp}} \ge L$, which means that the CP length must be higher than the delay spread of the multipath channel [6]. Additionally, the channel coefficients related to distinct paths are assumed uncorrelated. Then, the received signal has length $N_{\mathrm{t}} = N_{\mathrm{cp}} + N + L - 1$ and can be modeled as

$$\mathbf{y}_{cp} = \mathbf{h} * \mathbf{x}_{\mathrm{cp}} + \boldsymbol{\nu}_{\mathrm{cp}}, \tag{5}$$

where the symbol $*$ symbolizes linear convolution operation, $\boldsymbol{\nu}_{\mathrm{cp}}$ is the AWGN signal with variance σ_ν^2 and it is also represented by a vector of length N_{t}.

Before starting decoding process, the CP introduced at the transmitter needs to be removed. The frequency-domain equalization (FDE) properties can be employed so that the linear convolution in (5) becomes a circular convolution. So, the resulting received vector after CP removal can be expressed as

$$\mathbf{y} = \mathbf{H}_{\mathrm{ch}}\boldsymbol{A}\mathbf{d} + \boldsymbol{\nu}, \tag{6}$$

where vector $\boldsymbol{\nu}$ represents the AWGN signal of length N with variance σ_ν^2 and $\mathbf{H}_{\mathrm{ch}}$ is the $N \times N$ circular Toeplitz matrix based on vector $\mathbf{h}$, and can be written as[7]:

$$\mathbf{H}_{\mathrm{ch}} = \begin{bmatrix} h_1 & 0 & \cdots & 0 & h_L & \cdots & h_2 \\ h_2 & h_1 & \cdots & 0 & 0 & \cdots & h_3 \\ \vdots & & \ddots & & & \cdots & \vdots \\ h_L & h_{L-1} & \cdots & \cdots & \cdots & \cdots & 0 \\ 0 & h_L & \cdots & \cdots & \cdots & \cdots & 0 \\ \vdots & & \ddots & & & \cdots & \vdots \\ 0 & 0 & & h_L & \cdots & \cdots & h_1 \end{bmatrix}. \tag{7}$$

The matrix $\mathbf{H}_{\mathrm{ch}}$ has a very special pattern. Specifically, every row is the same as the previous row, just shifted to the right by 1 (wrapping around "cyclically" at the edges). That is, each row is a circular shift of the first row. To estimate the transmitted complex data symbols $\hat{\mathbf{d}}$, we consider a matrix $\mathbf{G}$ using the following relationship

$$\hat{\mathbf{d}} = \mathbf{G}\ \mathbf{y}, \tag{8}$$

where $\mathbf{G}$ denotes the MMSE receiver matrix.

Mathematically, the MMSE receiver matrix $\mathbf{G}$ is defined by the following:

$$\mathbf{G} = (\mathbf{H}_{\mathrm{ch}}\mathbf{A})^\dagger\ (p\mathbf{I}_N + (\mathbf{H}_{\mathrm{ch}}\mathbf{A})^\dagger(\mathbf{H}_{\mathrm{ch}}\mathbf{A}))^{-1}, \tag{9}$$

where the operator $(.)^\dagger$ represents the Hermitian-conjugate of a matrix, $\mathbf{I}_N$ is a $N \times N$ identity matrix, and p is the average signal-to-noise ratio (SNR), given by $p = \sigma_d^2/\sigma_\nu^2$. Based on the MMSE receiver, it can be shown that the SINR of the nth data symbol can be expressed as

$$\Gamma_n = \frac{1}{\mathrm{MMSE}_n} - 1 = \frac{1}{\left[(\mathbf{I}_N + \frac{p}{N}(\mathbf{H}_{\mathrm{ch}}\mathbf{A})^\dagger\mathbf{H}_{\mathrm{ch}}\mathbf{A})^{-1}\right]_{nn}} - 1. \tag{10}$$

Note that (10) has the same form of [8, Eq. (7.49)], being therefore not restricted to binary signals and its derivation is based on the second-order statistics of the input signals [9].

III. Approximation Approach for Γ_n

By analyzing (10), it can be verified that the product $\mathbf{H}_{\mathrm{ch}}\mathbf{A}$ is not a circular matrix. In this case, a closed-form expression for the joint PDF of the eigenvalues seems unfeasible. However, an accurate approximation for such statistics has been previously proposed in [5]. This approximation follows some assumptions that are described in the following subsections. Firstly, we will describe how the joint PDF of the eigenvalues of the matrix $\mathbf{H}_{ch}$ is obtained. Then, we will provide further insights on how to obtain the joint PDF of the eigenvalues of the matrix $\mathbf{H}_{ch}\mathbf{A}$. Finally, we will describe the procedure to obtain the approximation of the PDF of the SINR of Γ_n, which will be based on a Gamma approximation.

A. Joint Probability Density of Eigenvalues of $\mathbf{H}_{ch}$

Let us consider a general matrix $\mathbf{H}$, as defined in [10], where each channel coefficient is represented by h_r $(r = 1, ..., N)$ defined by a complex Gaussian distribution with zero-mean and variance σ_r^2. Thus, the PDF of h_r (independent and identically distributed Rayleigh channel realizations) can be expressed by

$$p_{h_r}(h_r) = \frac{1}{2\pi\sigma_r^2} \exp\left(-\frac{|h_r|^2}{2\sigma_r^2}\right). \tag{11}$$

The matrix $\mathbf{H}$ is defined as

$$\mathbf{H} = \begin{bmatrix} h_1 & h_N & \cdots & h_2 \\ h_2 & h_1 & \cdots & h_3 \\ \vdots & \vdots & \cdots & \vdots \\ h_N & h_{N-1} & \cdots & h_1 \end{bmatrix}. \tag{12}$$

From probability theory concepts, it can be shown that the joint PDF of $\{h_1 \ldots, h_N\}$ can be expressed as

$$p_{\mathbf{h}}(h_1, ..., h_N) = \prod_{r=1}^{N} \frac{1}{2\pi\sigma_r^2} \exp\left(-\frac{|h_r|^2}{2\sigma_r^2}\right). \tag{13}$$

Following the property of circulant matrices, as the one expressed in (12), the normalized eigenvectors are always the same [10]. Thus, the normalized k-th eigenvector $\mathbf{v}^{(k)}$, where $k = 0, 1, \ldots, N-1$, can be expressed as

$$\mathbf{v}^{(k)} = \frac{1}{\sqrt{N}} \left(\omega_N^{0k}\ \omega_N^{1k}\ \omega_N^{2k}\ \ldots\ \omega_N^{(N-1)k}\right)^T, \tag{14}$$

In this case, the variables ω_N^{jk} can be determined as

$$\omega_N^{jk} = e^{\frac{2\pi i}{N} jk}, \tag{15}$$

where i represents the imaginary unit, and $j = 0, 1, \ldots, N-1$. Note that (15) represents the Nth root of unity.

By its turn, the matrix $\mathbf{F}$, whose columns are the eigenvectors, can be defined as

$$\mathbf{F} = \left(\mathbf{v}^{(0)}\ \mathbf{v}^{(1)}\ \mathbf{v}^{(2)}\ \ldots\ \mathbf{v}^{(N-1)}\right), \tag{16}$$

which has the following entries

$$\mathbf{F}_{jk} = \mathbf{v}_j^{(k)} = \omega_N^{jk}. \tag{17}$$

Note that the operation of multiplying a vector by matrix $\mathbf{F}$ represents the discrete Fourier transform (DFT) of that vector. With this in mind, we can define the vector $\hat{\mathbf{c}}$ as

$$\hat{\mathbf{c}} = \mathbf{F}\mathbf{c} = \left(\lambda_0^*, \lambda_1^*, \lambda_2^*, \ldots, \lambda_{N-1}^*\right), \tag{18}$$

where $\mathbf{c}$ denotes the first row of $\mathbf{H}$, and $\hat{\mathbf{c}}$ stands for the DFT of vector $\mathbf{c}$, also representing the vector composed by the eigenvalues of $\mathbf{c}$.

We proceed similarly with $\mathbf{F}$, which is also a unitary matrix, to diagonalize $\mathbf{H}$ based on the following relationship

$$\text{diag}(\lambda_j^*) = \mathbf{F}^\dagger \mathbf{H} \mathbf{F}, \tag{19}$$

where, for both cases, λ_j^* has entries defined by

$$\lambda_j^* = \sum_{k=0}^{N-1} h_k \omega_N^{kj}. \tag{20}$$

Based on the fact that each h_k is complex Gaussian distributed with zero-mean and variance σ_r^2, the complex eigenvalues λ_j^* have joint PDF being given by

$$p_{\boldsymbol{\lambda}^*}(\lambda_1^*, ..., \lambda_N^*) = \prod_{j=1}^{N} \frac{1}{2\pi\Phi_{\text{h}}^2} \exp\left(-\frac{|\lambda_j^*|^2}{2\Phi_{\text{h}}^2}\right), \tag{21}$$

where $\Phi_{\text{h}}^2 = \sum_{r=1}^{N} \sigma_r^2$, leading to a PDF that has zero-mean and variance Φ_{h}^2 for both real and imaginary parts.

Note that all the previous analysis was related to matrix $\mathbf{H}$. In order to extend the procedure to matrix channel $\mathbf{H}_{\text{ch}}$, we now consider the limit $\sigma_r \to 0$ for $r = (L+1), (L+2), \ldots, N$ so that we are able to analyze $\mathbf{H}_{\text{ch}}\mathbf{A}$. Let us first use the following relationship defined by

$$\text{diag}(\lambda_j) = \mathbf{F}^\dagger \mathbf{H}_{\text{ch}} \mathbf{F}. \tag{22}$$

To obtain the complex eigenvalues λ_j of $\mathbf{H}_{ch}$, we first define the joint PDF of the eigenvalues as

$$p_{\boldsymbol{\lambda}}(\lambda_1, ..., \lambda_N) = \prod_{j=1}^{N} \frac{1}{2\pi\Phi^2} \exp\left(-\frac{|\lambda_j|^2}{2\Phi^2}\right). \tag{23}$$

Then, we can finally write the variance of matrix $\mathbf{H}_{\text{ch}}$ as $\Phi^2 = \sum_{r=1}^{L} \sigma_r^2$.

B. Joint Probability Density of the Eigenvalues of $\sqrt{p}\ \mathbf{H}_{ch}\mathbf{A}$

By inspection, one can notice that the product $\mathbf{H}_{\text{ch}}\mathbf{A}$ is not necessarily a circulant matrix. Let us consider the main product factor of (10) that is represented by $p\,(\mathbf{H}_{\text{ch}}\mathbf{A})^\dagger \mathbf{H}_{\text{ch}}\mathbf{A}$, which is an Hermitian matrix. We can employ a singular value decomposition strategy so that

$$\sqrt{p}\,\mathbf{H}_{\text{ch}}\mathbf{A} = \mathbf{V}\mathbf{M}\mathbf{U}, \tag{24}$$

where $\mathbf{V}$ and $\mathbf{U}$ are unitary matrices, and $\mathbf{M} = \text{diag}(\mu_1, ..., \mu_N)$ contains the singular values of $\sqrt{p}\,\mathbf{H}_{\text{ch}}\mathbf{A}$. From (24), we obtain

$$p\,(\mathbf{H}_{\text{ch}}\mathbf{A})^\dagger \mathbf{H}_{\text{ch}}\mathbf{A} = \mathbf{U}\mathbf{M}^\dagger\mathbf{M}\mathbf{U}^\dagger, \tag{25}$$

since $\mathbf{V}^\dagger\mathbf{V} = \mathbf{I}$.

From (10), Γ_n can be rewritten in terms of α_n so that

$$\Gamma_n = \frac{1}{\alpha_n} - 1, \tag{26}$$

where α_n is defined based on (25) as

$$\begin{aligned} \alpha_n &= \left[\left(\mathbf{I} + \frac{p}{N}(\mathbf{H}_{\text{ch}}\mathbf{A})^\dagger \mathbf{H}_{\text{ch}}\mathbf{A}\right)^{-1}\right]_{nn} \\ &= \left[\mathbf{U}\left(\mathbf{I} + \frac{1}{N}\mathbf{M}^\dagger\mathbf{M}\right)^{-1}\mathbf{U}^\dagger\right]_{nn}. \end{aligned} \tag{27}$$

Using summation notation, (27) can be re-expressed by

$$\alpha_n = \sum_{r,s=1}^{N} \mathbf{U}_{nr}\Big(1+\frac{1}{N}|\mu_r|^2\Big)^{-1}\delta_{rs}\mathbf{U}^*_{ns}, \tag{28}$$

or by

$$\alpha_n = \sum_{r=1}^{N} \Big(1+\frac{1}{N}|\mu_r|^2\Big)^{-1}|\mathbf{U}_{nr}|^2. \tag{29}$$

Based on the condition that $\mathbf{H}_{\text{ch}}\mathbf{A}$ is a circulant matrix, then $\mathbf{U}$ holds same condition as the DFT matrix given by (19) and (14). As a result, the square of the absolute value of $\mathbf{U}_{nr}$, represented by $|\mathbf{U}_{nr}|^2$, is equal to $1/N$. In this case, the eigenvalue $\{\mu_r\}$ equals to the product of $\sqrt{p}$, eigenvalues of $\mathbf{H}_{\text{ch}}$, and eigenvalues of $\mathbf{A}$. Consequently, α_n can be approximated by

$$\begin{aligned}\alpha_n &\approx \sum_{r=1}^{N}\Big(1+\frac{1}{N}|\mu_r|^2\Big)^{-1}\Big|\frac{1}{\sqrt{N}}\Big|^2\\ &\approx \sum_{r=1}^{N}\frac{1}{N+|\mu_r|^2}.\end{aligned} \tag{30}$$

As properly demonstrated in [5], this assumption holds very well for different parameter configurations of matrix $\mathbf{A}$, including different roll-off factors of prototype filter $g[n]$.

Based on above, the symmetrized joint PDF of $\{\mu_j\}$, $j = 0, 1, \ldots, N-1$), can be accurately approximated by

$$\begin{aligned}p_{\boldsymbol{\mu}}(\mu_1, ..., \mu_N) \approx \frac{1}{N!}\sum_{\{q(j)\}}\Bigg[\prod_{j=1}^{N}\frac{1}{2\pi p\Phi^2|\chi_{q(j)}|^2}\\ \times\exp\left(-\frac{|\mu_j|^2}{2p\Phi^2|\chi_{q(j)}|^2}\right)\Bigg],\end{aligned} \tag{31}$$

where the sum involves all $N!$ permutations of $\{q(1), q(2), ..., q(N)\}$, with $q(j)$ being the indices of $\{\chi\}$, which are the eigenvalues of the matrix A.

Now, considering the joint PDF of eigenvalues of $\sqrt{p}\,\mathbf{H}_{ch}\mathbf{A}$, as shown in Eq. (31), the next step is to find accurate approximations for the PDF of the random variables α_n and Γ_n, which will be detailed next.

C. Statistics for α_n and Γ_n

In order to compute an approximation for the PDF of α_n, we should first obtain its mean (μ) and variance (σ^2). To this end, we depart from the joint PDF given in (31) and use the relation given in (30), which results in the mean value for α_n [5]

$$\mu = \mathbb{E}[\alpha_n] = -\sum_{j=1}^{N}\left[\frac{1}{\Psi_j^2}\exp\left(\frac{N}{\Psi_j^2}\right)\text{Ei}\Big(-\frac{N}{\Psi_j^2}\Big)\right]. \tag{32}$$

We proceed similarly to compute the variance of α_n, which is given by [5]:

$$\begin{aligned}\sigma^2 &= \mathbb{E}[\alpha_n^2] - (\mathbb{E}[\alpha_n])^2\\ &= \sum_{j=1}^{N}\left[\frac{1}{N\Psi_j^2}+\frac{1}{\Psi_j^4}\exp\left(\frac{N}{\Psi_j^2}\right)\text{Ei}\Big(-\frac{N}{\Psi_j^2}\Big)\right.\\ &\quad\left.-\frac{1}{\Psi_j^4}\exp\left(\frac{2N}{\Psi_j^2}\right)\text{Ei}^2\Big(-\frac{N}{\Psi_j^2}\Big)\right],\end{aligned} \tag{33}$$

where $\text{Ei}(x)$ represents the exponential integral function, which is defined by

$$Ei(x) = -\int_{-x}^{\infty}\frac{e^{-t}}{t}dt. \tag{34}$$

In addition, Ψ_j^2 is given by the following relation:

$$\Psi_j^2 = 2p\Phi^2|\chi_j|^2, \tag{35}$$

where $\Phi^2 = \sum_{r=1}^{N}\sigma_r^2$ and χ_j denotes the jth eigenvalue of matrix A.

Then, the PDF of α_n can be approximated in terms of the incomplete Gamma function as

$$p_\alpha(\alpha_n) \approx \frac{1}{\Gamma(k)\,\theta^k}\,\alpha_n^{k-1}\exp\left(-\frac{\alpha_n}{\theta}\right), \tag{36}$$

where $\Gamma(\cdot)$ denotes the Gamma function [11, Eq. (8.310)], $\theta = \sigma^2/\mu$, and $k = \mu^2/\sigma^2$.

Based on the approximation above, we can easily reach at an accurate approximation for the PDF of Γ_n after appropriate substitutions and using standard statistical procedure for random variables transformation, i.e.,

$$p_\Gamma(\Gamma_n) \approx \frac{1}{\Gamma(\kappa)\,\theta^\kappa}\,(1+\Gamma_n)^{-1-\kappa}\exp\left(-\frac{1}{(1+\Gamma_n)\theta}\right). \tag{37}$$

IV. Achievable Sum Rate

Assuming independent decoding at the receiver, the achievable ergodic sum rate for MMSE receiver is given by [12]:

$$\mathcal{R}^{\text{mmse}}(\Gamma_n, N) = \sum_{n=1}^{N} E_{\Gamma_n}[\log_2(1+\Gamma_n)], \tag{38}$$

which can be rewritten as

$$\begin{aligned}\mathcal{R}^{\text{mmse}} &= \sum_{n=1}^{N}\int_0^\infty [\log_2(1+\Gamma_n)]\; p_\Gamma(\Gamma_n)\; d\Gamma_n\\ &\approx \sum_{n=1}^{N}\int_0^\infty\left[\log_2(1+\Gamma_n)\;\frac{1}{\Gamma(\kappa)\,\theta^\kappa}\,(1+\Gamma_n)^{-1-\kappa}\right.\\ &\quad\left.\exp\left(-\frac{1}{(1+\Gamma_n)\theta}\right)\right]d\Gamma_n,\end{aligned} \tag{39}$$

to solve the Integral in (39) let $\alpha = -1/\theta$ and consider that

$$\begin{aligned}\int_0^\infty\frac{\log(x+1)}{(x+1)^p}\mathrm{d}x &= -\frac{\mathrm{d}}{\mathrm{d}p}\int_0^\infty\frac{\mathrm{d}x}{(x+1)^p}\\ &= \frac{1}{(p-1)^2}, \Re(p) > 1\end{aligned} \tag{40}$$

and

$$\exp\left(\frac{\alpha}{(1+\Gamma_n)}\right) = \sum_{j\geq 0} \frac{\alpha^j}{j!\ (\Gamma_n+1)^j} \tag{41}$$

the equation for $\mathcal{R}^{\text{mmse}}$ could be re-written as

$$\begin{aligned}
\mathcal{R}^{\text{mmse}} &\approx \frac{N\ (-\alpha^\kappa)}{\Gamma(\kappa)\log(2)} \left(\sum_{j\geq 0} \int_0^\infty \frac{\log(1+\Gamma_n)}{(1+\Gamma_n)^{\kappa+1}} \frac{\alpha^j}{j!\ (1+\Gamma_n)^j} \mathrm{d}\Gamma_n \right) \\
&\approx \frac{N\ (-\alpha^\kappa)}{\Gamma(\kappa)\log(2)} \left(\sum_{j\geq 0} \frac{\alpha^j}{j!} \int_0^\infty \frac{\log(1+\Gamma_n)}{(1+\Gamma_n)^{j+\kappa+1}} \mathrm{d}\Gamma_n \right) \\
&\approx \frac{N\ (-\alpha^\kappa)}{\Gamma(\kappa)\log(2)} \left(\sum_{j\geq 0} \frac{\alpha^j}{j!}\ \frac{1}{(j+\kappa)^2} \right) \\
&\approx \frac{N\ (-\alpha^\kappa)}{\Gamma(\kappa)\log(2)} \left(\kappa^2\ {}_2F_2(\kappa,\kappa;\kappa+1,\kappa+1;\alpha) \right)
\end{aligned} \tag{42}$$

where ${}_2F_2(\cdot,\cdot;\cdot,\cdot;\cdot)$ represents the Generalized Hypergeometric function [13, pp.555-566.]. Then, using the residue theorem to the integral representation of the function $G_{p,q}^{m,n}\left(\begin{matrix} a_1,\ldots,a_p \\ b_1,\ldots,b_q \end{matrix} \middle| z \right)$, which is the Meijer's G-function [11, Eq. (9.301)] and replacing $\theta = -1/\alpha$, the Eq. (42) could be finally defined as

$$\begin{aligned}
\mathcal{R}^{\text{mmse}} \approx \frac{N}{\Gamma(\kappa)\log(2)} \Bigg(&\Gamma\Big(\kappa, \frac{1}{\theta}\Big)\Big(\log(1/\theta) + \log(\theta)\Big) + \\
&G_{2,3}^{3,0}\left(\begin{matrix} 1,1 \\ 0,0,\kappa \end{matrix} \middle| \frac{1}{\theta} \right) - \Gamma(\kappa)(\log(\theta) + \psi^{(0)}(\kappa))) \Bigg),
\end{aligned} \tag{43}$$

where $\Re(\kappa) > 0$, and $\psi^{(0)}(z) = \Gamma'(z)/\Gamma(z)$ is the Polygamma function.

V. Outage Capacity

Considering that the variable Γ_n represents the SINR, it is possible to calculate the non-ergodic capacity C_{Γ_n} of the nth data symbol by $C_{\Gamma_n} = \log_2(1+\Gamma_n)$ [14], [15]. However, to calculate the outage capacity of the system, it should be considered that there are $N = S \times K$ symbols. Then, we calculate the GFDM system capacity by

$$C_\Gamma = \sum_{n=1}^{N} \log_2(1+\Gamma_n) = N\ \log_2(1+\Gamma_n). \tag{44}$$

So, as we know the PDF of Γ_n from (37), it is possible to calculate the PDF of the random variable C_Γ, which is represented by $f_{C_\Gamma}(C_\Gamma)$ and computed using random variable transformation, i.e.,

$$\begin{aligned}
f_{C_\Gamma}(C_\Gamma) &= \frac{(1+\Gamma_n)^{-1-\kappa}\ e^{\frac{-1}{\theta(1+\Gamma_n)}}}{\Gamma(\kappa)\theta^\kappa\ \frac{N}{\log(2)\ (1+\Gamma_n)}} \Bigg|_{\Gamma_n = 2^{C_\Gamma/N}-1} \\
&= \frac{e^{-\frac{2^{-C_\Gamma/N}}{\theta}} \left(\frac{2^{-C_\Gamma/N}}{\theta}\right)^k \log(2)}{N\Gamma(k)},
\end{aligned} \tag{45}$$

The outage probability of the system associated with a given transmission rate is defined as the probability that the random variable C_{Γ_n} falls below an arbitrary data rate value, which is named as R_{out}. Accordingly, the outage probability for the GFDM system is therefore given by

$$\begin{aligned}
P_{\text{out}} &= P[C_\Gamma < R_{\text{out}}] \\
&= F_{C_\Gamma}(R_{\text{out}})
\end{aligned} \tag{46}$$

where $F_{C_\Gamma}(C_\Gamma)$ is the cumulative distribution of C_{Γ_n} defined by

$$F_{C_\Gamma}(C_\Gamma) = \int_\infty^{R_{\text{out}}} f_{C_\Gamma(C_\Gamma)}\ \mathrm{d}C_\Gamma \tag{47}$$

In order to solve the (47), we use the following variable substitution: $t = \frac{2^{\frac{-C_\Gamma}{N}}}{\theta}$ in (45). So, $\mathrm{d}t = \frac{-2^{-C_\Gamma/N}}{N\ \theta}\log(2)\ \mathrm{d}C_\Gamma$.

$$F_{C_\Gamma}(C_\Gamma) = \int_{\frac{2^{-C_\Gamma/N}}{\theta}}^{\infty} \left(e^{-t}\ t^{\kappa-1}\right)\mathrm{d}t = \frac{\Gamma\left(\kappa, \frac{2^{\frac{-C_\Gamma}{N}}}{\theta}\right)}{\Gamma(\kappa)}, \tag{48}$$

where the function $\Gamma(a,x) \equiv \int_x^\infty t^{a-1}e^{-t}\mathrm{d}t$ is the upper incomplete Gamma function.

VI. Performance Analysis

To validate the analytical formulations of the achievable sum rate and outage capacity defined in (39) and (46), we employ Monte Carlo simulation to demonstrate the accuracy of the proposed models. The simulation considers different parameters for the GFDM system, namely the prototype filter defined by a root raised cosine (RRC) with a specific roll-off factor, and the number of sub-carriers and symbols. The channel is modeled as a FSFC, for different sizes of the L, power delay profile modeled by $\sigma_m^2 = e^{-0.2m}$, $m = 1,\ldots,L$. The power transmission for data symbols (σ_d^2) is equal to 1. So, the SNR values ($p = \sigma_d^2/\sigma_v^2$) depend only of the noise variance.

A. Achievable sum rate results

Figure 1 presents the achievable sum rate for some number of sub-carriers as $K = 8, 32, 128$, number of sub-symbols as $S = 3, 5$, the roll-off factors $= 0.1, 0.9$, and the number of channels steps is $L = 2$. In all cases, the analytical approximation (represented by lines) matches with high accuracy with the Monte Carlo simulation (represented by markers), indicating the effectiveness of the proposed approach.

As the performance analysis itself, the achievable sum rate is presented as a function of the SNR (p) using a logarithmic scale in the achievable sum rate axis. The greater the $N = S.K$, the higher the achievable sum rate value. For example, when the SNR is 30 dB the achievable sum rate for the case with K=8 and S=3 is less than 100 bps/Hz. For the same SNR value, the achievable sum rate for K=128 and S=5 is approximately 400 bps/Hz. Based on this result, we can conclude that the mathematical model described in (39) is approximating the achievable sum rate with acceptable accuracy in scenarios using a roll-off=0.1 and roll-off=0.9.

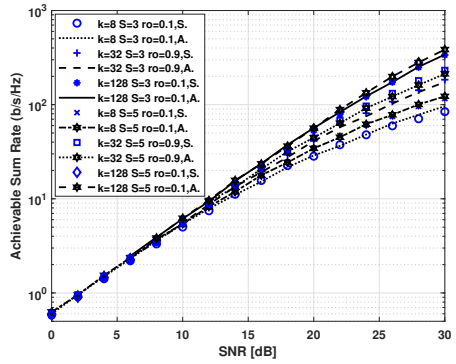

Fig. 1. Simulated and analytic achievable sum rate for GFDM for different values of k,S, roll-off, and L. The abbreviations S. and A. mean simulation and analytical respectively.

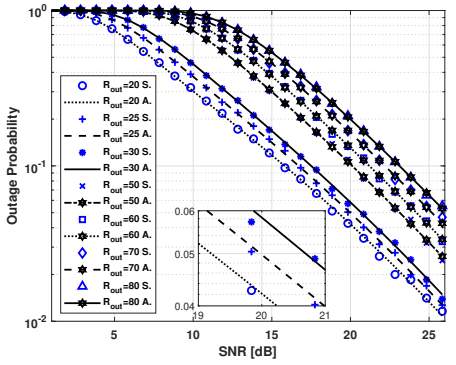

Fig. 2. Probability of outage versus SNR for different values of R_{out} for GFDM ($S = 3$, $K = 32$, $L = 2$) with Roll-off= 0.9. Every R_{out} is in bps/Hz, and the abbreviations S. and A. means simulation and analytical, respectively.

B. Outage results

We considered the following GFDM parameters: $K = 32$, $S = 3$, $L = 2$, and roll-off= 0.1. Many curves were generated based on the assumption that an arbitrary data rate is fixed. These data rates vary from 20 bps/Hz until 80 bps/Hz. As less the value of the data rate, much is the chance of a specific scenario to be in outage. For example, for a $R_{\text{out}} = 20$ bps/Hz and a SNR value of 10 dB the outage probability is equal to 0.3. In the same analyse point, for a $R_{\text{out}} = 80$ bps/Hz the outage probability is increased to 0.95.

VII. Conclusion and Future Works

In this paper, we studied the achievable sum rate and the outage for a GFDM system in closed-form employing MMSE receivers over FSFC based on a Gamma-distribution approximation for the random variable that define the SINR. the accuracy of the proposed model was evaluated with different GFDM parameters and channel conditions. For instance, that the outage probability when the SNR= 20 for the $R_{\text{out}} = 25$ bps/Hz is less than 5%. As future works, we plan to extend this work to more performance metrics, providing a thorough comparison of the GFDM and other techniques as OFDM.

Acknowledgements

This paper is supported by Academy of Finland via: (a) ee-IoT project n.319009, (b) FIREMAN consortium CHIST-ERA/n.326270, and (c) EnergyNet Research Fellowship n.321265/n.328869. The work of D. B. da Costa was financially supported by FUNCAP (Edital PRONEM, 01/2016) and by CNPq (Grant no. 302863/2017-6). The work of G. Fraidenraich was financially supported by CNPq (Grant no. 301777/2019-5).

References

[1] G. Wunder, P. Jung, M. Kasparick, T. Wild, F. Schaich, Y. Chen, S. T. Brink, I. Gaspar, N. Michailow, A. Festag, L. Mendes, N. Cassiau, D. Ktenas, M. Dryjanski, S. Pietrzyk, B. Eged, P. Vago, and F. Wiedmann, "5GNOW: non-orthogonal, asynchronous waveforms for future mobile applications," *IEEE Communications Magazine*, vol. 52, no. 2, pp. 97–105, February 2014.

[2] N. Michailow, M. Matthé, I. S. Gaspar, A. N. Caldevilla, L. L. Mendes, A. Festag, and G. Fettweis, "Generalized frequency division multiplexing for 5th generation cellular networks," *IEEE Transactions on Communications*, vol. 62, no. 9, pp. 3045–3061, 2014.

[3] M. Towliat and S. M. J. A. Tabatabaee, "GFDM Interference Mitigation Without Noise Enhancement," *IEEE Communications Letters*, vol. 22, no. 5, pp. 1042–1045, 2018.

[4] S. Han, Y. Sung, and Y. H. Lee, "Filter Design for Generalized Frequency-Division Multiplexing," *IEEE Transactions on Signal Processing*, vol. 65, no. 7, pp. 1644–1659, April 2017.

[5] D. Carrillo, S. Kumar, G. Fraidenraich, and L. L. Mendes, "Bit Error Probability for MMSE Receiver in GFDM Systems," *IEEE Communications Letters*, vol. 22, no. 5, pp. 942–945, May 2018.

[6] C. Shin, R. W. Heath, and E. J. Powers, "Non-Redundant Precoding-Based Blind and Semi-Blind Channel Estimation for MIMO Block Transmission With a Cyclic Prefix," *IEEE Transactions on Signal Processing*, vol. 56, no. 6, pp. 2509–2523, June 2008.

[7] S. Tiwari, S. S. Das, and K. K. Bandyopadhyay, "Precoded Generalized Frequency Division Multiplexing System to Combat Intercarrier Interference: Performance Analysis," *IET Communications*, vol. 9, no. 15, pp. 1829 – 1841, May 2015.

[8] A. Paulraj, R. Nabar, and D. Gore, *Introduction to space-time wireless communications*. Cambridge university press, 2003.

[9] P. Li, D. Paul, R. Narasimhan, and J. Cioffi, "On the Distribution of SINR for the MMSE MIMO Receiver and Performance Analysis," *IEEE Trans. Inf. Theory*, vol. 52, no. 1, pp. 271 – 286, Jan 2006.

[10] R. M. Gray, "Toeplitz and Circulant Matrices: A Review," *Commun. Inf. Theory*, vol. 2, no. 3, pp. 155–239, Aug. 2005.

[11] I. S. Gradshteyn and I. M. Ryzhik, *Table of Integrals, Series, and Products*, 7th ed., San Diego, CA: Academic, 2007.

[12] C. Zhong, M. Matthaiou, A. Huang, and Z. Zhang, "On the sum rate of MIMO Nakagami-m fading channels with MMSE receivers," in *2012 IEEE 7th Sensor Array and Multichannel Signal Processing Workshop (SAM)*, June 2012, pp. 49–52.

[13] M. Abramowitz and I. Stegun, *Handbook of Mathematical Functions*, New York, NY: Dover, 1972.

[14] A. Maaref and S. Aissa, "Closed-form expressions for the outage and ergodic Shannon capacity of MIMO MRC systems," *IEEE Transactions on Communications*, vol. 53, no. 7, pp. 1092–1095, July 2005.

[15] P. Wijesinghe, U. Gunawardana, and R. Liyanapathirana, "An Efficient Algorithm for Capacity and Outage Probability Estimation in MIMO Channels," *IEEE Communications Letters*, vol. 15, no. 6, pp. 644–646, June 2011.

ACTA UNIVERSITATIS LAPPEENRANTAENSIS

1048. KARJUNEN, HANNU. Analysis and design of carbon dioxide utilization systems and infrastructures. 2022. Diss.

1049. VEHMAANPERÄ, PAULA. Dissolution of magnetite and hematite in acid mixtures. 2022. Diss.

1050. GOLOVLEVA, MARIA. Numerical simulations of defect modeling in semiconductor radiation detectors. 2022. Diss.

1051. TREVES, LUKE. A connected future: The influence of the Internet of Things on business models and their innovation. 2022. Diss.

1052. TSERING, TENZIN. Research advancements and future needs of microplastic analytics: microplastics in the shore sediment of the freshwater sources of the Indian Himalaya. 2022. Diss.

1053. HOSEINPUR, FARHOOD. Towards security and resource efficiency in fog computing networks. 2022. Diss.

1054. MAKSIMOV, PAVEL. Methanol synthesis via CO2 hydrogenation in a periodically operated multifunctional reactor. 2022. Diss.

1055. LIPIÄINEN, KALLE. Fatigue performance and the effect of manufacturing quality on uncoated and hot-dip galvanized ultra-high-strength steel laser cut edges. 2022. Diss.

1056. MONTONEN, JAN-HENRI. Modeling and system analysis of electrically driven mechatronic systems. 2022. Diss.

1057. HAVUKAINEN, MINNA. Global climate as a commons — from decision making to climate actions in least developed countries. 2022. Diss.

1058. KHAN, MUSHAROF. Environmental impacts of the utilisation of challenging plastic-containing waste. 2022. Diss.

1059. RINTALA, VILLE. Coupling Monte Carlo neutronics with thermal hydraulics and fuel thermo-mechanics. 2022. Diss.

1060. LÄHDEAHO, OSKARI. Competitiveness through sustainability: Drivers for logistics industry transformation. 2022. Diss.

1061. ESKOLA, ROOPE. Value creation in manufacturing industry based on the simulation. 2022. Diss.

1062. MAKARAVA, IRYNA. Electrochemical recovery of rare-earth elements from NdFeB magnets. 2022. Diss.

1063. LUHAS, JUKKA. The interconnections of lock-in mechanisms in the forest-based bioeconomy transition towards sustainability. 2022. Diss.

1064. QIN, GUODONG. Research on key technologies of snake arm maintainers in extreme environments. 2022. Diss.

1065. TAMMINEN, JUSSI. Fast contact copper extraction. 2022. Diss.

1066. JANTUNEN, NIKLAS. Development of liquid–liquid extraction processes for concentrated hydrometallurgical solutions. 2023. Diss.

1067. GULAGI, ASHISH. South Asia's Energy [R]evolution – Transition towards defossilised power systems by 2050 with special focus on India. 2023. Diss.

1068. OBREZKOV LEONID. Development of continuum beam elements for the Achilles tendon modeling. 2023. Diss.

1069. KASEVA, JANNE. Assessing the climate resilience of plant-soil systems through response diversity. 2023. Diss.

1070. HYNNINEN, TIMO. Development directions in software testing and quality assurance. 2023. Diss.

1071. AGHAHOSSEINI, ARMAN. Analyses and comparison of energy systems and scenarios for carbon neutrality - Focus on the Americas, the MENA region, and the role of geo-technologies. 2023. Diss.

1072. LAKANEN, LAURA. Developing handprints to enhance the environmental performance of other actors. 2023. Diss.

1073. ABRAMENKO, VALERII. Synchronous reluctance motor with an axially laminated anisotropic rotor in high-speed applications. 2023. Diss.

1074. GUTIERREZ ROJAS, DANIEL. Anomaly detection in cyber-physical applications. 2023. Diss.

1075. ESANOV, BAKHTIYOR. Adaptive user-controlled personalization for virtual journey applications. 2023. Diss.

1076. SILTANEN, JUKKA. Laser and hybrid welding of high-strength structural steels. 2023. Diss.

1077. NOUSIAINEN, JALO. Model-based reinforcement learning and inverse problems in extreme adaptive optics control. 2023. Diss.

1078. USTINOV, STANISLAV. Fast and accurate simulation of fluid power circuits in the presence of small volumes using advanced methods and models for numerical stiffness elimination. 2023. Diss.

1079. HUSSAIN, HAFIZ MAJID. Heuristic-based packetized energy management for residential electricity demand. 2023. Diss.

1080. HÄMÄLÄINEN, MINNA. Principals managing entrepreneurship education in schools. 2023. Diss.

1081. WANG, ZHAO. Photocatalytic degradation of pharmaceutical and person care products (PPCPs) by commercial and synthesized catalysts under UV irradiation. 2023. Diss.

1082. LOHRMANN, ALENA. The water footprint of the global power sector: Status quo, challenges, and opportunities for tackling the global water crisis. 2023. Diss.

1083. PONOMAREV, NIKOLAI. A salt and alkali synergy for synthesising active carbons from lignin: porosity development and techno-economic assessment. 2023. Diss.

1084. AFANASYEVA, SVETLANA. Wind farm layout optimization: project economics and risk. 2023. Diss.

1085. VOSTROV, KONSTANTIN. Reduction of non-circulating bearing currents by electrical machine design. 2023. Diss.

ISBN 978-952-335-963-5
ISBN 978-952-335-964-2 (PDF)
ISSN 1456-4491 (Print)
ISSN 2814-5518 (Online)
Lappeenranta 2023